FOSSIL

DOE/MC/25046-2875
(DE90015334)

THE EXTRACTION OF BITUMEN FROM WESTERN TAR SANDS

Final Report

By
A. G. Oblad
J. W. Bunger
F. V. Hanson
J. D. Miller
J. D. Seader

May 1989

Work Performed Under Contract No. FG21-88MC25046

For
U.S. Department of Energy
Morgantown Energy Technology Center
Morgantown, West Virginia

By
University of Utah
Salt Lake City, Utah

DISCLAIMER

This report has been reproduced directly from the best available copy.

Available to DOE and DOE contractors from the Office of Scientific and Technical Information, P.O. Box 62, Oak Ridge, TN 37831; prices available from (615)576-8401, FTS 626-8401.

Available to the public from the National Technical Information Service, U. S. Department of Commerce, 5285 Port Royal Rd., Springfield, VA 22161.

Price: Printed Copy A09
Microfiche A01

Printed in the United States of America, Office of Scientific and Technical Information, Oak Ridge , Tennessee

DOE/MC/25046--2875

DE90 015334

The Extraction of Bitumen From Western Tar Sands

Final Report

A.G. Oblad
J.W. Bunger
F.V. Hanson
J.D. Miller
J.D. Seader

Work Performed Under Contract No.: DE-FG21-88MC25046

For
U.S. Department of Energy
Office of Fossil Energy
Morgantown Energy Technology Center
P.O. Box 880
Morgantown, West Virginia 26507-0880

By
University of Utah
Department of Fuels Engineering
Department of Metallurgical Engineering
Department of Chemical Engineering
Salt Lake City, Utah 84112

May 1989

TABLE OF CONTENTS

LIST OF FIGURES

LIST OF TABLES

EXECUTIVE SUMMARY

Alex G. Oblad Principal Investigator

This report represents the work done on contract DE-FG21-88MC25046 during the year of May 8, 1987 to June 9, 1988. This year was the first year of a five-year program. The overall objective of the latter is to advance the technologies for recovering bitumen from the tar sands by thermal and water assisted extraction means and upgrading of bitumen to synthetic crude, and conversion of bitumens to specialty products such as asphalt and resins to levels where realistic evaluations of technical and commercial potential can be made. Additionally, it is desired to have the data at a level which is adequate for design of pilot plants of appropriate size deemed necessary for commercial scale-up of the various processes being studied.

The main areas for studies covered in this report are modelling and optimization of the hydropyrolysis process for upgrading bitumens, bitumen recovery by pyrolysis of the Circle Cliffs tar sands in a fluid bed, pyrolysis of Whiterocks tar sand in a rotary kiln, modelling of the combustor in the coupled fluidized bed with interbed heat transfer using heat pipes, development of superior diluents for use in the water extraction of Utah's tar sands, and fractionation and characterization of the bitumens from Asphalt Ridge and Sunnyside tar sands.

Bitumen recovered from tar sands must be upgraded to produce refinery-acceptable materials. Hydropyrolysis has been studied extensively as a novel process for upgrading of bitumen to a crude oil in high yields, which are amenable for downstream catalytic processing. Emphasis in the current reporting period has focused on the development of a kinetic model for hydropyrolysis. Accordingly, a lumped component kinetic model was developed which expresses the yield distribution as a function of feed composition, temperature and residence time. Results of runs using both tar sand bitumen and Wilmington crude oil (geochemically similar to Uinta Basin tar sands) were used to establish kinetic constants. The kinetic model can be used in conjunction with the drop model previously developed (cf: final report, 1985) to mathematically represent the combined rate processes, e.g., heat and mass transfer and chemical reactions occurring. Results have confirmed that optimum process conditions are expected in the regime of 520-535 °C and residence times on the order of 1-10 seconds at 1800 psig. Research currently being conducted is focusing on process simulation and economic optimization of the process based on the kinetic model developed.

It has been previously reported that Circle Cliffs tar sand contained, besides quartz sand, considerable other mineral matter. The latter has now been identified as feldspar and kaolinite. Extensive analyses of the bitumen and these minerals have been undertaken. Carbon dioxide and water are produced upon heating of the spent sand obtained in pyrolysis of Circle Cliffs tar sand. Production of CO_2 and H_2O during pyrolysis is believed to have come from decomposition of carbonates and the kaolinite, respectively. The presence of

kaolin was suspected of giving the anomalous results obtained during pyrolysis of Circle Cliffs tar sand. Kaolinite is known to become catalytically active as a cracking catalyst for hydrocarbons upon heating. This was proved to be the case with the contained kaolin by studies of ammonia adsorption and the cracking of n-hexane with bitumen-free Circle Cliffs sand. The sand was found to exhibit cracking activity and to adsorb ammonia. The cracking activity of the active sand decayed with time, which is characteristic of catalytic cracking catalysts, as is the adsorption of ammonia by these catalysts.

A commercially available small scale rotary kiln was evaluated (at the facilities of a manufacturer of commercial kilns) as a means of conducting pyrolysis of tar sands. The results obtained were very encouraging in that the overall operability of the kiln with Utah sands was excellent. The results of the tests showed that product yields and distribution were approximately the same as those obtained in fluid bed pyrolysis. Furthermore, the C_5^+ liquid yield showed a trend of yield vs. residence time that was similar to that found in fluid bed pyrolysis.

As a step toward the ultimate goal of optimizing the configuration and operation of a coupled fluidized-bed process for the thermal pyrolysis of Utah tar sands, an extensive literature review was conducted regarding hydrodynamics, transport, and kinetics of fluidized beds. Subsequently, a preliminary mathematical model of the lower combustion bed was developed and an accompanying computer program was prepared. A preliminary test of the model was completed for a bed temperature of 575 °C. Future work includes extensive testing of the model over a wide range of the important operating variables and incorporation into the model of the pyrolysis bed with thermal coupling between the two beds.

The importance of reducing the viscosity of the bitumen contained in tar sands prior to water extraction has been well established at the University. The required reduction of bitumen viscosity has been accomplished by addition of a petroleum based hydrocarbon solvent such as kerosene as a diluent for the bitumen prior to extraction. As part of our program on improving our water-extraction technology, it was considered important to determine the effectiveness of a variety of solvents for viscosity reduction. Accordingly, six different materials of varying physical and chemical properties were evaluated using bitumens from Asphalt Ridge, P.R. Spring, and Sunnyside tar sands. The results showed that the most effective solvents for viscosity reduction were a highly aromatic heavy naphtha (SC-150) and a kerosene (both commercially available). Development of a rationale to explain the effectiveness of the various diluents in reducing bitumen viscosity proved to be complex. However, it was concluded from the information obtained in these studies and information from the literature that effective diluents are those with boiling ranges from heavy naphthas through kerosene (170 - 275 °C). Comparison of the effectiveness of SC-150 and kerosene as diluents for extraction was determined using Sunnyside tar sand. SC-150 proved to be more effective than kerosene; however, the bitumen concentrate quality and degree of separation were marginal at the test conditions employed. The results with Sunnyside tar sand corroborate previous results obtained on this tar sand. The marginal results are believed to be due to the very fine quartz sand material occurring in this tar sand. It is believed that improvement of our hot water extraction equipment will enable us to improve the quality of the concentrate and the separation efficiency for Sunnyside tar sand.

improvement of our hot water extraction equipment will enable us to improve the quality of the concentrate and the separation efficiency for Sunnyside tar sand.

To broaden our understanding of the causes of the widely different viscosity properties of the bitumens found in the various Utah tar sands, studies were carried out with Asphalt Ridge, and Sunnyside. These two bitumens have widely different viscosities, Sunnyside bitumen being 20 times more viscous than Asphalt Ridge. The studies included separation of the bitumens into saturates, aromatics, resins, and asphaltenes using standard procedures. The separate components were subjected to elemental analysis and C_{13} NMR and FTIR spectra determinations. The results obtained show significant differences in chemical composition between the two bitumens, the most significant being the carbonyl content of Sunnyside bitumen. The presence of carbonyl groups is believed to be an important factor in the much higher viscosity of Sunnyside bitumen.

A comparison of the resins contained in tar sands was made with those present in a Utah coal. Significant differences were found in both physical and chemical properties. The coal resins are characterized by lower heteroatom and aromatic contents and significantly different amounts and species of carbonyl compounds. Further studies are required to show whether or not resins obtained from tar sands can be used in place of coal resins in the commercial uses of the latter.

BITUMEN UPGRADING

James W. Bunger	Co-Principal Investigator
Hoil Ryu	Graduate Student
Soon-Yong Jeong	Graduate Student

INTRODUCTION

The objective of the bitumen upgrading tasks is to develop a predictive kinetic description of hydropyrolysis for incorporation into an integrated process model. A kinetic description of hydropyrolysis of heavy oil is complicated by the presence of large numbers of different molecules. Therefore, describing the kinetics of each individual species present in a complex mixture is not feasible. In practice, it has always been necessary to group, or concentrate, many of the individual species into pseudospecies, or lumped species, and then to develop kinetics based on the simplified reaction network. Long before lumping analysis became popular in reaction engineering, it was common in the petroleum industry to lump large numbers of molecular species together, depending on the type of chemical or physical analysis employed.

Some of the theoretical developments of lumping are listed[1-25] in Table 1. Aris and Gavalas[1] and Aris[2,3] performed some of the earliest theoretical work describing the nature of lumped systems. They found that when all reactions are first-order, the initial distributions of components can determine the functional form of the rate expression. In a comprehensive treatment, Wei and Kuo[4,5] have established criteria for lumping species together so as to preserve the important characteristics of the monomolecular reaction system. They have also shown the error involved in lumping systems which are not exactly lumpable in terms of overall system behavior. In an extension of this work, Ozawa[11] has established criteria on which species should be lumped in the absence of complete information on the system rate constants for a monomolecular system.

Recently, the lumping of nonlinear kinetics in a continuous mixture has been actively studied. Nonlinear lumping techniques have been used successfully to predict yields from various processes such as fluid catalytic cracking,[26-33] hydrocracking,[34-37] and coal conversion,[38-44] etc. A major disadvantage to this approach is that a change in product specifications or in the number of lumping products require reformulating the model and refitting the data.

MODEL DESCRIPTION

One of the key problems in describing the kinetics of complex systems is how to lump the many components so that the resultant lumped kinetics describe the system behavior adequately. There is no a priori method for defining the lumps of complex systems. As a matter of practicality, most industrial systems

Table 1

Theoretical Developments in Lumping

Main Contents	Reference
Foundations for the stoichiometry, thermodynamics, and kinetics in continuous mixtures and outlining several techniques for solving the resulting integro-differential equations	Aris (1965)[2] Aris and Gavalas (1966)[1] Aris (1968)[3]
A lumping analysis of the exact and approximate comparable monomolecular reaction system with numerical examples illustrating the lumpability concept	Wei and Kuo (1969)[4] Kuo and Wei (1969)[5]
Methods of exact and approximate lumping for mixtures in which many parallel first-order irreversible reactions are occurring	Hutchinson and Luss (1970)[6]
A priori estimates of the sensitivity and uncertainty involved in lumped rate expressions of many parallel n^{th} order reactions	Luss and Hutchinson (1971)[7]
A priori prediction of the conditions under which a unique steady state solution exists for chemically reacting systems	Luss (1971)[8]
Validation of lumped kinetic models for reaction mixtures containing a continuum of components in both reversible and irreversible reactions	Bailey (1972)[9]
Temperature effect on the reaction rate of grouped species on parallel n^{th} order irreversible reactions	Golikeri and Luss (1972)[10]
Method of finding a lumping matrix experimentally and geometrical configuration of the eigenvectors of a lumpable monomolecular system	Ozawa (1973)[11]
Observer theory approach for the lumping analysis of the general monomolecular reaction systems with constant or time-dependent rate coefficient in discrete and continuous mixtures	Liu and Lapidus (1973)[12]
Investigation of the behavior of a mixture with many coupled irreversible consecutive first-order reactions	Golikeri and Luss (1974)[13]
Different behavior with certain empirical lumped reaction rate expressions for the different reactor types	Luss and Golikeri (1975)[14]
A general purpose kinetic model for mixtures with many first-order reactions	Lee (1977)[15]

Table 1, continued

Synthesizing a kinetically consistent structure of reaction mixtures of irreversible first-order reactions without knowing the initial lumps	Lee (1978)[16]
Exact lumping of a mono- or/and bimolecular system	Li (1984)[17]
Apparent second-order kinetics	Ho and Aris (1987)[18]
A systems-mathematics approach to chemical-kinetic lumping analysis and addition of cluster analysis to provide a basis for analyzing large empirical data sets	Coxson and Bischoff (1987a)[19] (1987b)[20]
Lumping of the kinetics of mixtures described by a continuous distribution function of concentration in nonlinear reactions	Astarita and Ocone (1988)[21] Astarita (1989)[22]
Kinetic lumping for continuous reaction mixtures in nonlinear reactions by introduction of a reactant-type distribution function	Chou and Ho (1988)[23]
Lumping coupled nonlinear reactions of a Langmuir-Hinshelwood type and a bimolecular type in continuous mixtures	Chou and Ho (1989)[24]
Generalization of nonlinear reactions in continuous mixtures	Aris (1989)[25]

are strongly constrained to lumping those species which can be readily identified and used. There is also a strong incentive to lump species in terms of those that are the final products of the process. Another important consideration is that the lumping should be correlative with accurate relations between easily accessible effluent properties and the operating variables. When a certain property is used for grouping the species into pseudocomponents, the reliability of the derived kinetic model depends on the correlation between that property and the kinetics of the individual components.

Process Variables and Reaction Order

Although extensive studies[45-48] have been carried out on the hydropyrolysis of Utah tar sand bitumen, most have dealt with the product distribution,[49] chemical and physical properties of the reaction products,[50] and the development of new hydropyrolysis processes.[51] The kinetics for complex mixtures have received much less attention. The present work was initiated to determine the kinetics of the hydropyrolysis reactions of Utah tar sand bitumen and to establish a simple reaction mechanism for these reactions in terms of lumped species.

The main process variables involved in hydropyrolysis are temperature, hydrogen partial pressure, residence time, gas-to-oil feed ratio, and oil recycle ratio. The last two variables can be correlated with residence time under an excess hydrogen environment. It is quite complicated to investigate the effects of these process variables for real complex mixtures.

McCologan and Parsons[52] investigated the effects of hydrogen pressure on product yields. The hydrogen pressure effects are largely complete by 1000 psi. Further increase in pressure has little effect on product composition and properties. Previous studies[45-47] at the University of Utah show that the pressure has little effect on the product yield (max. 4% increase in liquid yield in the range of 1200-2200 psi hydrogen pressures) without much change on product quality. Therefore, the effect of residence time and temperature on product yield are considered the more important process variables for study in this work.

Hydrocracking of hydrocarbons is first-order with respect to the hydrocarbon molecule in most of the published kinetics studies.[53-59] The hydropyrolysis reactions of heavy oils and their fractions are assumed to be pseudo first order with respect to the concentration of hydrogen due to the high hydrogen partial pressures used. Similar conclusions were reached by Qader and Hill[53-57] based on the magnitude of the activation energies for the hydrocracking reactions of coal liquids. This result is not surprising, since hydrogen is present in such large excess and its concentration changes negligibly during the reaction. Another explanation for the first-order reaction is that rapid attainment of equilibrium between the gas and liquid phase[60] keeps the hydrogen concentration constant in the liquid phase. The rate of hydrogen transfer across the gas-liquid interface was also found to be negligible in the hydrogenation of coal.[60]

Lumping and Model Formulation

It has previously been reported[45,47-49] that at high hydrogen partial pressures production of coke is virtually eliminated. Bunger[61,62] speculated that the coke forming reactions are inhibited first by the simple dilution of the aromatics through vaporization in hydrogen. Second, aromatic free radicals are terminated through metathesis reactions, first mentioned by Shabtai et al.,[45] with molecular hydrogen ($Ar\bullet + H_2 = ArH + H\bullet$). Thus, this inhibits the aromatics transformation into coke-like substances because aromatic free radicals represent the principal precursors to coke formation, at least in the temperature regime of less than 600 °C.[63] Third, the concentration of vinyl arenes (styrene-types) is reduced through attack on the vinylic bond by hydrogen, rendering the species unreactive to diene-type reactions. Fourth, hydrogen atoms add to aromatic rings (preferentially polycondensed aromatics) to hydrogenate aromatics and reverse the growth of aromatics.[62] This coke inhibition was also reported[64] by others working in the area of thermal hydrocracking of heavy oils. Hence, coke is not included as a lump in this work.

The primary objective of hydropyrolysis is molecular weight reduction. Molecular weight is the single most important factor that determines the physical and thermodynamic properties of heavy oils; boiling point is a sensitive indicator of molecular weight. Therefore, the feed and product streams are assumed to contain a continuum of compounds that can be characterized solely by boiling point and density.

Simulated distillation,[65] a gas chromatographic method for obtaining boiling point distribution, has been applied to a Wilmington crude oil. Simulated distillation allows results to be obtained up to a nominal boiling point of 538 °C without the danger of thermal decomposition associated with actual distillation of high boiling petroleum fractions. Detailed information in simulated distillation of bitumens has been previously reported.[66] Good agreement between true boiling point (tbp) distillation and simulated distillation values for Wilmington crude oil (which is used for this work) was reported.[67] Also, simulated distillation and chromatographic separation data[68] indicate that, in general, the tar sand bitumens most closely resemble Wilmington petroleum with respect to hydrocarbon/non-hydrocarbon distribution, especially in the nondistilling portion (the distilling portion, mainly hydrocarbons, are similar for all samples in the referenced studies). Therefore, the experimental results of hydropyrolysis of Wilmington crude distillate (<320 °C b.p.)[48] and whole Wilmington crude[69] can be used to estimate the kinetics of the hydropyrolysis reactions of Utah tar sand bitumens.

The complex mixture is separated into specified boiling ranges to provide individual products of commercial importance such as residual (R), total gas oil (T), middle distillate (M), and gases (G). The four lumped components, R, T, M, and G, are used for representing the overall kinetics by considering that the molecular weight of hydrocarbon compounds has a strong relation to their boiling points. The kinetics also recognizes that in hydropyrolysis material of high molecular weight cracks to lower molecular weight and that retrogressive reactions (e.g., polymerization, condensation, etc.) are almost totally inhibited.

R is the weight fraction of residue boiling at 1 atm above 538 °C; T is the weight fraction of total gas oil boiling at 1 atm from 275 up to as high as 538

°C; M is the weight fraction of middle distillate boiling at 1 atm up to 275 °C (C_5-275 °C); and G represents the weight fraction of gases (C_4-, dry gas). The reaction can be represented by the scheme:

$$A_i + H_2 \xrightarrow{k_i} products \qquad (i=1,2,3,\ldots,n) \tag{1}$$

and the rate equation by:

$$\frac{d[A_i]}{dt} = -k_i [A_i]^1 [H]^0 \tag{2}$$

where n is the number of lumped species, $[A_i]$ and [H] represent concentration of the *ith* lump and hydrogen, respectively, and k_i is the apparent rate constant (1/time).

Possible reactions involving these four lumps are:

$$\begin{array}{cccc} \overset{1}{R \longrightarrow T} & \overset{4}{T \longrightarrow R} & \overset{7}{M \longrightarrow R} & \overset{10}{G \longrightarrow R} \\ \overset{2}{R \longrightarrow M} & \overset{5}{T \longrightarrow M} & \overset{8}{M \longrightarrow T} & \overset{11}{G \longrightarrow T} \\ \overset{3}{R \longrightarrow G} & \overset{6}{T \longrightarrow G} & \overset{9}{M \longrightarrow G} & \overset{12}{G \longrightarrow M} \end{array} \tag{3}$$

Based on the experimental results,[45-49,68] important reactions are identified for use in the model. Since M and G are considered to be final products, reactions 7, 8, 10, 11, and 12 can be eliminated. Reactions 2 and 3 are eliminated from the reaction scheme because the formation of M and G is considered to be a secondary reaction in the hydropyrolysis of residues. Also, experimental results suggest that residue formation is most unlikely to occur because of continuous decrease in its concentration. This reaction step (reaction 4) is therefore eliminated. The final form of the reaction model is described by the following:

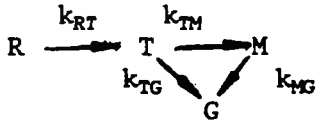

(4)

The apparent rate constants calculated from the model are:

k_{RT} = rate constant for total gas oil formation;
k_{TM} = rate constant for total gas oil cracking to middle distillate;
k_{TG} = rate constant for total gas oil cracking to gas;
k_T = overall rate constant for total gas oil cracking = $k_{TM} + k_{TG}$;
k_1 = k_{TM}/k_T = selectivity ratio for middle distillate formation; and

k_{MG} = rate constant for middle distillate cracking to gas.

In normal kinetic practice with well-defined chemical species, reaction rates are expressed in terms of molar concentrations. However, the convention that is commonly adopted for lumped kinetics is to express the reaction rates in terms of mass fractions. Therefore, the kinetic rate equations for these pseudo-first-order irreversible reactions may be written as follows:

$$\frac{dR}{dt} = -k_{RT}R \tag{5}$$

$$\frac{dT}{dt} = k_{RT}R - (k_{TM} + k_{TG})\,T \tag{6}$$

$$\frac{dM}{dt} = k_{TM}T - k_{MG}M \tag{7}$$

$$\frac{dG}{dt} = k_{TG}T + k_{MG}M \tag{8}$$

where t is the residence time which is measured by the reactor volume divided by the volumetric flow rate at reaction conditions.

DATA FITTING AND INTERPRETATION

Sets of data at four residence times and reaction temperatures are shown in Figure 1 for hydropyrolysis of Wilmington crude[48,69] in once-through operation (H_2 pressure, 1800 psig; liquid hourly space velocity [LHSV] = 3.1/hr). These plots represent the change of concentration of each lump with respect to residence time at 758, 783, 808, and 833 K. The concentration of each lump at zero time was taken to be equal to the concentration in the original feedstock. It can be seen that:

1. The concentrations of lighter lumps (middle distillate and gas) increased continuously with time for experimental temperature ranges.

2. The concentrations of heavier lumps (residue and gas oil) decreased continuously with time and the rate of decrease was greater at the beginning of the reaction. These concentrations decreased more rapidly with increasing temperature. In general, temperature affects the yield of each lump more than does residence time over the experimental ranges.

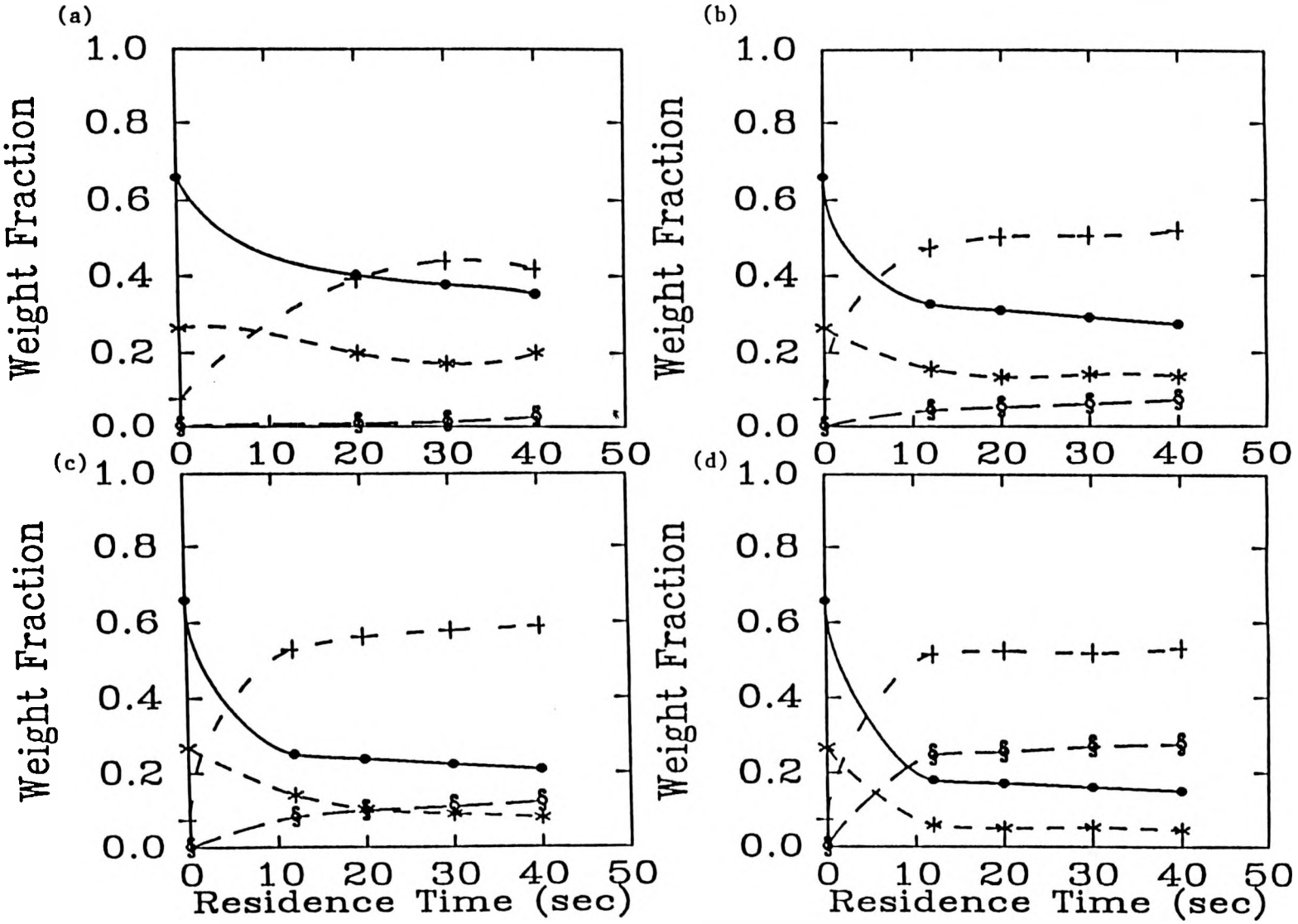

Figure 1. Product Yield of Hydropyrolysis of Wilmington$_1$ Crude. H_2 pressure = 1800 psig; Liquid Hourly Space Velocity (LHSV) = 3.1 hr^{-1}. Reaction Temperature: (a) 485°C; (b) 510°C; (c) 535°C; (d) 560°C. Symbols used: • - Residue (R); * - Total Gas Oil (T); + - Middle Distillate (M); § - Gas (G)

3. The concentration of middle distillate above 808 K reached a maximum, after which a decline in concentration occurred. This behavior suggests that at higher temperatures cracking of middle distillates to gas becomes predominant over the production of middle distillate from total gas oil according to the reaction scheme.

The kinetic parameters of the rate constants in a simultaneous reaction system were first obtained to give the best fit to all the experimental results, simultaneously by the numerical Simplex method as listed in Appendix A. Then these values were used as initial guesses to recalculate the individual apparent kinetic rate constants more accurately by using the Simusolv, the modeling and simulation software developed by Dow Chemical Co.[70,71] The program file and run-time command file are listed in Appendix B. In Simusolv, the equations are solved by numerical integration techniques and the Log Likelihood Function (LLF) is used as a criterion for judging whether a set of parameter values or a model was the best one.[72] LLF is defined as follows:

$$LLF = \log(LF) = -n \log(\sigma\sqrt{2\pi}) - \sum_{i=1}^{n} \frac{(y_i - y)^2}{2\sigma^2} \qquad (9)$$

where n is the total number of measurements, σ is the true standard deviation of the measurements, y_i is the value obtained for the *ith* measurement, and y is the measured value.

The parameter estimation and the Arrhenius expressions obtained by using the Simusolv are shown in Tables 2 and 3, respectively. The plot of apparent rate constants vs. reciprocal temperature shown in Figure 2 indicates no obvious deviation from linearity. Figure 3 shows the relationship between the experimental values and the values calculated using the equations in the preceding section with the kinetic parameters in Table 3 and gives 14.4% AAD, which is defined by:

$$\%AAD = \frac{1}{n} \sum_{i=1}^{n} \left| \frac{y_{e,i} - y_{c,i}}{y_{e,i}} \right| x\ 100 \qquad (10)$$

where $y_{e,i}$ is the experimental value, $y_{c,i}$ is the predicted value, and i is a component ($1 \leq i \leq N$). Also, a linear least-squares fit to these data gives the correlation of determination (R^2 value) of 0.884. The value of R^2, the ratio of the sum of squares of the model to that of the data, is a relative indicator of the fit of the model to the data.

Table 2
Rate Constants[a] and Their Standard Deviation

Temperature, °C (K)	485 (758)	510 (783)	535 (808)	560 (883)
k_{RT}	0.0183 ± 0.002	0.0272 ± 0.004	0.0362 ± 0.005	0.0620 ± 0.011
k_{TM}	0.0497 ± 0.006	0.0894 ± 0.015	0.1187 ± 0.016	0.2297 ± 0.071
k_{TG}	0.0018 ± 0.002	0.0128 ± 0.004	0.0263 ± 0.007	0.1260 ± 0.043
k_T	0.0515 ± 0.006	0.1022 ± 0.015	0.1450 ± 0.017	0.3557 ± 0.083
k_1	0.9651 ± 0.167	0.8748 ± 0.223	0.8186 ± 0.178	0.6458 ± 0.387
k_{MG}	9.95×10^{-5} ± 0.002	1.24×10^{-4} ± 0.001	4.93×10^{-4} ± 0.0001	8.0×10^{-4} ± 0.005
LLF	53.913	53.332	53.828	50.847

[a]All constants in sec^{-1}.

Table 3
Arrhenius Constant and Activation Energy

Rate Constants	Activation Energy (Kcal/mol)	Frequency Factor (1/sec)	Coefficient of Determination
k_{RT}	19.68 ± 2.0	8.42×10^{3}	0.9778
k_{TM}	24.37 ± 2.7	5.29×10^{5}	0.9766
k_{TG}	67.16 ± 7.6	4.91×10^{16}	0.9751
k_{MG}	38.13 ± 7.8	8.09×10^{6}	0.9229

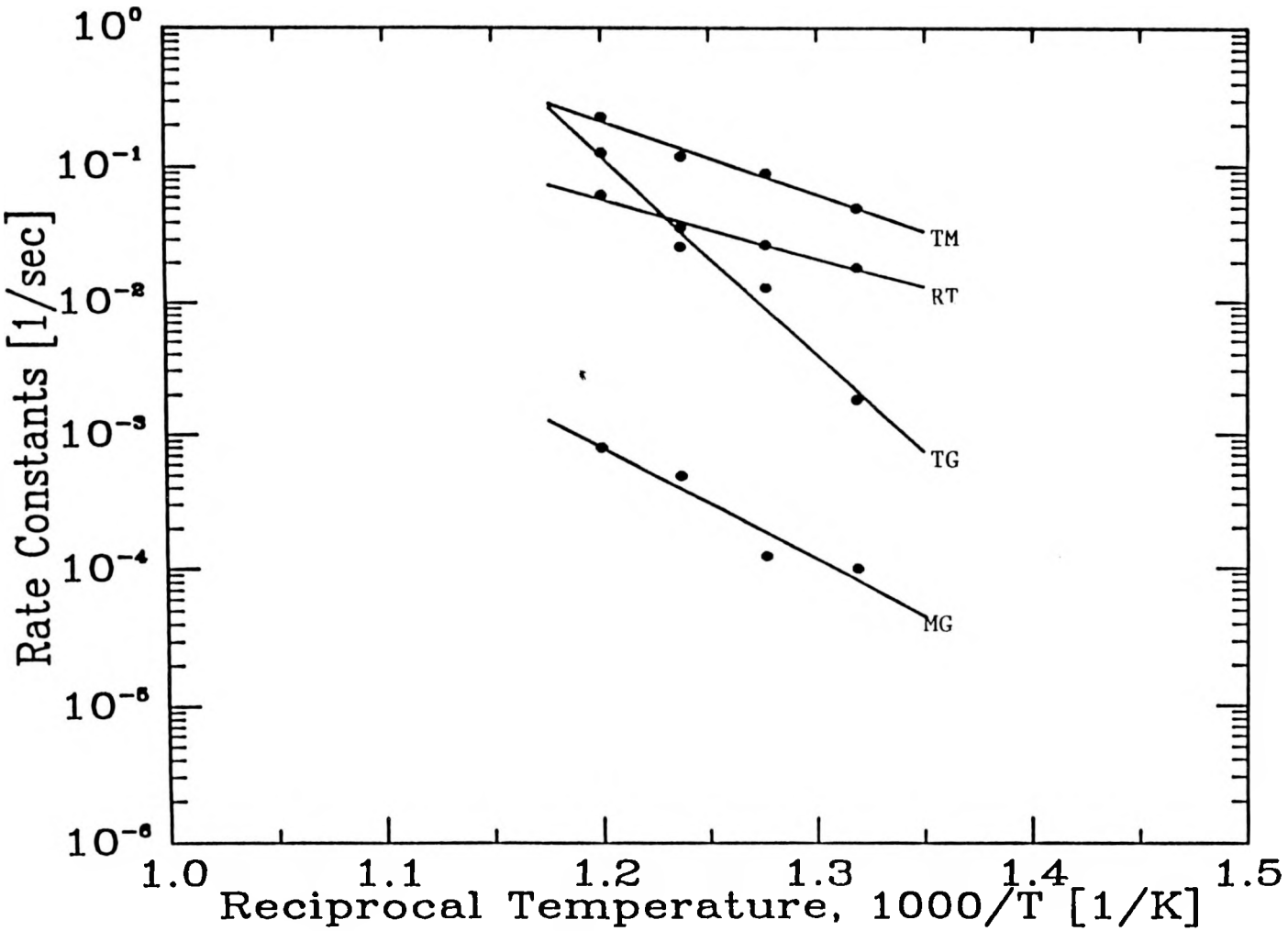

Figure 2. Arrhenius Plot for Hydropyrolysis of Wilmington Crude. (a) Rate constant for total gas oil cracking to middle distillate (k_{TM}); (b) Rate constant for total gas oil formation (k_{RT}); (c) Rate constant for total gas oil cracking to gas (k_{TG}); (d) Rate constant for middle distillate cracking to gas (k_{MG})

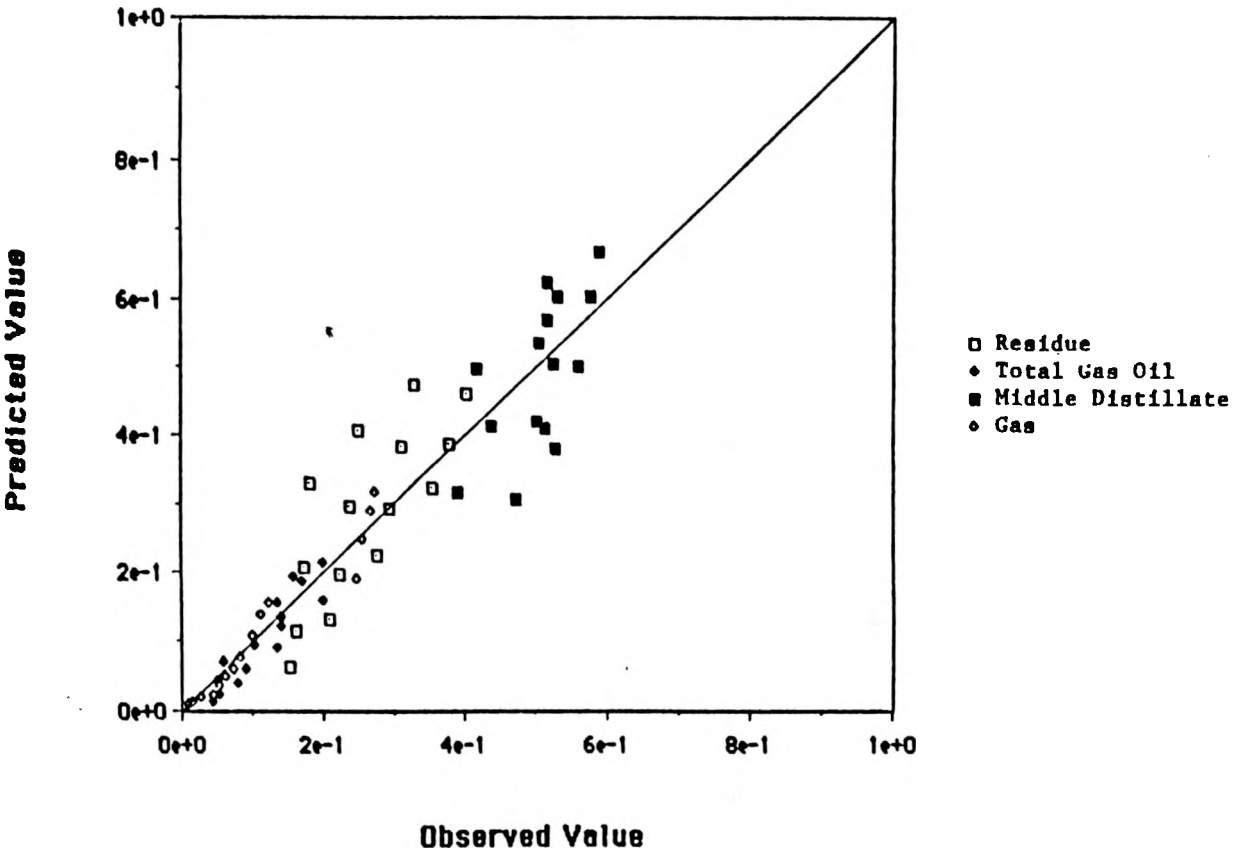

Figure 3. Parity Plot of Predicted Yield Versus Measured Yield of Lumping Species of Hydropyrolysis of Wilmington Crude

As can be seen, a good fit and minimal biases were found by this relatively simple reaction scheme. Therefore, the concentration change behavior of each lump for hydropyrolysis of Utah tar sand bitumen (e.g., TS-IIC bitumen from a N.W. Asphalt Ridge Utah site, produced by the Laramie Energy Technology Center)[48,49] can be predicted with reasonable accuracy as shown in Figure 4, where each lump yield is plotted as a function of residence time at different reaction temperatures, 475-575 °C, of commercial interest.

Although this four-lump model gives a reasonable description of current experimental results, further studies would be valuable to improve the accuracy and generality of the lumped kinetic model through theoretical development and its experimental configurations.

The concept of reaction severity index arises naturally in the model. Noting the apparent relation between residence time and temperature (i.e., long residence times at lower temperatures produce yields equivalent to short residence times at higher temperatures in many cases), the concept of reaction severity of those variables appeared to be a potentially useful parameter. Also, the gas lump can be considered as a good indicator of reaction severity among lumps. Therefore severity, a combination of residence time and temperature, is arbitrarily defined as the sum of the residence time (sec) multiplied by a coefficient plus a term T - 430 where T is the temperature of reaction and 430 is the temperature at which the onset of hydropyrolysis becomes apparent.

To examine the sensitivity of the fit to the way severity is defined, a number of fits to the data were made multiplying the residence time (sec) by a variety of coefficients from 0 to 1.0. The best result (R^2 = 0.721) was found for a coefficient of 0.31. Thus, S = 0.31(t) + (T - 430°C). This reaction severity index shows fairly good linear relationship with gas yield up to 535°C (R^2 = 0.9691), but starts to deviate at higher temperatures due to large amounts of gas production. Figure 5 shows this linear least-squares fit of the gas yield as a function of severity index. The gas yield distinctly increases at a severity level > 125, indicating that the operations above 555 °C are not desirable due to high hydrogen consumption. Hydrogen consumption is directly related to the noncondensable gas production.[46,49,69] Severity would appear to be a useful parameter, if good correlations between severity and processing variables are provided. The severity index may then be correlated with process yields, reducing the number of variables to consider in reaction modelling.

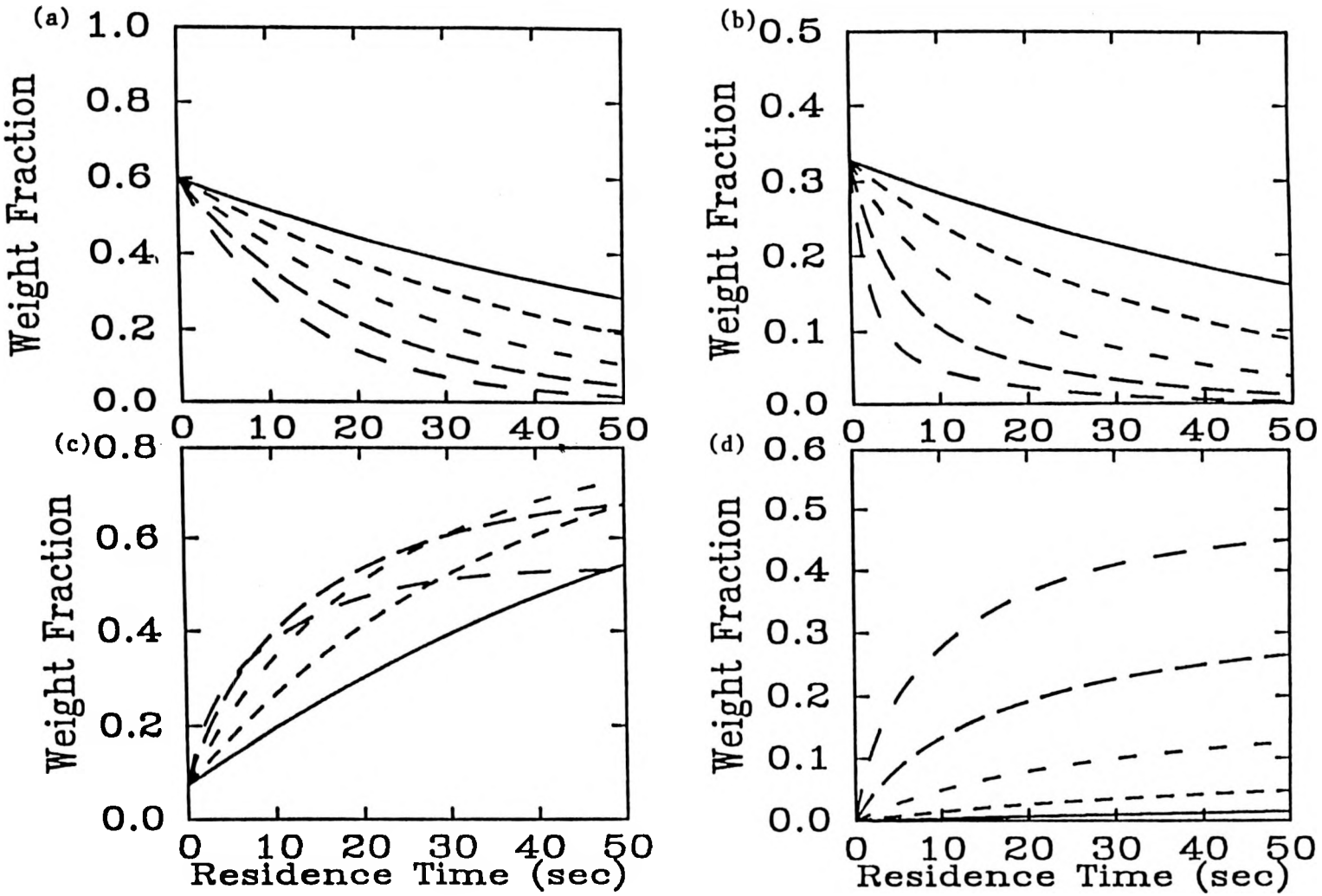

Figure 4. Concentration Change of Each Lump for Hydropyrolysis of Tar Sand Bitumen. (a) Residue; (b) Total gas oil; (c) Middle distillate; (d) Gas. Increasing temperature symbolized by escalating size and spacing of dashes: 475, 500, 525, 550 and 575 °C.

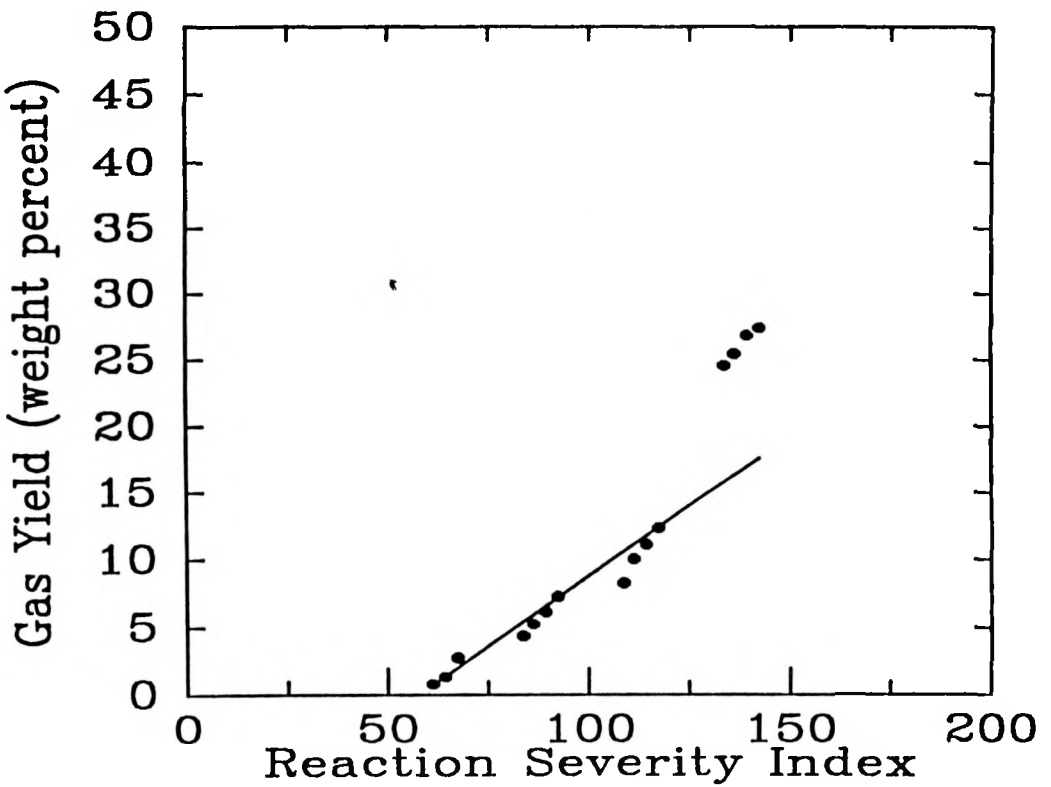

Figure 5. Relationship Between Gas Yield and Reaction Severity Index

FLUIDIZED-BED PYROLYSIS OF BITUMEN-IMPREGNATED SANDSTONE

Francis V. Hanson	Co-Principal Investigator
Soon-Man Cha	Graduate Student
Liang Ching Lin	Postdoctoral Fellow
Dowon Shun	Graduate Student
Seung-Hyun Sung	Graduate Student

SMALL-DIAMETER FLUIDIZED-BED REACTOR STUDIES

The small-diameter fluidized-bed tar sand pyrolysis reactor studies focused on the analysis of the Circle Cliffs mineral matter to determine its influence on the product distribution. This report summarizes the analysis performed on the Circle Cliffs mineral matter to date.

X-Ray Diffraction

The X-ray diffraction pattern indicated that the major constituents of the Circle Cliffs tar sand mineral matter were α-quartz (SiO_2), potassium feldspar ($KalSi_3O_8$), and kaolinite ($Al_2Si_2O_5(OH)_4$). The mineral constituents of the host rock for several Utah tar sands are presented in Table 4.

Table 4
Mineral Analysis of Selected Utah Tar Sand

Origin	Circle Cliffs	P.R. Spring Rainbow I	Whiterocks
Compounds	SiO_2	SiO_2	SiO_2
	$KalSi_3O_8$	$KalSi_3O_8$	$KalSi_3O_8$
	$Al_3Si_2O_5(OH)_4$		$NaAlSi_3O_8$

The basic difference in the constituents of the Circle Cliffs tar sand host rock relative to that of the other Utah tar sands--P.R. Spring Rainbow I and Whiterocks--was the presence of kaolinite.

The connate water content determined by the Karl Fisher titration method was only 0.3%. Like other Utah tar sands, Circle Cliffs tar sand was also moisture free. However, considerably more water was produced along with the bitumen-derived liquid product during pyrolysis in the fluidized-bed reactor. This could be explained as water bonded to kaolinite which is released with the bitumen-derived hydrocarbon vapor at the pyrolysis temperature, which was about 773 K. The release of bonded water was determined by heating bitumen-free mineral matter in a muffle furnace at specified temperatures for periods of 15 hours. The weight loss due to dehydroxylation occurred in the range of 725 K to 825 K. The decomposition of mineral carbonates occurred in the range of 873 - 1073 K. The release of bonded water and the decomposition of mineral carbonates overlap slightly in the range 823 - 873 K, which will be explained in the thermogravimetric analysis section. The water release data obtained in the muffle furnace experiments are presented in Table 5.

Table 5
Muffle Furnace Heating of Bitumen-Free Circle Cliffs Mineral Matter

Temperature, K	Weight Loss, wt %
673	0.004
723	1.01
773	2.38
823	3.21

Photomicrographs

The bitumen-impregnated sandstones of the Circle Cliffs are consolidated; that is, the sand grains form a continuous matrix bound together by calcareous cement. The electron photomicrographs of the bitumen-free mineral matter are presented in Figure 6. These figures reveal the shapes of the consolidated particles and of the voids or pores. The brighter regions in the lower figures are α-quartz particles, and the darker grains are mostly a mixture of quartz and feldspar. The kaolinite is not identifiable in the figures.

The low bitumen content (less than 4 wt%) of the Circle Cliffs tar sand results in a noncontinuous bitumen film on the sand grains and an incomplete filling of the void spaces between the sand particles. Figure 7 shows the microscope image of Circle Cliffs tar sand. The bright islands are bitumen-filled pores.

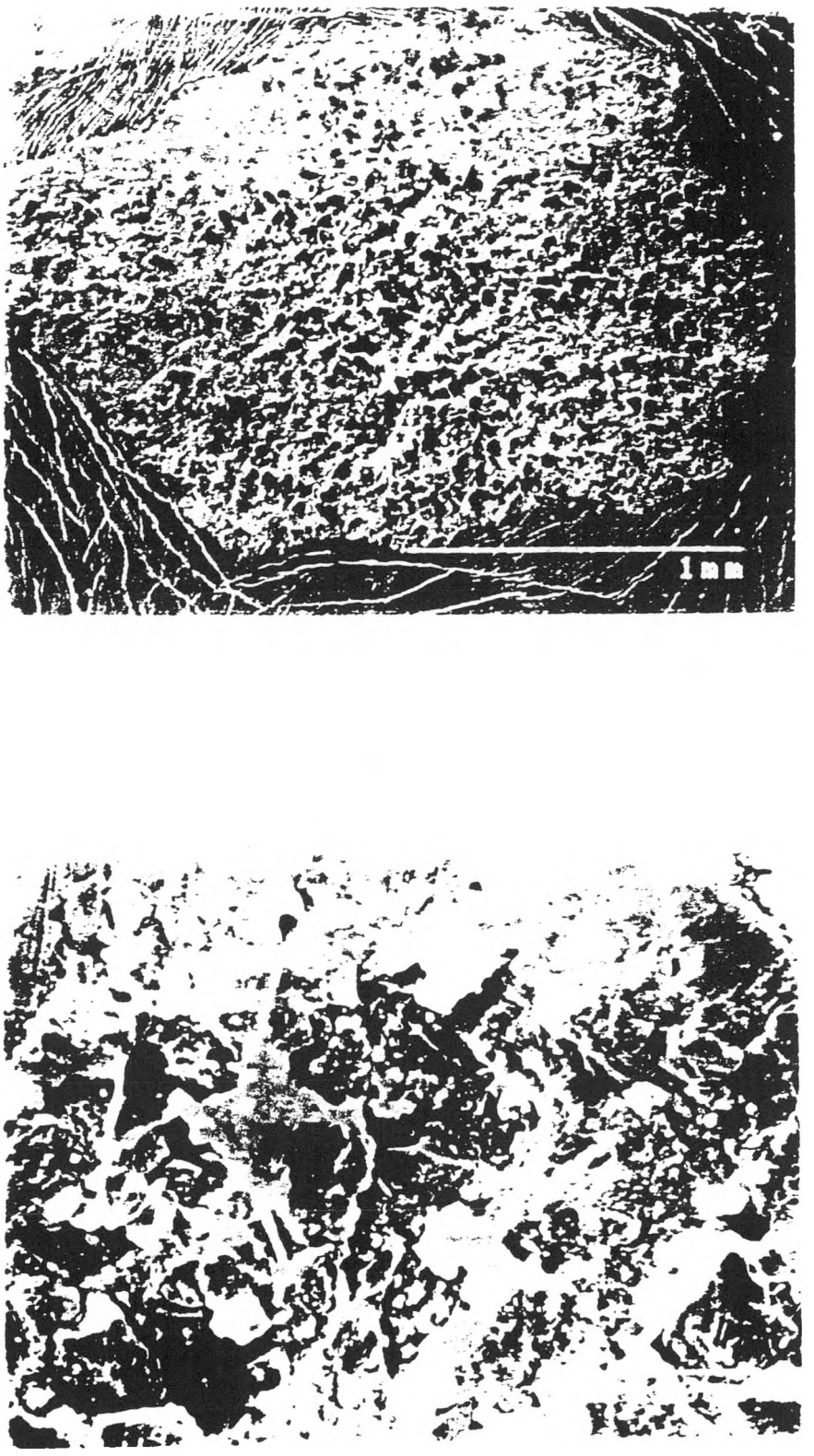

Figure 6. Electronmicrographs of the Circle Cliffs Tar Sand

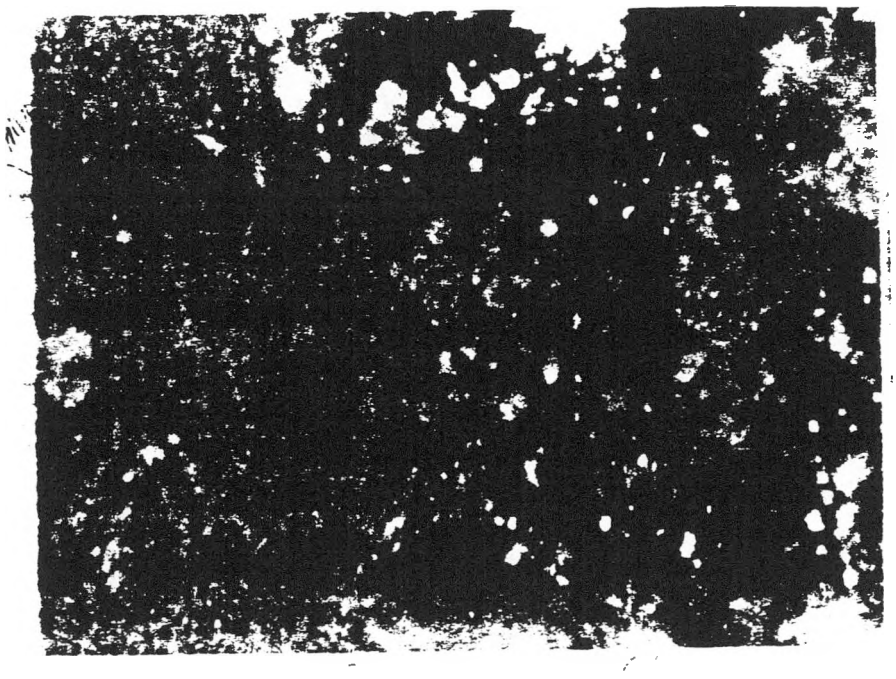

Figure 7. Micrograph of Circle Cliffs Tar Sand

Elemental Analysis of Sand Matrix

The elemental analysis of the Circle Cliffs tar sand host rock indicated that the major constituents were silicon, calcium, magnesium, aluminum, iron, and potassium. The maximum possible amount of each mineral constituent identified in the X-ray analysis and other experiments, such as thermogravimetric analysis (TGA) and differential scanning calorimetry (DSC), was computed from the elemental analysis. The results of these calculations are presented in Table 6.

Table 6
Elemental Analysis of Tar Sand Matrix
Circle Cliffs Tar Sand

Element	Weight Percent	Possible Compound	Maximum Possible Concentration, wt %
Fe	1.2	FeO, Fe_2O_3, $FeCO_3$	
Ca	8.3	$CaCO_3$	20.7
Mg	5.3	$MgCO_3$	5.3
K	0.94	$KAlSi_3O_8$	6.7
Al	3.66	$Al_2Si_5(OH)_4$	14.4

The calculations indicated that the Circle Cliffs host rock could contain as much as 14.4 wt% kaolinite, 26% mineral carbonate, and small yet significant amounts of iron oxide. If these minerals were activated at pyrolysis conditions, they could function as cracking catalysts, thus influencing the yield of the C_5^+ bitumen-derived hydrocarbon liquid. Concomitant with this decline in liquid yield, an increase in the gas make and carbonaceous residue would be expected and was observed in the pyrolysis experiments.

Infrared Spectra of Sand Matrix

Infrared spectra of bitumen-free extracted tar sand matrix indicated the presence of four distinct strong hydroxyl groups at 3689, 3666, 3649, and 3618 cm^{-1} (Figure 8). These peaks are presumed to represent four different types of hydroxyl groups on kaolinite, and it is assumed that some of these hydroxyl groups are released at the pyrolysis temperature of bitumen. An infrared spectrum of the Whiterocks tar sand host rock is presented in Figure 9 for comparison to the Circle Cliffs host rock spectrum. The Whiterocks spectrum revealed no OH peaks near the 4000 cm^{-1} region.

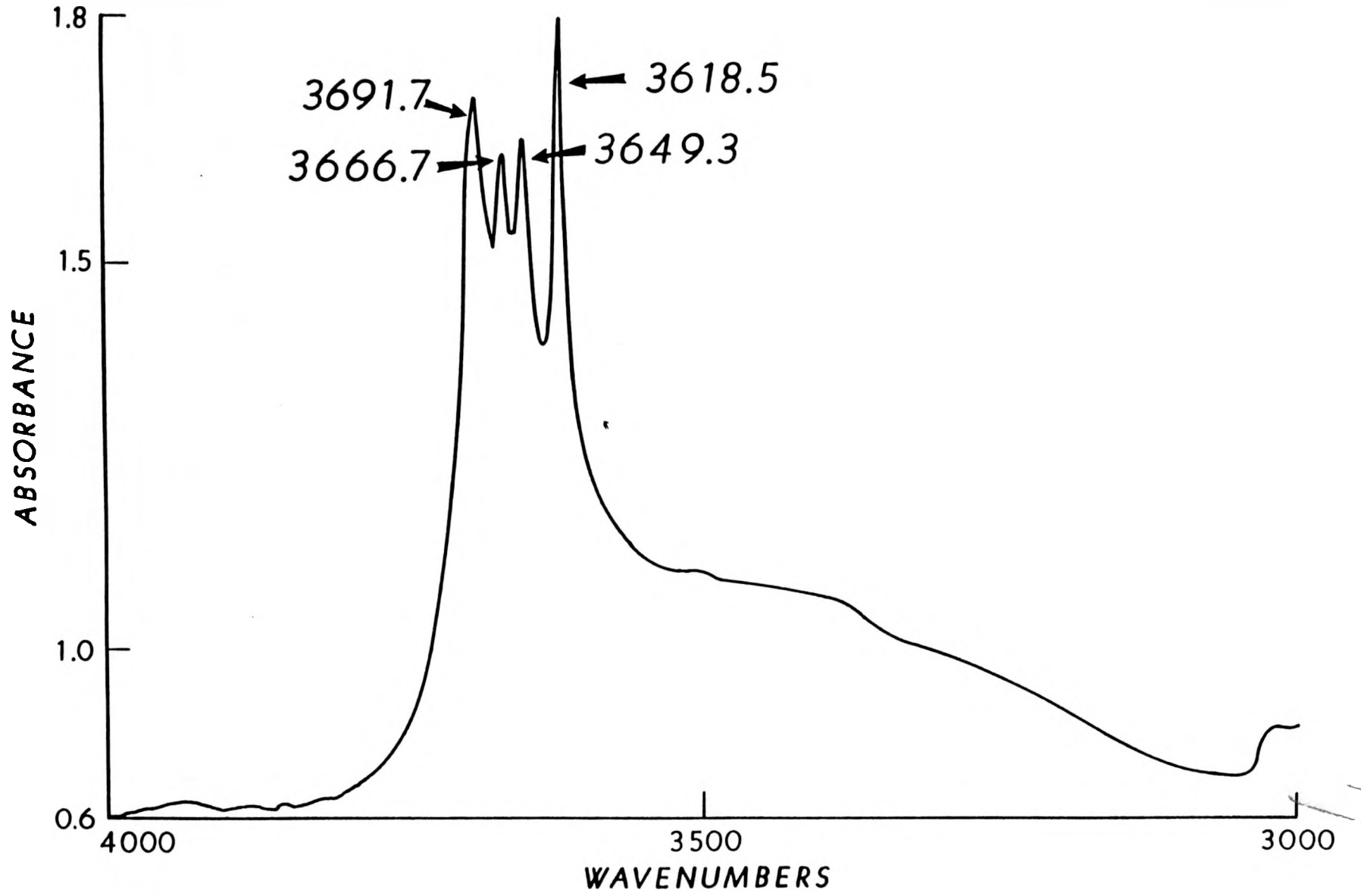

Figure 8. Infrared Spectrum of Bitumen-Free Circle Cliffs Tar Sand

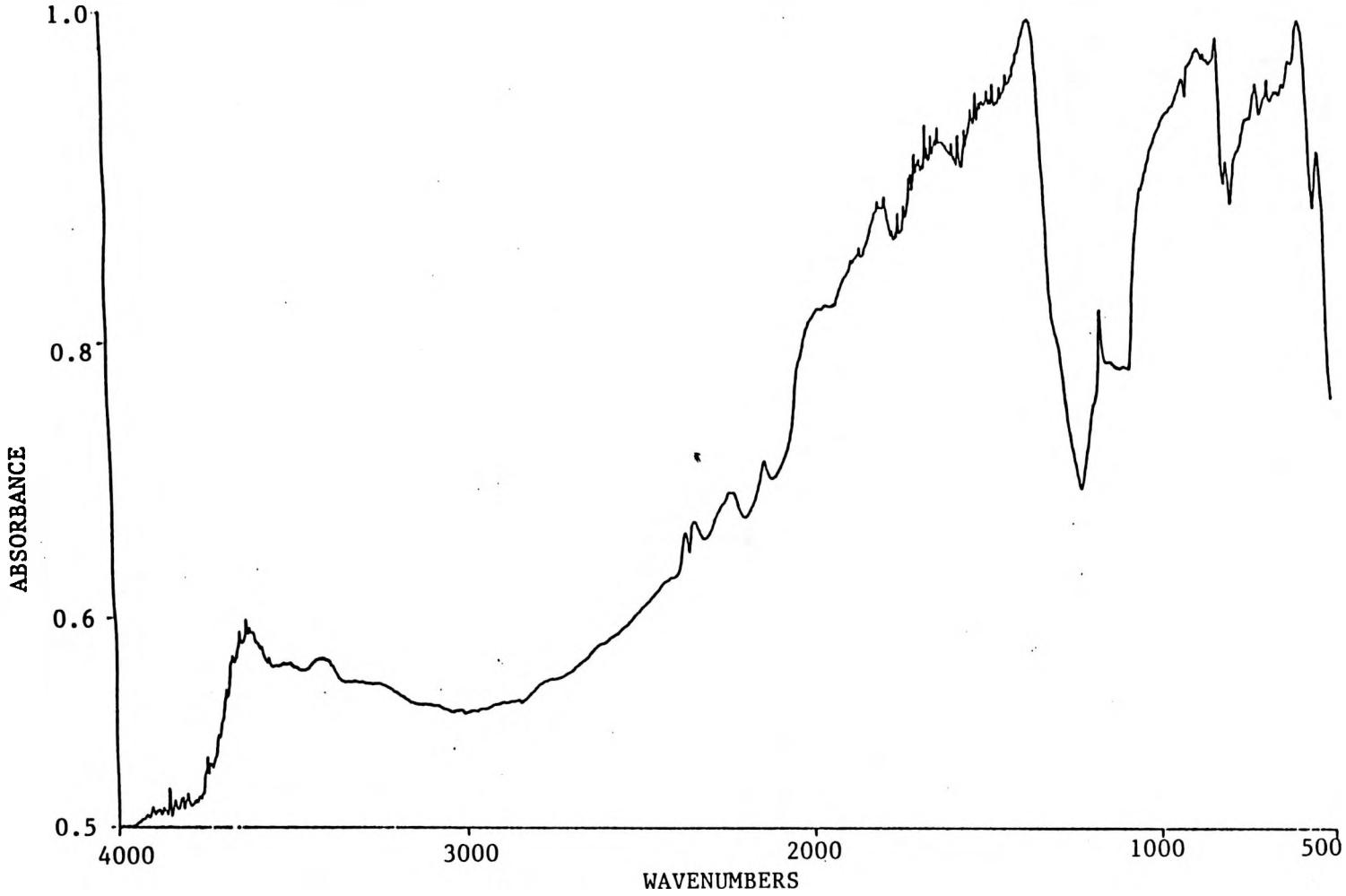

Figure 9. Infrared Spectrum of Bitumen-Free Whiterocks Tar Sand

The coked sand samples collected from several pyrolysis experiments at different pyrolysis temperatures were also analyzed. The spectrum of spent sand from the pyrolysis of the Circle Cliffs tar sand is presented in Figure 10. The intensities of the peaks were reduced; however, the positions of the peaks did not shift, indicating the decomposition of the OH groups. A comparison of peak intensities for the spent sand from the pyrolysis of the Circle Cliffs tar sand at various temperatures is presented in Figure 11. As the temperature increases from 723 to 873 K, the intensities of the peaks were reduced and eventually disappeared.

Infrared Spectra of Bitumen

Infrared spectra of the bitumen usually do not give much qualitative information because of the extreme complexity of the compounds in the bitumen, but do give general indications of the groups present in the bitumen. Fourier Transform Infrared (FTIR) spectra of toluene-extracted Circle Cliffs tar sand bitumen indicated the presence of several distinctive peaks.

Strong peaks at 2950 cm^{-1}, 2920 cm^{-1}, and 2850 cm^{-1} were indicative of carbon hydrogen stretching in both aliphatic and aromatic hydrocarbons. In the fingerprint region, 1600-1300 cm^{-1}, there are two more small peaks which are related to stretching between hydrocarbon and heteroatoms. Unlike coal, liquid bitumen has no phenolic OH bond in the 3400 cm^{-1} region. Thus, we can expect relatively stronger aging resistance than is found in coal, due to carboxylation of phenolic OH to COOH. Still, there is an oxygen-carbon (C=O) band at the 1700 cm^{-1} region, which explains the locale of 2% oxygen determined from elemental analysis (Figure 12).

Surface Area Measurement

It is presumed that two factors may determine the global rate of pyrolysis: (1) vaporization of light hydrocarbons; and (2) thermal cracking of heavy hydrocarbons on the surface of the host rock. The rate and reaction pathways of thermal pyrolysis are presumed to be affected by size and structures of the pores of host rock.

The surface area of the bitumen-free host rock from the Circle Cliffs tar sand deposit was determined by using a BET surface area apparatus with nitrogen as the adsorbing gas. Two samples were prepared for this analysis. The first was the solvent-extracted sand matrix that contained about 2% water, which was chemically bound to the kaolinite present in the mineral matter. The nitrogen adsorption-desorption isotherm is presented in Figure 13. This isotherm shows a small but definite hysteresis of the sand indicating the existence of micropores. The BET plot for this sample is presented in Figure 14. The surface area of this sample was determined to be 1.37 m^2/g. The second sample was the same solvent-extracted host rock; however, it was calcined at 773 K for 15 hours to remove water before the surface area was determined. The surface area of this sample was 0.7 m^2/g. Thus, the Circle Cliffs host rock had a surface area in the range of 1 to 2 m^2/g sand.

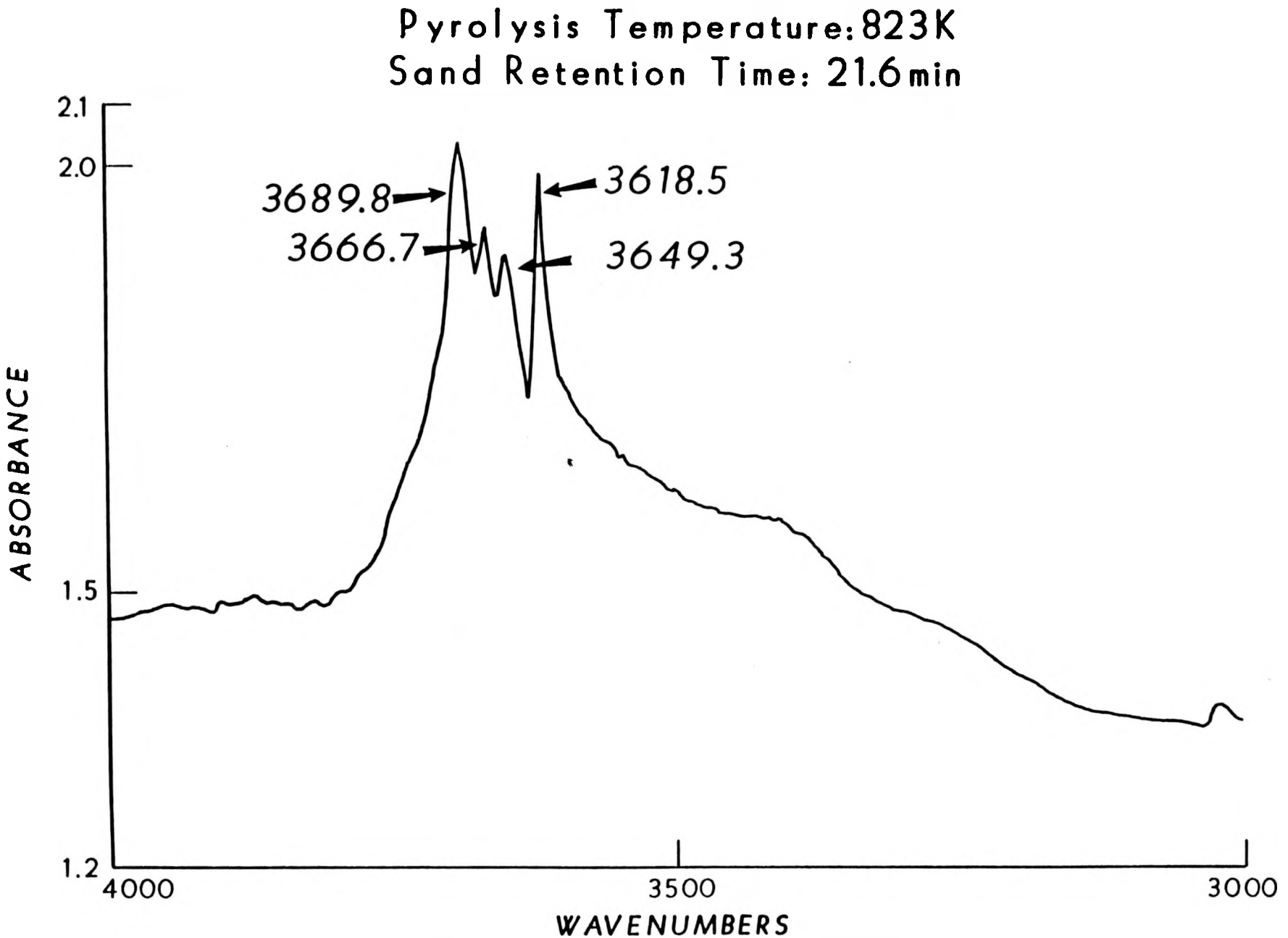

Figure 10. Infrared Spectrum of Spent Circle Cliffs Tar Sand

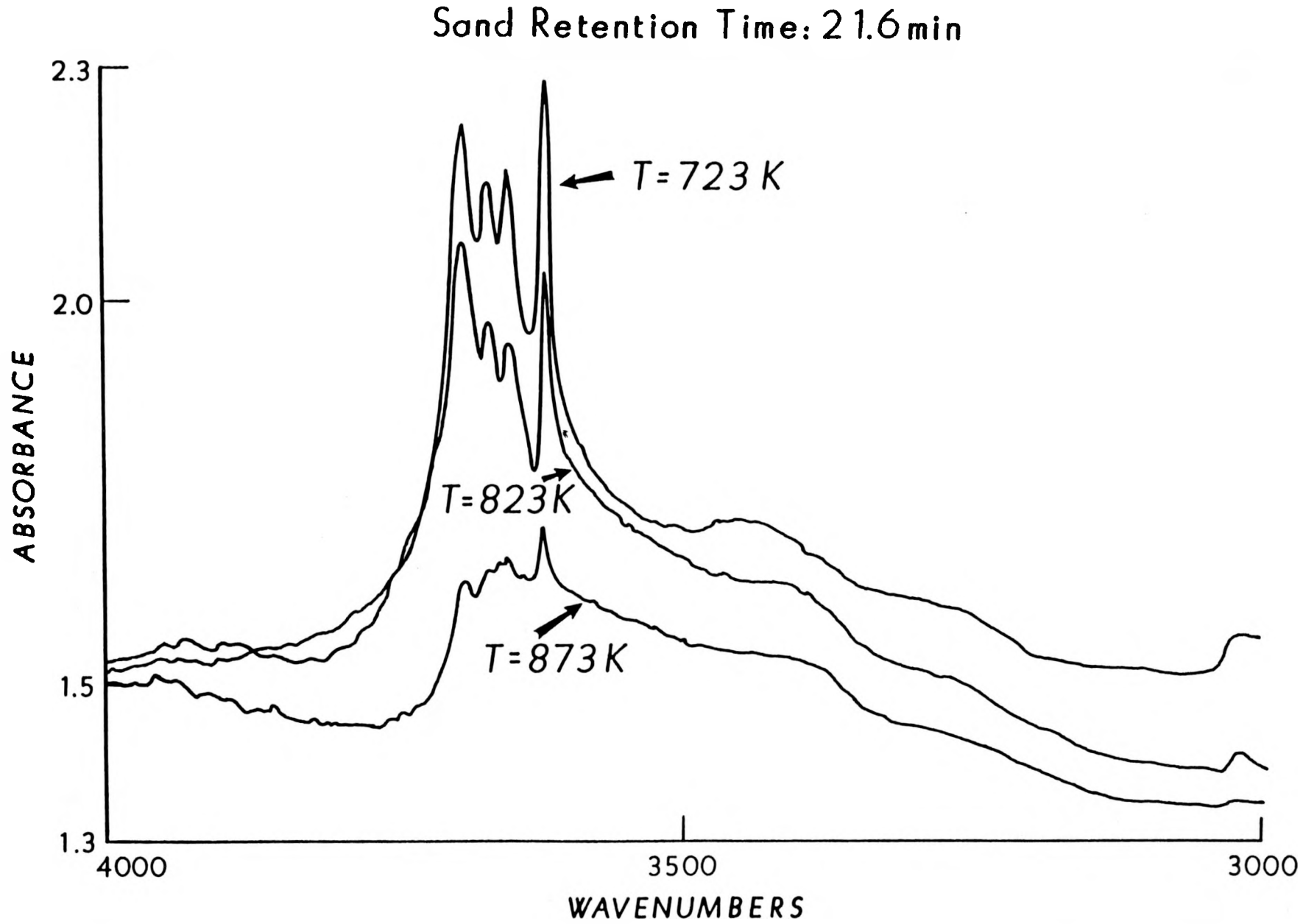

Figure 11. Infrared Spectrum of Spent Whiterocks Tar Sands

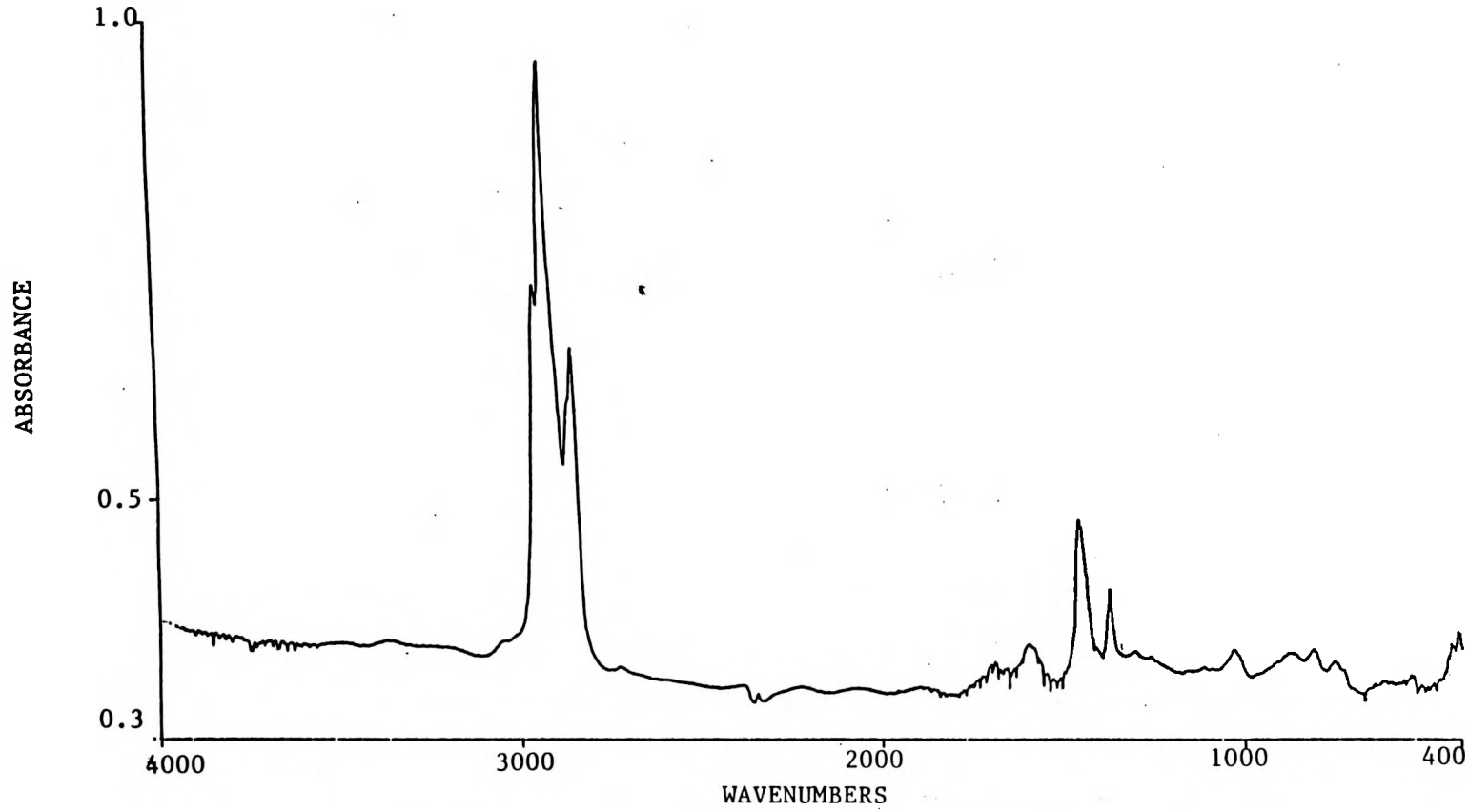

Figure 12. Infrared Spectrum of Extracted Bitumen (Circle Cliffs)

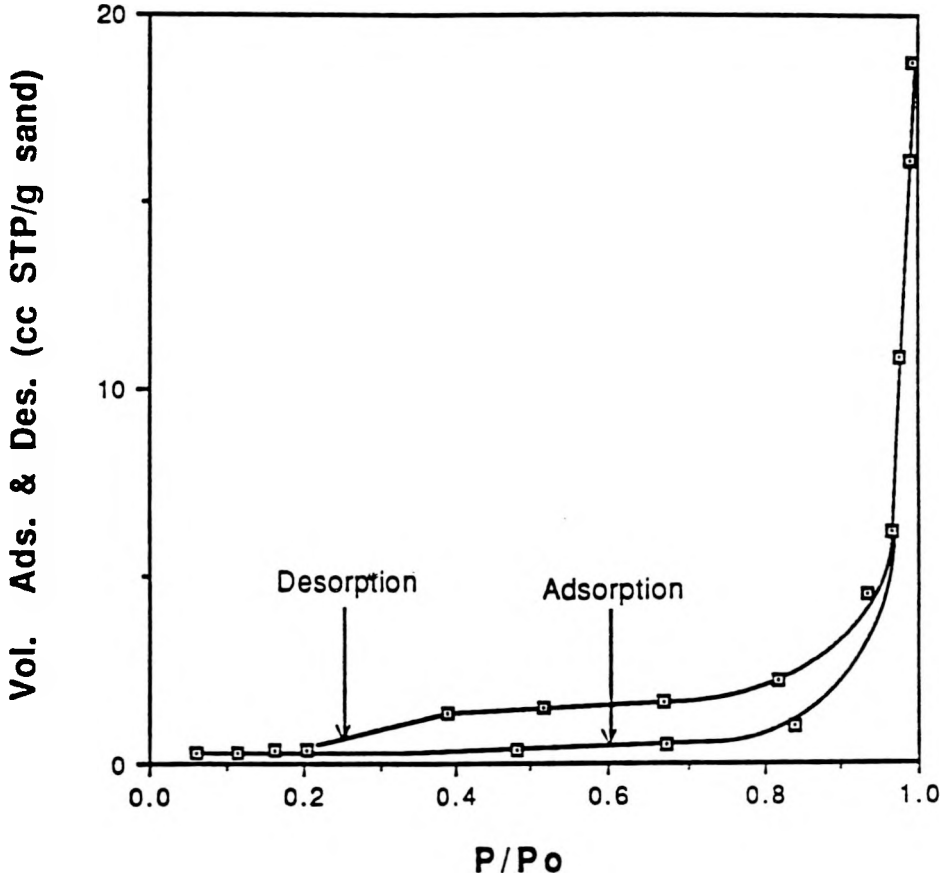

Figure 13. Adsorption/Desorption Isotherms for Nitrogen on Circle Cliffs Tar Sand Matrix

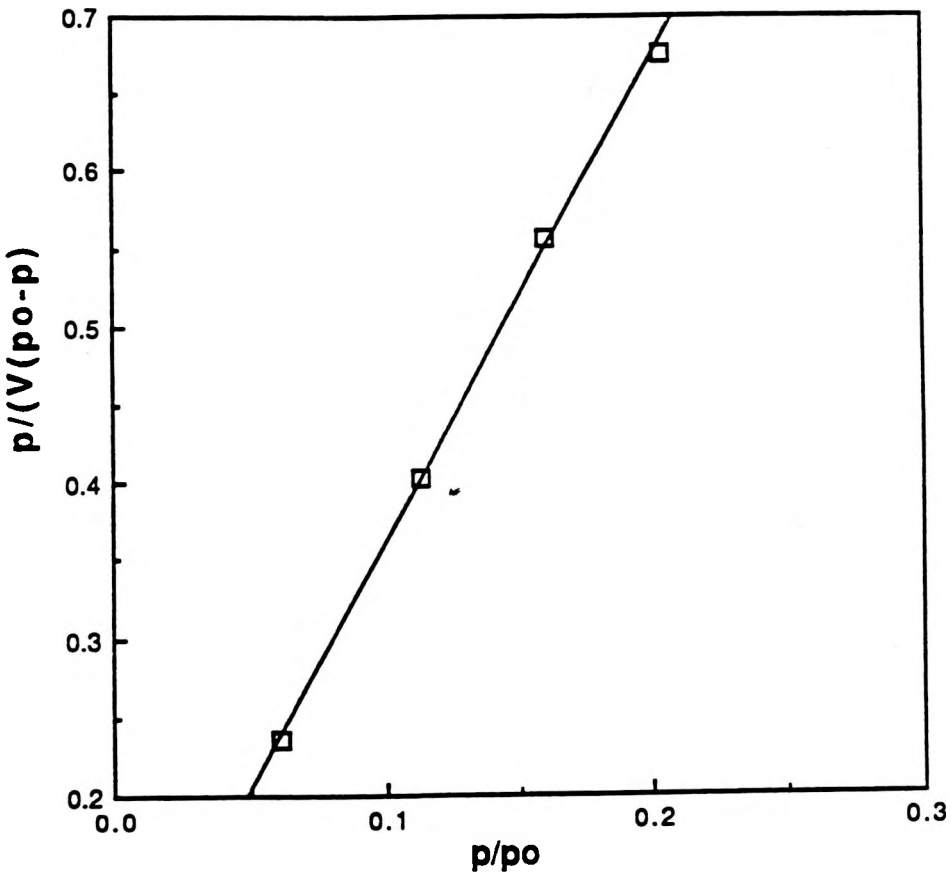

Figure 14. BET Plot of the Circle Cliffs Tar Sand Matrix

The pore volume and size distribution were determined with a mercury porosimeter. The bitumen-free Circle Cliffs host rock and the bitumen-free Whiterocks tar sand host rock were used in these experiments. The mercury porosimeter data for both host rock samples are presented in Table 7. The pore size distribution of both host rock samples are presented in Figures 15 and 16. These data indicate that the Circle Cliffs host rock had a wider micropore size distribution than the Whiterocks host rock.

Table 7
Mercury Intrusion Data

Origin	Circle Cliffs	Whiterocks
Intrusion volume, cc/g	0.2194	0.2814
Pore area, m^2/g	5.5792	1.1107
Bulk density, g/cc	1.6750	1.4924
Skeletal density, g/cc	2.6483	2.5731

Ammonia Adsorption

Ammonia adsorption was used to titrate the acid sites present on the Circle Cliffs mineral matter. The sand used in this experiment was the same sample used for the subsequent hexane cracking experiment and was prepared as follows:

1. Circle Cliffs bitumen-free was placed in a muffle furnace and calcined at 773 K for 15 hours.

2. The calcined sand was put in a microcatalytic reactor and moisture was absorbed at 473 K for five hours in a flowing helium at a rate of 25 cc/min at STP conditions (0 °C, 1 atm).

3. The excess unbound water was evaporated from the sand surface in flowing helium at 573 K for 15 hours.

4. The sample was placed in the ammonia adsorption chamber and degassed at 573 K for 10 hours, after which the ammonia was introduced into the chamber.

The amount of ammonia adsorbed increased with increasing ammonia pressure. A long period of time was required to establish adsorption equilibrium. The isotherm appears to be a Type II isotherm, as presented in Figure 17. The isotherm does not equilibrate but continues further adsorption for a long period of time. This phenomena was first explained by Oblad et al.[74] In solid aluminosilicates, some alumina forms a four

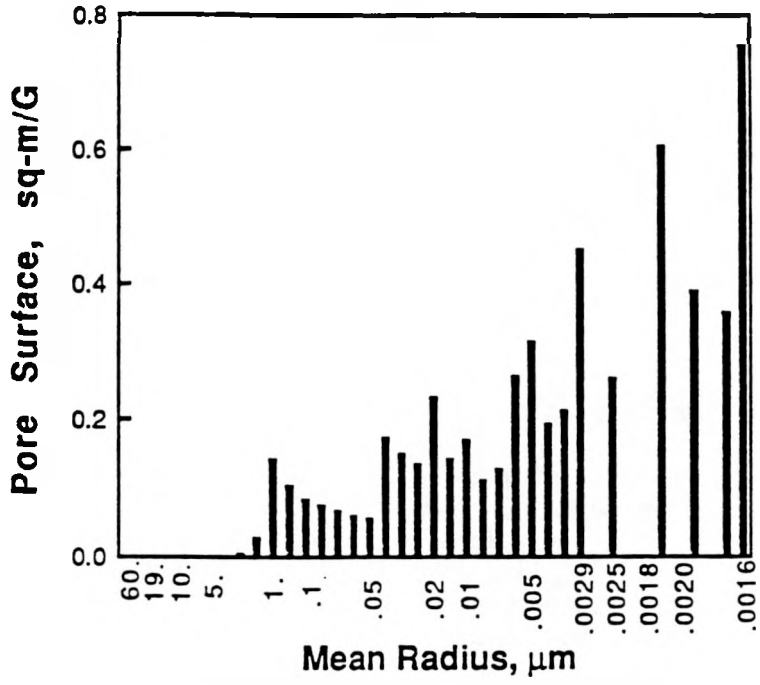

Figure 15. Pore Distribution of Circle Cliffs Sand

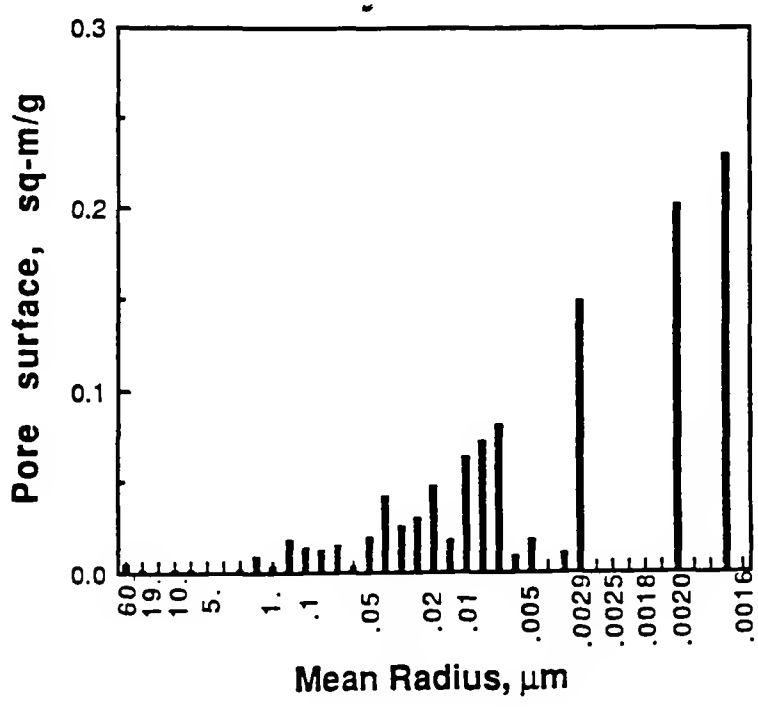

Figure 16. Pore Distribution of Whiterocks Sand

coordinated site with silica and the remainder exists in the six coordinated bulk form. These six coordinated sites are not catalytically active. Ammonia, introduced to silica-alumina can form a positive ion, which involves the formation of silicon-oxygen-aluminum bonds. The highly stable silica structure would be expected to induce a corresponding coordination of the oxygen ions around the aluminum ion. The alumina in the bulk state emerges to the surface and bonds with silicon to form an aluminate which gives rise to an acid site upon which ammonia can adsorb. It is a very slow reaction and requires a very long period of time for equilibrium to be reached. A Langmuir plot of the isotherm data calculated from the first flat of the adsorption curve is presented in Figure 18.

Thermogravimetric Analysis

Spent sand produced from pyrolysis of Circle Cliffs tar sand was analyzed thermogravimetrically in a DuPont TGA 951 system. A thermogram of the oxidation of the spent sand at a 5 °C heating rate in air is presented in Figure 19. The derivative of the thermogram indicated that coke oxidation took place near 723 K, decomposition of hydroxyl groups on the kaolinite took place near 773 K, and the decomposition of mineral carbonates started a little above 873 K and peaked near 1000 K. The first two reactions definitely overlap (i.e., both oxidation of coked sand and decomposition of kaolinite hydroxyl groups occur simultaneously). This overlap makes it technically difficult to determine coke content on the spent sand.

The differential scanning calorimeter thermograms for various Circle Cliffs tar sand host rock samples are compared to Georgia kaolinite. All the dehydroxylation peaks coincide near 800 K, supporting the previous suggestion in Figure 20 regarding hydroxyl group decomposition as a source of produced water. The small peak associated with the dehydroxylation peak for the Circle Cliffs tar sand is related to the phase transformation of quartz.

KAOLINITE EFFECT ON PRODUCT YIELD AND POSSIBLE CRACKING ACTIVITY OF TAR SAND MATRIX

The pyrolysis of the Circle Cliffs tar sand gave a low yield of liquid plus a relatively high yield of gases. Also, it generated 5-20% of carbon dioxide in the reducing environment of pyrolysis. This seems to indicate that a heterogeneous surface reaction is involved in the pyrolysis reaction.

A series of experiments was carried out with the bitumen-free tar sand matrix in a microcatalytic reactor[73] to determine the catalytic influence of the Circle Cliffs mineral matter on the pyrolysis reactions.

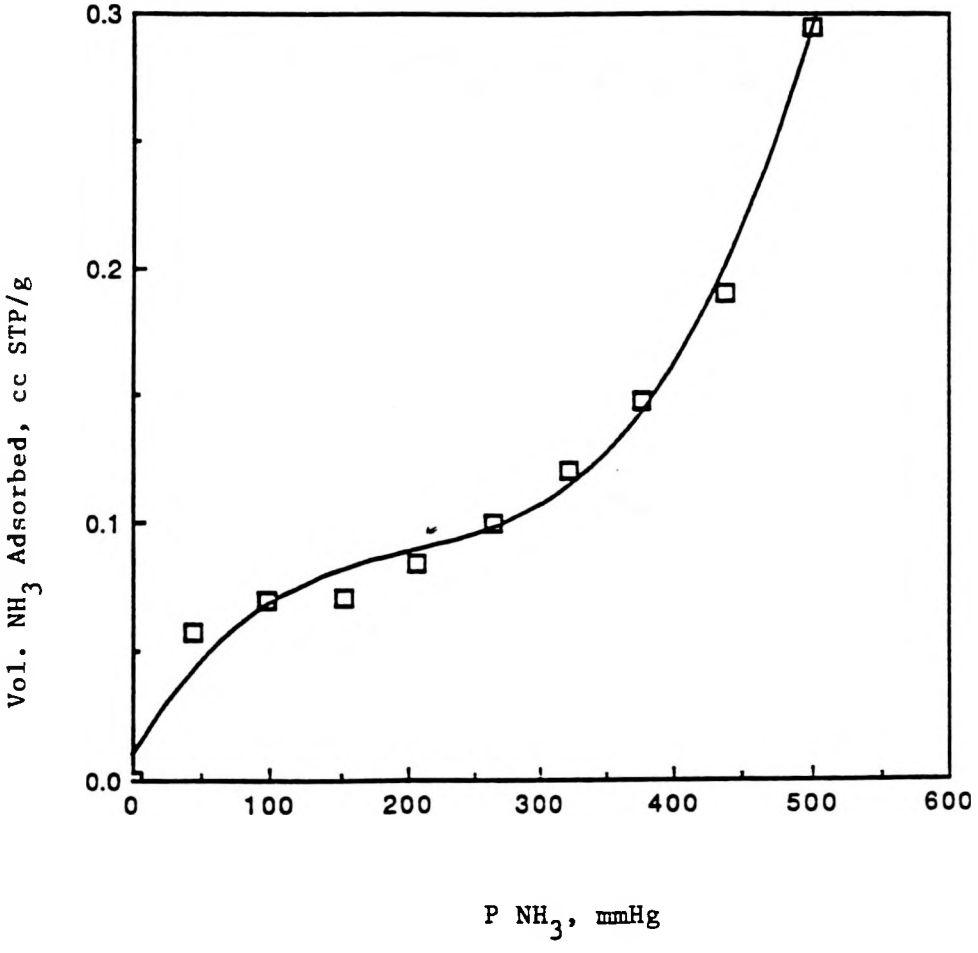

Figure 17. Ammonia Adsorption on Bitumen-Free Mineral Matter

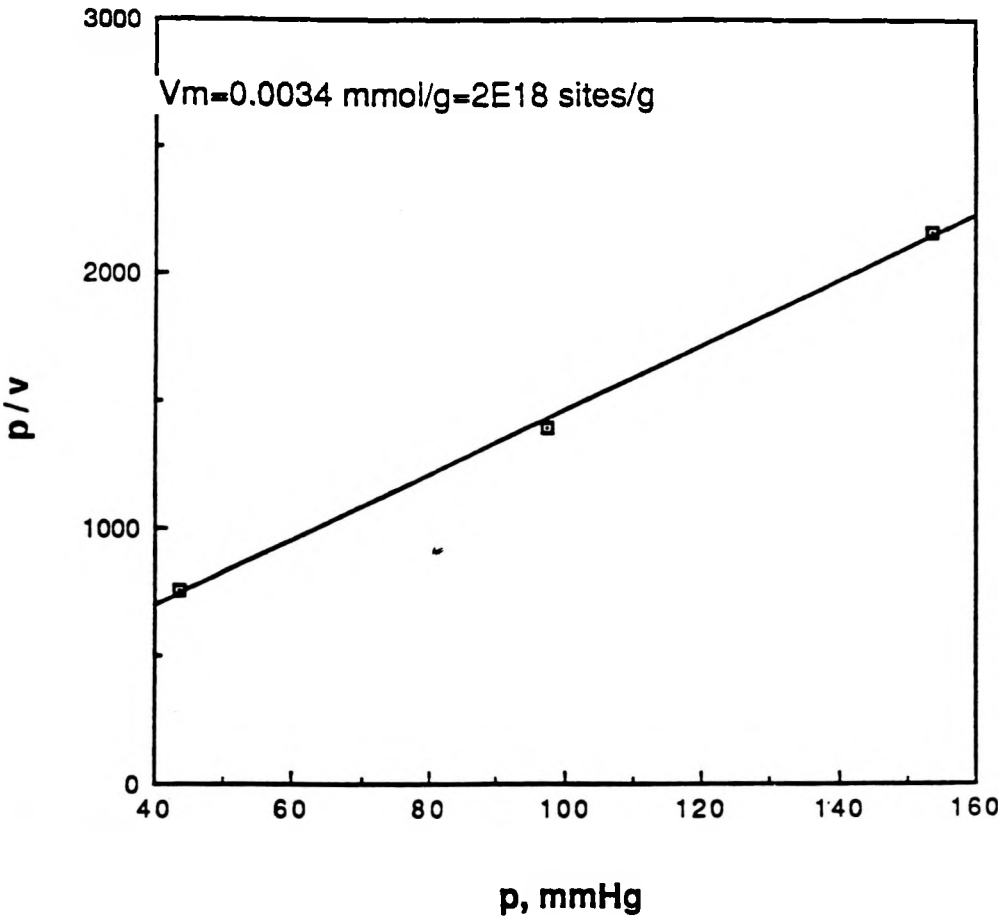

Figure 18. Langmuir Isotherm of Ammonia Adsorption

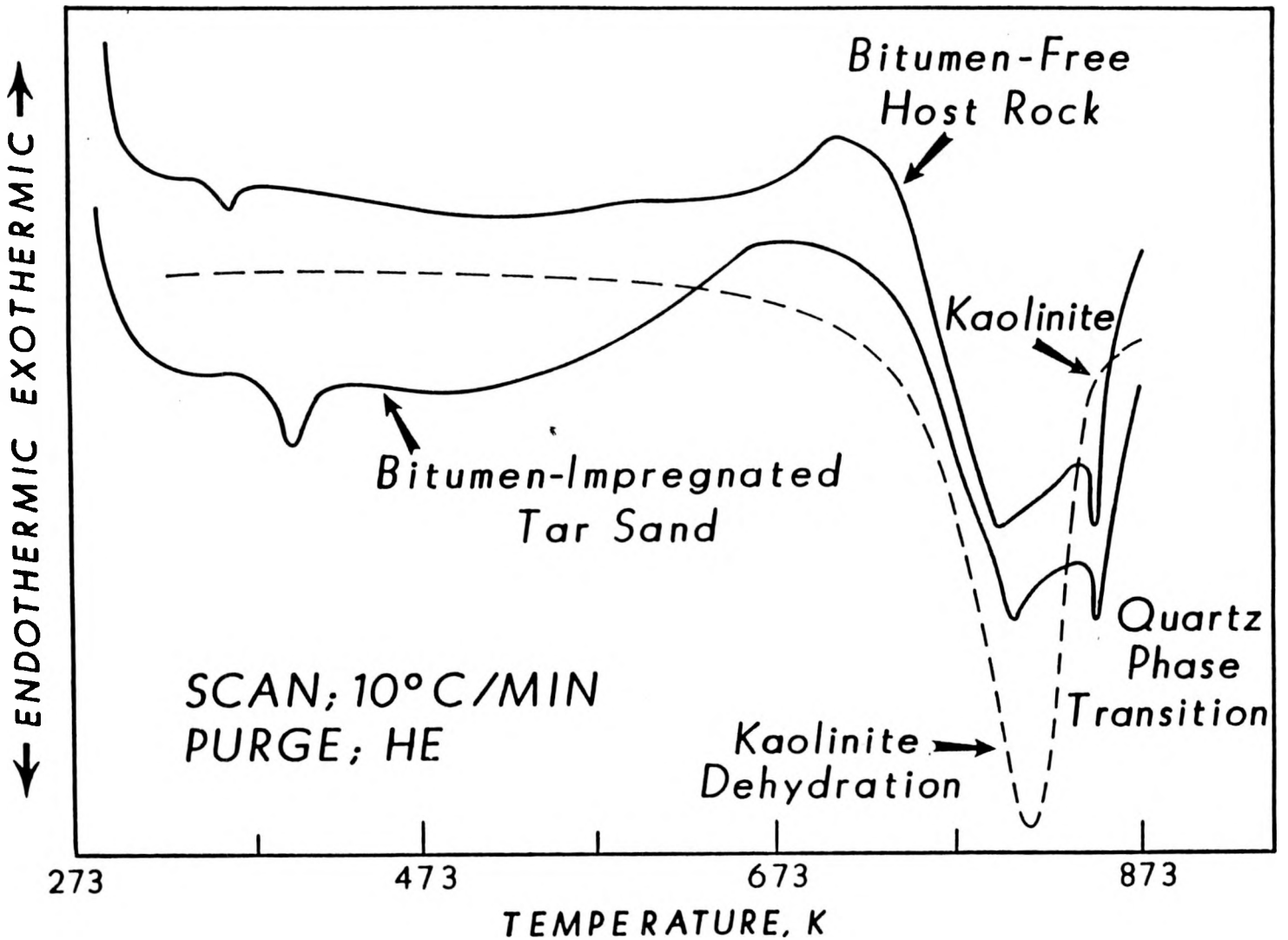

Figure 19. DSC Curve for Circle Cliffs Tar Sand

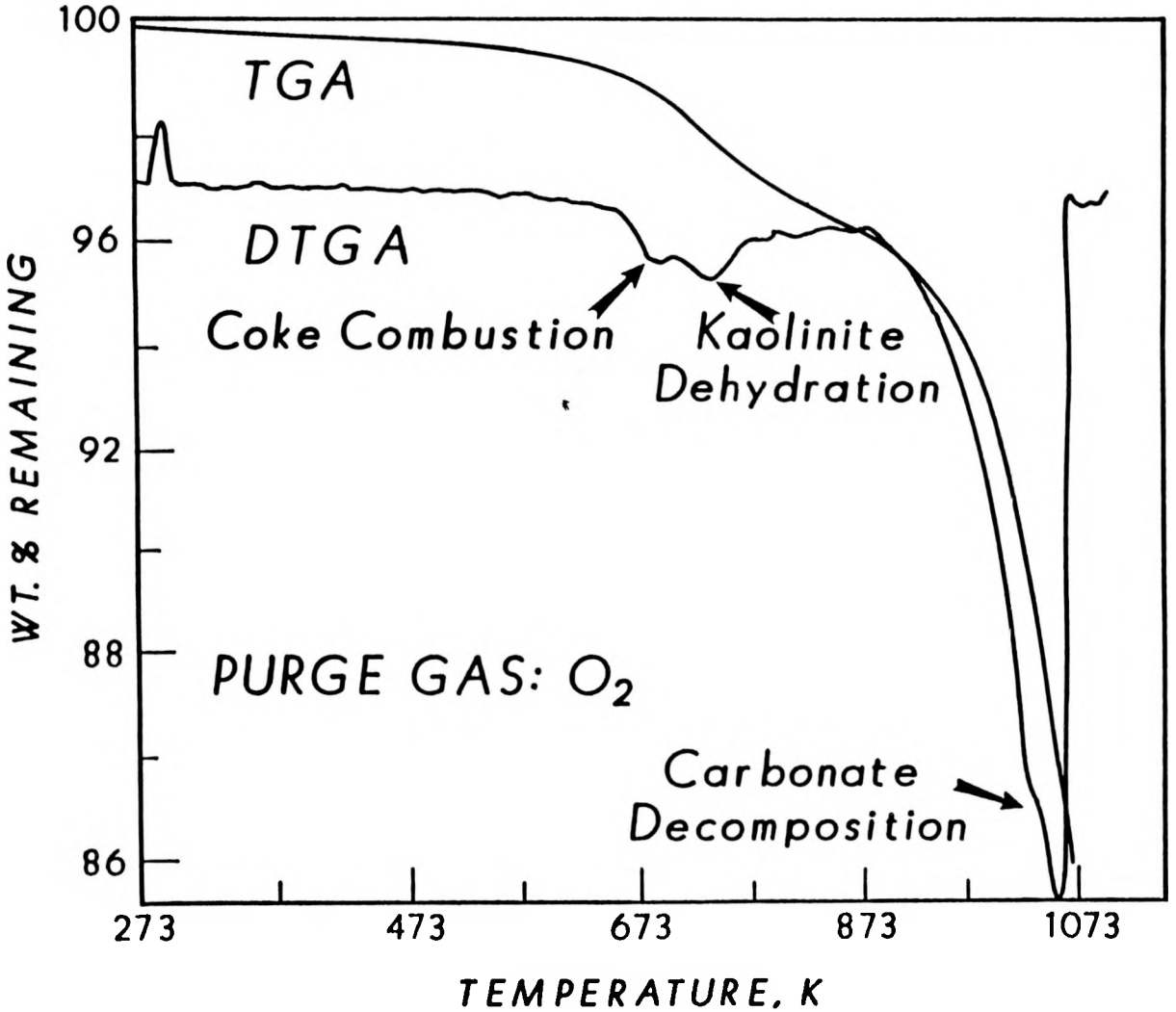

Figure 20. TGA Curve for Circle Cliffs Coked Sand

Sample Preparation

The bitumen was removed from the sandstone in a Soxhlet extractor for more than 72 hours, and the solvent was removed from the host rock in a vacuum desiccator. Pure (99+%) n-hexane and cumene were selected as feedstocks for the catalytic cracking experiment. Helium was used as a carrier gas in all experiments.

A 1.00 ± 0.005 g sample of the bitumen-free host rock was loaded in the center region of a tubular reactor. Glass wool was placed in both the inlet and outlet regions of the reactor to prevent displacement of the sand bed during the reaction. The sample was dried at 573 K in the carrier gas flow overnight before the experiment.

The fresh or spent sand matrix was calcined in air for 4+ hours. Helium saturated with water vapor was then passed through the catalyst bed for 4+ hours. After these treatments, the sand was dried at 573 K in flowing helium overnight.

Microcatalytic Flow Reactor

A tubular isothermal microcatalytic flow reactor was used for these experiments. The reactor was made of glass with dimensions 12 mm I.D. and 45 cm long. Feed hydrocarbon was transported from the bubbler upstream of the reactor by the carrier gas into the reactor. The hydrocarbon feed was passed over the catalyst for ten minutes; the product sample was collected by syringe and injected into a gas chromatograph (Hewlett Packard GC 5830 with TCD detector). A schematic of the reactor is presented in Figure 21. The operating conditions for these experiments are presented in Table 8.

Table 8
Reaction Conditions

Sample Source:	Circle Cliffs tar sand matrix (bitumen washed out by toluene)
Bed Weight:	1 g
Particle Size:	445 μ
Carrier Gas/Flow Rate:	He, 30 ml/min
Feed Flow:	Helium flow saturated with hexane; pulse injection for 10 min

Hexane Cracking

The results of the hexane cracking experiments with the untreated tar sand matrix are presented in Table 9. These data indicate significant hexane cracking activity at 723 K. Subsequently, this activity disappeared. Following a second injection of hexane, the activity further

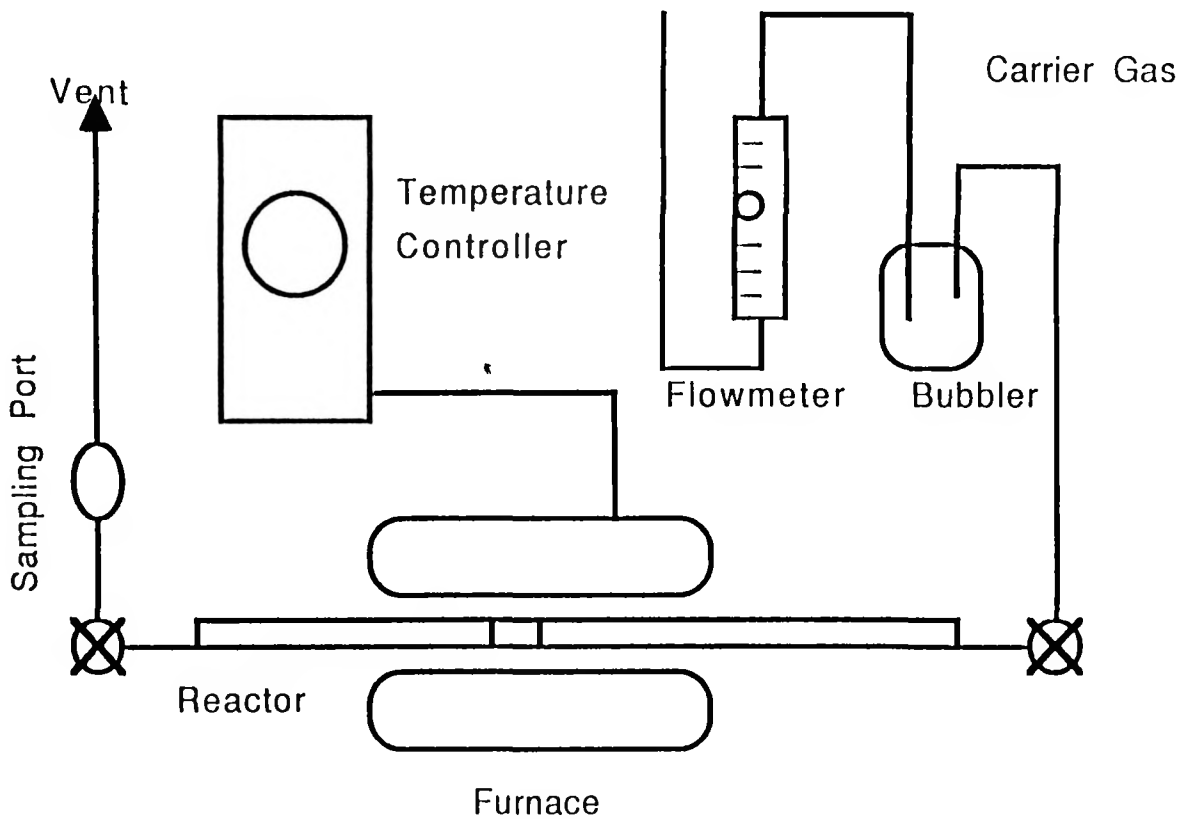

Figure 21. Diagram of Microflow Reactor

decreased, and thermal cracking slowly overrode catalytic cracking as the temperature was raised to 853 K. Table 10 shows that activity decreased with subsequent injections. This observation may be related to coking of residual bitumen in the micropores of the Circle Cliffs host rock that was not removed in the solvent extraction procedure. The nature of the hexane cracking which occurred was identified by comparing the products of the cracking with those obtained in catalytic or thermal cracking of n-paraffins. The distribution of the C_1-C_4 hydrocarbons produced in these two modes of cracking are distinctly different.

Regenerated Catalyst

The activity of tar sand matrix was improved following a calcination pretreatment. The fresh tar sand matrix (washed bitumen-free with toluene) was calcined in the microreactor at 773 K for several hours. Water-saturated helium was then passed through the reactor in the temperature range 373-673 K for several hours. The interaction of the adsorbed water with the calcined host rock led to the regeneration of the hydroxyl bonds removed in the calcination step. It is believed that this procedure was effective in creating Brönsted acid sites. After this step of water adsorption was completed, the sample was dried in a helium flow at 573 K overnight to remove excess water. Following these treatments, a helium flow saturated with hexane was reintroduced. The regenerated sand showed increased conversion of feed hexane.

The activity of the regenerated host rock was dependent upon regeneration parameters (i.e., calcination time, water adsorption/absorption time, and temperature). The sand regenerated at 473 K showed higher activity than that regenerated at 373 K.

The higher activity of the regenerated sand matrix relative to the original matrix at 723 K is indicated in Table 11. The activity of the regenerated sand seemed to decay very quickly (i.e., in 20 minutes in the hexane flow, the hydrocarbon yield was drastically reduced). This observation may be related to coking of the silica alumina such that the active sites are blocked. The deactivated sand was again regenerated; however, the second regeneration did not improve the activity as much as the first regeneration and the activity decayed in 20 min. The rapid decay may be due to a loss of silica alumina surface area during calcination.

At 773 K, the hexane cracking activity does not appear to die out rapidly (Tables 12 and 13). Rather, it appears to approach an equilibrium state, which is a common effect for silica-alumina catalysts.

Table 9

Hexane Cracking on Tar Sand Matrix
(Circle Cliffs Solvent Washed)

I.D.: N26-31
Sample wt: 1.06 g
Carrier Gas Flow Rate: 22.28 cc/min @ STP

#	Temp, K	HC Conv., %	CO_2/HC	H_2O/HC
1	723	6.153	0.032	0.021
2	723	0.0	0.014	0.009
3	773	1.840	0.005	0.001
4	823	1.796	0.003	0.001
5	857	6.6265	0.005	0.001

Table 10

Hexane Cracking on Tar Sand Matrix
(Circle Cliffs Solvent Washed/Calcined)

I.D.: N26-32, N26-24
Sample wt: 1.19 g
Carrier Gas Flow Rate: 25.09 cc/min @ STP

#	Temp, K	HC Conv., %	Thermal Cracking, wt%
1	723	0.094	0.145
2	773	0.487	0.25
3	823	2.242	--
4	833	--	2.823
5	853	5.881	--

Table 11

Hexane Cracking on Regenerated Sand
(Circle Cliffs)

I.D.:	N26-36
Sample wt:	1.01 g
Carrier Gas Flow Rate:	25.09 cc/min @ STP
Water Treatment Temp:	473 K

1st Regeneration

Temp, K	Inj. #	HC Conv., %	CO_2/HC	H_2O/HC
723	1	18.66	0.042	0.010
	2	2.78	0.026	0.002
	3	0.328	0.013	0.011

2nd Regeneration

Temp, K	Inj. #	HC Conv., %	CO_2/HC	H_2O/HC
723	1	5.7	0.017	0.031
	2	0.4	0.011	0.002

I.D.:	N26-35
Sample wt:	0.99 g
Carrier Gas Flow Rate:	25.09 cc/min @ STP
Water Treatment Temp:	373 K

1st Regeneration

Temp, K	Inj. #	HC Conv., %	CO_2/HC	H_2O/HC
773	1	4.279	0.023	0.034
	2	2.021	0.007	0.033

Table 12

Hexane Cracking on Regenerated Sand
(Circle Cliffs)

I.D.:	N26-40
Sample wt:	1.00 g
Carrier Gas Flow Rate:	25.09 cc/min @ STP
Water Treatment Temp:	473 K

1st Regeneration

Temp, K	Inj. #	HC Conv., %	CO_2/HC	H_2O/HC
773	1	25.88	0.114	0.020
	2	20.65	0.069	0.003
	3	16.83	0.055	0.003
	4	18.87	0.046	0.018
	5	17.16	0.041	0.003

Table 13

Hexane Cracking on Regenerated Sand

I.D.:	N26-33
Sample wt:	1.19 g
Carrier Gas Flow Rate:	25.09 cc/min @ STP
Water Treatment Temp:	373 K

1st Regeneration

Temp, K	Inj. #	HC Conv., %	CO_2/HC	H_2O/HC
773	1	7.281	0.012	0.016
823	2	6.201	0.003	0.009
853	3	6.060	0.002	0.003
853	4	5.060	0.002	0.003
853	5	4.134	0.002	0.002
853	6	3.656	0.002	0.002

Carbon Dioxide Yield

Significant amounts of carbon dioxide were produced during the pyrolysis of the Circle Cliffs tar sand. The probable explanation based on the experimental results is that the carbon dioxide is produced from the decomposition of minerals such as siderite ($FeCO_3$), dolomite ($CaMg(CO_3)_2$), or calcite ($CaCO_3$). Tables 9-13 indicate that the carbon dioxide and water yields decrease as the reaction proceeds.

Water Yield

Detectable amounts of water were also produced during hexane cracking. The production of water was attributed to hydroxyl group decomposition. Because of difficulties in measurement, the quantitative analysis for produced water is not listed in the tables. The simultaneous production of H_2O and CO_2 may also be related to oxidation of the hydrocarbon feeds.

Cumene Cracking

Cumene was passed over various host rock samples obtained from the Circle Cliffs deposit; however, cumene cracking was not observed in any of these experiments. A sample of sand was calcined at 1023 K to remove CO_2. The resulting calcined mineral matter, while expected to possess cracking activity, showed no activity with either cumene or hexane.

Conclusions

A portion of the Circle Cliffs mineral matter is activated as a cracking catalyst at pyrolysis conditions such that the hydrocarbon vapors produced in the dense phase fluidized bed undergo a combination of thermal and catalytic cracking at the reaction temperature of 723-873 K. The activity of the sand matrix decayed significantly after 20 minutes for hexane cracking at low temperature. The regenerated mineral matter exhibited higher catalytic activity at higher temperatures; however, the cracking activity usually died out in 30 minutes when exposed to hydrocarbon.

The carbon dioxide yield may be related to the reduction of the oxidized mineral matter, whereas the water yield is related to the dehydroxylation of the kaolinite component of the host rock.

None of the samples tested exhibited the ability to crack cumene in the temperature range 723-873 K. The cracking activity seemed to be related to the extent of dehydration of the mineral matter and thus indirectly to the bound water.

ROTARY KILN REACTOR STUDIES

INTRODUCTION

The rotary kiln is one of the most important high-temperature process furnaces and the most widely-used industrial reactor for contacting gases and solids. Kilns are mainly used for calcining, drying, nodulizing, incinerating, or reducing solid materials. Although pyrolytic kilns have already been used for various applications, the rotary kiln has not been extensively evaluated for the pyrolysis of Utah's tar sands, with the exception of early process studies conducted by Lurgi.

Preliminary continuous-flow pyrolysis experiments were recently conducted in a 6-inch I.D., 120-inch long rotary kiln reactor at the research and development facilities of the Harper Electric Furnace Corporation in Lancaster, New York. The mined, crushed, and screened ore from the Whiterocks tar sand deposit was used as the feed sand in these experiments. The objectives of this preliminary investigation were as follows:

1. determination of the feasibility of the pyrolysis of bitumen-impregnated sandstone in a commercially-available rotary kiln reactor;

2. determination of the feasibility of material balance closure in a continuous rotary kiln reactor;

3. preliminary determination of the influence of process variables on kiln operation; and

4. analysis and characterization of the bitumen-derived liquids produced in the rotary kiln pyrolysis experiments.

Nature of the Feed Bitumen

The feed tar sands used in this investigation were obtained from the Whiterocks tar sand deposit in the Uinta Basin of northeastern Utah. The feed tar sand was an outcrop sample that was obtained from the Fausett Pit, as shown in Figure 22.

Physical and chemical properties of the native Whiterocks bitumen are presented in Table 14. The bitumen content of the Whiterocks tar sand was about 7.2 wt%. As the bitumen content of the Whiterocks tar sand is relatively higher than other deposits (i.e., Circle Cliffs), the crushed and screened tar sands tended to agglomerate again in the storage barrel and the feed hopper. Therefore, the feed sand had to be mixed with coked sand in a weight ratio of 1:1 to ensure that it would flow freely from the feed hopper and the screw feeder.

LOCATION OF SAMPLE SITE ON THE WHITEROCKS TAR SAND DEPOSIT

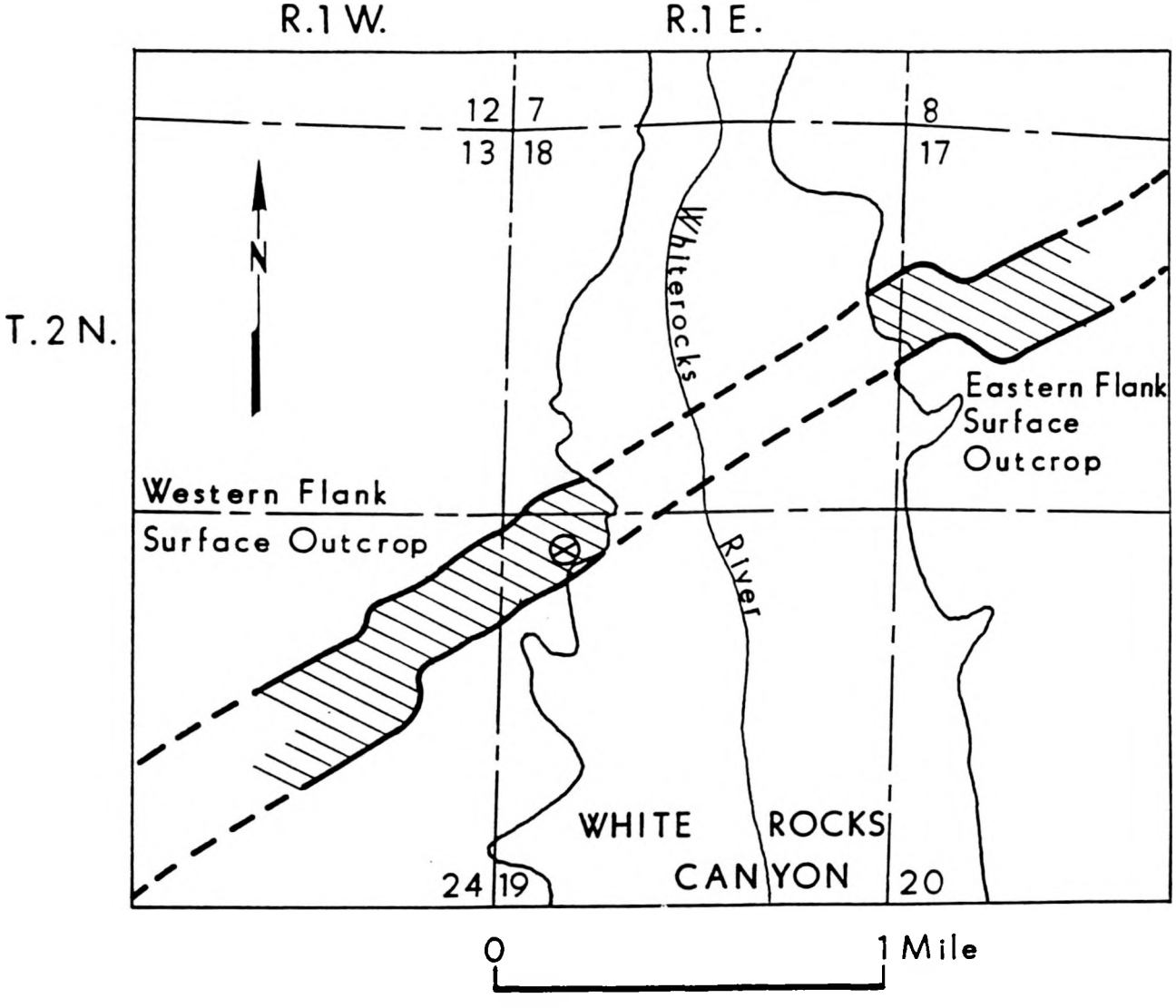

⊗ *Sample Site from Fausett Pit*

Exposed Surface Outcrop

Portion of Deposit

Overlain by Overburden

Figure 22. Location of Sample Site on the Whiterocks Tar Sand Deposit

Table 14

Native Bitumen Properties,
Whiterocks Tar Sand

Bitumen content, wt%	72
API gravity, °API	11.9
Viscosity, cps (@ 358 K)	2665
Conradson carbon residue, wt%	8.1
Ash content, wt%	1.3
Pour point, °F	135
Simulated Distillation	
Volatility, wt%	40.5
IBP-400°F, wt%	0.0
400-650°F, wt%	4.9
650-1000°F, wt%	35.6
> 1000°F, wt%	59.5
IBP, °F	464
Elemental Analysis	
C, wt%	83.3
H, wt%	11.0
N, wt%	1.3
S, wt%	0.3
O, wt%	4.1
H/C Atomic Ratio	1.58
Molecular Weight, g/mol	402
Ni, ppm	67
V, ppm	< 5

The native bitumen was obtained by solvent extraction with toluene in a Soxhlet apparatus for characterization. The extracted bitumen was a semisolid at room temperature. The viscosity was measured at a temperature of 185 °F and was 2670 cps. The Conradson carbon residue and ash content were 8.1% and 1.3% by weight, respectively. The carbon residue was lower than that obtained for other Utah bitumens, and it was anticipated that the carbonaceous residue yield would be less than that expected from the pyrolysis of Sunnyside and P.R. Spring bitumens.

The volatility of the native bitumen was 40% and the residual fraction was 60% by weight as determined by simulated distillation. The atomic H/C ratio was 1.58 and the sulfur and nitrogen contents, 0.3 and 1.3 wt%, respectively, were consistent with published data.

EXPERIMENTAL APPARATUS AND PROCEDURES

Rotary Kiln Reactor System

The reactor system utilized in this investigation was a commercially-available rotary kiln reactor which was designed and constructed by Harper Electric Furnace Corporation (Harper Rotary Tube Furnace Model No. HOU-6D60-RTA-25). The reactor was 6 inches in diameter, 120 inches in length, and was designed for a maximum operating temperature of 1150 °C with an alloy tube and 1350 °C with a suitable ceramic tube. The reactor system consisted of a rotary kiln reactor assembly, a tar sand feeding system, a spent sand discharge system, and a liquid product recovery system. A schematic of the rotary kiln pyrolysis reactor apparatus is presented in Figure 23. Also, a detailed discussion of equipment specifications is presented below.

Feeder Section

This part of the reactor system features an Acrison Model 105Z volumetric screw feeder with an 050-2A controller. A tachometer feedback provides for precise speed control and repeatability through adjustment of a digital thumbwheel speed selector. All contact parts of the feeder are made from 304 stainless steel and include a 1 cubic foot hopper to provide for storage of unprocessed material. The screw feeder consists of two concentric different-sized augers: a large screw auger (12-inch diameter) and a small screw auger (1-inch diameter). Both the screw augers are located in the feed hopper. The large screw auger helps to crush and mix agglomerated feed sands so that the feed sands will flow freely. In order to prevent feed sands being driven into the corner of the hopper, the half-portion of the screw auger is oriented in the opposite direction. The small screw auger carries feed sand from the hopper to the reactor. The end of the screw feeder is located directly at the beginning of the rotary kiln, and the other end of the screw shaft is connected to the drive motor assembly. A schematic of the feeding system is shown in Figure 24.

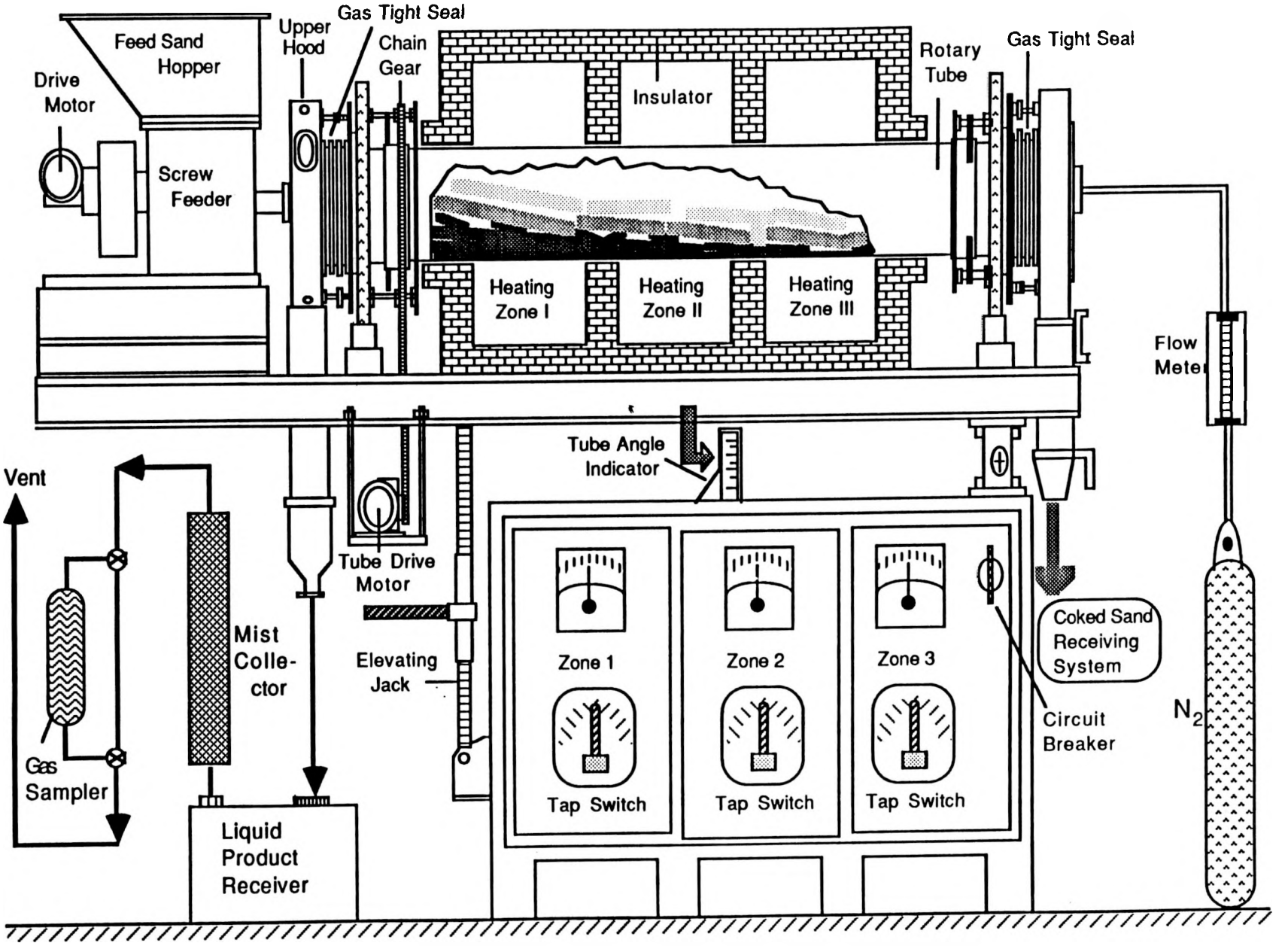

Figure 23. Schematic of the Rotary Kiln Reactor Apparatus

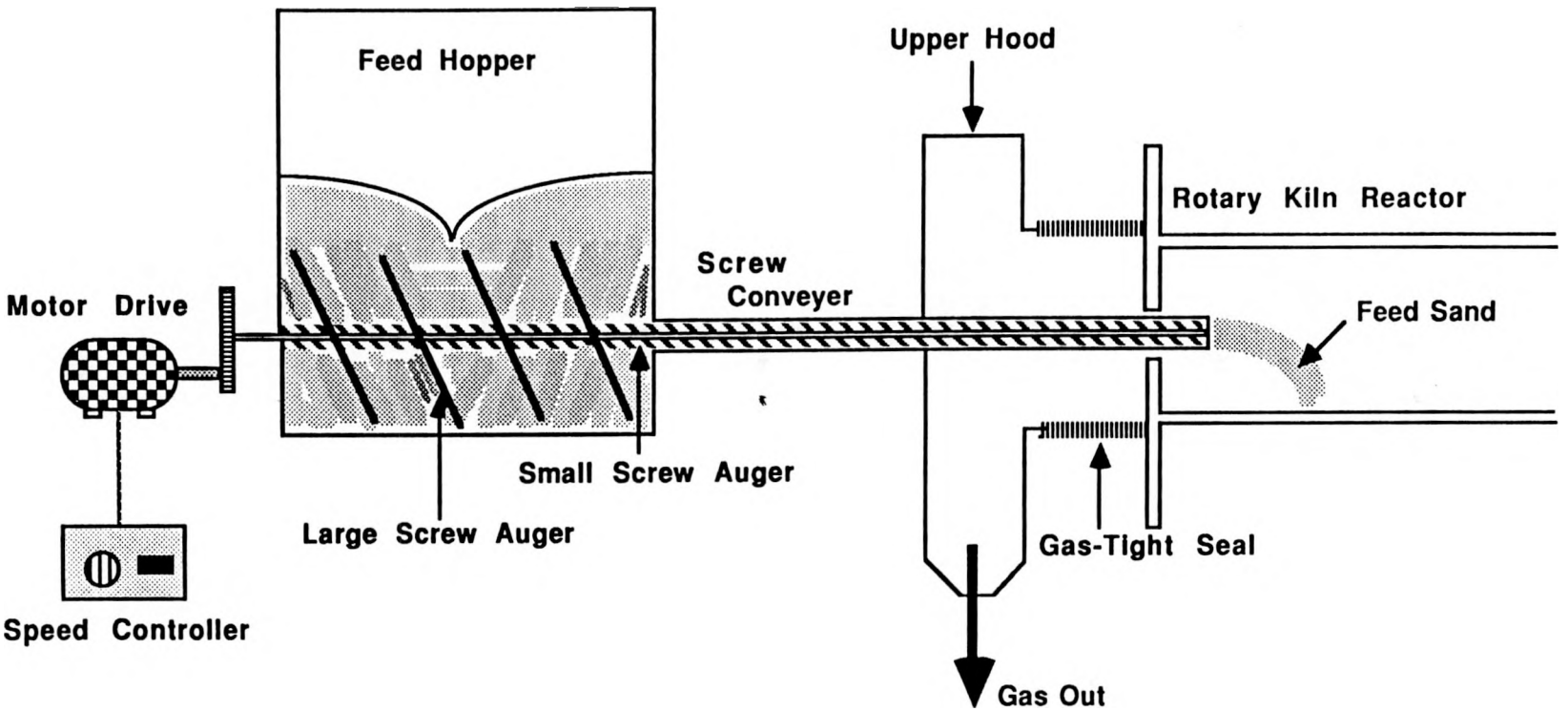

Figure 24. Schematic of the Feeding System

Heating Section

Thermal energy is supplied to the reactor by the stationary electric heater. Two baffles divide the chamber into three dimensionally equal sections. Silicon carbide heating elements are mounted horizontally above and below the tube. Sixty total inches of heated length are provided over the three zones. The heating element terminal compartments are conveniently located on both sides of the furnace to facilitate both installation and removal of heating elements. Three thermocouple ports are located through the top of the furnace, with one thermocouple located at the midpoint of each zone. A probe thermocouple port, located on the exit hood, allows for placement of a probe thermocouple inside the furnace tube. A temperature profile of the rotary kiln reactor is shown in Figure 25 for the case when the temperature of the reactor was set to be 798 K. Temperatures were measured every foot along the axis of the kiln when the kiln did not contain solid material.

Tube Assembly

The furnace features a cast HT alloy tube 6 inches I.D. by 6-1/2 inches O.D. with an overall length of 120 inches, 60 inches of which is heated. This tube can be operated at temperatures of up to 1150 °C. The tube also has an entrance dam to prevent backspilling of the product. Tire assemblies support the tube on the entrance and exit end of the furnace. A three-piece clamp fixes the tube to the support system.

Tube Seals

Atmosphere gas-tight rotary tube seals are used to seal the rotating tube and to prevent the passage of gas through the annular opening between the rotating tube and the stationary hood. The seal has several springs in the ring to maintain tension on the contact surfaces. Self lubrication graphite wiper seals provide for low maintenance.

Hood Assemblies

The breech type hoods are constructed from 304 stainless steel and located on both the entrance and exit ends of the furnace. These hoods are equipped with cleanout ports, sight ports, and atmosphere vent assemblies. A ball valve is located on both the entrance and exit hoods. In the exit hood, a removable 90 CFM duct fan is supplied to mix the atmosphere inside the furnace.

Tube Drive

The tube drive system incorporates a DC gear motor, reducer, and SCR variable speed controller to effectively control the rotational speed of the tube from 0-10 RPM. The tube drive features a Minarik Digi-lock DLC 100 converter. Set speed for this unit is achieved by adjustment of a four-decade thumbwheel. The required rotational speed set by the operator would be entered using a switch on the front panel of the converter. This unit features a magnetic pickup unit directly coupled to the motor shaft. The signal from this unit is converted and displayed on the front panel as the tube rotational speed.

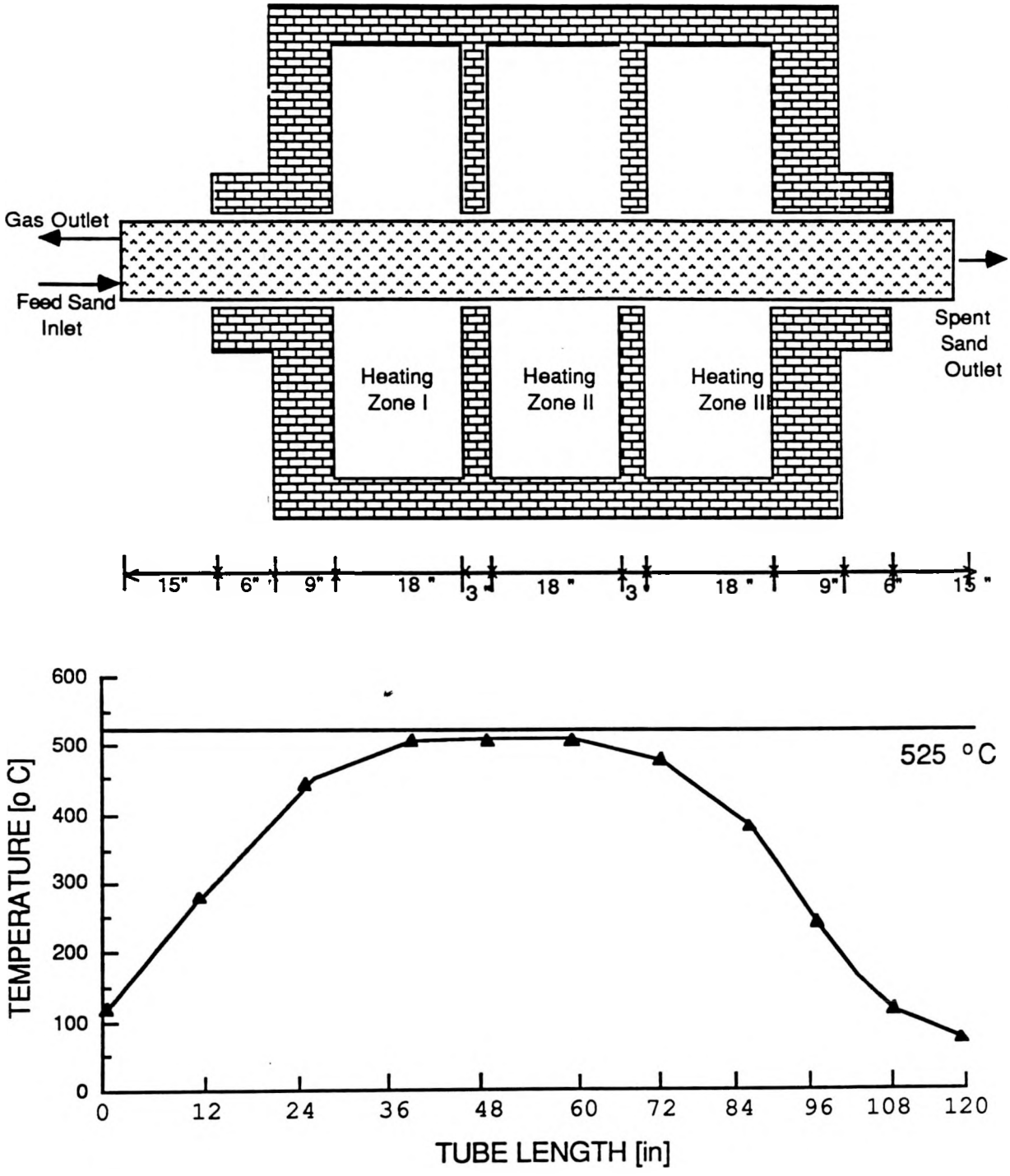

* 3-heating zones temperature setpoint = 525 C (798 K).
* Temperature was measured when the kiln was empty.
* 'K' type thermocouple (120" long) was used.
* Maximum temperature recorded = 520 C.

Figure 25. Rotary Kiln Temperature Profiles

Furnace Stand

The stand, in addition to supporting the furnace, houses the power supply and temperature control instrumentation. A manual ratcheting jack permits the furnace to be adjusted from -5 to 10° from the horizontal. A calibrated scale and pointer allow for repeatability of the angle.

Nitrogen Flow Control Panel

In all experiments, nitrogen is used as the sweep gas, counterflow to the direction of flow of the tar sand. A nitrogen flow control panel is mounted on the furnace. It is designed for use with a regulated 3 psi nitrogen supply. A 0-250 CFH flow meter regulates the flow of nitrogen into the furnace tube. The panel also features flow meters for nitrogen into the following locations: feeder hopper; entrance hood discharge chute; entrance sight ports; discharge sight port; entrance bellows seal (graphite ring); discharge bellows seal (graphite ring); and discharge chute.

Power Control System

The power control system is mounted and wired in the furnace stand. The heating elements are arranged electrically into three circuits for three zones of independent power control. The power control system is rated at 45 KW and consists of the following components:

1. Three-phase angle-fired SCR power controllers with current limit to proportion power independently to the three zones.

2. One shunt trip circuit breaker to open the primary circuit of the power control system in the event of overtemperature conditions.

3. One pneumatic time delay relay to eliminate nuisance tripping of the circuit breaker due to momentary power interruptions.

4. Three 15 KVA insulating step-down transformers with eight individual voltage taps. Increased voltage is used to compensate for an increase in resistance in the heating elements due to aging.

5. Three eight-point tap switches used for changing transformer taps.

Temperature Control Instrumentation

The temperature control system is mounted and wired in the base of the furnace. This system consists of the following:

1. Three Barber-Coleman Model 560 microprocessor-based controllers.

2. Three Barber-Coleman Model 121 series set point controllers, which are used for overtemperature protection. In event of

overtemperature conditions, the shunt trip circuit breaker will open the primary heating circuits.

3. One audio/visual alarm system with silencing switch to alert operating personnel to overtemperature conditions.

4. One control transformer to reduce line voltage to instrumentation operating voltage.

5. Six type "S" thermocouples (three dual) equipped with mullite protection tubes. Three thermocouples are dedicated to temperature control and the other three to overtemperature protection.

6. One type "K" probe thermocouple.

7. One Digital Display for the probe thermocouple to be mounted in the furnace base.

8. All switches, relays, lamps, and peripheral electrical equipment required to make a safe and complete electrical system.

Spent Sand Discharge system

The spent sand discharge system consists of an upper ball valve and a lower ball valve to prevent the produced gas from leaving the reactor during the spent sand withdrawal step due to the pressure differential across the sand discharge tube. The upper valve is connected to the lower hood where the coked sand is first collected from the kiln tube. When this valve is opened, the coked sand in the lower hood is transferred to the spent sand discharge tube. After the upper valve is closed, the bottom valve is opened and the coked sand is removed from the spent sand discharge tube. A schematic of the spent sand discharge system is presented in Figure 26.

Feed Preparation

The continuous-flow rotary kiln reactor was operated to investigate the recovery of a bitumen-derived hydrocarbon liquid from the Whiterocks tar sands of Utah. The Whiterocks tar sand samples used in this study were consolidated bitumen-impregnated sandstone rock.

The feed was prepared as follows: the Whiterocks tar sand was initially crushed in a large jaw crusher, screened and recycled to a roll crusher. On the first screening, about 60 wt% of the material recovered from the jaw crusher passed through the screen. The overhead (material that did not pass through the screen) was passed through a roll crusher with the rolls set at a 1/2-inch spacing. After the first roll crushing of this material, 75 wt% of the material then passed through the 1/2-inch screen. The overhead from this screening had the appearance of flat disks and was referred to as "pancake material." After the second passage of this material through the roll crusher, the subsequent screening left

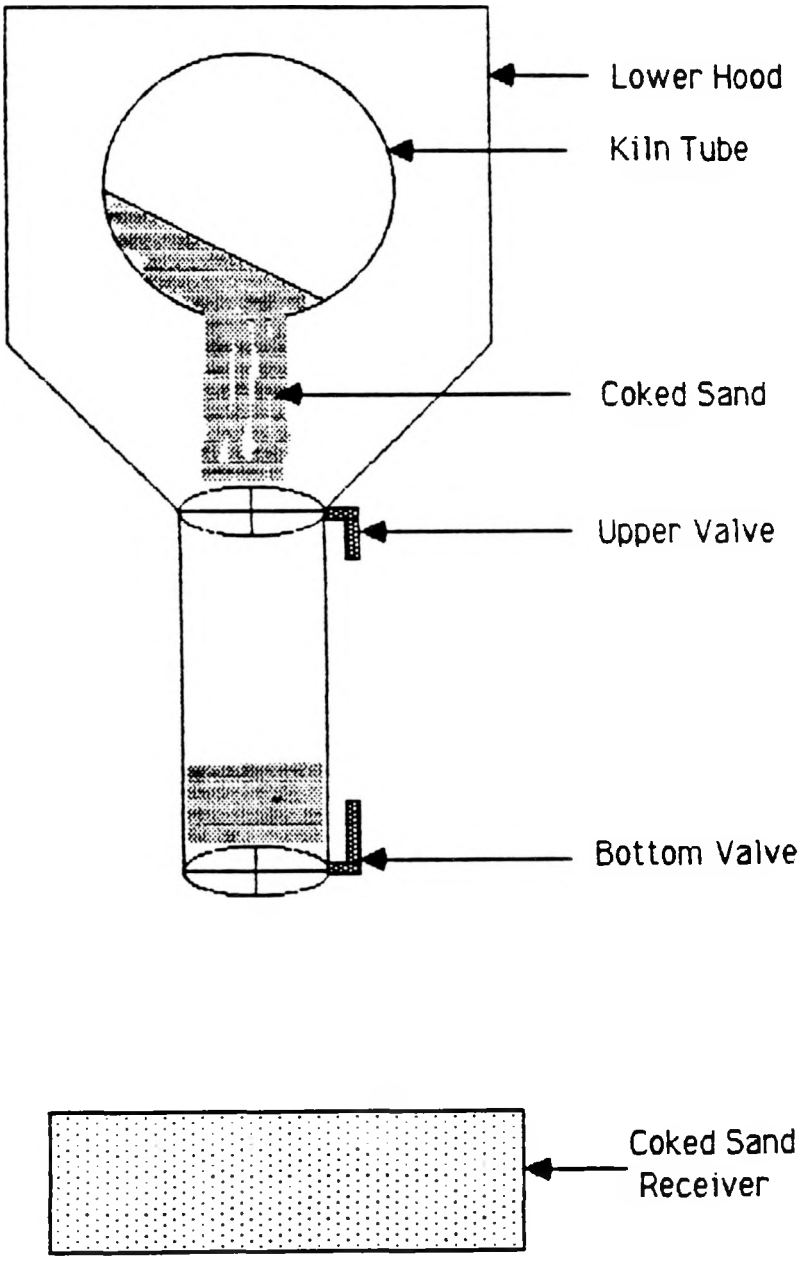

Figure 26. Schematic of the Spent Sand Discharge System

about 5 wt% of the original material or reject. This material was combined with ore from the jaw crusher that had been screened but not passed through the roll crusher. After rolling and crushing two more times, only five wt% of the original material that came from the jaw crusher remained larger than 1/2-inch mesh, indicating that the "pancake material" could be easily crushed in the roll crusher when fed in the presence of overhead material that had not been passed previously through the roll crusher. The screened Whiterocks tar sand agglomerated again in the storage barrel and had to be mixed with coked sand in a weight ratio of 1:1 to ensure that it would flow freely from the feed hopper and the screw feeder.

Experimental Procedures

The following start-up procedures were established for the rotary kiln reactor and were used in each experiment:

1. The reactor temperature for each heating section was set at 798 K. The inclination angle and the rotational speed of the kiln were set at the desired values.

2. The nitrogen gas cylinder valves were opened. The sweep gas flow rate was set at 75 SCFH and the purge gas flow rate was set at 2.5 SCFH using a rotameter. Thus, the total nitrogen gas flow rate entering the reactor was 77.5 SCFH.

3. The hopper was filled with the crushed and sized feed sand. During the continuous run, additional feed sand was placed in the hopper whenever the large screw auger was not completely covered by the feed.

4. When the reactor temperature reached the setpoint, 798 K, the screw feeder rate was set at the proper level by adjusting the speed of the drive motor and the feed sands were fed from the feed hopper to the reactor.

5. The amount of the coked sand discharged from the reactor was weighed every five or ten minutes until a steady state was obtained.

6. After the liquid recovery system was weighed, the run was started and the run time was recorded.

7. During the run, the amount of coked sands discharged was weighed every five minutes. The total weight of the coked sand discharged during each run was measured.

8. Produced gas samples were collected in the gas sampler 30 minutes after starting the run.

9. As soon as the run was completed, the screw feeder was turned off and the liquid recovery system was weighed. The holdup in

the reactor was determined by emptying the kiln tube and weighing the sand withdrawn from the tube.

EXPERIMENTAL RESULTS AND CHARACTERIZATION

It is well-established that the reactor temperature and the solids retention time affect the product distribution in fluidized-bed tar sand pyrolysis processes. Because of the limited time of our stay, the solids retention time was selected as the process variable to be investigated.

The process variable data were obtained in a rotary kiln reactor at 798 K at the solids retention times ranging from 9 to 31 minutes. The effect of solids retention time in the reactor on both pyrolysis product yields and bitumen-derived liquids properties was investigated.

The bitumen content of the Whiterocks tar sands was determined by burning the bitumen at 773 K for 15 hours. The error from water loss is small since the tar sand has no connate water. Three samples were prepared and placed in the muffle furnace, and the weight difference between the original bitumen-impregnated sample and the burned sample was defined as the bitumen content. The product gases that were collected during the experiment were analyzed by gas chromatography to determine the chemical composition for the material balance. The gas analysis was performed on a Hewlett-Packard Model 5830A gas chromatograph with dual thermal conductivity detectors. The coke saturation on the coked sand was determined in the same manner as the bitumen content of the feed tar sands.

Effect of Solids Retention Time on Product Yields

The solids retention time, t, was defined as follows:

$$t = \frac{W/2}{F}$$

where W is the weight of sand held up in the bed and F is the tar sand feed rate. Originally, the reactor heating system was designed and constructed to heat the center section (one-half the length of the tube) of the tube. Thus, the reaction or pyrolysis zone was confined to half of the entire tube length, thus the total bed holdup weight used in calculation of the solids retention time was divided by 2. Typical rotary kiln reactor temperature profiles are presented in Figure 25. In this investigation, the solids retention time was varied by changing the kiln rotation speed and the kiln inclination, which in turn changed the feed rate and the bed holdup.

The effect of solids retention time on product yields was investigated for the Whiterocks tar sands. It was difficult to obtain closure on the material balances due to the small amount of hydrocarbon gas collected during the experiments. Gas analyses were complicated by the necessity to

ship the collection vessels from Harper Electric to the University of Utah for chromatographic analysis. Thus, the gas yield data were normalized by adding the difference between the total hydrocarbon recovery and 100 for these preliminary experiments. The results of a series of experiments are presented in Table 15 and Figure 27.

Table 15
Effect of Solids Retention Time on Product Yields from Whiterocks Tar Sands

Run ID number	WR-RK-1	WR-RK-2	WR-RK-3	WR-RK-4
Reactor temp, K	798	798	798	798
Solids retention time, min	31	21	13	9
Sweep gas flow rate, SCFH	77.5	77.5	77.5	77.5
Feed rate, kg/h	9.02	9.78	10.09	29.55
Kiln slope, deg.	0.5	1.5	2.5	2.5
Kiln rotational speed, RPM	2	2.8	3.2	4.7
Product Yields				
Liquids, wt%	40.0	47.9	52.8	51.6
Gases,* wt%	32.3	30.0	21.4	21.5
Coke, wt%	27.8	22.2	25.9	26.9

*Normalized to 100 percent by weight of bitumen fed.

The liquid yield increased with decreasing solids retention time, while the gas yield decreased with decreasing solids retention time. This observation may be related to the fact that the bitumen-derived liquid also undergoes secondary cracking, which takes place in the vapor phase. Also, solids-vapor contact time affects the rate of this vapor-phase thermal cracking because the solids-vapor contact time is directly proportional to the retention time. Therefore, the decrease in the liquid yield as the solids retention time increased was accompanied by an increase in the gas yield. However, the coke yield was essentially insensitive to changes in solids retention time. Previously, the fluidized-bed studies indicated that the carbonaceous residue yield depends on the source of the tar sand feed rather than on operating variables.

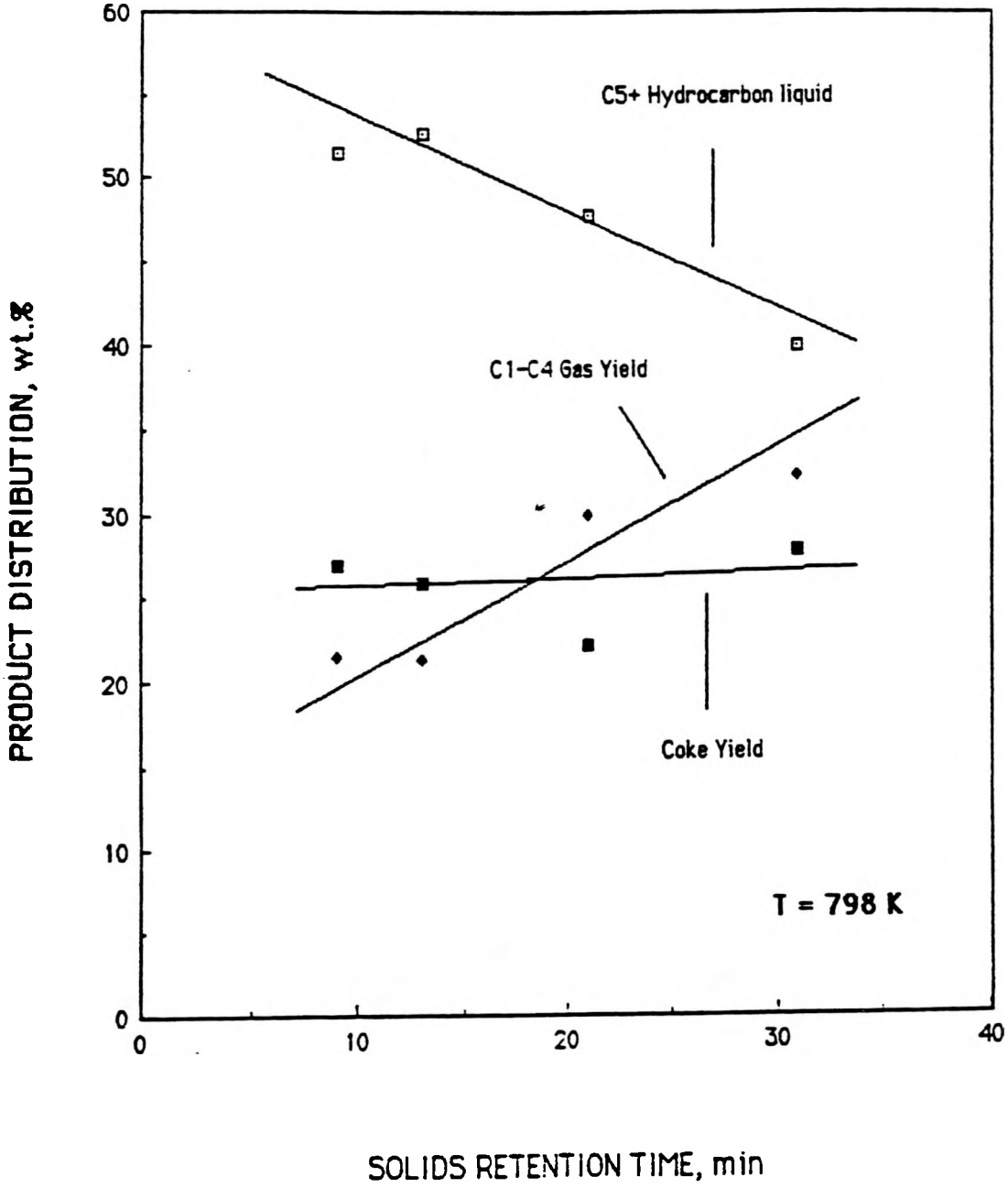

Figure 27. Product Distribution from the Rotary Kiln Reactor

Effect of Solids Retention Time on Properties of Bitumen-Derived Liquids

Detailed chemical and physical analyses of the bitumen-derived liquid produced by the rotary kiln pyrolysis of the Whiterocks tar sands were performed. Densities of the liquid products were measured on a Mettler/Parr Model DMA 40 digital density meter. The product liquid viscosities were measured on a Brookfield Model LVT viscometer with 1.565° cones. The pour points of the liquid products were determined according to ASTM method number D97-66. Conradson carbon residue and ash content of the liquid products were determined using ASTM methods D189-65 and D482-63, respectively. The simulated distillation data were obtained using a procedure similar to the ASTM method D2887-70T. The analysis was performed on a Hewlett-Packard 5730A gas chromatograph with dual flame ionization detectors. These physical and chemical properties are presented in Table 16. In addition, the effect of the solids retention time on various properties of product liquids from the Whiterocks tar sands is shown in Figures 28 through 32.

From Figure 28 it can be seen that the API gravities of the liquid products decreased at a constant reactor temperature as the solids retention time increased from 9 to 31 minutes. The thermal cracking in the reactor was enhanced by longer solids retention times. Moreover, the increased severity of thermal cracking caused an increase in the aromaticity of the product liquids, resulting in increased density or decreased API gravity. The viscosities of the liquid products increased with increasing solids retention time. The pour point and atomic H/C ratio of the product liquids remained essentially constant with respect to solids retention time. No clearly-established trend was observed with the Conradson carbon residue as the solids retention time decreased. Also, no clear trend was observed in the simulated distillation data with respect to solids retention time in these experiments.

Effect of Solids Retention Time on the Chemical Composition of Bitumen-Derived Liquids

The native bitumen and product liquids were fractionated using gradient elution chromatography (GEC). A schematic of the GEC apparatus is shown in Figure 33. The main column was packed uniformly with activated alumina. The ALCOA F-20 alumina was activated to <5% moisture by heating it at 773 K for 16 hours in a muffle furnace. About 10 grams bitumen-derived liquid sample were dissolved in dichloromethane ($MeCl_2$). The solution was absorbed on 60 to 65 grams of activated alumina. After the solvent was evaporated, the sample was packed in the sample column. Nitrogen pressure of 2-5 psig was maintained throughout the run. A series of solvents with increasingly eluting power was added sequentially to the solvent reservoir. The solvent sequence used in this analysis is shown in Table 17.

The mixing chamber provided a gradual and continual increase in the eluting power of the solvent entering the column. The balance between the adsorption sites on the alumina and the eluting power of the solvents accomplished the separation into defined fractions. The saturates, which

Table 16

Effect of Solids Retention Time on Bitumen-Derived Liquid Properties from Whiterocks Tar Sands

Run ID Number	WR-RK-1	WR-RK-2	WR-RK-3	WR-RK-4	
Reactor Temp., K	798	798	798	798	
Solids Retention Time, min	31	21	13	9	
N_2 Gas Flow Rate, SCFH	77.5	77.5	77.5	77.5	
Properties	**Bitumen-Derived Liquid**				**Native Bitumen**
Gravity, °API @ 298 K	18.3	18.9	19.5	20.3	11.9*
Viscosity, cps @ 298 K	534	516	464	381	2665.
Pour Point, K (F)	275. (36)	268. (23)	269. (25)	276. (38)	338. (149)
Conradson Carbon Residue, wt%	1.85	2.53	2.16	1.27	11.8
Ash Content, wt%	0.07	0.0	0.0	0.01	
Simulated Distillation, wt%					
IBP, °F	428	392	385	428	464
Volatility, wt%	90.7	86.6	92.3	88.2	40.5
IBP-400°F, wt%	0.7	0.9	1.1	0.0	0.0
400-650°F, wt%	23.9	22.2	26.7	24.4	4.9
650-1000°F, wt%	66.2	63.5	64.6	63.8	35.6
>1000°F, wt%	9.3	13.4	7.8	11.8	74.6
Elemental Analysis					
C, wt%	86.1	85.8	86.0	86.7	83.3
H, wt%	11.5	11.4	11.3	11.5	11.0
N, wt%	1.0	0.9	0.9	0.8	1.3
S, wt%	0.2	0.2	0.2	0.2	0.3
O, wt%	1.2	1.7	1.6	0.8	4.1
H/C Atomic Ratio	1.60	1.60	1.58	1.59	1.58

*Measured at 358 K.

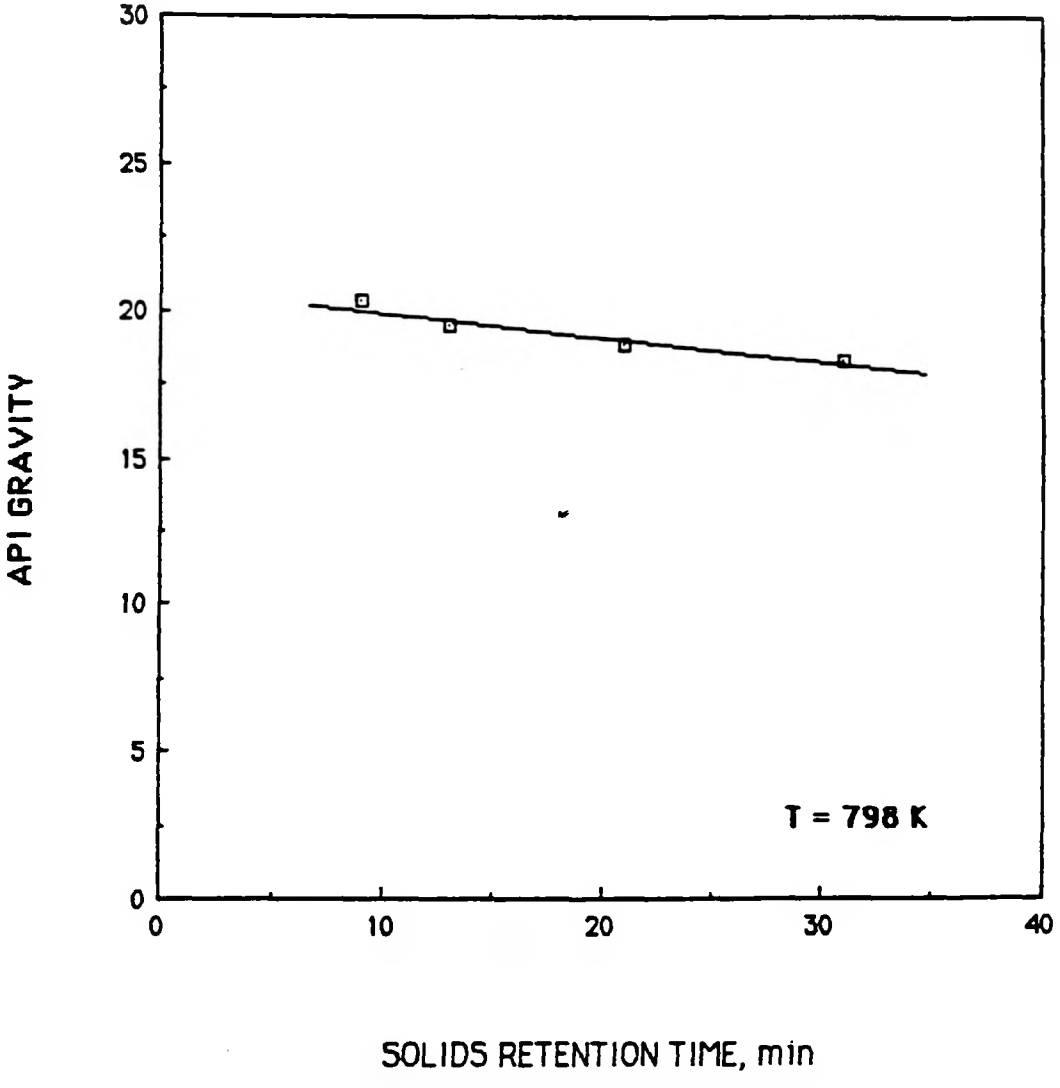

Figure 28. Effect of Solids Retention Time on API Gravity

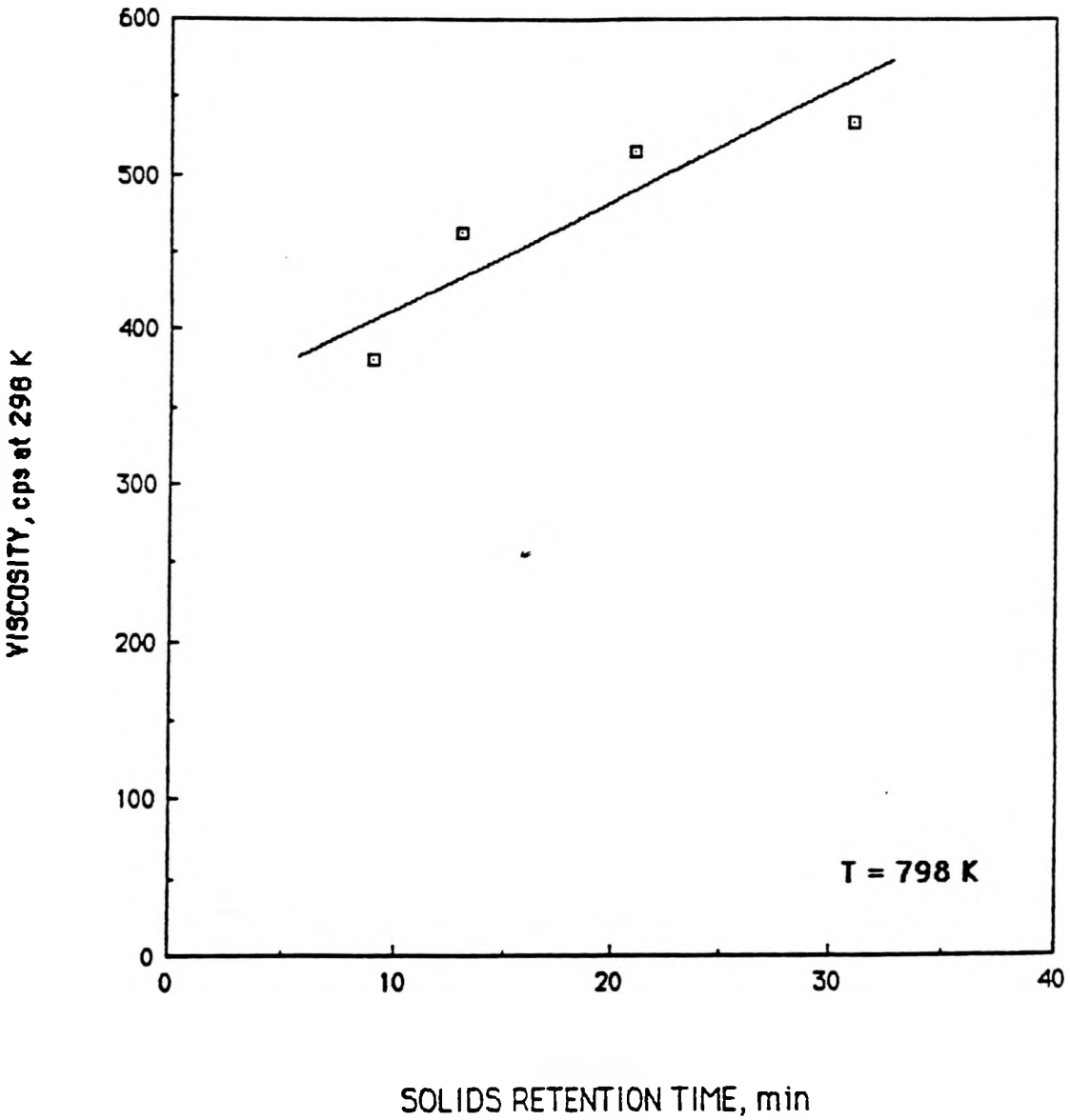

Figure 29. Effect of Solids Retention Time on Viscosity

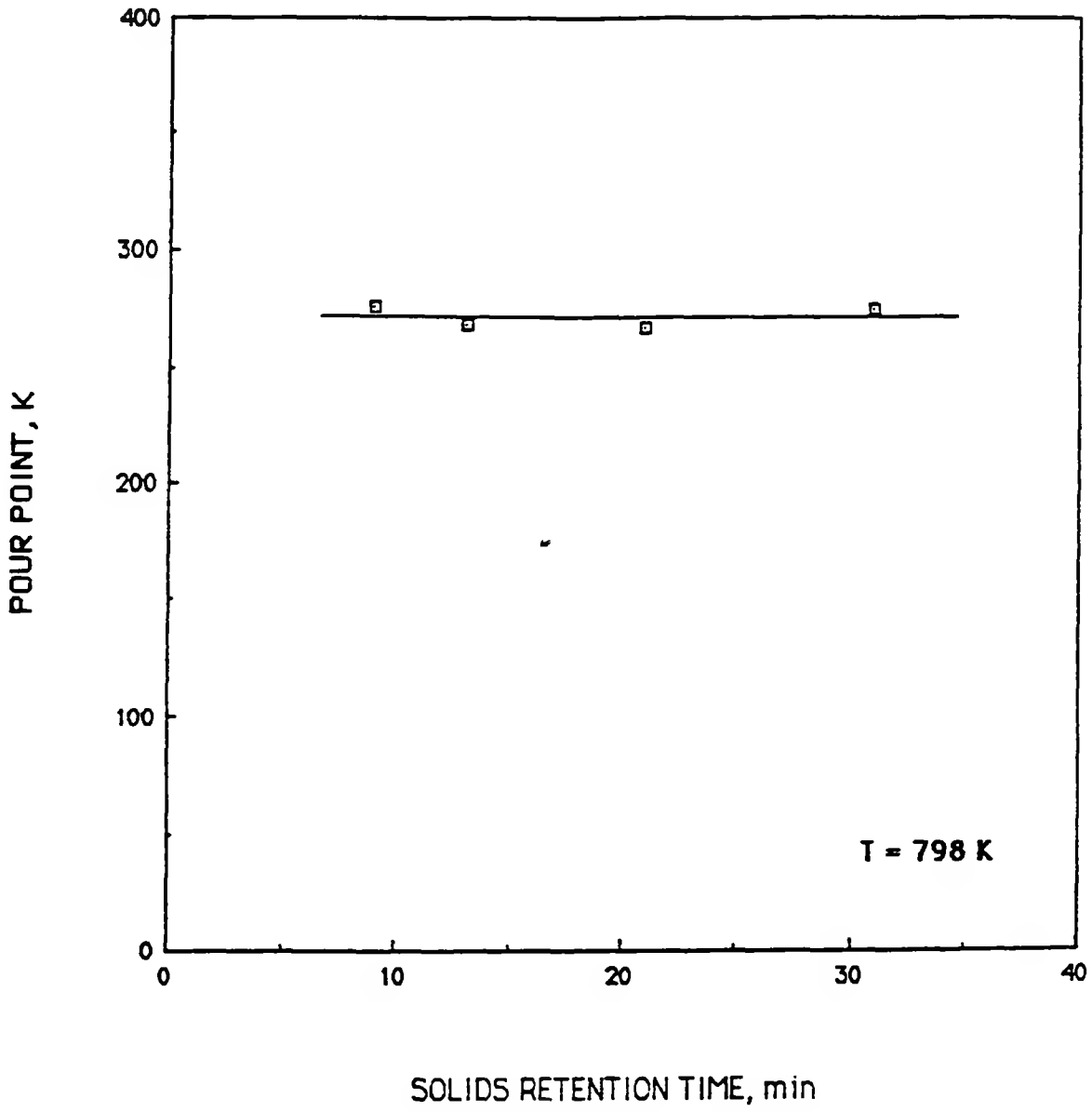

Figure 30. Effect of Solids Retention Time on Pour Point

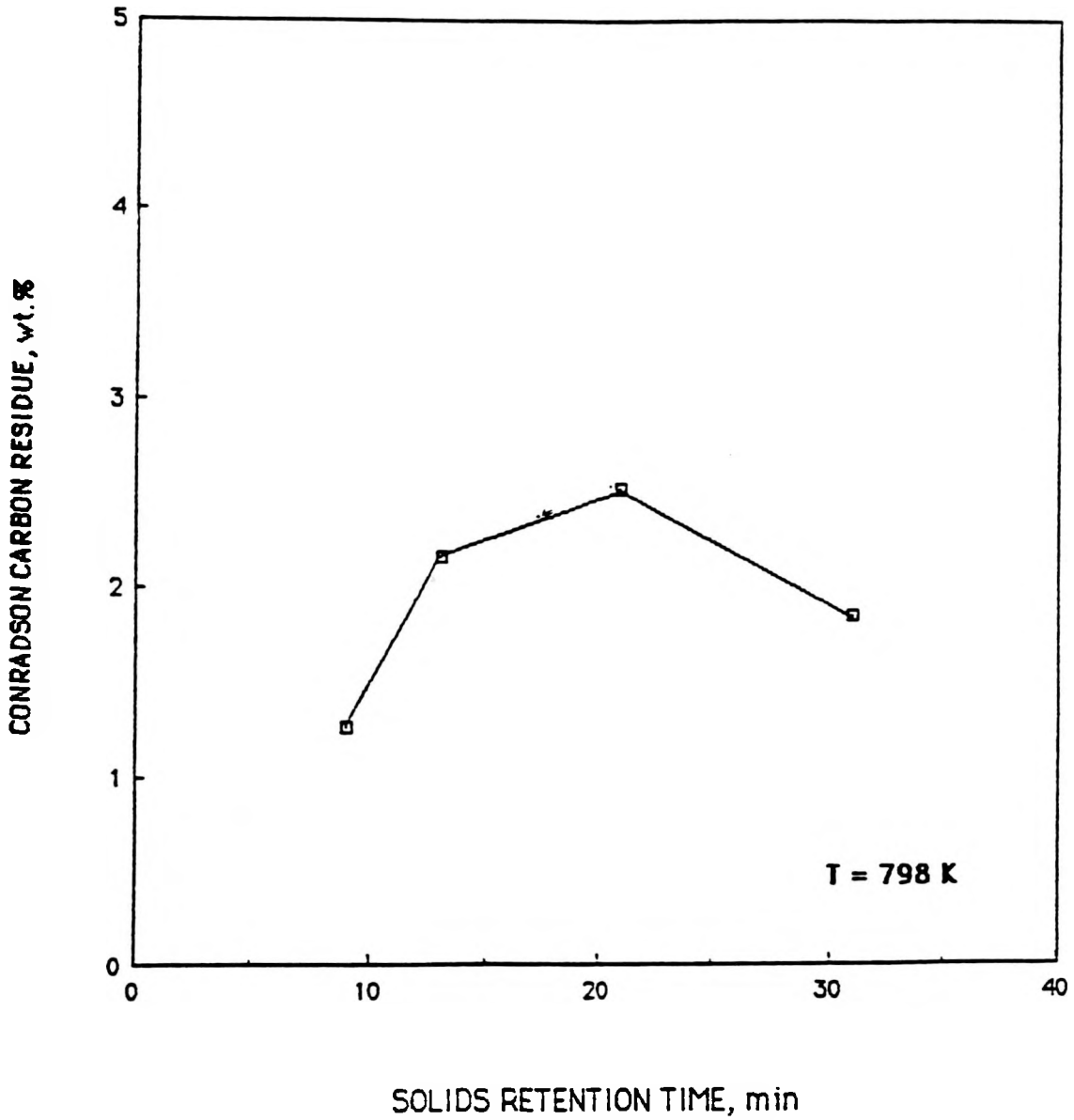

Figure 31. Effect of Solids Retention Time on Carbon Residue

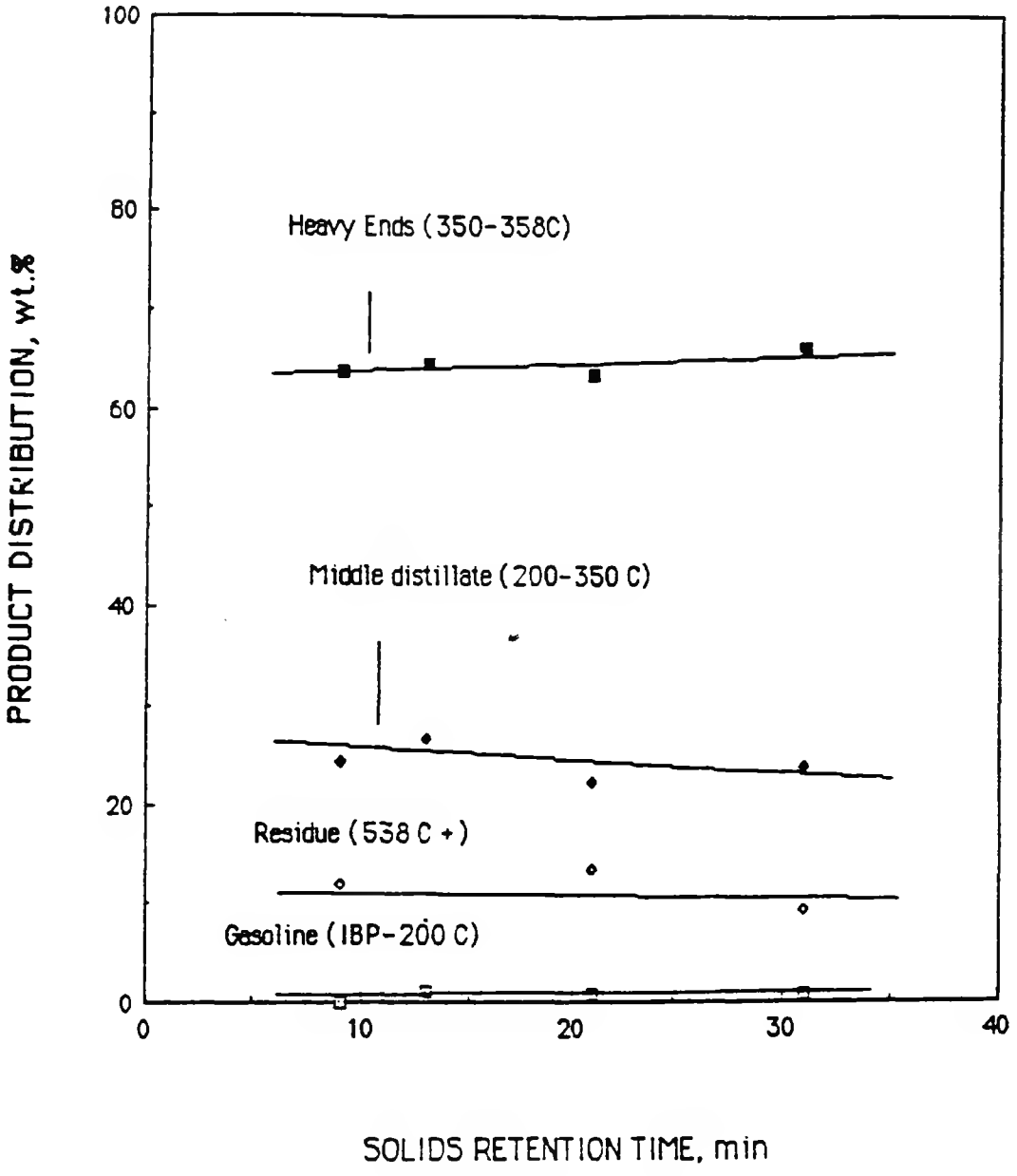

Figure 32. Effect of Solids Retention Time on Fractions of Product Liquids

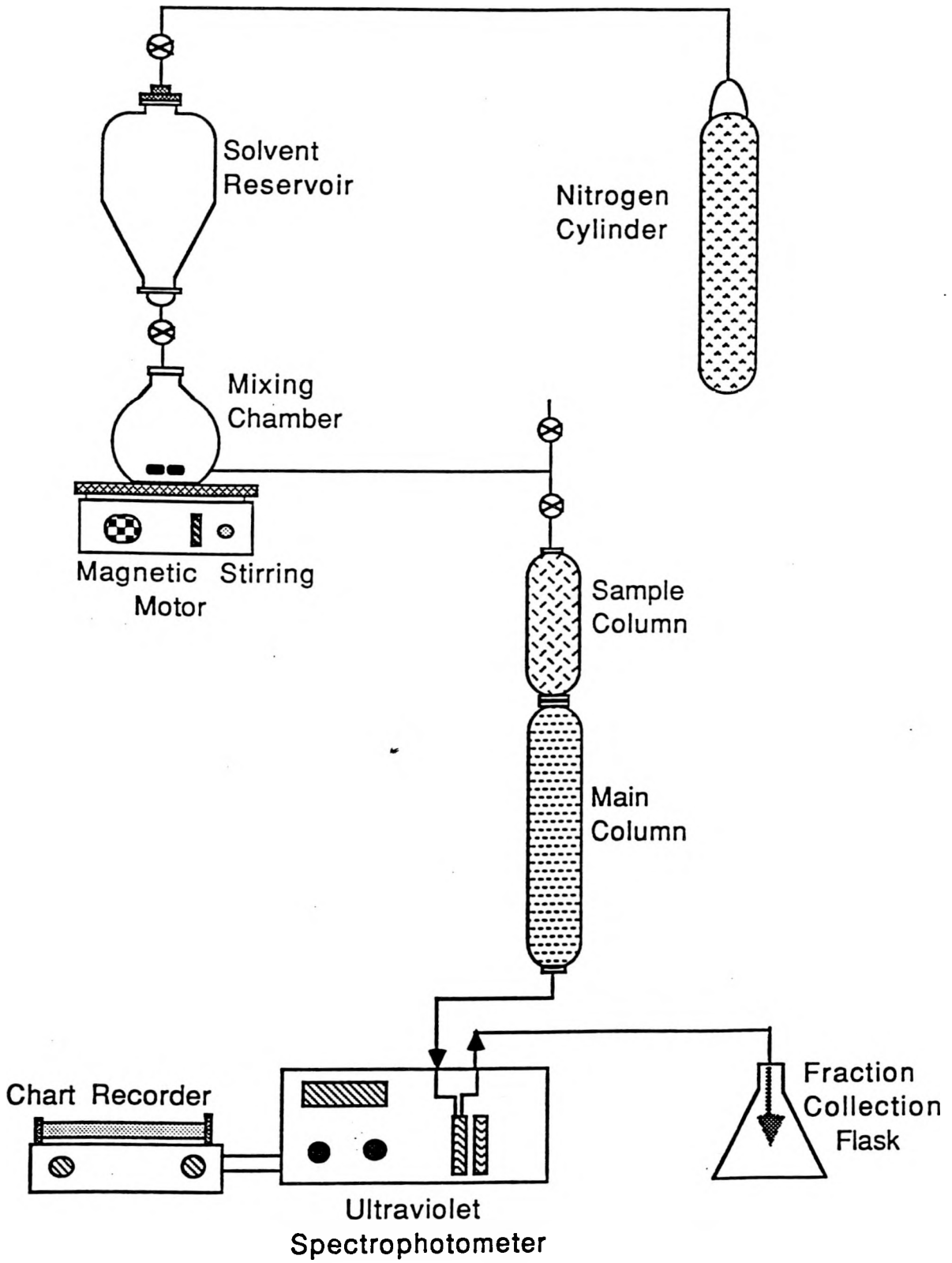

Figure 33. Schematic of the Gradient Elution Chromatography Apparatus

were weakly adsorbed on the alumina, were eluted first. The asphaltenes, which were bonded strongly to the alumina, were eluted last. The solvent flowing from the column passed through a Varian Techtrom Model 634S variable wavelength UV-VIS spectrophotometer. In order to obtain material balance the solvent was evaporated from each fraction by rotavapor (Büchi RE120) distillation. The losses in material were attributed to noneluted asphaltenes. The GEC procedure provided a method of quantifying the upgrading of the pyrolysis product liquids relative to the native bitumen by providing an overview of the shift from more refractive compounds in the native bitumen to more desirable compounds in the bitumen-derived liquids.

The GEC data for the native bitumen and the bitumen-derived liquids produced in the rotary kiln from the Whiterocks tar sand are presented in Table 18. In addition, the effect of the solids retention time on the chemical composition of the bitumen-derived liquids from the Whiterocks tar sands is shown in Figure 34.

The trends in API gravity with respect to solids retention time are consistent with the trends in chemical composition of the product liquids as shown in Figure 34. As the retention time was increased, the severity of thermal cracking was increased. Under these conditions, the alkyl side chains were cracked from the PNA groups and the linkages between the PNA groups were broken. The alkyl groups were cracked further to smaller groups which volatilized and passed from the reactor in the light gas. Thus, at longer retention time, the aromaticity of the product liquids was increased, along with a similar increase in the asphaltene content. The saturates content decreased significantly with increasing solids retention time. These trends are consistent with the decrease in API gravity of the product liquids and are indicative of the enhancement of thermal cracking by increased solids retention times. A similar trend was obtained with the P.R. Spring tar sands in a fluidized-bed pyrolysis study.

DISCUSSION

Originally, the rotary kiln unit used a water trap as a product recovery system on the gas outlet to ensure positive pressure (1-inch H_2O) inside the kiln. However, a large amount of mist (liquid vapor) passed from the reactor through the flue gas pipe to the stack. Because vapor bubbles were formed in the water and they carried the mist and dust to the flue gas pipe, most of the mist was not collected by the water trap. Thus, this water trap recovery system was modified using two water traps in series on the gas outlet. Unfortunately, the same mist problem occurred. These water traps did not work at all for the tar sand pyrolysis case. Another modification of the recovery system included using a 5-gallon solvent disposal container and a 1-inch diameter PVC tubing with cellulose fiber. The five-gallon container was used as the liquid product accumulator, and PVC tubing with cellulose fiber was used as a series of mist collectors. For the mist collectors, large-diameter tubing (1-inch diameter) was selected to reduce the pressure drop in the unit. Finally, most of the mist was collected by this recovery system when the cellulose fiber in the tubing was saturated by the liquid product.

Table 17
Solvent Order for GEC

Order	Composition
1.	360 cc n-pentane
2.	7.5 cc $MeCl_2$ + 242.5 cc n-hexane
3.	15 cc $MeCl_2$ + 235 cc-hexane
4.	22.3 cc $MeCl_2$ + 5 cc THF + 222.5 cc n-hexane
5.	30 cc $MeCl_2$ + 10 cc THF + 210 cc n-hexane
6.	375 cc $MeCl_2$ + 15 cc THF + 197.5 cc n-hexane
7.	45 cc $MeCl_2$ + 20 cc THF + 185 cc n-hexane
8.	52.5 cc $MeCl_2$ + 25 cc THF + 172.5 cc n-hexane
9.	62.5 cc $MeCl_2$ + 30 cc THF + 157.5 cc n-hexane
10.	250 cc THF
11.	37.5 cc MeOH + 212.5 cc THF
12.	37.5 cc MeOH + 10 cc H_2

where THF = Tetrahydrofuran
$MeCl_2$ = Dichloromethane
MeOH = Methanol
H_2O = Distilled Water

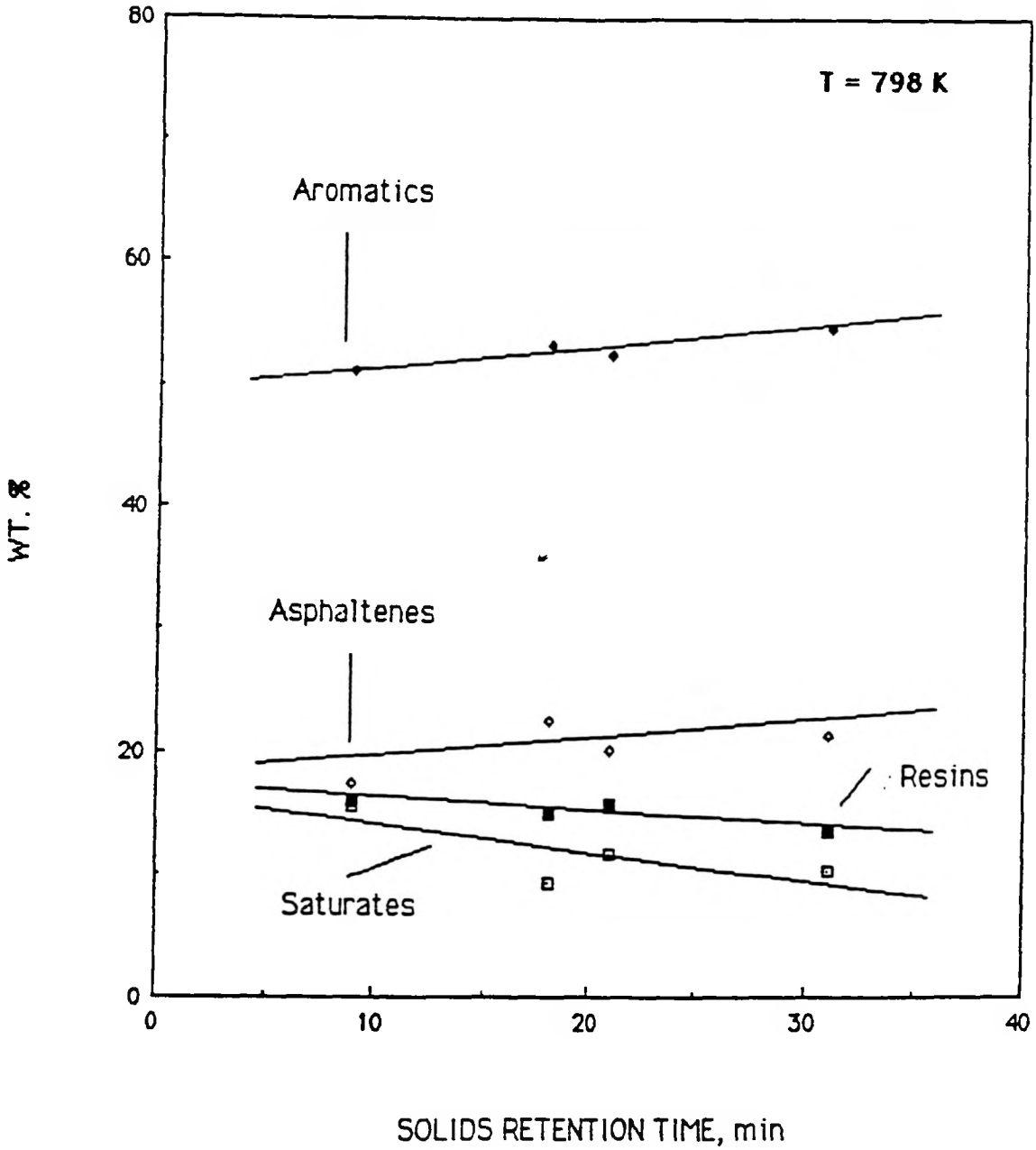

Figure 34. Effect of Solids Retention Time on the Chemical Composition of the Product Liquids

Table 18

Chemical Composition of the Bitumen-Derived Liquids from the Whiterocks Tar Sands

Run ID Number	WR-RK-1	WR-RK-2	WR-RK-3	WR-RK-4	Native Bitumen
Reactor Temp., K	798	798	798	798	
Solids retention time, min	31	21	13	9	
N_2 gas flow rate, SCFH	77.5	77.5	77.5	77.5	
Gradient Elution Chromatography					
Saturates, wt%	10.3	11.7	9.4	15.5	18.3
MNA/DNA oil, wt%	36.7	41.7	41.4	39.7	5.5
PNA oil, wt%	18.1	10.8	11.9	11.5	11.3
Soft resin, wt%	11.4	12.5	12.0	13.3	13.8
Hard resin, wt%	0.9	1.5	1.2	1.3	3.0
Polar resin, wt%	1.3	1.7	1.7	1.3	1.6
Asphaltenes, wt%	12.9	12.9	13.1	9.5	29.6
Noneluted asphaltenes, wt%	8.4	7.2	9.3	7.9	16.9

The pressure drop in the rotary kiln had to be limited to 16 inches of H_2O, because any increase in the pressure drop within the kiln above this design specification caused the rotary seals to leak. This made it difficult to install the mist collector on the gas outlet because the mist collector created a pressure drop inside the unit.

The degree of mixing in the vapor space within the kiln appeared to be a significant parameter, especially at the higher feed rate. At low sweep gas flow rates, stratification of the nitrogen and hydrocarbon vapor phases took place. Thus, the heavier hydrocarbon vapor phase moved concurrently with the solid phase and condensed in the outlet region of the kiln rather than moving countercurrently to the product recovery section. At high sweep gas flow rates, the nitrogen and hydrogen vapors were well mixed and passed out of the reactor into the product recovery system.

The retention time of solids was not directly proportional to the screw feeder rates. According to the theoretical calculation of the dwell time in the rotary kiln, the theoretical dwell time is directly proportional to L/NDS where L is a hot zone length, N is a kiln rotational speed (rpm), D is a diameter of the kiln, and S is a slope of the kiln. Thus, at the constant rotational speed, the dwell time was only dependent on the kiln inclination in this unit.

In the temperature profiles of the rotary kiln, the maximum temperature of 793 K was obtained when the setpoint was 798 K. The temperature was measured when the kiln was empty. Thus, the temperature profile was not the same as that in the real run. Another temperature profile of the kiln has been measured by the Harper Electric Furnace Corporation when the temperature setpoint was 1100 °C. This profile showed that half of the entire kiln length was in the desired temperature range.

It is important to discuss the extent of upgrading of liquid products that takes place during the pyrolysis process. The good quality of the liquid products is one distinct advantage of a thermal processing scheme over alternate bitumen-sand separation technologies. Properties of the liquid products from the pyrolysis of the Whiterocks tar sands are presented in Tables 14 and 16, along with the properties of the native bitumen. It can be seen that in all cases the API gravity and volatility of the product liquids were increased substantially over the native bitumen while the viscosity, Conradson carbon residue, and pour point were markedly decreased. In addition, the amount of preferred components (mono- and dinuclear aromatics) in the product liquids were increased at the expense of asphaltenes.

CONCLUSIONS

A commercially-available rotary kiln reactor was evaluated for the Whiterocks tar sand pyrolysis at the Harper Electric Furnace Corporation. The feasibility of the pyrolysis of bitumen-impregnated sandstone in the commercially-available rotary kiln reactor in a continuous mode was demonstrated. Four steady-state experiments were completed at the reactor

temperature of 798 K for solids retention times ranging from 9 to 31 minutes. The effect of solids retention time on the product distribution was investigated and the bitumen-derived liquids produced in the rotary kiln pyrolysis process were also analyzed and characterized.

The liquid yield increased with decreasing solids retention time. The gas yield decreased steadily as solids retention time decreased. The increase in the liquid yield as the solids retention time decreased was accompanied by a decrease in the gas yield. The coke yield was essentially insensitive to changes in solids retention time. The API gravities of the liquid products decreased at a constant reactor temperature as the solids retention time increased. The viscosities of the liquid products increased with increasing solids retention time. The pour point and atomic H/C ratio of the liquid products remained essentially constant with respect to solids retention time, along with a similar increase in the asphaltene content. The saturates content decreased significantly as the solids retention time increased.

MODIFIED HOT-WATER SEPARATION TECHNOLOGY

J.D. Miller	Co-Principal Investigator
K. Bukka	Postdoctoral Fellow
Y.J. Yang	Graduate Student

The research work carried out during the period 1988-1989 is divided into three topics. The first is a continuation of the studies of water-assisted extraction of bitumen; the second is concerned with characterization studies of Asphalt Ridge and Sunnyside bitumens; while the third involves assessing the potential of bitumen fractions as specialty resins. More specifically, the three topics are:

1. Selection and evaluation of diluents in the modified hot-water process.

2. Fractionation and characterization of Asphalt Ridge and Sunnyside tar sand bitumens.

3. Comparison of Hiawatha coal resins with those derived from Asphalt Ridge and Sunnyside tar sand bitumens.

INTRODUCTION

Bitumens occurring in different Utah tar sand deposits show very divergent physical properties and chemical compositions. The characteristic features of Utah tar sands include bitumens of very high viscosity, relatively coarse sand grains, very low content of clays, and the consolidated nature of the sand. Some of these features are advantageous in the processing, while others make it difficult. Whereas chemical composition greatly influences[75] the upgrading and subsequent refining processes of the extracted bitumen, physical properties play a vital role in the way it is recovered from the tar sands. One remarkable difference in the physical property is in viscosity, a difference which prompted the development of different strategies to recover bitumen from these tar sands. This situation is in contrast to the Canadian tar sands, which have almost uniform properties and compositions, regardless of their location. The strategies developed for Utah tar sands include ambient temperature bitumen recovery,[76] hot water,[77] and modified hot-water[78] separation methods. Each one of these was developed for a particular deposit, and no one method of the three can be applied in a satisfactory manner to all Utah deposits, although the modified hot-water process is the most versatile of the three and can treat almost all tar sand types. In addition, the Utah tar sands are considered to be structurally unique in that they lack a fine layer of connate water around the sand particles as assumed for Canadian tar sands. Presence of this aqueous layer is considered[79] to be the single most characteristic and fortunate feature of

the Athabasca oil sand, as this is understood to facilitate relatively easy recovery of bitumen from tar sands by hot water processing. As the bitumen in Utah deposits is in intimate contact with the sand surface, greater forces are required to displace the bitumen.

The principle involved in the development of the modified hot-water processing method for Utah deposits has been the control of bitumen viscosity in the tar sands. The process essentially consists of the same two steps, *viz.*, digestion of tar sand pulp at temperatures in the range of 50 - 60 °C, followed by flotation. Control of bitumen viscosity in the tar sands is accomplished mainly by increasing the temperature during digestion in the cases of low and moderate viscosity bitumens, and a combination of diluent addition and high temperature in the case of high viscosity bitumens. For convenience, Utah tar sands have been categorized on the basis of bitumen viscosity into four different types. Table 19 lists the details of the criteria on which the classifications have been made. Although with the use of the modified hot-water process, bitumen recoveries have been realized in the laboratory and in pilot plant scale operations for tar sand containing light and moderate viscosity bitumens, they are not as effective for tar sands containing bitumen of high and very high viscosities. Since a very significant portion of the Utah deposits fall into this category, studies have been carried out to improve the efficiency of bitumen recovery from these tar sands containing highly viscous bitumen.

Table 19
Classification of Tar Sands According to Bitumen Viscosity

Tar Sand Type	Bitumen Character	Bitumen Viscosity @°C(Pa.S) 50	90	Recommendations for Hot-Water Processing
I	Light	10^0	10^{-1}	Diluent unnecessary
II	Moderate	10	10^{-1}-10^0	Diluent optional
III	Heavy	10^2-10^6	10^0	Diluent necessary
IV	Very heavy	$\geq 10^6$	10^3	Tar sand not amenable to hot-water separation

It has been determined from our earlier work that when the viscosity of bitumen in the tar sands at processing temperature is reduced to a value in the range 0.5 - 1.5 Pa.S recoveries were greatly improved.[78]

Addition of a diluent also facilitated higher recoveries at lower temperatures. In these studies, kerosene has been used as the diluent. The considerations for choosing kerosene are perhaps cost and availability, which are important factors from an industrial perspective.

In this study, an attempt was made to find whether or not the reduction of bitumen viscosity in tar sands can be optimized by changing the nature of the diluent. In these studies, a variety of diluents were selected and their effect on bitumen viscosities were examined. Since tar sands are processed at 50-95 °C, diluents of a higher boiling point/range were considered (with the exception of cyclohexane). Diluents used were cyclohexane, SC-2, SC-150, ethyleneglycol-di-butylether (EGBE), and xylene. Kerosene was also included for comparison purposes. The diluents SC-2 and SC-150 are designated industrial aromatic solvents which were obtained from Chemcentral Corporation. The differences between these two diluents and the details of diluents used are presented in Table 20. The choice of these diluents, besides being industrial solvents, was an arbitrary decision as a first step in determining optimum properties for diluents.

Table 20
Some Physical and Chemical Characteristics of Diluents

			Percentage Composition by Volume		
Diluent	Sp. Gravity	Boiling Point/Range Temp. °C	Saturates	Aromatics	C_{8+} Aromatics
Cyclohexane	0.779	81	100	0	0
Ethylene-glycol-n-dibutyl-ether	0.900	171	100	0	0
Kerosene	0.818	177-272	80	0	19
SC-2	0.844	138-153	18	8	74
SC-150	0.899	183-210	2	0	98
Xylene	0.871	138-140	0	26	74

EXPERIMENTAL

Bitumen samples for viscosity measurements were obtained from the respective tar sand deposits by the Dean-Stark extraction method using toluene as the solvent. Toluene solutions were centrifuged to separate fine solids, and the supernatants were removed by distillation using a rotary evaporator to obtain bitumen. Cyclohexane and xylene were reagent grade. The other diluents used, ethyleneglycol-n-dibutylether (EGBE), kerosene, SC-2, and SC-150, are commercial grade solvents obtained from Chemcentral Corporation. Bitumen samples selected for study were derived from Sunnyside, P.R. Spring, and Asphalt Ridge tar sands of Utah. These bitumens, which include bitumens of high viscosity (reported earlier),[80] are presented in Table 21. For comparison purposes, the value of Athabasca bitumen is also included.

Table 21
Comparison of Bitumen Viscosities Derived from
Different Tar Sands at 50°C

Source of Bitumen	Viscosity, Pa.S.
Sunnyside, Utah	1500
P.R. Spring	280
Asphalt Ridge	80
Athabasca, Alberta	5

Viscosity measurements of bitumen-diluent mixtures were made on a Wells-Brookfield cone and plate viscometer (Model 35XHBT). The cone and plate assembly were enclosed in a water jacket, and the temperature was controlled by circulating water from a thermostat. Measurements were made in the temperature range 25-65 °C. The ratio of bitumen to diluent was determined by the viscosity of pure bitumen and viscosity range of the instrument.

Diluent Evaluation in the Batch Processing of Sunnyside Tar Sands

Relative efficiencies of kerosene and SC-150 as diluents were evaluated in the bitumen recovery from Sunnyside tar sands using a low-shear energy digester. A schematic of the hot-water process for the recovery of bitumen from tar sands is outlined in Figure 35. Tar sand samples were ground, and only fractions that passed #4 mesh (Tyler, 4.7 mm

opening) were used in the test runs. Diluent was added to 4 kg batch of ground tar sand, mixed well, and set aside for 24 hours to permit the diluent to penetrate into the sample matrix. Processing was carried out in a 38 liter Denver type flotation cell. Solids concentration during digestion was maintained at 25-30%, and in the Ph range 7.5-9.0 which is controlled by the addition of sodium carbonate (4 gm). A rotorstator impeller turning at 900 rpm recirculated the slurry (the air suction valve was closed during digestion) combining shear, impact, collision, and circulation effects. After a specified period of digestion, the flotation cell was filled with water at the same temperature and the air suction valve was opened. The solids content in the flotation step was maintained at 10%. The bitumen concentrates collected in the froth were filtered and air-dried. In some cases, undigested feed (middlings) which reported to the tailings was separated by sievings (#28 Tyler mesh, 600 μ opening). Analysis of bitumen and solids in concentrates, middlings, and tailings was carried out by the Dean-Stark method.

The process efficiency was expressed by the term "separation coefficient," which is a measure of the fraction of the feed that undergoes a perfect separation.[81] For a binary system like tar sand, it can be shown that the separation coefficient (SC) is equal to the difference between percentage recovery of bitumen and sand in the concentrate.

RESULTS AND DISCUSSION

Viscosity data on various bitumen-diluent mixtures obtained as a function of temperature are presented in Tables 22-24. Each table clearly shows that viscosity reduction capacities of the diluents are quite varied, and in some cases the difference between the diluents for a given bitumen is almost one order of magnitude. In a similar study using Athabasca bitumen and hydrocarbon solvents, it has been shown[82] that the differences among the solvents were relatively small. It was concluded that for Athabasca bitumen, among the solvents used, those with features such as high molecular weight, branching in the solvent molecular structure, aromatic and alicyclic natures were less effective in reducing the viscosity than straight-chain low-molecular-weight hydrocarbons.

The large differences between the diluents in this study is perhaps not unexpected due to the complex nature of bitumen in which various constituent components are distributed in a characteristic assemblage. For a similar material like asphalt, it has been understood[83,84] that solid asphaltenes are suspended in liquid hydrocarbons and the suspension is stabilized by the resins which act as surfactants. Extending this view to bitumen, it can be imagined that these enhanced interactions lead to formation of a three-dimensional gel-like structure. With the addition of a diluent, the inherent physical structural network of bitumen is partially modified. It can be implied that a diluent which effectively brings about such a large structural disorganization could be expected to

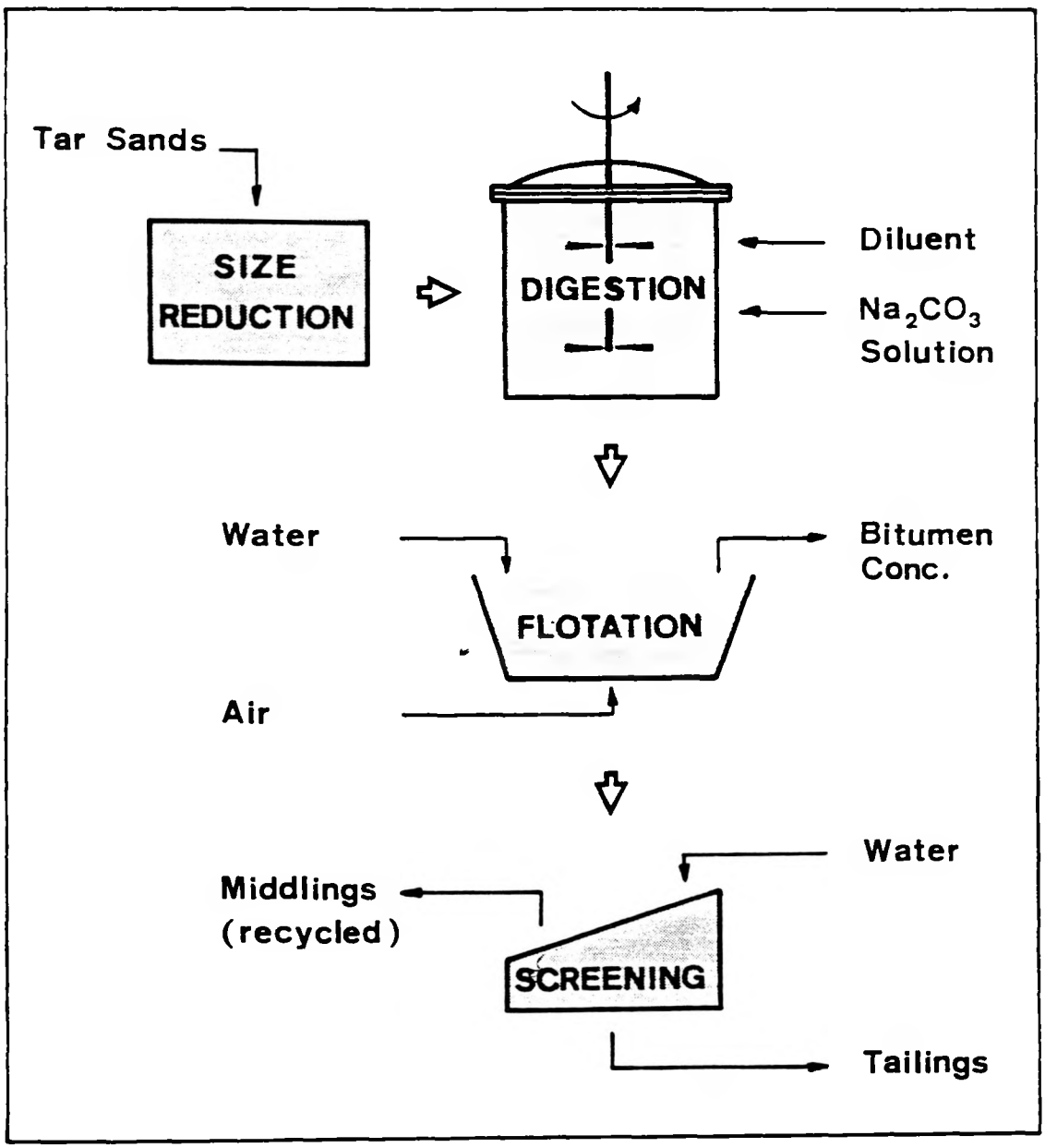

Figure 35. Schematic of the Hot Water Process for the Recovery of Bitumen from Tar Sands

Table 22
Viscosity of Asphalt Ridge Bitumen-Diluent Mixtures
(20% w/w Diluent)

Temp., °C	Viscosity, Pa.S.					
	Diluent					
	Xylene	Cyclohexane	SC-2	Kerosene	EGBE	SC-150
25	--	--	--	8.53	8.35	4.00
33	16.00	12.10	8.90	4.05	3.96	2.20
41	8.82	6.47	4.85	2.23	2.14	1.26
49	5.00	3.99	2.82	1.26	1.21	0.78
57	2.80	2.12	1.67	0.76	0.74	0.51
65	1.72	1.13	1.03	--	--	0.36

Table 23
Viscosity of P.R. Spring Bitumen-Diluent Mixtures
(36% w/w Diluent)

Temp., °C	Viscosity, Pa.S.					
	Diluent					
	Xylene	Cyclohexane	SC-2	Kerosene	EGBE	SC-150
25	7.44	--	15.10	2.70	11.65	2.07
33	3.96	11.40	7.90	1.55	5.91	1.21
41	2.31	5.62	4.40	0.84	2.75	0.75
49	1.42	3.12	2.72	0.46	1.71	0.48
57	0.94	1.90	1.67	0.30	0.99	0.34

Table 24

Viscosity of Sunnyside Bitumen-Diluent Mixtures
(36% w/w Diluent)

Temp., °C	Viscosity, Pa.S.				
	Diluent				
	Cyclohexane	Kerosene	EGBE	SC-150	Xylene
25	--	15.65	15.53	2.99	24.35
33	--	7.12	7.00	1.69	12.50
41	--	3.88	3.96	1.08	6.95
49	--	2.02	1.79	0.70	4.80
57	11.73	1.02	0.95	0.46	2.53
65	6.80	0.62	0.64	0.34	1.69

greatly reduce the viscosity. In other words, a diluent with better solvating properties will decrease the viscosity in a more efficient manner.

For the three bitumen samples studied, viscosity reduction capacities of the diluents at room temperature followed this order.

In the case of Asphalt Ridge bitumen,

SC-150 > EGBE > kerosene > SC-2 > cyclohexane > xylene.

In the case of P.R. Spring bitumen,

SC-150 > kerosene > xylene > EGBE > SC-2 > cyclohexane.

In the case of Sunnyside bitumen,

SC-150 > EGBE = kerosene > xylene > cyclohexane.

In most cases, the observed order of diluents for a given bitumen is maintained even at higher temperatures. It can be seen from Figures 36-38 that the lines representing the relationship between viscosity and temperature are almost parallel to each other. However, there is an exception in the case of P.R. Spring bitumen, in which two diluents, kerosene and EGBE, appear to improve their relative positions in the order at higher temperatures.

It also becomes apparent from the results that the observed order of diluents does not remain the same when the bitumen sample is changed. Except for diluent SC-150, the relative positions of the other diluents are significantly altered. Lack of consistency in the order of diluents suggests that there may be some specific interactions operating between diluent and bitumen. It also indirectly indicates that a change in the order of the diluents is a result of differences in the chemical compositions of bitumens. Bunger et al.[75] have amply demonstrated that there are significant differences in the chemical compositions of the bitumens occurring in Utah tar sands.

In an attempt to relate viscosity-reducing capacities of diluents to some of their properties, Table 19 is presented. Although it is difficult to identify any relationship with the outlined properties, it appears that an effective diluent would require a high boiling range with a blend of large amounts of aromatic and some aliphatic hydrocarbons. It has been found[85] that highly aromatic solvents dissolve bitumen faster than a paraffinic solvent such as kerosene. However, there is also evidence that solvent properties other than aromaticity are also important. Funk[86] from his spinning disc experiments on the dissolution of bitumen in paraffinic and aromatic solvents concluded that in the case of paraffinic solvents, the principal resistance to dissolution resides in the bitumen layer and not in the transport across the solvent-bitumen interface, whereas the aromatic solvents rapidly dissolve the bitumen but encounter resistance in the mass transport. From these considerations, it appears that a blend of aromatic and paraffinic components in the diluent SC-150 play supplementary roles in the task of reducing the viscosity of the bitumen. SC-150

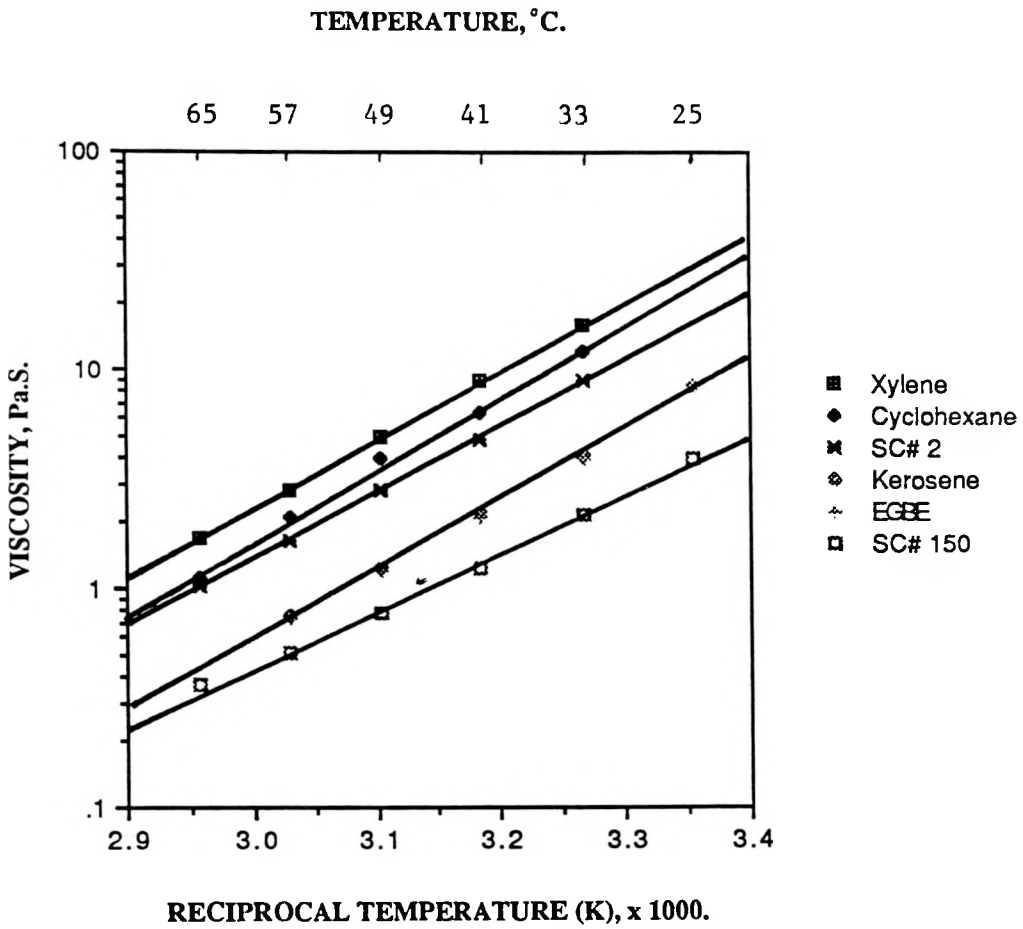

Figure 36. Variation of Asphalt Ridge Bitumen Viscosity with Temperature (20% Dil. w/w).

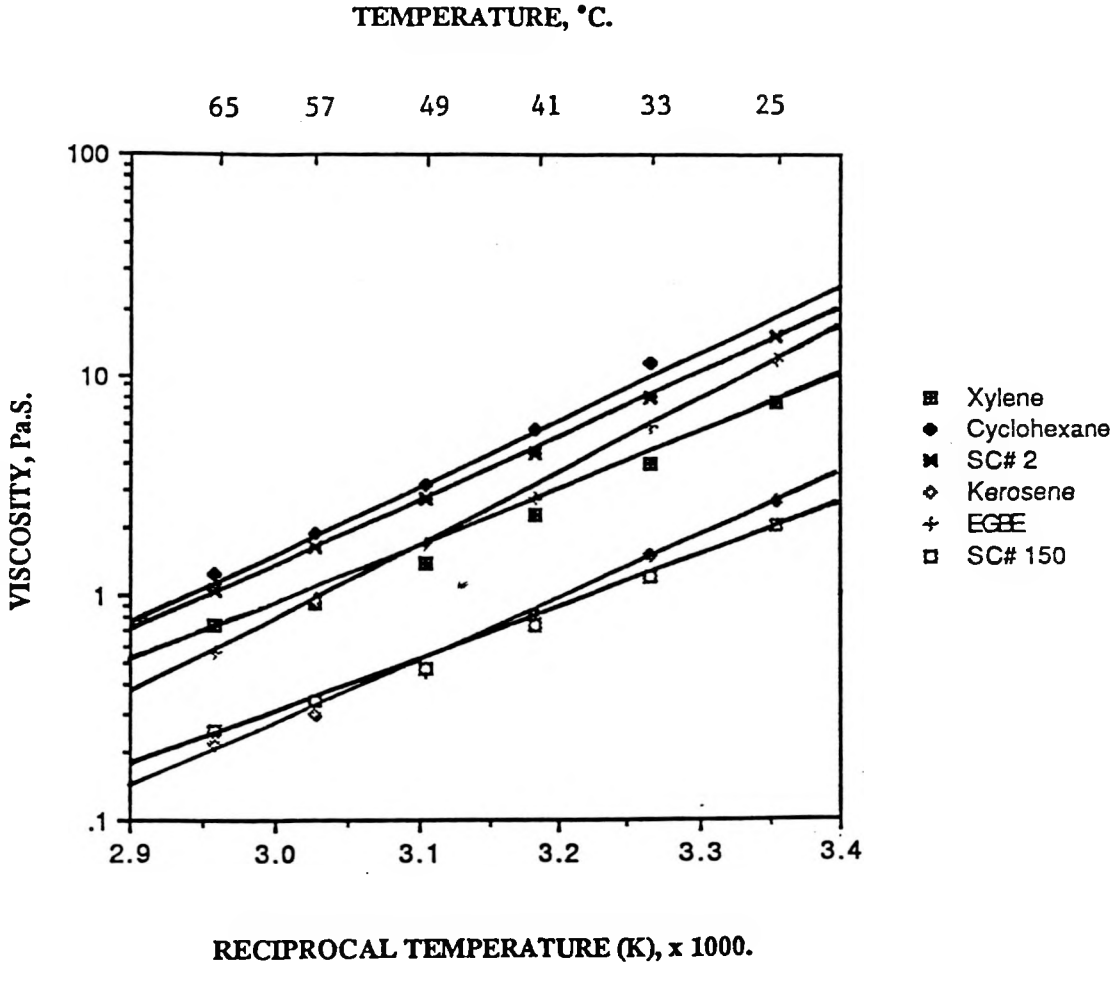

Figure 37. Variation of P.R. Spring Bitumen Viscosity with Temperature (36% Diluent, w/w).

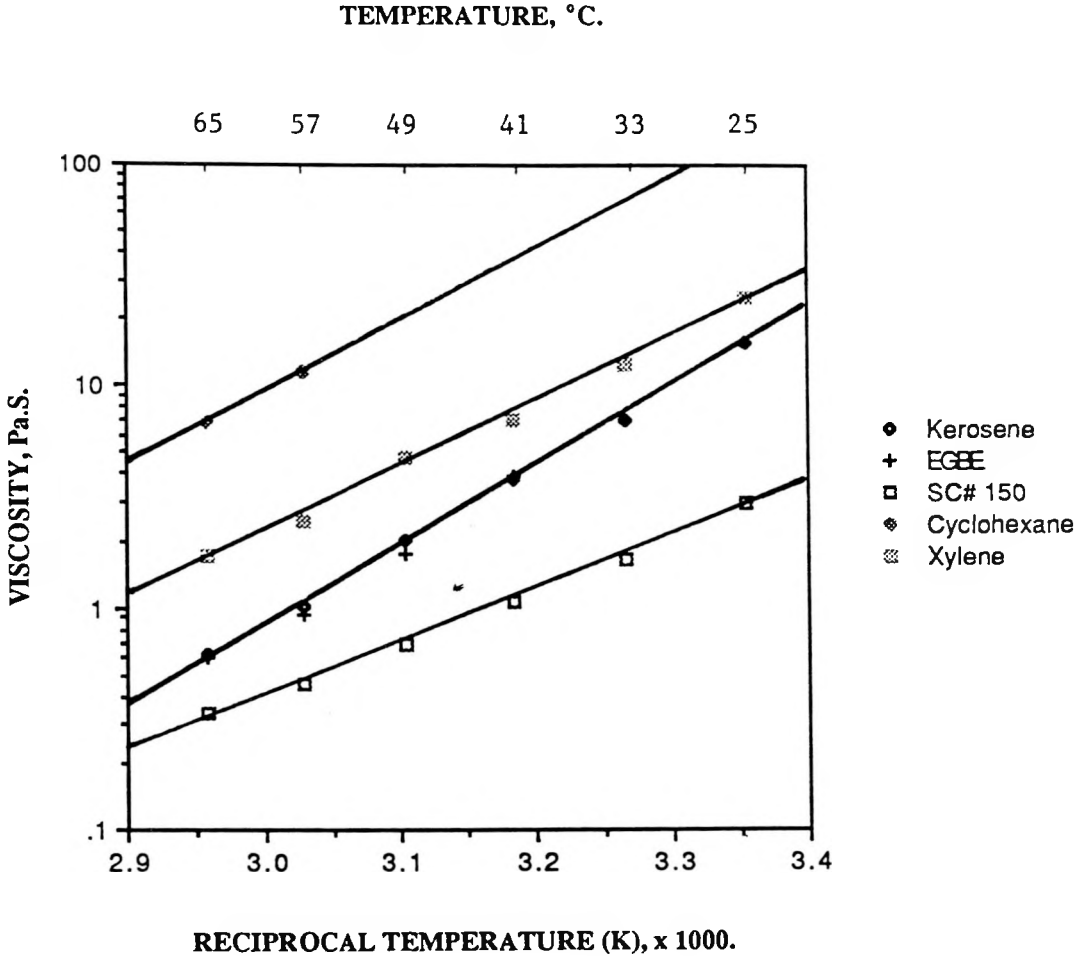

Figure 38. Variation of Sunnyside Bitumen Viscosity with Temperature (36% Diluent, w/w).

is a designated aromatic hydrocarbon solvent, consisting predominantly of C_{8+} components with a combination of methyl, ethyl, and propyl substitutions in the benzene ring.

Another interesting feature which is noticeable from this study is that while a highly viscous bitumen (Sunnyside) enhances the difference between two different diluents, *viz.*, kerosene and SC-150, low-viscosity bitumens (Asphalt Ridge) appear to diminish their viscosity-lowering capacity. This is perhaps indicative of the leveling effect. In other words, as described earlier, the structural network of low-viscosity bitumen is not extensive; therefore, the subtle differences in the effects of diluents become smaller.

The effect of temperature on the viscosity of bitumen-diluent mixtures are presented in Figures 36-38. Linear relationships were obtained when ln (viscosity) was plotted against reciprocal temperature (°K). The relationship is expressed as:

$$Viscosity = A\, e^{B/T}$$

From results presented in Tables 21-23, it is clear that diluent SC-150 consistently reduces the viscosities of all three bitumens in a most efficient manner. Since the principal consideration for using a diluent in a modified hot-water process is to reduce the viscosity of bitumen in tar sands, and thereby attain better recoveries, clearly SC-150 becomes a preferable diluent. In order to verify this point, SC-150 was chosen as a diluent for the recovery of bitumen from Sunnyside tar sands using the modified hot-water process. However, kerosene was also used to compare the test results with those obtained from SC-150. The choice of Sunnyside tar sands is based on the fact that its high-viscosity bitumen seems to accentuate the difference between kerosene and SC-150.

Evaluation of Diluent in the Modified Hot-Water Processing of Sunnyside Tar Sands

A total of 14 test runs were made at two different temperatures and at three levels of diluent additions. Among these are included two control runs without any diluent addition. The amount of diluent added is expressed as a weight percentage of the sum of the bitumen present in the feed and diluent. Evaluations of diluents are made on the basis of their effects on recovery parameters such as quality of bitumen concentrates, tailings, amount of middlings remaining in the tailings, and finally the separation coefficient. The separation coefficient is the fraction of feed that undergoes perfect separation. For a two-component system like tar sand, the coefficient of separation (CS) is defined as follows:

$$CS = \frac{a_1 M_1}{a_o M_o} - \frac{b_1 M_1}{b_o M_o}$$

where:

M_o, M_1 = Mass of feed and concentrate, respectively;
a_o, a_1 = weight fraction of bitumen in the feed and concentrate, respectively; and
b_o, b_1 = weight fraction of sand in the feed and concentrate, respectively.

Results of test runs made at 50 °C, presented in Table 25, show that there are only small differences between the two diluents. The bitumen recoveries have been corrected by subtracting the amount of diluent added in each case. However, this correction is made with the assumption that all the diluent reports exclusively to the bitumen in the bitumen concentrate.* It is seen in Table 26 that, among the recovery variables, separation coefficient and the amount of middlings left in the tailings show noticeable differences between the two diluents. Despite poor recoveries, all comparisons between the two diluents show SC-150 to be a better diluent, although by a very small margin.

Results from the test runs made at 80 °C are presented in Table 27. As expected, these results show improved values in all categories of recovery parameters, and differences between the two diluents are relatively more pronounced. Superiority of SC-150 over kerosene can be noticed in all comparisons. The differences between the two diluents are progressively enhanced as the diluent amounts increase. The best results are noticeable at 30% diluent addition.

Differences between the two diluents were also noticed with regard to the solids content of bitumen product. The differences observed were not only in the amount of solids reported to the bitumen product, but also in their size distribution. Table 28 lists the details of the particle size distribution observed for both diluents at 30% addition. It is seen that while there are only small differences in the proportion of coarse particles, that of fines reported to the product in the case of SC-150 is more than twice that in the kerosene case. This may indicate the superiority of the diluent SC-150 in terms of liberating the bitumen from finer sand grains.

The results of viscosity determinations made on bitumen-diluent mixtures indicated that the diluent addition (30%) and the temperature (80°C) employed in the batch extraction runs are adequate to reduce the viscosity of bitumen to the range 0.5-1.5 PaS. so that its disengagement from the sand surface is complete. However, the results presented in Table 27 do not concur with this assumption. This discrepancy may be attributed to the insufficient digestion of the feed and, possibly, to our incorrect estimation of bitumen viscosity in the tar sand, particularly as there is no known method of in-situ viscosity measurement of bitumen

---

* It must be noted that a very small portion of diluent is carried away by the tailings as a result of its solubility in water and its adsorption on sand. But it is considered to be very small and does not seriously affect the comparisons that are made between the two diluents.

Table 25

Summary of Low-Shear Energy Digestion
Test Runs at 50°C

Tar Sand (Sunnyside), kg	= 4
Wetting Agent (Na_2CO_3), gm	= 4
Digestion Time, Minutes	= 30
% Solids During Digestion	= 25
% Solids During Flotation	= 10
Duration of Pretreatment, Hours	= 24

Diluents: K = Kerosene, S = SC-150

	No Diluent	10% Diluent		20% Diluent		30% Diluent	
		K	S	K	S	K	S
% Bitumen in conc.	20.0	21.1	22.6	22.3	23.1	26.5	28.8
% Bitumen in tails†	4.0	3.5	3.3	3.4	3.1	3.0	3.0
% Bit. in middlings	8.8	7.8	7.5	7.0	6.7	6.0	5.7
% Tails as middlings	47.0	37.5	29.2	28.7	26.3	27.5	23.2
% Recovery	61.3	69.6	72.5	73.8	75.6	75.6	76.2
Separation Coeff.	0.32	0.38	0.43	0.43	0.45	0.46	0.54

†Excluding middlings.

Table 26

Summary of Low-Shear Energy Digestion
Test Runs at 80°C

Tar Sand (Sunnyside), kg = 4
Wetting Agent (Na_2CO_3), gm = 4
Digestion Time, Minutes = 30
% Solids During Digestion = 25
% Solids During Flotation = 10
Duration of Pretreatment, Hours = 24

Diluents: K = Kerosene, S = SC-150

	No Diluent	10% Diluent		20% Diluent		30% Diluent	
		K	S	K	S	K	S
% Bitumen in conc.	21.2	23.0	23.5	23.4	24.7	31.9	36.8
% Bitumen in tails †	3.6	3.3	3.2	2.9	2.0	2.8	2.4
% Bit. in middlings	7.6	7.2	7.0	6.1	4.4	5.8	4.2
% Tails as middlings	37.8	30.5	22.0	25.2	19.0	18.5	12.2
% Recovery	68.8	72.0	75.7	75.1	85.6	77.0	81.7
Separation Coeff.	0.38	0.43	0.46	0.44	0.53	0.47	0.65

†Excluding middlings.

Table 27

Differences in the Size Fractions[a] of the Solids Reported to Bitumen Concentrates for Sunnyside Tar Sand Processed at 80°C at 30% Diluents

	Percentage of the Total Solids	
Particle Size, μ	Kerosene	SC-150
> 106	56.6	54.6
90-106	7.8	7.3
75-90	6.2	4.3
45-75	12.3	8.0
38-45	7.4	4.5
< 38	9.7	21.3

[a]Based on dry sieving.

Table 28
Percentage Compositions of Asphalt Ridge and Sunnyside Bitumens

Components	Asphalt Ridge	Sunnyside
% Saturates	32.4	24.9
% Aromatics I	22.4	18.1
% Aromatics II	n.d.	0.5
% Resins I	37.6	30.0
% Resins II	n.d.	0.6
% Asphaltenes	7.3	23.7

n.d.: not determined.

present in the tar sand. Further, it must be emphasized that these were batch runs, and no streams (middlings or tailings) could be recycled for better recoveries. In our earlier work (Hupka et al., 1987) on Sunnyside tar sands, better recoveries were realized using the high-shear reactor with the digestion step carried out at 70-75% solids. Since the high-shear reactor was not operable for these experiments, low-shear digestion was employed.

The quality of bitumen concentrates obtained in these test runs is characteristically low. This is due to a typical feature of Sunnyside tar sands, which are known[87] to contain relatively large proportions of fine particles. In fact, it has been determined in this study that >30% of the solids reporting to the bitumen concentrate are of sizes <45 microns. However, infrared analysis of fine particles (< 38 microns) showed that there are no significant amounts of clays. They consisted mainly of fine silica and small amounts of carbonate minerals such as calcite and dolomite, as a characteristic absorption band for CO_3^{2-}, were observed at 1420 cm^{-1}. Even though bitumen disengagement from the sand surface can be achieved by using an efficient diluent, in the subsequent flotation step fine particles rise to the surface along with the bitumen. These fine particles are naturally hydrophilic, but with the adsorption of bitumen components on their surface they become hydrophobic[88,89] and rise to the surface. This problem has been well-recognized in the case of low-grade Athabasca tar sands with significant amounts of clays. In addressing this problem, efforts must be made to selectively float the bitumen to the exclusion of solids. In order to improve the flotation process, it is essential to study the electrical and other relevant surface properties of solids accompanying the bitumen in the concentrates.

CONCLUSIONS

The modified hot-water process developed at the University of Utah is based on the control of bitumen viscosity, which is achieved by selection of temperature and the addition of diluent to tar sand. For tar sands containing highly viscous bitumen, it is important to select a diluent which is efficient in its role of reducing bitumen viscosity. In this effort, several diluents have been considered. Viscosity measurements of bitumen-diluent mixtures were carried out on toluene-extracted bitumen, and selection of a diluent was made on the basis of its capacity to reduce bitumen viscosity. It has been found that SC-150, a diluent predominant in aromatic hydrocarbons, is better suited for reducing the viscosity of bitumens in tar sands.

In order to verify the conclusions made on the basis of viscosity experiments, kerosene and SC-150 were chosen for the separation of bitumen from Sunnyside tar sands. Batch experiments were conducted in which the tar sand was subjected to hot water processing using the low-shear energy digestion. The results obtained confirm that SC-150 is indeed a better diluent. However, the bitumen concentrate quality and separation coefficient is short of a satisfactory level. This is due to the nature of Sunnyside tar sand, which is known to contain relatively large amounts of fine sand particles. Modifications of our procedures will be attempted in order to improve the quality of the concentrate.

FRACTIONATION AND CHARACTERIZATION OF ASPHALT RIDGE AND SUNNYSIDE TAR SAND BITUMENS

Asphaltenes are known to enhance the viscous behavior of bitumen.[91] The relative amount of asphaltenes in two different bitumen samples do not necessarily indicate that the one with larger amounts of asphaltenes renders the respective bitumen with higher viscosity than the other bitumen with lower asphaltene content. This can be readily illustrated with examples of Asphalt Ridge and Athabasca bitumens. Asphalt Ridge bitumen, though it contains only 7.3% asphaltenes, has a value of viscosity (80 Pa.S.) that is nearly an order of magnitude higher than Athabasca bitumen (5 Pa.S.) which contains 16.5% asphaltenes.[92] This observation leads one to conclude that viscosity of a bitumen is a complex variable and depends not only on its composition but also on the nature of components.

To determine additional factors which may influence the viscosity of bitumen, an attempt was made to fractionate the representative bitumen samples and conduct a characterization study of their fractions. Sunnyside (SS) and Asphalt Ridge (AR) tar sand bitumens were chosen for this study, as their respective viscosity values are known to represent extreme cases. Sunnyside tar sands are known to be less yielding to bitumen recoveries in the hot water separation methods. The difficulty encountered in the processing of these deposits is mainly attributed to extremely high viscosity of the bitumen therein (nearly 20 times that of Asphalt Ridge bitumen). It was therefore considered important to fractionate this bitumen and analyze its components. This analysis is anticipated to provide information on the nature of components of bitumen and their potential intermolecular attractions that render the bitumen with such high viscosity.

The names assigned to the fractions of bitumen such as aromatics, resins, and asphaltenes, are merely operational definitions for groups of compounds. These groups are broadly separated on the basis of their differences in polarities. In an equally complex material like coal, somewhat similar broadly applicable terms have been used to describe its various components. Among them is the resinite maceral in coals. Fossil resin found in the Wasatch plateau coal of Utah is considered to be a valuable commodity. Although its content in coal on average is estimated to be about 7-10%, its economic value is either equal to or greater than that of coal. In view of this, a study was undertaken to isolate resin fractions from bitumens and compare their chemical and physical properties with resin obtained from coal.

EXPERIMENTAL

Fractionation of Bitumens

The method adopted for fractionation of bitumen is mainly based on considerations of solubility in a particular solvent and polarities of constituent components which exhibit differences in adsorption properties on a given support material. The fractionation scheme followed in this study is illustrated in Figure 39. The determination of bitumen

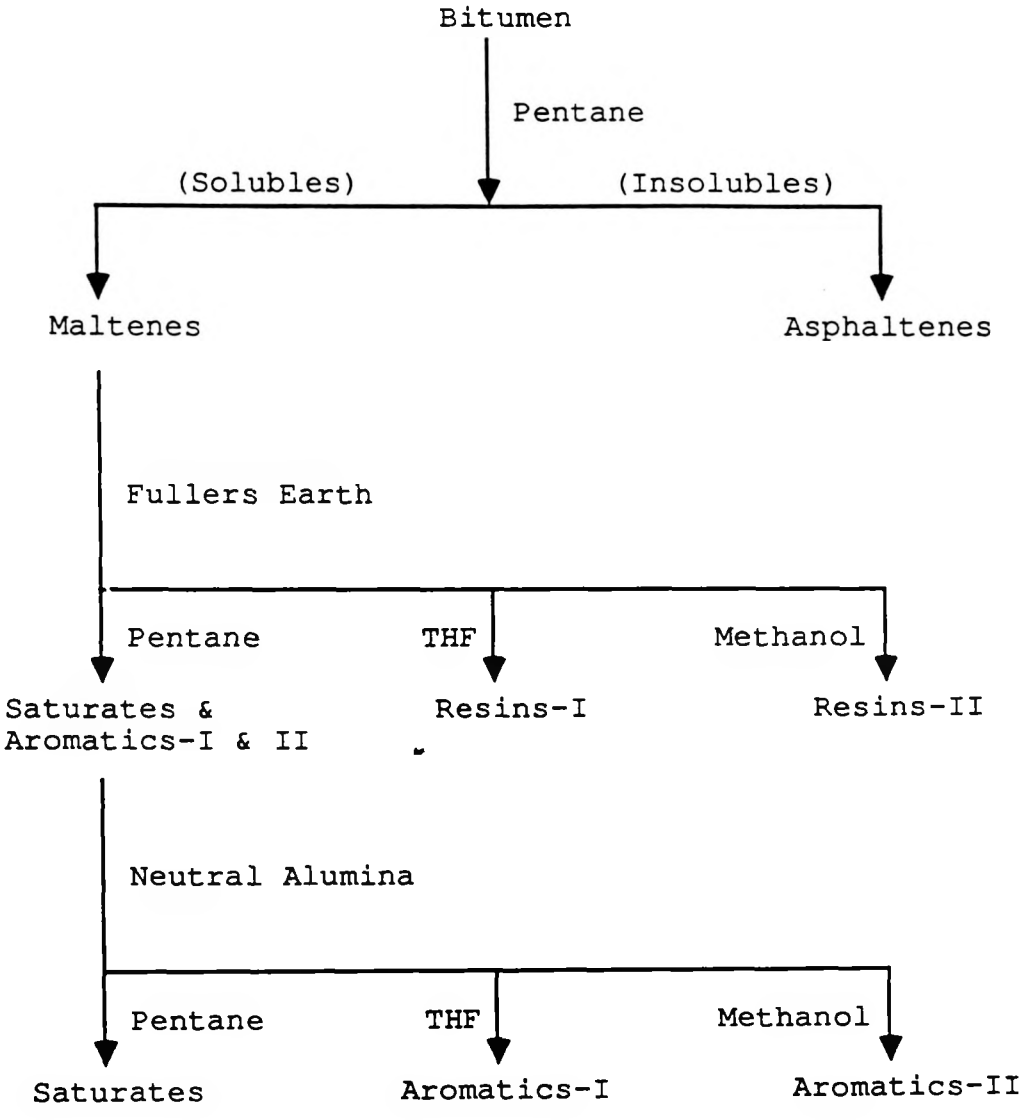

Figure 39. Bitumen fractionation scheme.

composition depends on the nature of the solvent and, to some extent, on the nature of the adsorbent used. For the initial separation of bitumen into maltenes and asphaltenes, the most commonly used solvents are C_5-C_7 normal alkanes. The solvating ability of the alkanes for bitumen increases with carbon chain length yielding progressively less insolubles (asphaltenes).[93] Since the boiling point of individual solvents in a class of solvents increases gradually with molecular weight of the solvent, and since its removal from the separated bitumen fractions cannot be accomplished without the use of elevated temperatures, it was decided to use n-pentane as the solvent. The consequence of this choice would be that the estimation of the polar fractions in the bitumen is slightly lower.

The fractionation scheme consisted of the following procedure. Bitumen was weighed in an erlenmeyer flask (250 ml) to which toluene was added (1 ml of toluene per g of bitumen). This was followed by n-pentane (40 times volume of toluene). The resulting suspension was thoroughly shaken and stored in the dark for 16-20 hours. The solids (asphaltenes) from the suspension were separated from maltenes by filtration. The asphaltenes were further extracted with n-pentane in a soxhlet extraction unit for the recovery of residual maltene. The inorganic materials from asphaltenes were removed by dissolving in dichloromethane and centrifuging at 10,000 rpm for 30 minutes. Finally, the asphaltene solution is subjected to solvent removal on a Rotavap and the resulting solids were dried in the oven at 110 °C for 1 hour.

Maltenes were obtained from the filtrate by evaporation of solvent on a Rotavap and vacuum drying at 40 °C for an extended period of time (12-16 hrs) to remove final traces of solvent. The resulting maltenes were further divided into a mixture consisting of saturates, aromatics, and resins. This separation was carried out by loading maltenes onto Fullers Earth (mesh size 30-60) in a glass fritted thimble (maltenes: Fullers Earth = 1:10), and extracting successively with solvents of increasing polarity in a soxhlet extraction unit. Extraction with each solvent was made until the extracts were colorless. Solvents used were n-pentane, tetrahydrofuran, and methanol. The extracts thus obtained were labeled as a mixture of saturates and aromatics, resin I, and resin II, respectively. In each case the solvent was removed as mentioned in the previous paragraph.

In the final step, the mixture containing saturates and aromatics was separated by column chromatography. Neutral alumina, dried at 110 °C for 40 hours, was used as support material. A ratio of support material to saturates and aromatics mixture was maintained at 15:1. The void or holding volume of the column was determined by running solvent through it. The saturates and aromatics mixture was dissolved in n-pentane, and the solution was loaded onto the column. The column was eluted with the same solvents sequence as described earlier. Solvents were removed from each of the fractions and labeled as saturates, aromatics I, and aromatics II. The fractionation results thus obtained are quantitatively presented in Table 28.

Table 29

Elemental Compositions of the Bitumen Fractions Derived from Asphalt Ridge (AR) and Sunnyside (SS) Tar Sands

Property	Saturates		Aromatics		Resins		Asphaltenes	
	AR	SS	AR	SS	AR	SS	AR	SS
% Carbon	86.51	86.57	85.83	85.85	79.95	83.38	84.26	83.49
% Hydrogen	12.83	12.89	10.51	10.51	10.07	10.37	9.19	8.68
% Nitrogen	0.09	0.1	0.65	0.53	1.58	1.13	2.23	1.56
% Sulfur	0.07	0.04	0.41	0.43	0.42	0.40	0.51	0.64
% Oxygen[a]	0.50	0.40	2.60	2.68	7.98	4.80	3.71	5.63
H/C Ratio	1.78	1.79	1.47	1.47	1.51	1.49	1.31	1.23
Aromaticity[b]	0.04	0.04	0.31	0.27	0.18	0.17	0.26	0.27
Molecular Wt.	388	403	465	480	1510	670	1100	2240

[a]Values obtained by difference. No provision was made for metals present in all these fractions which are considered to be very small in comparison.

[b]Determined from the ^{13}C NMR spectral analysis.

Characterization of Bitumen Fractions

Compositional differences between AR and SS bitumens are outlined in Table 29. The mass balances obtained in the fractionation scheme are 99.7 and 97.8 percent for AR and SS bitumens, respectively. The greater loss observed in the case of SS bitumen was mainly confined to the step involving the separation of saturates and aromatics. The major difference between the two bitumens lies in their relative amounts of asphaltenes. The separated fractions of bitumens were subjected to a variety of analyses to determine their intrinsic differences. Since two of the fractions obtained, resins II and aromatics II, were extremely small, no characterization studies could be attempted on these. The saturate fractions of both bitumens were clear, viscous liquids with a faintly yellow color for AR bitumen and colorless for SS bitumen. Physically there were no apparent differences between aromatics and resin fractions. When the resins were freshly separated they were black crystalline solids which soon became viscous semisolids, possibly due to their low melting points. Both the asphaltene fractions were glossy crystalline solids. The analytical methods employed in this study for comparison purposes were elemental analysis, molecular weight determination, and ^{13}C NMR and FTIR spectral examinations.

Elemental Analysis and Molecular Weight Determination

Elemental analysis was conducted on all separated fractions of bitumens. Carbon, hydrogen, and nitrogen contents of bitumen fractions were determined by LECO-600 and of sulfur by LECO-SC132 analyzers. Results of the analyses are presented in Table 30. As seen from this table that while carbon content in each fraction remains almost similar, hydrogen content gradually decreases from saturates to asphaltenes fraction. As expected, oxygen, nitrogen, and sulfur gradually increase from saturates to asphaltenes. From the bitumenwise comparison of fractions, it appears that AR has noticeably more nitrogen in every fraction. The amount of sulfur is practically similar in all fractions except in asphaltenes where SS bitumen appears to contain a higher amount. Oxygen appears to vary randomly between the two bitumens. It must be emphasized that oxygen values are not directly measured and caution must be exercised in their interpretation. From the calculated atomic ratios of H/C for both bitumens, it indicates that while both bitumens are similar in nature and aromatics fractions, they are slightly different in resins and asphaltene fractions. All the above analytical indicators show that there are no major differences between the two bitumens used in the study.

Molecular weights of bitumen fractions were determined in a commercial laboratory. These were carried out using a WESCAN model 233 vapor phase osmometer. Toluene was used as the solvent. Concentrations of the fractions were varied over an order of magnitude (5 g/lit to 0.5 g/lit). The molecular weights thus determined are listed in Table 29. It is observed that while the molecular weights of saturate and aromatic fractions of AR and SS bitumens show almost similar values, the resin and asphaltene fractions show reverse trends. The surprising result is that in the case of AR bitumen, the compounds with the highest molecular weight are found in the resin fraction, whereas in SS bitumen those with the highest molecular weights are observed in the asphaltene fraction.

Table 30

Absorption Bands Observed in the FTIR Spectra of Bitumen Fractions and Some of Their Probable Designations

Wave Number, cm^{-1}	Band Designation
3648	O-H stretching in non H-bonded primary alcohols
3480	N-H stretching in pyrrolic type compounds
3500-3200	O-H and N-H stretching in multiple H-bonded compounds
3956	C-H stretching (asymmetrical) in $-CH_3$
2929	C-H stretching (asymmetrical) in $-CH_2$
2852	C-H stretching (symmetrical) in $-CH_3$
2829	C-H stretching (symmetrical) in $-CH_2$
2728	C-H stretching in -CHO group (aldehyde)
1700	C=O stretching in aldehydes and ketones
1600	C=C stretching (conjugated) and skeletal ring vibrations
1460	C-H deformation in $-CH_2$
1370	C-H deformation in $-CH_3$
1314	O-H deformation in phenols
1267	C-O stretching in aromatic and cyclic ethers
1231	C-O-H deformation
1215	
1196	C-O stretching in tertiary alcohols
1158	C-O stretching in alkyl ethers ($-CH_2-O-CH_2$)
1121	Aliphatic C-O and/or S=O stretching
1071	C-O-C stretching in alkyl ethers and C-N stretching
1033	C-O-H deformation
933	
907	
879	Lone aromatic C-H out of plane bending vibrations
860	--- ---
810	Two adjacent C-H groups on the aromatic ring
747	Four adjacent C-H groups on the aromatic ring
727	$-CH_2$ rocking

Here, too, no clues are offered as to the possible differences between AR and SS bitumens.

^{13}C NMR Spectra

The ^{13}C NMR spectra of both AR and SS bitumen saturate fractions show that the principle bands are in the region 10-70 ppm, which is characteristic of the saturated carbon. These spectra are presented in Figures 40 and 41. The unsaturated carbon or what is termed as the aromatic region 90-170 ppm[94] in these fractions is very small, amounting to less than 4% of the saturated carbon. These samples exhibit identical spectral features and similar relative intensities for all major bands. Since the saturate fraction, like any other fraction of the bitumen, is a complex mixture of numerous unknown compounds, band assignments are at best qualified guesswork. Consequently, a precise analysis is considered to be extremely difficult.

Based on the study of model compounds like phytane (2,6,10,14-tetramethylhexadecane) and farnesane, some recent attempts have been made to identify the observed bands in ^{13}C NMR spectra of Athabasca bitumen fractions[95] and coal extracts[96] to carbon atoms with certain structural characteristics. Although these band assignments are useful for identification purposes, the overall information that is derived from ^{13}C NMR data still appears to be of limited value.

The ^{13}C NMR spectra of aromatics and resin fractions from both bitumens show remarkably similar features (Figures 42-45). The only difference between the two is in the relative intensities of some of the bands. For these bands the intensities are invariably higher in AR than the SS bitumen. The aromaticities of both AR fractions are marginally higher than those of SS fractions (Table 29).

^{13}C NMR spectra of asphaltene fractions are shown in Figures 46 and 47. There are marked differences between the two asphaltene fractions in the region of saturated carbon both in the number of bands observed as well as their relative intensities. It is also noticeable that the aromatic carbon content of the asphaltene fraction in both the bitumens is relatively higher than that observed for other fractions (except aromatics).

Apparent aromaticities of all saturate, resin, and asphaltene fractions of both the bitumens were determined from ^{13}C NMR spectral data. These values were derived from the relative integrated intensities of the aromatic region (90-160 ppm) and the aliphatic region (10-60 ppm). The empirical aromaticity values thus determined are presented in Table 29.

FTIR Spectra

Relatively, FTIR spectra of the bitumen fractions are expected to furnish more detailed information on the nature of components present. In the ^{13}C NMR technique, two different atoms, regardless of their bonding characteristics, are expected to show absorption bands of equal intensities. In the infrared technique band, intensities for vibrational modes of more polar groups are disproportionately higher than less polar groups.

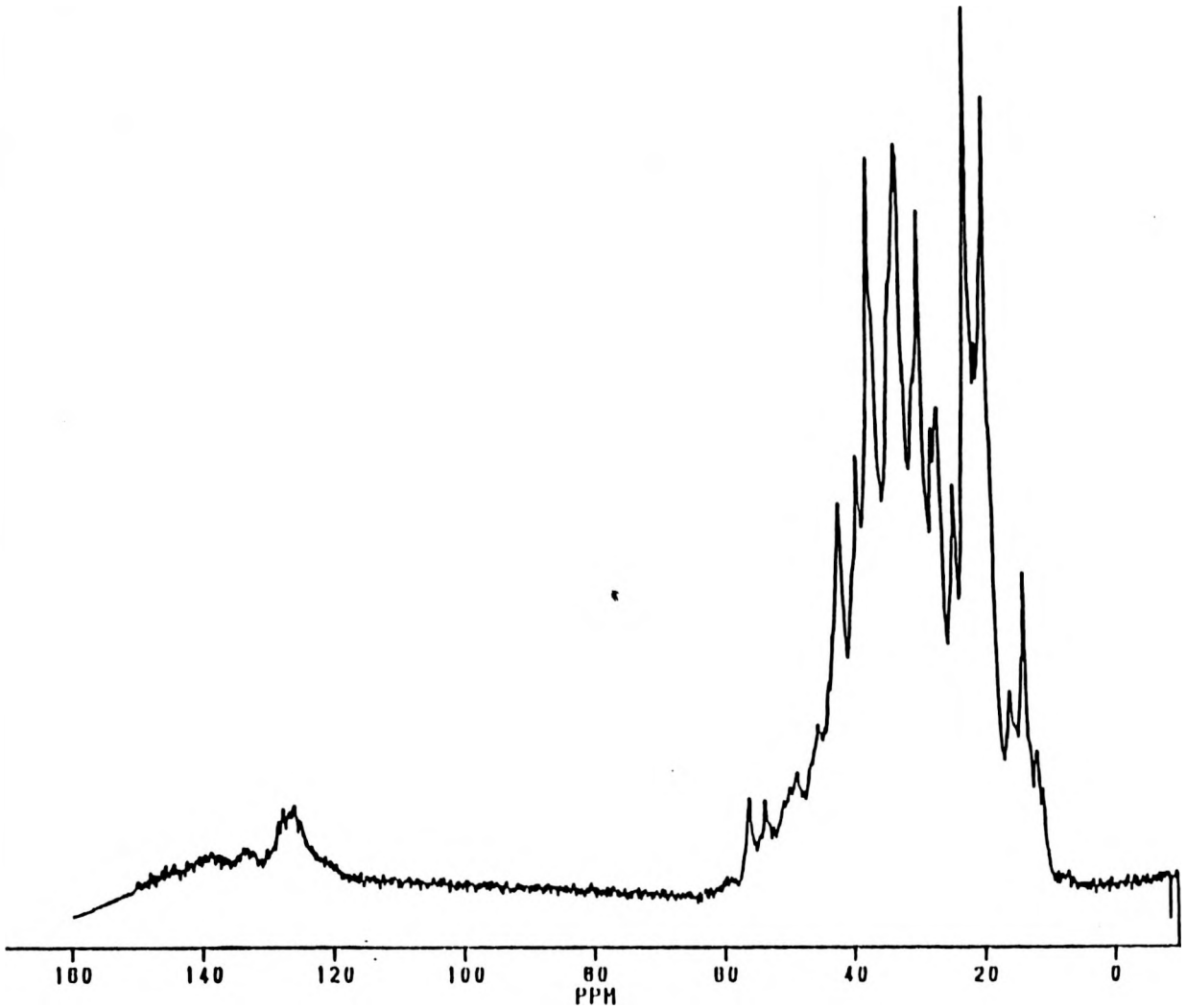

Figure 40. ^{13}C NMR Spectrum of AR Bitumen Saturate Fraction

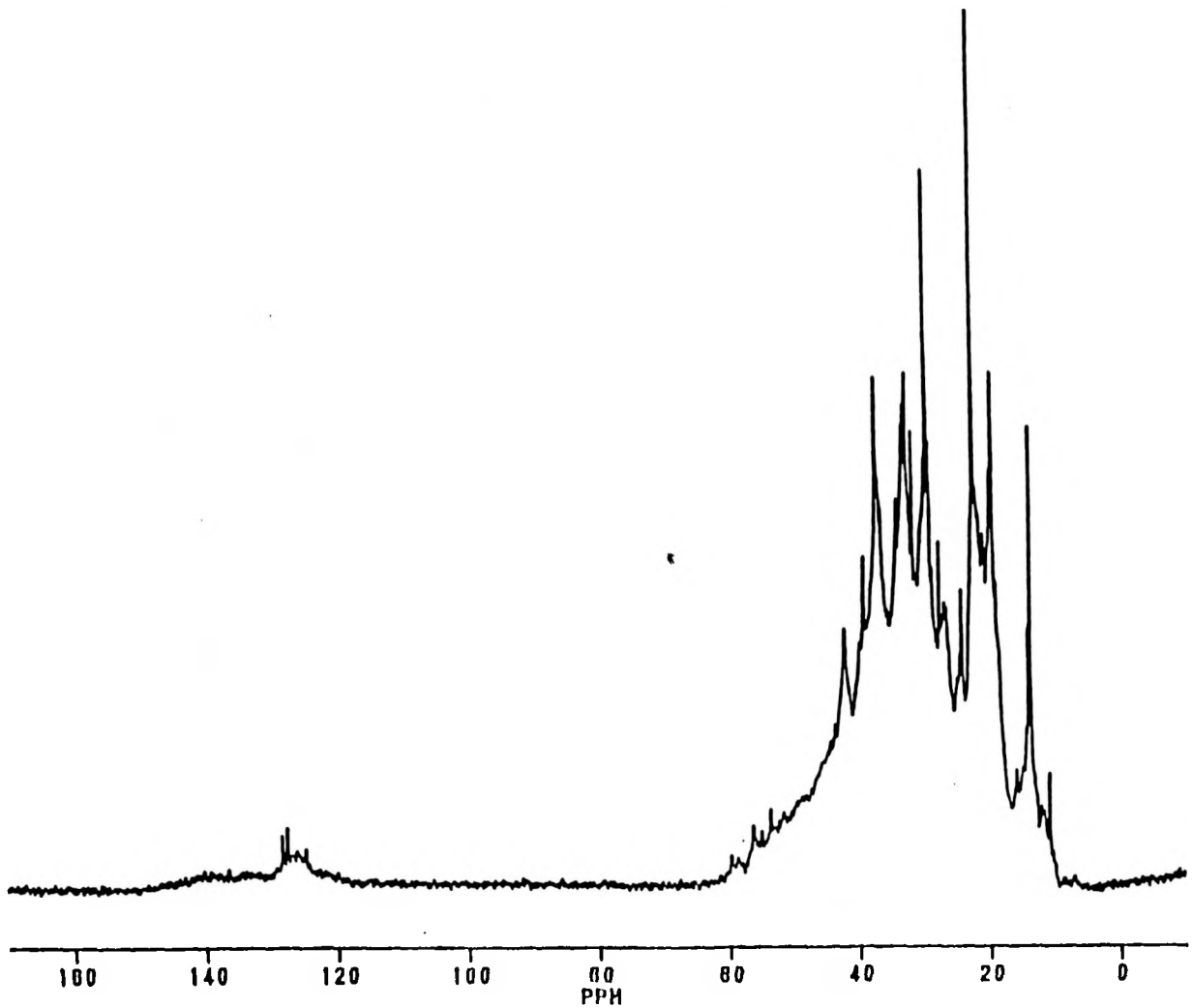

Figure 41. ^{13}C NMR Spectrum of SS Bitumen Saturate Fraction

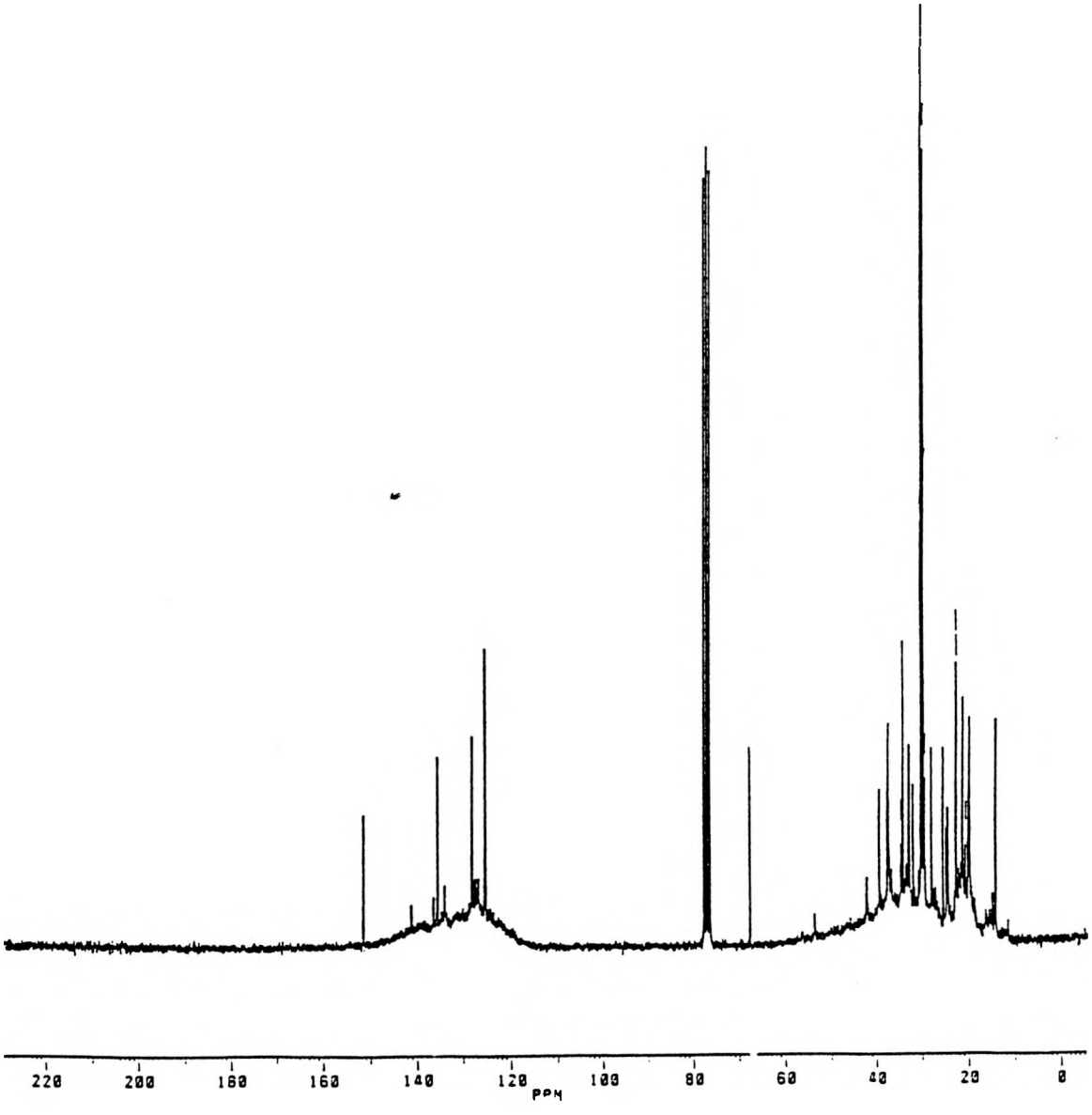

Figure 42. Solution ^{13}C NMR ($CDCl_3$) Spectrum of AR Bitumen Aromatic Fraction.

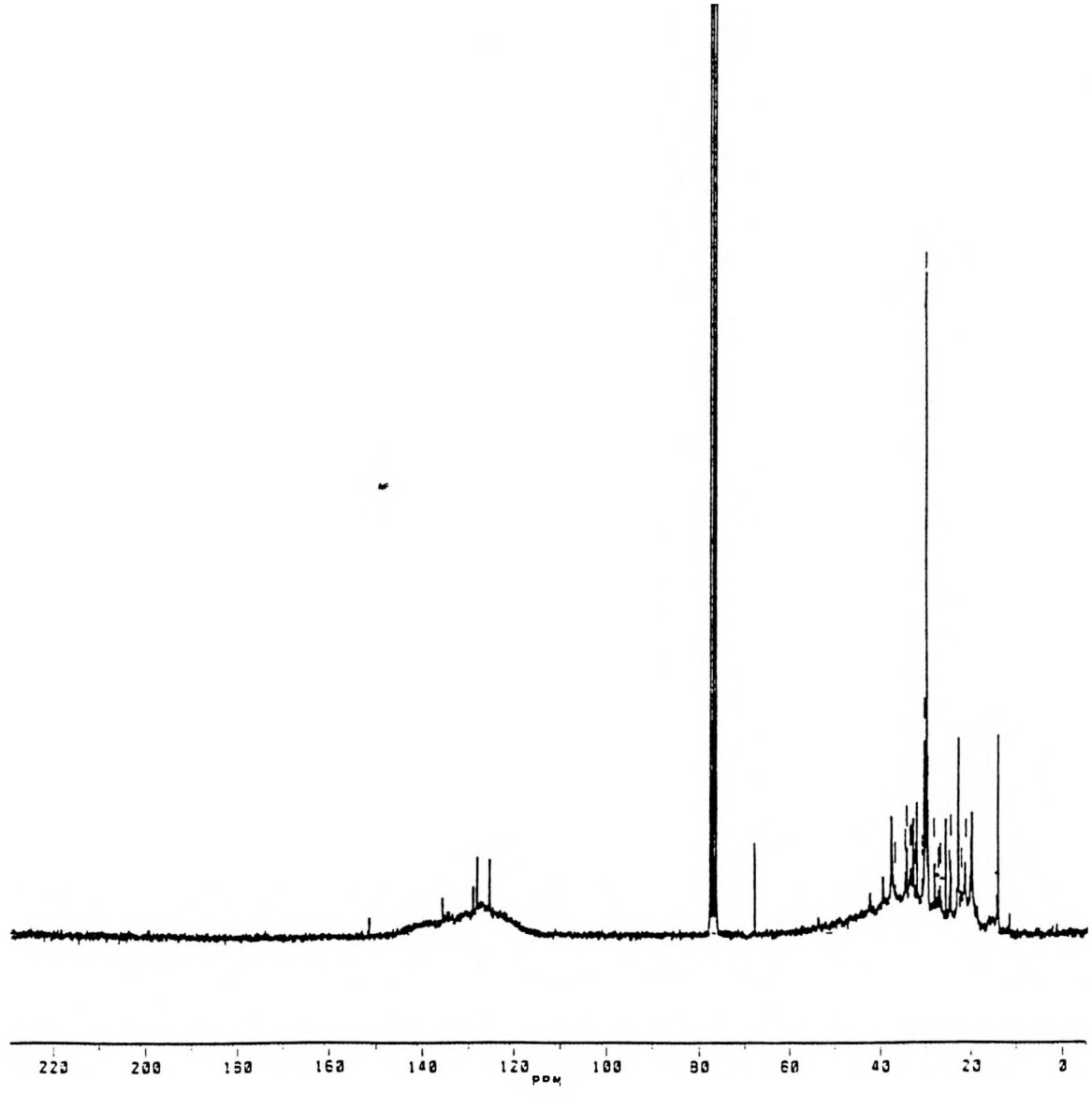

Figure 43. Solution ^{13}C NMR ($CDCl_3$) Spectrum of SS Bitumen Aromatic Fraction

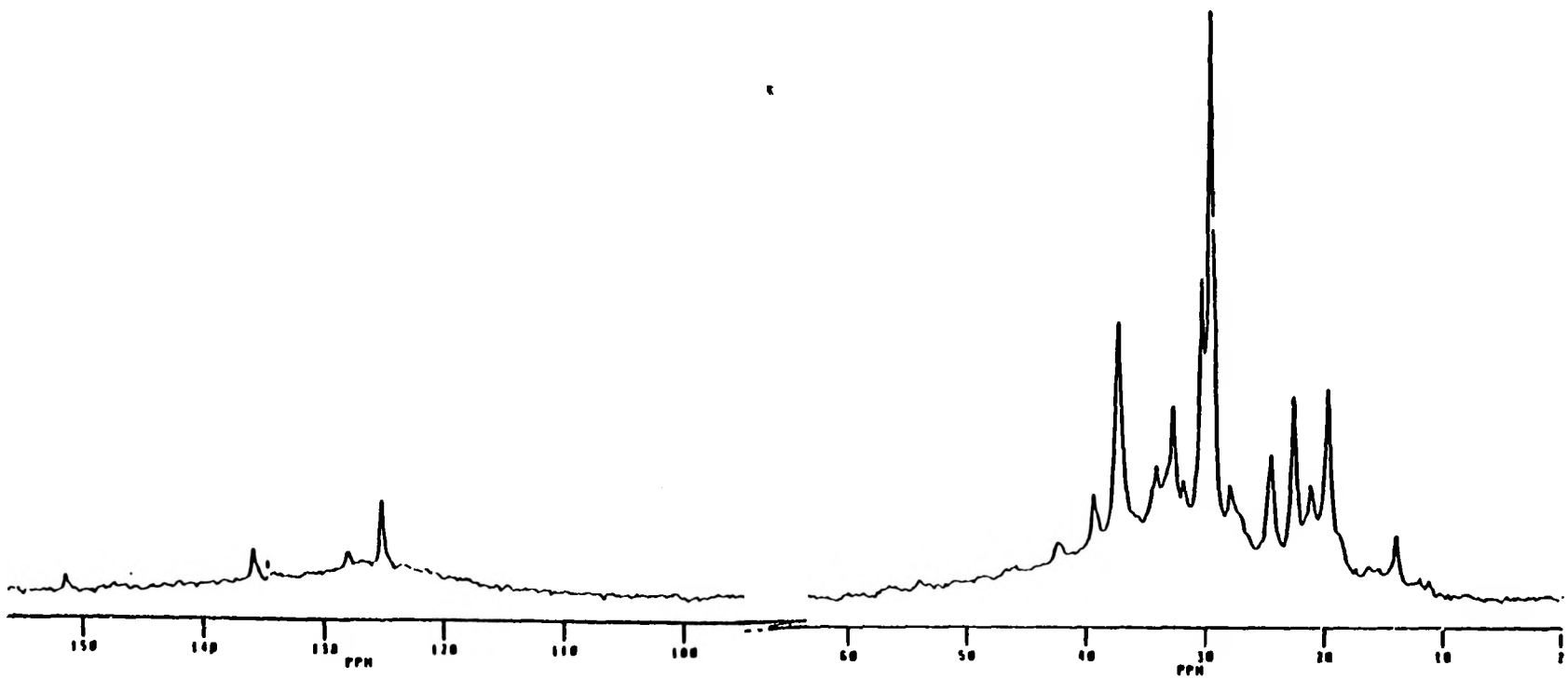

Figure 44. Solution ^{13}C NMR ($CDCL_3$) Spectrum of AR Bitumen Resin Fraction

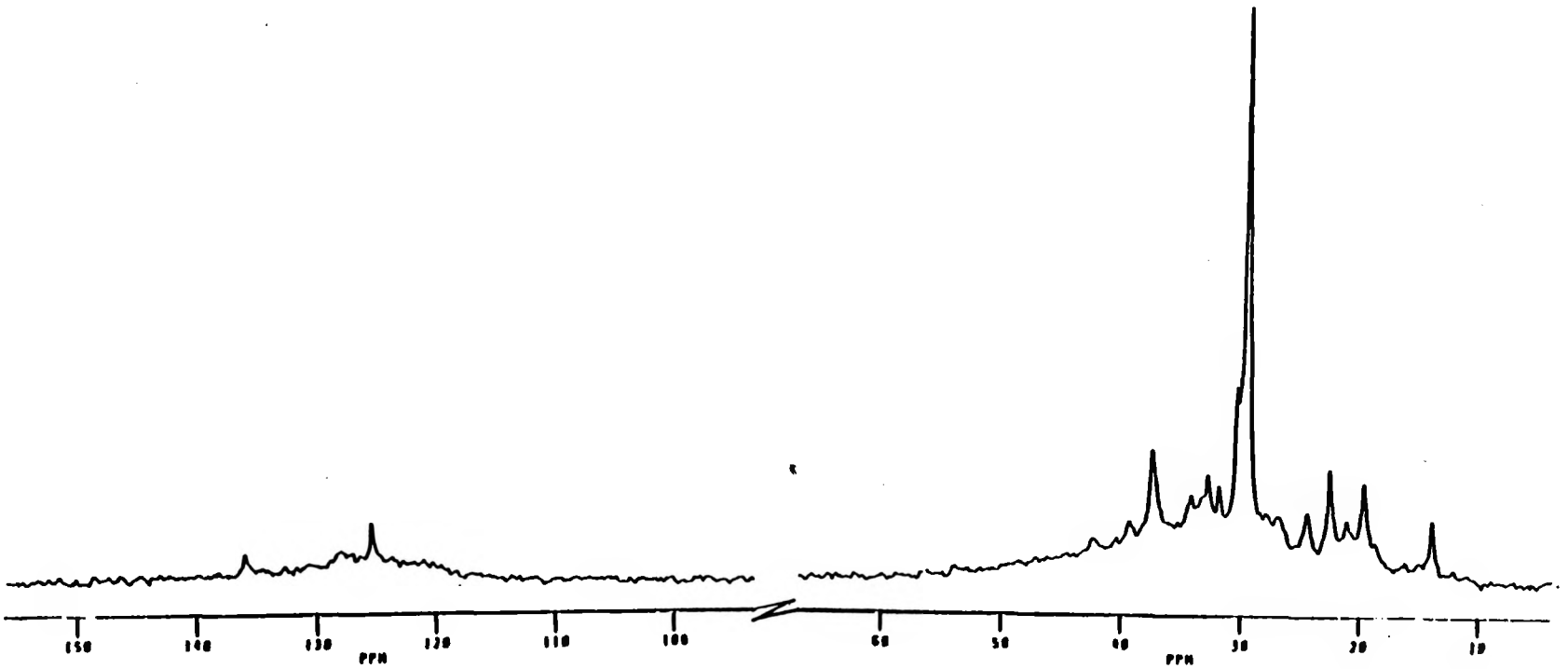

Figure 45. Solution ^{13}C NMR ($CDCl_3$) Spectrum of SS Bitumen Resin Fraction

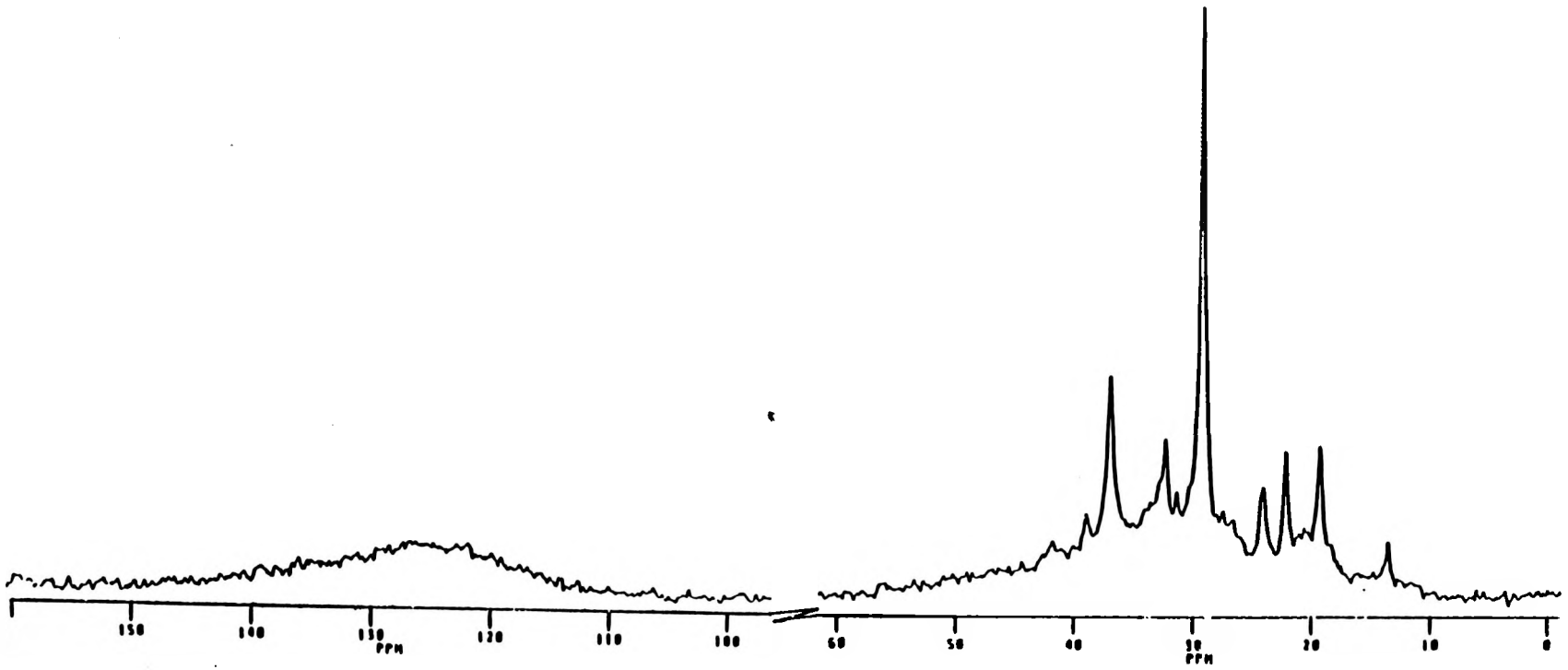

Figure 46. Solution ^{13}C NMR ($CDCl_3$) Spectrum of AR Bitumen Asphaltene Fraction

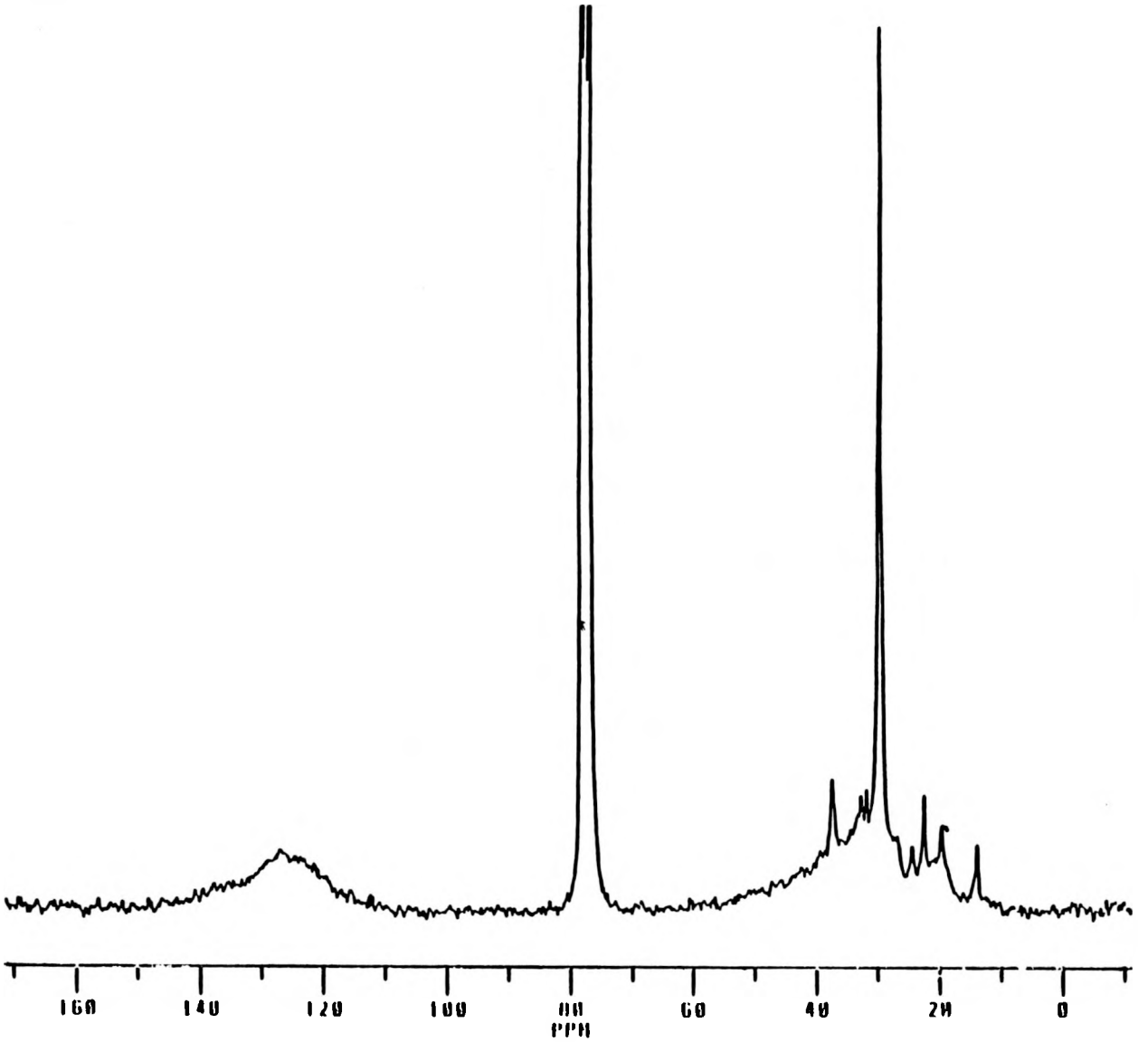

Figure 47. Solution ^{13}C NMR ($CDCl_3$) Spectrum of SS Bitumen Asphaltene Fraction

This difference in techniques enables one to identify certain less abundant compounds containing higher polar groups in the IR spectrum which are otherwise invisible in the NMR spectrum. The FTIR spectra of each of the fractions for both bitumens are outlined in the following paragraphs.

Spectra of the saturate fractions are entirely featureless in accordance with their expected compositions. These are presented in Figure 48. The only observable major bands are due to C-H stretching and bending vibrations. The other bands are very weak and appear almost to be of no significance. In this particular case, ^{13}C NMR spectral data provide comparatively more information than FTIR data on the nature of components, since the former technique is capable of distinguishing various types of saturated carbon atoms that are presented in the saturates fraction.

Spectra of aromatic fractions of bitumens are presented in Figure 49. The differences between AR and SS bitumens are very clear, both in terms of band characteristics and their relative intensities. The principle bands that are observed and identifiable are listed in Table 30. From the elemental analyses of aromatics fractions, as outlined in Table 29, it is clear that both of these fractions have similar amounts of oxygen. A close examination of the spectra, however, indicates that the oxygen content is distributed in both fractions in a very different manner.

In the aromatics fraction of the AR bitumen, the majority of the oxygen is distributed in the absorption bands appearing at 3648 cm^{-1}. This indicates the presence of non-hydrogen bonded free O-H groups, and in bands appearing in the region 1330-1100 cm^{-1}, a region characteristic of CH_2O-H, CO-H deformation modes of vibrations and antisymmetrical bridge stretching for cyclic ethers.[97] The remaining small portion of the oxygen is bound in carbonyl groups, which is indicated by a weak band observed at 1704 cm^{-1}.

In case of the aromatic fraction of SS bitumen, distribution of oxygen appears to be opposite to that observed in the case of AR bitumen. Here most of the oxygen is distributed in carbonyl groups as indicated by the relatively more intense band at 1703 cm^{-1}. The amount of oxygen contained in O-H groups is relatively insignificant, as can be seen in the intensities of the bands observed at 3648 cm^{-1} and in the region 1330-1100 cm^{-1}. These subtle differences in composition, as indicated by FTIR spectra, would contribute significantly to physical properties of the bitumen, as will be discussed later.

Other differences between the aromatic fractions of AR and SS bitumens are minor and are found in the region 900-700 cm^{-1}, which is characteristic of the nature of substitution in six-membered aromatic compounds. However, these small differences are not assumed to play any significant role in the composite physical properties of the parent bitumens.

FTIR spectra of the resin fractions also show some interesting differences between AR and SS bitumens. These are displayed in Figure 50. From the design of the fractionation scheme, one would expect an accumulation of polar compounds in resins. Among the noticeable features

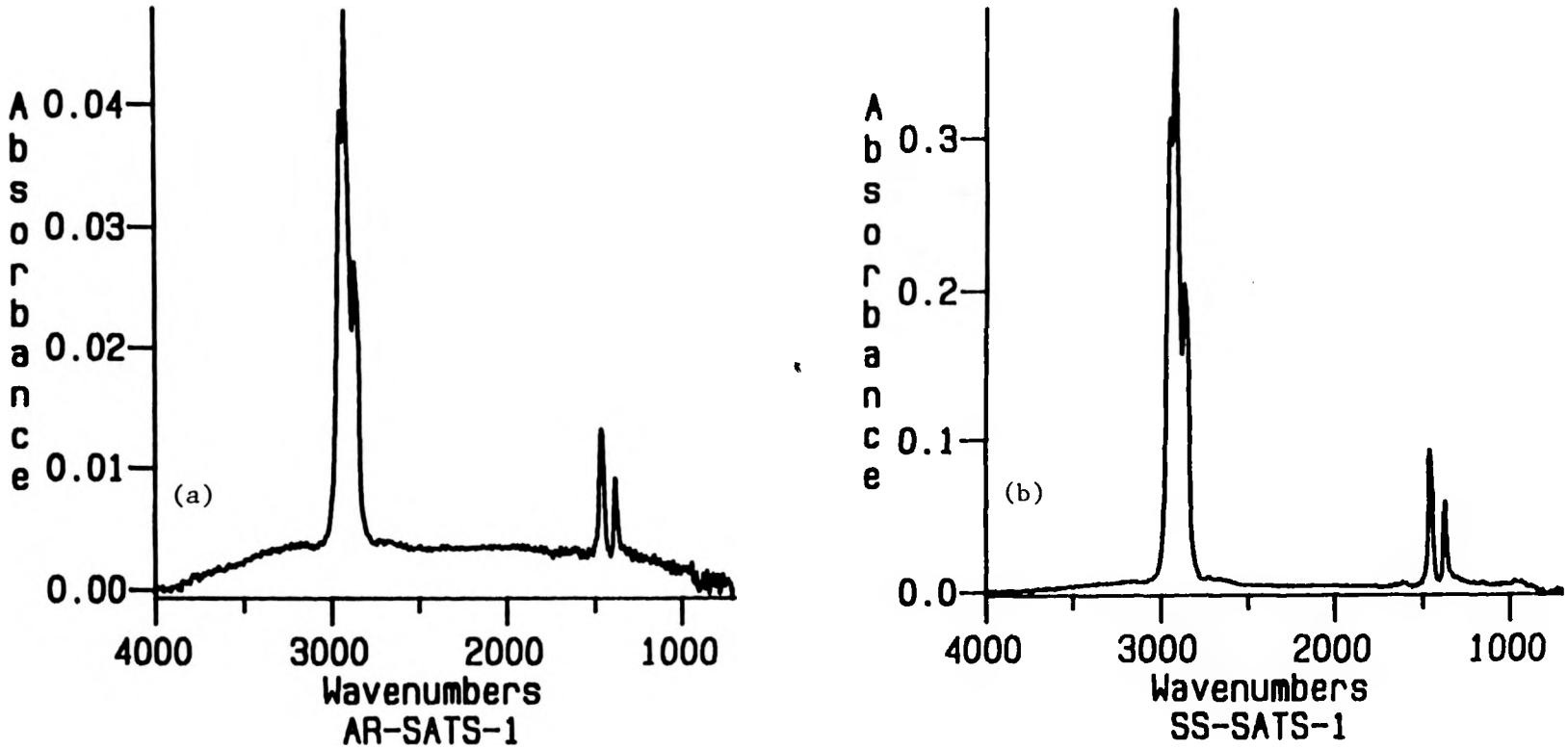

Figure 48. FTIR Spectra of (a) AR Bitumen and (b) SS Bitumen Saturate Fractions

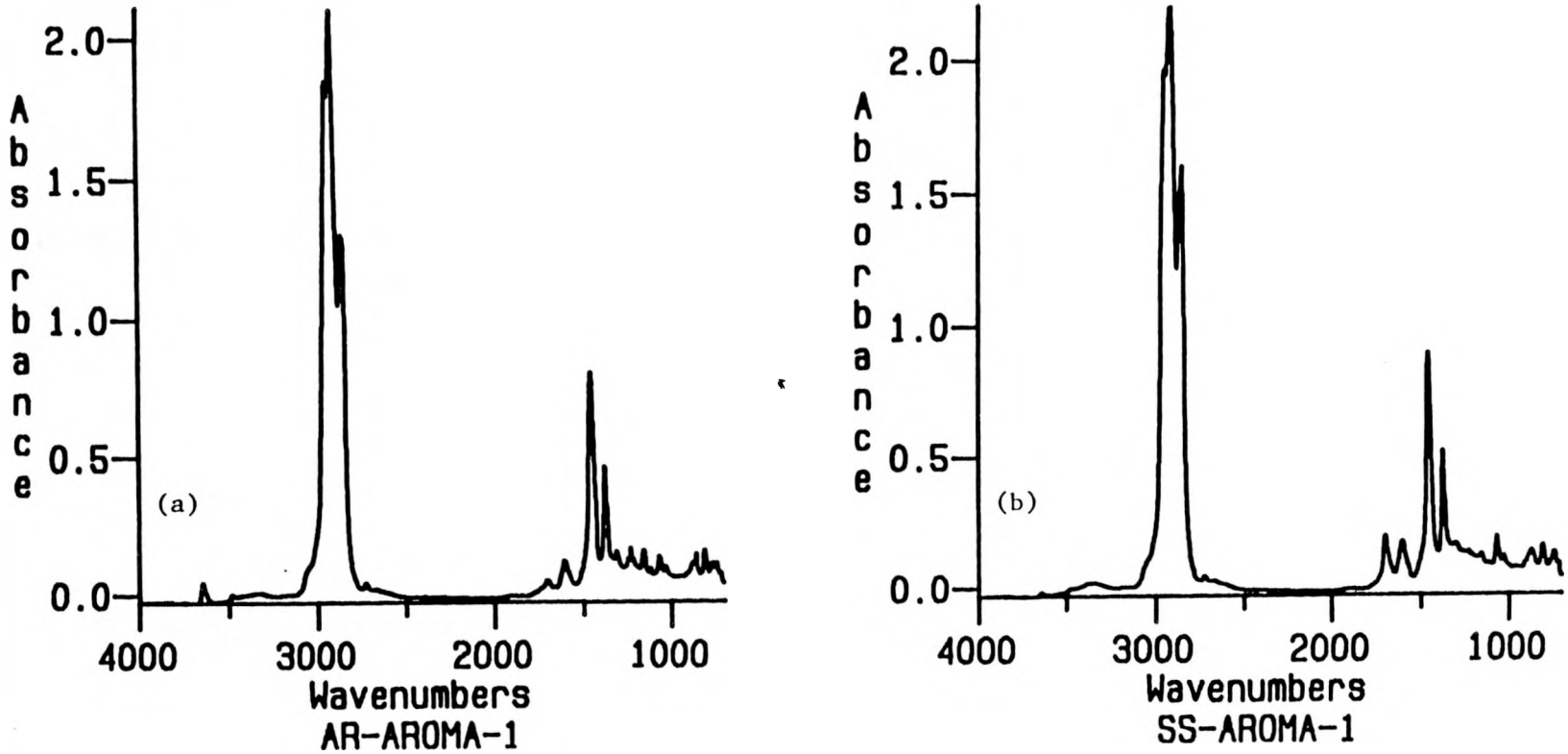

Figure 49. FTIR Spectra of (a) AR Bitumen and (b) SS Bitumen Aromatic Fractions

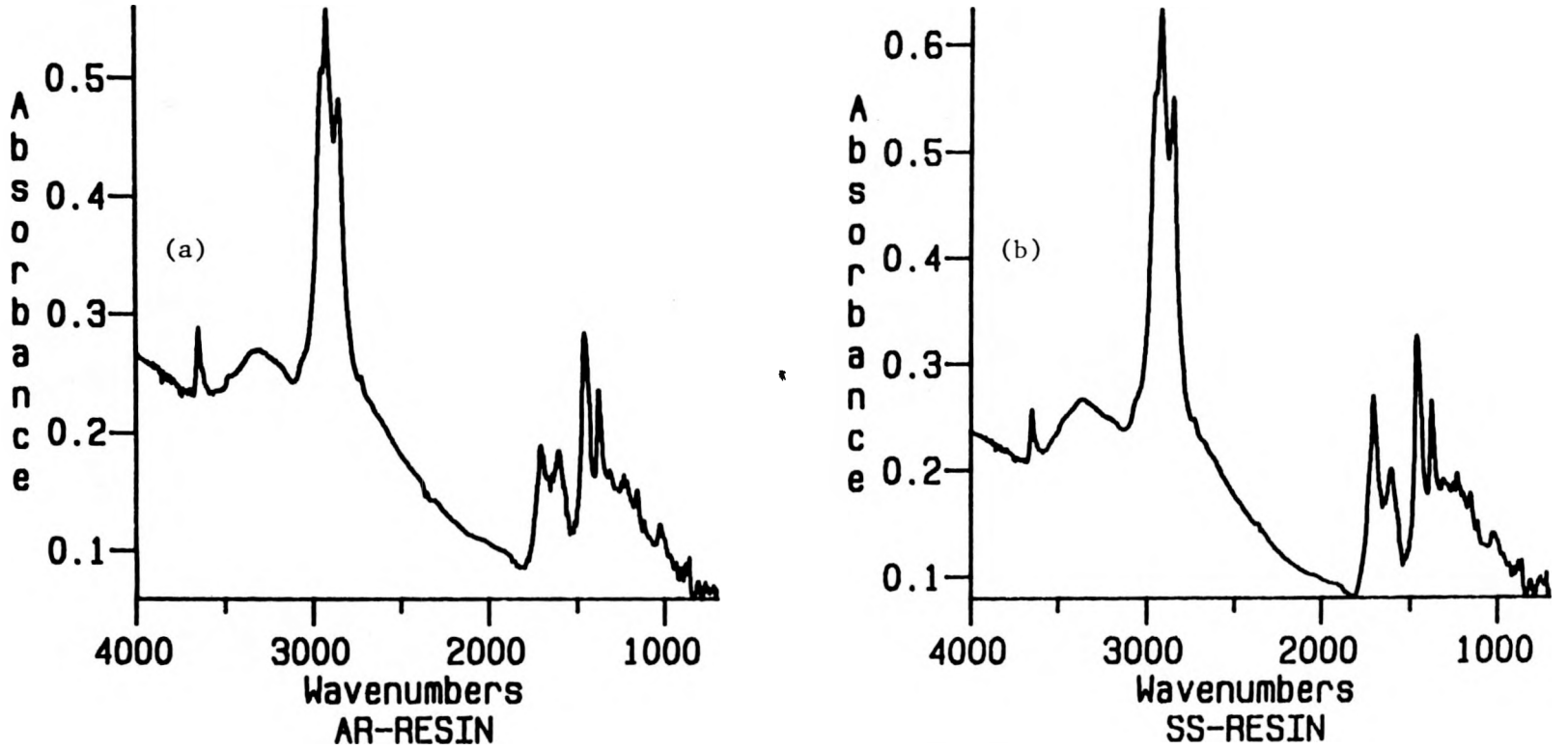

Figure 50. FTIR Spectra of (a) AR Bitumen and (b) SS Bitumen Resin Fractions

are the presence of a broad band in the region 3500-3200 cm^{-1}, indicating the presence of O-H (from both alcoholic and carboxylic compounds), possibly NH_2 and NH groups which are capable of taking part in both inter- and intramolecular hydrogen bond formation. Also, the band at 3648 cm^{-1} is more intense in resins than aromatics fraction. Perhaps the most distinguishing feature between the two resin fractions is the difference in carbonyl band intensities. The trend observed in the aromatics fraction is also maintained in the resins fraction. Here again the carbonyl content of the SS bitumen resin fraction is significantly greater than that of the AR bitumen resin fraction. In addition, there are some other minor differences in the region 900-700 cm^{-1}, the implications of which cannot be satisfactorily explained.

Asphaltene fractions are considered to be the most polar components of the bitumen. FTIR spectra of these fractions are presented in Figure 51. In general, the spectra of these fractions are simpler than those of resin fractions. The noticeable features in these are the absence of a band at 3648 cm^{-1} representing the compounds containing free O-H groups, a small broad band in the region 3500-3200 cm^{-1} indicating a moderate amount of O-H groups involved in hydrogen bonding, and also less intense (in comparison to resin fractions) carbonyl bands. The weaker bands that are observed for AR asphaltenes at 975, 948, and 918 cm^{-1} are missing entirely for the SS asphaltenes. These may be attributed to the cyclohexane and cyclobutane ring vibrations and are perhaps less abundant in SS asphaltenes. Once again, the major difference between these two is in the intensity of the carbonyl band at 1659-93 cm^{-1}. A slight shift in the carbonyl wave number is not considered to be significant, particularly when it represents not a single compound but a group of related compounds.

Influence of Chemical Composition on Physical Property

From the above characterization study of bitumen fractions, it becomes apparent that FTIR spectroscopy provides the best distinguishing technique in terms of identification of distinct functional groups and their variations.

Using this technique, an attempt was made to show in the following lines how the differences in the chemical nature of bitumen fractions influence the physical properties of the composite bitumen. Bitumens derived from AR and SS tar sands represent extreme cases in terms of viscosity value. The difference between the two is greater than one order of magnitude. The characterization undertaken in this study was partly to explore the causes which are responsible for these two bitumens to have such divergent viscosity values.

The saturate fractions of both bitumens are identical in every respect (see Table 29), including ^{13}C NMR and FTIR spectroscopic profiles. However, the similarities diminish as the comparison is extended to other fractions of bitumen. Beginning with aromatic fractions, distinct differences between the two are noticeable. These differences become apparent only in the spectroscopic profiles, and of the two techniques employed in this study, only FTIR spectroscopy yields useful information. This is attributed mainly to its superior sensitivity and extensive range.

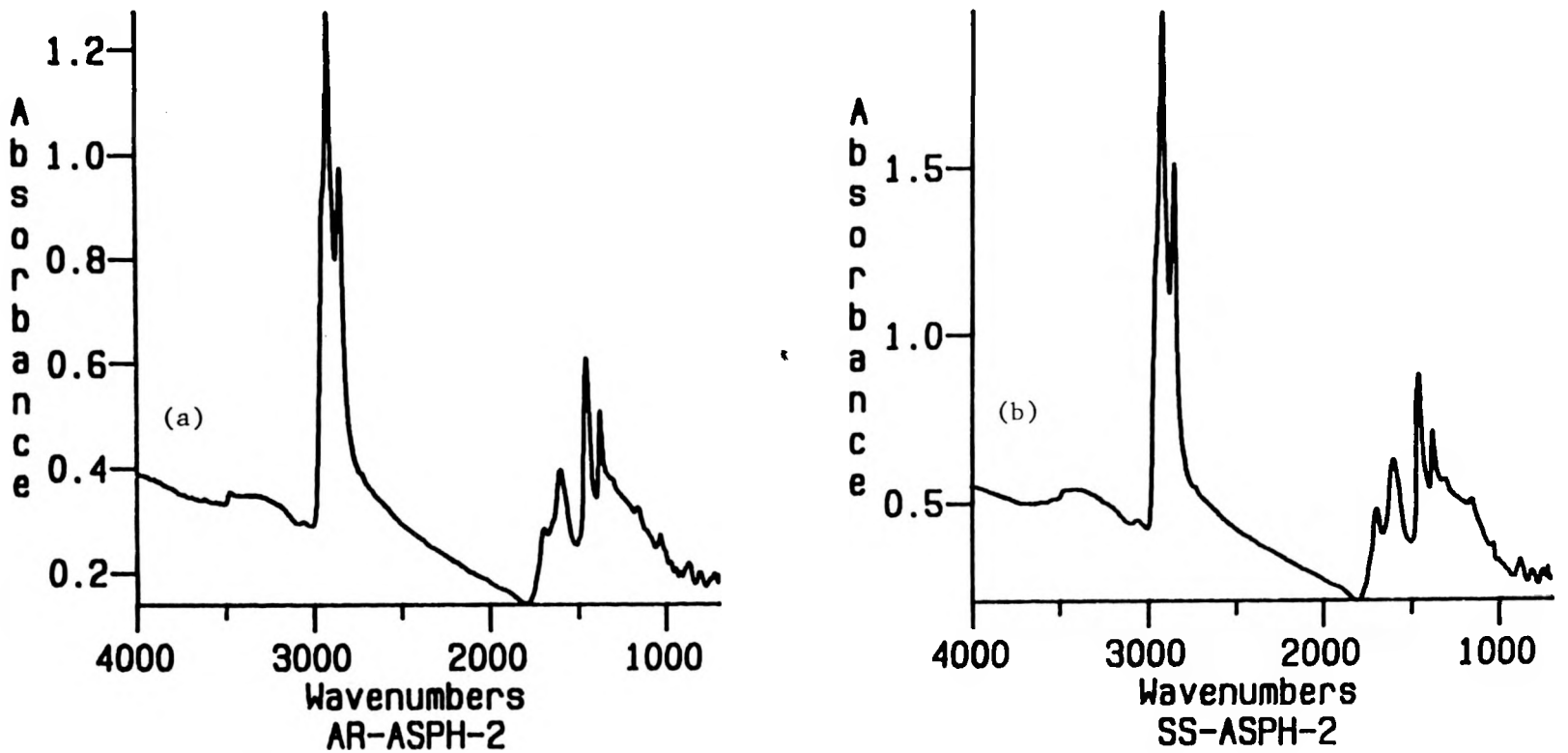

Figure 51. FTIR Spectra of (a) AR Bitumen and (b) SS Bitumen Asphaltene Fractions

In the FTIR profiles, differences are observed in several regions of the scanned spectrum. Since all the absorption bands in the spectrum cannot be satisfactorily accounted for due to the complex nature of the sample, attention was focused only on the region where large differences are observed. Also, it was expected that the major differences between the fractions are brought about by differences in the abundance of polar functional groups and possibly by heteroatom content. A close examination of the spectra of AR and SS bitumen fractions (other than saturates) reveals that significant differences between them are found in the spectral region characteristic to the carbonyl bond stretching. As mentioned earlier, the differences observed in the other region of spectra, *viz.*, 1000-700 cm^{-1}, are mainly related to the differences in the aromatic ring substitutions and also possibly due to the relative abundance of cycloparaffin compounds in both AR and SS bitumens. However, these differences are not expected to contribute significantly to the enhancement of the physical property such as viscosity. The impact of other functional groups involving heteroatoms such as nitrogen and sulfur cannot be fully appreciated because their content in the fractions is small in comparison to oxygen, and their characteristic compounds are too weak and difficult to identify to provide any meaningful interpretation. This is probably due to their relatively small molar extinction coefficients.

The carbonyl band intensities (observed at 1700 ± 6 cm^{-1}) of all the three fractions--aromatic, resin, and asphaltene--derived from both bitumens show very informative trends. The occurrence of an absorption band in this region indicates the presence of carbonyl groups containing compounds such as aldehydes, ketones, carboxylic acids, and esters. However, as carbonyl groups in esters absorb at 1740 cm^{-1}, their presence can be discounted. The amounts of aldehydes and carboxylic acids can be qualitatively evaluated by the intensities of the bands observed at 2728 cm^{-1} (characteristic of C-H stretching band adjacent to C=O group) and 3500-3200 cm^{-1} (broad band indicating the presence of O-H group and its involvement in the hydrogen bond formation), respectively. Spectra presented in Figures 49-51 show that for both AR and SS bitumens the amount of carbonyl compounds increases from aromatic to resin fraction and then decreases in the asphaltene fraction. These variations become evident even when the intensities of carbonyl bands are measured relative to either the C-H stretching or bending vibrational bands observed at 2925 and 1460 cm^{-1}, respectively. A decrease of carbonyl band intensity in the asphaltene fraction is surprising, as it is considered to be the most polar fraction of the bitumen. These spectra also furnish other corroborative evidence (as obtained from ^{13}C NMR spectroscopy; see Table 30), in that aromaticities of the bitumen fractions increase gradually from saturates to asphaltenes as determined by the intensities of the band observed at 1600 cm^{-1}, which is considered to be characteristic of aromatic and conjugated C=C bonds (Painter et al., 1985). However, the aromatic fractions in both bitumens constitute an exception.

Carbonyl band intensities also help differentiate similar fractions of different bitumens. Figures 49-51 indicate that every SS bitumen fraction consistently shows higher intensity (several folds) for the carbonyl band observed at 1700 cm^{-1} than AR bitumen. Since in resin and asphaltene fractions of both bitumens the corresponding bands at 2728 cm^{-1}

and 3500-3200 cm^{-1} are very similar, it can be concluded that differences in the intensities observed for the band at 1700 cm^{-1} are entirely due to the ketonic carbonyls. Even in the aromatic fraction of bitumens, the differences, as described earlier, would only indicate the relatively more ketonic carbonyls in SS bitumen. By virtue of the abundance of these carbonyl group containing compounds in SS bitumen, very strong inter- and intramolecular attractions are fostered among its various constituents, resulting in high viscosity values. This conclusion becomes inevitable, as there are no other identifiable features in any of the chemical characterizations made for these two bitumens which would satisfactorily explain the large difference in their viscosities. It is rather surprising to find that of all possible functional groups present in bitumen, only carbonyl groups would so influence the viscosity. It has been known that viscosity is in some way related to the internal structure of the bitumen. For a similar material like asphalt, a model has been developed which describes the bitumen as a composite material consisting of solid asphaltenes suspended in liquid hydrocarbons (saturates), and the suspension is stabilized by the resin and aromatics which function as surfactants.[83] As a result of these interactions, the internal structure of bitumen is considered to have a three-dimensional network. Results from this study not only lend support to this model, but also point to the specific group of compounds that are responsible for the enhanced interactions among the various fractions of bitumens.

The influence of carbonyl groups on bitumen viscosity can be further illustrated by the fractionation and characterization studies of Athabasca tar sand bitumen. The polar fractions--aromatics, resins, and asphaltenes--derived from Athabasca bitumen have been observed to contain even lower levels of carbonyl groups than Asphalt Ridge bitumen (unpublished results). This observation provides strengthening evidence to the important role of carbonyl groups in enhancing the viscosity of bitumen. It also becomes apparent that the role of asphaltenes in the determination of bitumen viscosity is secondary in comparison to that of carbonyl group compounds. As pointed out in the earlier section that even though Athabasca bitumen contains about 16.5% asphaltenes, its viscosity (5 Pa.S.) is about one order of magnitude less than that of Asphalt Ridge bitumen (80 Pa.S.) with only 7% asphaltenes. This clearly demonstrates the influence of the chemical nature of bitumen fractions on viscosity rather than the relative abundance of asphaltenes present.

The only mechanism of carbonyl group participation in the enhancement of bitumen structure will be through hydrogen bond formation with alcohols, carboxylic acids, amides, amines, and imines. Presumably all these compounds are present in the bitumen, although some of them are extremely low. However, a careful analysis of the FTIR spectra should reveal that, excepting the carbonyls, the amounts of all these other groups are very similar in both AR and SS bitumens. From the above characterization study, it would appear that the amounts of carbonyls in the composition of AR bitumen are very low. As a result, they cannot optimally engage the other groups mentioned above in a structure-building H- bond formation. In the case of SS bitumen, however, there are adequate levels of carbonyls with which to form an extensive structural network, hence high viscosity.

COMPARISON OF HIAWATHA COAL AND BITUMEN-DERIVED RESINS

Coal resins are a complex mixture of yellow to brownish-yellow colored solids which begin to melt at relatively higher (>136 °C) temperatures. On the other hand, bitumen-derived resins, when freshly separated from bitumen, appear as black crystalline solids which melt at low temperatures. They appear as glossy semisolids at room temperature. Elemental analyses of both types of resins are presented in Table 31. The data outlined indicate that the three elements other than hydrogen and carbon are relatively low in coal resins, while the carbon content is slightly higher. Aromaticity of coal resins, as determined by ^{13}C NMR analysis, is significantly lower.

Table 31

Comparison of the Properties of Coal and Bitumen-Derived Resins

Property	Coal Resin	Asphalt Ridge Bitumen Resin	Sunnyside Bitumen Resin
% Carbon	85.75	81.20	83.38
% Hydrogen	10.63	10.85	10.63
% Nitrogen	0.35	1.58	1.14
% Oxygen	3.07	5.95	4.45
% Sulfur	0.19	0.42	0.40
H/C Ratio	1.49	1.60	1.53
Aromaticity	0.09	0.18	0.17

^{13}C NMR analysis of coal resin does reveal some distinguishing features from that of bitumen resins. The spectrum obtained for the coal resin is displayed in Figure 52. The bands in the region characteristic to unsaturated carbon indicate similar features to those observed for bitumen resins. However, from the location of principal bands observed in the saturated carbon region, it may imply that the basic skeletal structure in coal resins is quite different from those of bitumen resins (Figures 44-45).

FTIR spectra of coal resin are presented in Figure 53. As pointed out earlier, this method of comparison is more useful for differentiation

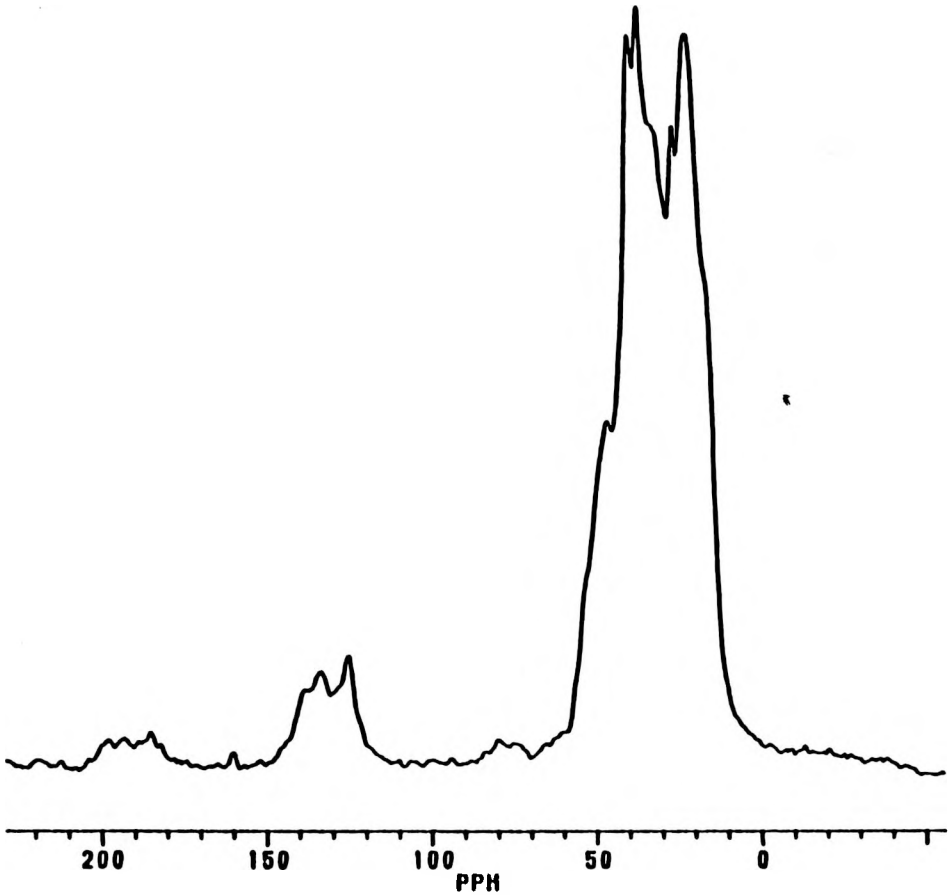

Figure 52. Solid ^{13}C NMR Spectrum of Utah Wasatch Plateau Coal Resin

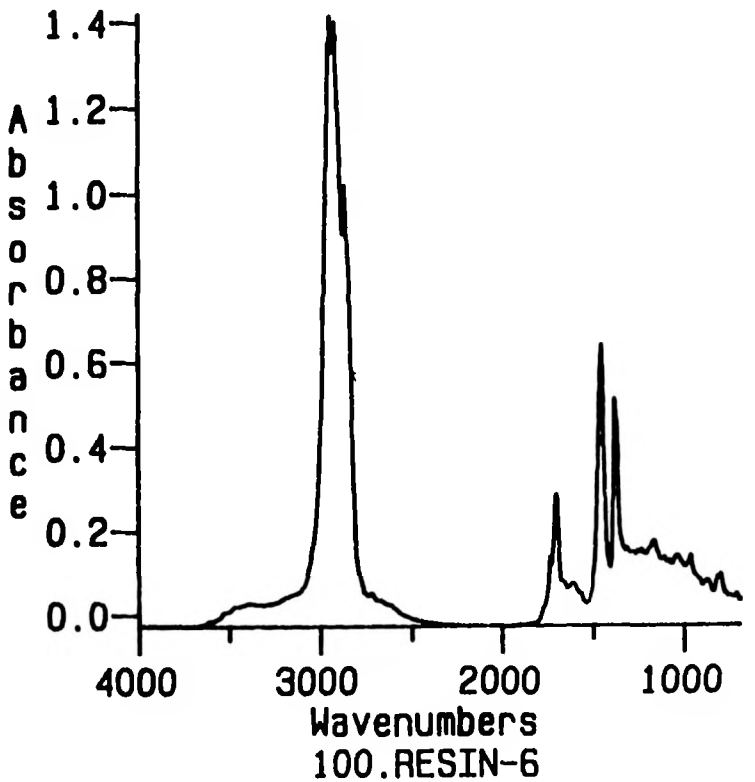

Figure 53. FTIR Spectrum of Utah Wasatch Plateau Coal Resin

and better identification of the constituent components. There are several features in the spectrum of coal resins which are distinctly different from those of bitumen resins. Among these are the following.

1. Absence of free -OH group containing compounds, as there is no characteristic band at 3648 cm^{-1}.

2. The broad band in the region 3500-3200 cm^{-1} is extremely small.

3. A relatively intense band observed at 2958 cm^{-1} indicates the presence of a large number of methyl groups in coal resins. However, in comparison with bitumen resins, there is no correspondingly enhanced peak at 2958 cm^{-1} representing the symmetrical stretching vibration of the same -CH bond of the methyl group. Perhaps this may be explained by the restrictions imposed on this vibration by steric considerations.

4. A band at 1740 cm^{-1} indicates the presence of carbonyl groups associated with esters. This band is not noticeable in the case of bitumen resins.

5. The aromatic content of coal resins, as characterized by the band at 1600 cm^{-1}, is extremely low.

6. Coal resins have very low intensity bands in the region 1270-1200 cm^{-1}, which indicates low amounts of compounds containing alcohols and ethers.

7. Although less intense, a distinct band is observed for coal resins at 973 cm^{-1}, which is characteristic of C-H stretching of trans-isomer of olefinic linkages ($^{H}>C=C>_{H}$).

8. The bands observed in the region 900-700 cm^{-1}, which are considered to represent, among others, the -CH deformation modes of multiple-substituted aromatic compounds, are relatively weak. This is in agreement with the weak band observed at 1600 cm^{-1}. Position of most of the observed bands are entirely different from those of bitumen resins. Although precise identification of these bands is not possible, those observed can be attributed to the -CH stretching of cis isomers of olefinic compounds.

These comparisons between coal and bitumen resins indicate significant differences between them. Bitumen resins have higher aromatic and heteroatom contents. Their FTIR spectra also show that they are composed of relatively more diverse numbers of compounds. This study was initiated only to compare the chemical characteristics of coal and bitumen resins. However, to evaluate bitumen resins as substitutes for existing coal resin markets, further studies of separated resins would have to be undertaken.

CONCLUSIONS

Since viscosity of the bitumen is an important property which plays a decisive role in its recovery from the tar sand deposits of Utah, a study was undertaken to relate the differences in the viscosities of two different bitumens to their chemical composition.

Sunnyside and Asphalt Ridge bitumens of Utah, which greatly differ in their viscosities, were subjected to fractionation and characterization. The composition of these bitumens in terms of their relative amounts of fractions was found to be different. Among the analytical techniques used in the characterization of fractions, FTIR spectroscopic analysis was shown to be most informative. This analysis reveals that there are significant differences between the AR and SS bitumens in every fraction with the exception of the saturates fraction.

The notable difference between a given fraction of AR and SS bitumens is observed in the relative intensities of the carbonyl band located at 1700 cm^{-1}. In every SS bitumen fraction, the intensity of this band is proportionally higher than that of AR bitumen. From this observation it was concluded that bitumen viscosity is directly related to the amounts of various carbonyl compounds present in the bitumen. It is the relative abundance of these carbonyl compounds in SS bitumen which renders such high viscosity. The role of carbonyl compounds in the mechanism of increased viscosity for SS bitumen can obviously be attributed to their ability to form extended hydrogen bonding within a complex molecule (intramolecular) or with its neighbor (intermolecular). Further, since there appears to be no observable differences in the amounts of -OH and -NH containing compounds between AR and SS bitumens, it can only be argued that these compounds are effectively utilized for the hydrogen bond formation in the case of SS bitumen.

It is known that asphaltenes affect the viscosity of bitumen. From this study it has become clear that viscosity is also influenced by the presence of carbonyl compounds. The relative importance of these two variables on the magnitude of viscosity can be demonstrated by a comparison of Athabasca and AR bitumens. Athabasca bitumen contains 16.5% asphaltenes where AR bitumen contains only 7.3%, yet the viscosity of Athabasca bitumen is an order of magnitude less than that of AR bitumen. This large difference in viscosity can be explained if one takes into account the carbonyl compounds present in each of them. Athabasca bitumen has lower amounts of carbonyl compounds than AR bitumen and hence has lower viscosity. This clearly demonstrates that carbonyl compounds contained in the bitumen play a more dominant role in the determination of viscosity than its constituent asphaltenes.

Finally, a comparison of the bitumen-derived resins with that obtained from Hiawatha coal shows some significant differences, both in their physical and chemical properties. Coal resins are characterized by lower heteroatom and aromatic contents. Even the nature of carbonyl compounds that are present in coal resins, as determined by the FTIR spectrum, are different.

EXTRACTION OF BITUMEN FROM WESTERN TAR SANDS
ENERGY EFFICIENT THERMAL METHOD

J.D. Seader — Co-Principal Investigator
Charles J. Coronella — Graduate Student

In order to accurately scale up and optimize a coupled fluidized-bed process for the thermal pyrolysis of Utah tar sands, an in-depth mathematical model must be developed for computer simulation of the process. Using the combustion bed as a starting point, a literature review was first conducted to gather information on the hydrodynamics, transport, and kinetics of fluidized beds. An appropriate model was selected. Experimental work was done in order to confirm some of the conclusions about bed operation reached as a result of the above literature search. Fluidization studies were done with spent (clean) tar sand with the goal of verifying minimum fluidization velocity correlations and conclusions regarding bed pressure drop, void fraction, bubble diameter, and fluidization quality. The kinetics of coke combustion and the subsequent oxidation of CO were explored. Conclusions were reached regarding the heat transfer to the heat pipes which thermally link the pyrolysis bed with the combustion bed. Mass and energy balance equations were derived and a procedure for finding a solution was outlined. Additionally, the phenomenon of particle mixing was investigated. An algorithm was developed for solving the differential equations which model the reactions in the combustion bed, and subsequently, FORTRAN coding has been written and preliminary results obtained as presented here.

Hydrodynamics

The dynamics of a fluidized bed are determined by the regime in which the bed is operating. As the rate of gas flow, u_o, through a packed bed of particles is gradually increased, a point is reached at which the particles begin to rise slowly, until the point of minimum fluidization, when they are free to move about. Increasing the gas velocity from this minimum fluidization velocity, u_{mf}, causes the particles to move about more rapidly until the gas reaches the minimum bubbling velocity, u_{mb}, at which point large bubbles of gas containing very small amounts of entrained particles pass through the bed, essentially bypassing the solids. Increasing the gas velocity above u_{ms} can cause the bubbles to grow until their diameter becomes that of the reactor, at which point slugging begins, which is characterized by large bullet-shaped bubbles passing through the bed. At even higher velocities, where $u_o > u_k$, the bed enters the turbulent regime, characterized by small tongues of air shooting rapidly through the bed.

In order to model a bed, the regime of operation must first be determined. Four criteria for the superficial gas velocity, u_o, must be met to ensure operation in the bubbling regime. They are:

$$u_o > u_{mf} \tag{1}$$

$$u_o > u_{mb} \tag{2}$$

$$u_o < u_{ms} \tag{3}$$

$$u_o < u_k \tag{4}$$

An empirical correlation given by Geldart and Abrahamsen[98] for the minimum bubbling velocity is:

$$u_{mb} = 2.07 \overline{d_p} \rho_g^{0.06} \mu_g^{-0.347} \exp(0.716\, m_f) \tag{5}$$

where $\overline{d_p}$ is the average particle size, ρ_g is the gas density, μ_g is the gas viscosity, and m_f is the mass fraction of particles of a diameter less than 45 μm. (All variables are in SI units). Taking d_p as 140 μm, m_f as 3%, and air at 575 °C and 1 atm, all typical values, we calculate u_{mb} = 0.010 m/s for the combustion bed, which corresponds to a mass velocity of 3.16 lb/hr • ft^2. Interpolating from the experimental results of Jayakar[99] to a temperature of 575 °C, a minimum fluidization mass velocity of 5.2 lb/hr • ft^2 is found. This indicates that at all fluidizing conditions, the bed is bubbling, which is supported by Geldart,[100] who states (very broadly) that sand, which falls into his Group B category, will bubble immediately upon reaching its minimum fluidization velocity.

Presumably, an industrial column will not experience slugging because of a large column diameter and the presence of vertical heat pipes spaced evenly through the bed, which will have the effect of decreasing the allowable bubble size.[101,102] This phenomenon is discussed in greater detail below.

Yerushalmi and Cankurt[103] derived an empirical relation for the threshold of the turbulent regime:

$$u_k = 7.0 \sqrt{\rho_g \overline{d_p}} - 0.77 \tag{6}$$

where all quantities are given in SI units. This correlation was developed for air at atmospheric conditions, and predicts $u_k/u_{mf} = 160$. Since u_{mf} decreases with increasing temperature, it is to be hoped that this ratio will be no worse at the true operating conditions of the bed. Therefore, each of the equations 1 through 4 are satisfied under all conditions for which $u_{mf} < u_o < u_k$; so the combustion bed will operate in the bubbling regime for a very wide range of fluidizing gas velocity.

In order to simulate a fluidized bed, values are required for the void fraction at minimum fluidization, ε_{mf}, and the minimum fluidization velocity, u_{mf}. For the combustion bed, ε_{mf} was determined by Guo Di and Seader[104] and is given by:

$$\varepsilon_{mf} = 0.476\ Re_{mf}^{-0.02} \tag{7}$$

where $Re_{mf} = \overline{d_p}\ \rho_g u_o/\mu_g$. Note the slight dependence on Re_{mf}. This finding is supported by the conclusions of Mathur et al.,[105] Saxena and Mathur,[106] Yang et al.,[107] and Shrivastava et al.,[108] who maintain that when minimum fluidization occurs in the laminar regime ($Re_{mf} < 2$), the void fraction will remain virtually constant with changing temperature. From Jayakar's data,[99] Re_{mf} of clean sand varies from 0.2 at ambient temperature to 0.03 at 600 °C, and the bed, therefore, is always operating under laminar-flow conditions.

There are a myriad of correlations for the minimum fluidization velocity. Some are based on theoretical concepts, some are empirical; some are valid for a large particle-size distribution, others are for high temperatures, and so on. Many of the more recent correlations are based on the Ergun equation,[109] which was developed to give the pressure drop in a packed bed of particles of height L:

$$\Delta P = \frac{150\mu_g\, uL\,(1-\varepsilon)^2}{\phi_s^2\, d_p^2\, \varepsilon^3} + \frac{1.75\rho_g\, u^2 L\,(1-\varepsilon)}{\phi_s\, d_p\, \varepsilon^3} \tag{8}$$

When this is combined with the following relation which equates the weight of the particles to the pressure drop in a fluidized bed,

$$\Delta P/L_{mf} = (\rho_s - \rho_g)\ g\ (1-\varepsilon_{mf}) \tag{9}$$

we obtain

$$\frac{A\ Re_{mf}^2}{\phi_s\ \varepsilon_{mf}^3} + \frac{B\ Re_{mf}\ (1-\varepsilon_{mf})}{\phi_s^2\ \varepsilon_{mf}^3} = Ar \qquad (10)$$

where A = 1.75 and B = 150. In these equations, μ_g is the gas viscosity, u is the superficial gas velocity, L is the length or height of bed, ε is the void fraction, ϕ_s represents the particle shape factor, d_p is the average particle size, ρ_g is the gas density, Re_{mf} is the particle Reynolds number at minimum fluidization, and Ar is the Archimedes number defined as

$$Ar = g\ \overline{d_p}^3\ \rho_g(\rho_s - \rho_g)/\mu_g^2 \qquad (11)$$

Equation 10 can be rearranged to give an explicit equation for Re_{mf}:

$$Re_{mf} = [(0.5\ K_2/K_1)^2 + Ar/K_1]^{0.5} - (0.5\ K_2/K_1) \qquad (12)$$

where $K_1 = A/(\phi_s\ \varepsilon_{mf}^3)$ and $K_2 = B(1-\varepsilon_{mf})/(\phi_s^2\ \varepsilon_{mf}^3)$.[110] Recently, many researchers have discovered that this modified Ergun equation works well under various conditions with different values or expressions for K_1 and K_2.[111-121] At the low Reynolds numbers at which the combustion bed will operate, the first term of equation 10 can be dropped, leaving

$$Re_{mf} = Ar\ \phi_s^2\ \varepsilon_{mf}^3/[B(1-\varepsilon_{mf})]. \qquad (13)$$

The correlation of Hartman and Svoboda[119] gives an explicit temperature dependence of equation 12 by setting $A = \alpha + \beta T$. Using the data of Jayakar[99] for spent sand from Tar Sand Triangle over a temperature range of 23.5 °C to 600 °C, α and β were found by linear regression to be -40.45 and 0.8895, respectively. Using these values, the average error is 5.9% and the maximum error is 9%.

To compute an average particle size $\overline{d_p}$ when the particles cover a wide size distribution, nearly all researchers use the harmonic mass fraction average as suggested by Kunii and Levenspiel[113] and Yang et al.:[107]

$$\frac{1}{\overline{d_p}} = \sum_I \frac{w_I}{d_{p,I}} \qquad (14)$$

The literature search was extended into examining how the presence of vertical heat pipes in the fluidized bed will affect the bed hydrodynamics. Harrison and Grace[122] outlined these effects. Bubble size is reduced, mass transfer and reaction conversion are increased, but heat

transfer and solids mixing (which are promoted by particle mixing caused by rising bubbles) are reduced. Nearly all these effects are the result of the reduced bubble size and corresponding bubble rise velocity. Yates et al.,[123] Sitnai and Whitehead,[124] Kunii and Levenspiel,[102] and Volk et al.[125] confirm Harrison and Grace's conclusion that the presence of vertical tubes reduces bubble size. Yates et al.[123] and Harrison and Grace[122] agree that the bubbles tend to "climb" narrow tubes, that the bubbles have a tendency to become elongated when doing this, and that the bubble rise velocity is faster when climbing a rod than the corresponding velocity of an equally sized bubble in an open bed. Harrison and Grace[122] recommend vertical tubes as the best baffles when heat transfer is required. Along with Volk et al.,[125] they also claim that the extent of reaction conversion in industrial-scale reactors baffled with vertical tubes is approximately the same as that in laboratory-scale reactors. Despite this attention from several researchers, there are no data available to quantitatively predict the bubble size reduction.

There is a wide distribution of particle size in many tar sands, with the particle diameter ranging typically from less than 38 μm to greater than 1,000 μm. This leads to the suspicion that there may be segregation by particle size through the bed, which would then need to be accounted for in a mathematical model of the bed according to a solids mixing model.

The mechanisms of solids mixing in gas-fluidized beds are well understood.[126] Gas bubbles rising through a fluidized bed carry behind them a wake of particles which is approximately 20% of the volume of the bubbles.[127] If it is assumed that all the gas in excess of that required for minimum fluidization passes through the bed as bubbles, a result of the simple two-phase theory,[128] the mass flux of particles rising through the bed via bubble wakes can be quite significant.

It is well known that particle segregation is much more likely when there is a difference in particle density, as compared to a difference in particle size alone.[126,129] Also it is known that particle segregation due to size distribution will occur at gas velocities near u_{mf}.[130,131] However, under these same circumstances (no density difference and large particle-size distribution), there is adequate experimental evidence to conclude that a bed will be well mixed at higher gas velocities.[126,132,133]

Therefore, it is guardedly concluded that particle-size distribution will be constant throughout the lower combustion bed. This conclusion will not be true in the case that the superficial gas velocity is near the minimum fluidization velocity.

There are many models of fluidized-bed reactors available in the literature, and the only thing they all have in common is that they are all statistically inadequate.[134] A very brief survey of models which may be applicable to this system is presented here.

The model of Orcutt, Davidson, and Pigford[135] is an early attempt to predict reaction conversions in fluidized-bed reactors. This model assumes the simple two-phase theory, which says that a bed is made up of a bubble phase and a dense (or emulsion) phase, which is always at minimum

fluidization conditions. All gas in excess of that required for minimum fluidization flows into the bubble phase. In the Orcutt model, bubbles are said to be of a single size and free of solids.

The pioneering bubbling-bed model of Kunii and Levenspiel[102] models three phases: a solids-free bubble phase, a dense (emulsion) phase, and a cloud/wake phase. Single-sized bubbles are assumed to be evenly distributed throughout the bed. The model is recommended by its authors for the case where vertical tubes cause a single bubble size. This model accounts for reaction in the cloud region and for solids mixing due to entrainment of the wake in the bubble.

The bubble assemblage model of Kato and Wen[136] is a two-phase model which was developed for catalytic reactions. The reactor is represented by several well-mixed regions in series, the height of each assumed equal to the diameter of the bubbles in that region. This model accounts for the growth of bubbles by means of coalescence.

Darton[137] presents a fluidized-bed reaction model based on the earlier elegant, theoretically derived bubble-growth model of Darton et al.[138] The bubble growth is predicted by:

$$d_b = 0.54\ (u_o - u_{mf})^{0.4}\ (z + 4\sqrt{A_o})^{0.8}\ g^{-0.2} \qquad (15)$$

The model is characterized by a perfectly mixed dense phase and a solids-free bubble phase which passes through the bed in plug flow. This model computes an average residence time for the gas in the bed, which subsequently is used to compute a mean conversion, a great simplification. Even the author states that this model embodies too many simplifications, and should only be used when there are little or no experimental data available.

Grace[139] presented a two-phase bubbling bed model which is a simplification of Kunii and Levenspiel's bubbling bed model.[102] The primary simplification is the inclusion of the cloud/wake phase with the bubble phase, thereby eliminating the need to determine several parameters and including some particles in the bubble phase. According to Johnsson et al.,[140] the cost in lost accuracy of this simplification is quite small or nonexistent.

Darton's model[137] is just too simple: the reactor is treated essentially as a well-mixed reactor with a characteristic mean residence time. The model of Orcutt et al.[135] is inaccurate because it does not account for solids reacting within the bubble phase. The mass transfer coefficient used by Kato and Wen[136] does not recognize the importance of throughflow between the bubble and dense phases. This leaves the models of Kunii and Levenspiel[102] and Grace,[139] which is a simplification of the former.

Grace[101] indicates that using a single characteristic bubble size is warranted, since the added computation of d_b is an unnecessary complication with little or no additional accuracy. However, the bubble growth model

of Darton et al.,[138] referenced in equation 15, is quite simple and generally well accepted by most researchers today. Therefore, the combustion bed will be modelled using Grace's two-phase bubbling bed model with the added feature of accounting for bubble growth using equation 15.

Kinetics of Combustion

The coke combustion reaction goes through four steps, any of which may limit the rate of reaction: (1) diffusion of oxygen through a boundary layer to the particle surface; (2) adsorption of oxygen; (3) chemical reaction; and (4) desorption and diffusion of product from the particle to the free stream.[141] For small particles burning at low temperatures (temperatures below 1200 K are low in this frame of reference), such as coked sand particles in the combustion bed, the reaction rate is limited by the chemical reaction step.[142] Therefore, oxygen concentration at the particle surface will be essentially the local free-stream concentration.

There are several reactions which can occur during the combustion of coke. Carbon can react heterogeneously with CO_2, O_2, H_2, and H_2O. However, Skinner and Smoot[141] maintain that the rate of oxidation is several orders of magnitude larger than the other rates at these lower temperatures and that an adequate oxygen concentration precludes the other reactions. Thus, there are two heterogeneous reactions and one homogeneous reaction occurring in the combustion bed:

$$C_{(s)} + O_{2(g)} \text{ ---- } CO_{2(g)} \tag{16}$$

$$C_{(s)} + 1/2\ O_{2(g)} \text{ ---- } CO_{(g)} \tag{17}$$

$$CO_{(g)} + 1/2\ O_{2(g)} \text{ ---- } CO_{2(g)} \tag{18}$$

The relative amounts of carbon dioxide and carbon monoxide produced by the oxidation of carbon is given by the empirical correlation of Arthur[143] as:

$$\frac{CO}{CO_2} = 2500 \exp\left(\frac{-6240}{T_p}\right) \tag{19}$$

where 730 K < T_p < 1170 K. At a typical combustion bed temperature of 575 °C, we find CO = 1.6 CO_2. Therefore, significant amounts of carbon monoxide will be oxidized homogeneously.

Some researchers[142] claim that internal pore diffusion can occur during coke combustion, but Smoot and Smith[144] maintain that treating the combustion reaction as a surface reaction is adequate. Additionally, the coke on the sand is essentially a two-dimensional surface with a very

small thickness. Therefore, pore diffusion need not be considered and the reaction may be modelled as a surface reaction according to Smoot and Smith:[144]

$$-r_c = k_p A_p p_{O_2} \tag{20}$$

where r_c is the combustion rate of coke (g/s), k_p is the rate coefficient (g/cm^2-s-atm O_2), A_p is the external surface area (cm^2), and p_{O_2} is the partial pressure of oxygen (atm). The temperature dependence of the rate constant, k_p, is given by:

$$k_p = k_o \exp\left(\frac{-E}{R\,T_p}\right) \tag{21}$$

Unfortunately, values of k_o and E are very dependent on the history and composition of the specific char. Mulcahy and Smith[145] recommend the values of Field et al.,[142] $k_o = 8.71 \times 10^3$ gm/cm^2 atm O_2, and E = 35.7 kcal/mol, which correlated many experimental data within a factor of two for T > 1000 K. Although this work was done at temperatures higher than that with which we are concerned, at least the activation energy E given above is in good agreement with that of Walsh and Green,[146] who found for combustion of petroleum coke at 550 °C, E = 41 kcal/mol.

There are several other characteristics of the specific char that can influence the combustion rate. It is well known[142,144,146] that the presence of trace amounts of minerals can dramatically increase the combustion rate. However, Walsh and Green[146] maintain that this effect does not occur when the temperature is greater than 550 °C, so that it can be ignored in the application here. Certainly the presence of volatiles in the coke would increase the combustion rate, but it is assumed that all volatiles were extracted from the bitumen in the upper pyrolysis bed. The particle temperature is an important parameter in the rate equation, but because the particles are so small and because they come from the upper bed (where the temperature is less than 100 °C below that in the combustion bed), it will be assumed that the particles are at the same temperature as the bed (which is assumed isothermal).

The oxidation of CO is a very complex reaction which cannot be categorized as either fully homogeneous or heterogeneous.[147,148] Based on experimental data, Hottel et al.[149] presented a rather simple rate equation:

$$\frac{-d\,C_{CO}}{dt} = 12 \times 10^{10} \exp\left(\frac{-16,000}{RT}\right) y_{O_2}^{0.3}\, y_{CO} y_{H_2O}^{0.5} \left(\frac{P}{RT}\right)^{1.8} \qquad (22)$$

where C_{CO} is in g mol/ml, t is in seconds, y_i is a mole fraction, T in Kelvin, P in atm, and R = 82.057 ml atm/(g mol K). Doubts about the validity of equation 22 have been raised,[150] and more complex models have been presented.[150,151] However, the simplicity of this equation is appealing, and it has been used by other researchers in modelling fluidized-bed combustion.[152]

Therefore, the coke combustion will be modelled by equations 16 through 22 with $T_p = T$, $A_p = \pi (\phi_s d_p)^2$, and p_{O_2} found from the local free-stream oxygen concentration. The values of k_o and E will be those given by Field et al.[142] Carbon monoxide oxidation will be treated as a homogeneous reaction with kinetics as determined by Hottel et al.[149]

Heat Transfer

Although the mechanism of heat transfer in a fluidized bed with internal vertical tubes is not yet well understood, some generalizations can be made. The bed size does not seem to affect the tube-to-bed heat transfer coefficient, h_t, appreciably; both bed diameter[153] and bed height[154] effects have been investigated. It is generally recognized that heat transfer coefficients to vertical tubes are about 10% higher than those to horizontal tubes.[155] This is because particles tend to "rest" both above and below a horizontal tube, essentially creating a stagnant zone of reduced heat transfer. White et al.[156] reported that for heat transfer in a fluidized bed composed of particles falling in Geldart's Type B classification[100] (small, heavy particles, fluidization of which generally exhibits bubbling bed behavior at all fluid velocities in excess of u_{mf}), such as sand, increasing the tube diameter may increase h_t, but only slightly. According to Gelperin and Einstein,[154] radiation accounts for less than 5% of heat transfer in a fluidized bed at temperatures below 1,000 °C. Since the combustion bed will typically operate at 575 °C, possible radiation effects in the determination of a heat transfer coefficient, h_t, to the heat pipes will be ignored.

The problem of accurately predicting heat transfer coefficients is notoriously difficult, and there is widespread disagreement among researchers of even seemingly basic concepts. In particular, Noe and Knudsen[157] maintain that the presence of more than one vertical tube will cause an increase in h_t; Saxena et al.[158] claim that multiple tubes have little or no effect on h_t; and according to Gelperin and Einstein,[154] the presence of tube bundles causes a reduction in h_t.

After a review of about thirty papers, four correlations were selected,[159-162] and a plot of the predicted Nusselt number as a function of the Reynolds number was made as shown in Figure 54. It is apparent

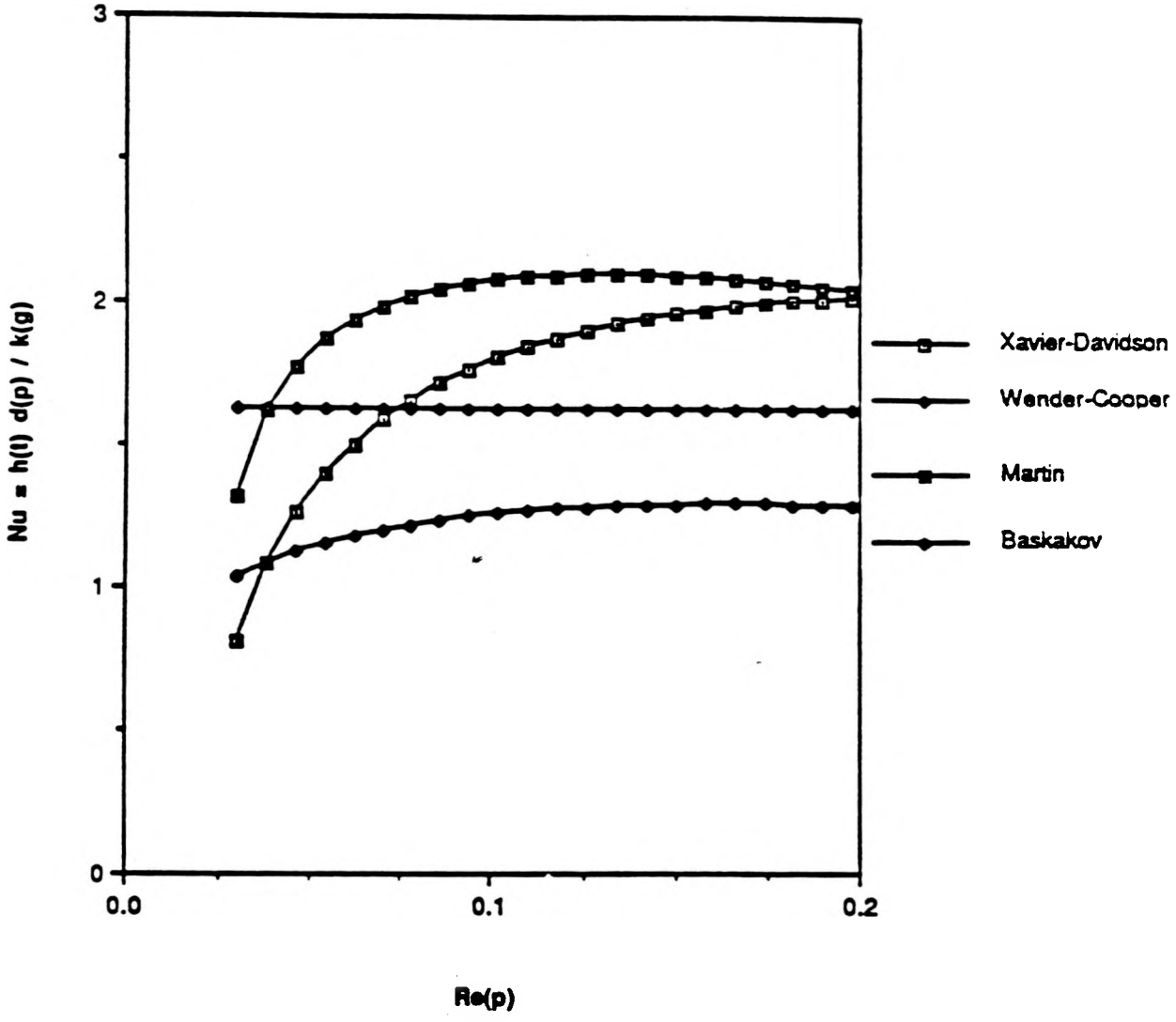

Figure 54. Heat Transfer to a Vertical Tube in a Fluidized Bed

that the predicted Nusselt numbers vary by about a factor of two. The correlation of Wender and Cooper[161] predicts the lowest (most conservative) value, and has been used by many researchers, including Jayakar[99] and Bezama,[163] to model the system here. This correlation is strictly empirical and is given by:

$$h_T = 3.10\frac{k_g}{d_p}(1-\varepsilon)\left(\frac{k_g}{C_g\rho_g}\right)^{-0.43} Re^{0.23}\left(\frac{C_s}{C_g}\right)^{0.8}\left(\frac{\rho_s}{\rho_g}\right)^{0.66} \qquad (23)$$

where the dimensional term $(k_g/C_g\rho_g)$ has the units m^2/s.

It is well known that a plot of Nu_p vs. Re_p should reach a maximum at some optimum gas flow rate. A correlation developed by Gelperin and Einstein[154] gives Nu_{max} for heat transfer to a vertical tube bank:

$$Nu_{max} = 0.75\, Ar^{0.22}\,(1 - d_t/s_H)^{0.14} \qquad (24)$$

For the same operating conditions as those used to generate the curves in Figure 54, we find $Nu_{max} = 1.45$, which is in surprisingly good agreement with the curve generated by equation 23. Bearing in mind the conclusion of Zabrodsky et al.[164] that all correlations of heat transfer in fluidized beds "will be of limited accuracy," it is therefore proposed to use equation 23 to predict h_t.

EXPERIMENTAL WORK

Experimental studies were done with spent (clean) tar sand with the goal of confirming minimum fluidization velocity correlations, and conclusions regarding bed pressure drop, void fraction, bubble diameter, and fluidization quality. These experiments were done in a four-inch column constructed by Smith.[165] In order to study the effect of heat pipes, a bed insert composed of three 3/4-inch diameter vertical aluminum rods in an equilateral triangle configuration was constructed. These rods were supported at the top of the column and extended to about 1.5 inches above the distributor for a length of 73 inches.

The following is a brief description of the experimental procedure employed in these experiments. A sample of the sand used in the column was sieved to determine the particle diameter. The distributor pressure drop was determined as a function of the flow rate through an empty column. Then a large sample of sand, 8.8 lbs., was poured into the column for the fluidization studies. Air flow was initiated, at first very slowly. At each flow rate, the total pressure drop, the flow meter reading, and the bed height were recorded. Unfortunately, the bed was fluidized at a very low flow rate with respect to the valves and flow meter, so it was difficult to take more than a few readings before the bed fluidized. In order to gain information on bubble size, the surface of the bed was photographed at a few different flow rates, both with and without the vertical-rod column inserts.

The sand used in the experimental studies has a wide size distribution, ranging in particle diameter from below 38 microns to above 1190 microns with an average particle size, as defined by equation 14, of $\overline{d_p}$ = 177.3 μm. The density of the sand was determined to be ρ_s = 2590 kg/m^3. The particle shape factor, ϕ_s, was determined by the method of Casal et al.[166] and then confirmed using Ergun's equation.[109] The slope of the line in Figure 55 is ϕ_s^{-2}, which corresponds to ϕ_s = 0.80.

The Reynolds number at minimum fluidization is found from the intersection of two straight lines on a log-log plot of Reynolds number vs. pressure drop.[113] From Figure 56, we find Re_{mf} = 0.210 and the corresponding u_{mf} = 0.0222 m/s. It should be noted here that Jayakar[99] found Re_{mf} = 0.207 for a similar clean sand at ambient temperature.

Many minimum fluidization correlations were applied with varying degrees of success. The method of Hartman and Svoboda,[119] discussed above, was the most successful. Using α = -40.45 and β = 0.8895 K^{-1} determined from Jayakar's minimum fluidization velocity data,[99] we calculate Re_{mf} = 0.200, which is only a 5% error. It should be noted that the value of A used here is A = 221.2, which is more than one hundred times the value of A = 1.75 originally used by Ergun,[109] and it may be incorrect to take such a high value for A. Also, Jayakar's data were taken from sand with a different particle size distribution, so the good agreement may simply be serendipitous. However, the obvious success of the correlation cannot be ignored.

It may be best to use the modified Ergun equation applicable at low Reynolds numbers. Using equation 13, we calculate Re_{mf} = 0.278, which is in error by 32%. This equation will be used in the model because of its simplicity and the high regard with which it is held.

A total of fifteen other correlations were compared with the experimental data. Leva's correlation,[167] which was used by Jayakar,[99] overpredicted Re_{mf} by 46%. The method developed by Guo Di and Seader,[104] intended for use with systems with a wide particle distribution, gave quite unsatisfactory results, underpredicting Re_{mf} by 98%. With respect to this correlation, the minimum fluidization velocity of the mixture is said to be proportional to that of the smallest particles in the bed. Perhaps the cause of the error is the difficulty in identifying the smallest particles in a particle mixture with such a wide size distribution.

The void fraction was found from the known particle density, total weight of solids in the bed, and the measured bed height. The void fraction at minimum fluidization, ε_{mf}, was determined to be 0.45, which compares favorably with values reported in the literature.[113] A correlation for the void fraction as a function of the fluidizing velocity can be found from the simple two-phase theory, first postulated by Davidson and Harrison in 1963.[128] Yates[168] derives an equation for the height of the surface of the bed, L, as a function of the fluidizing velocity, u:

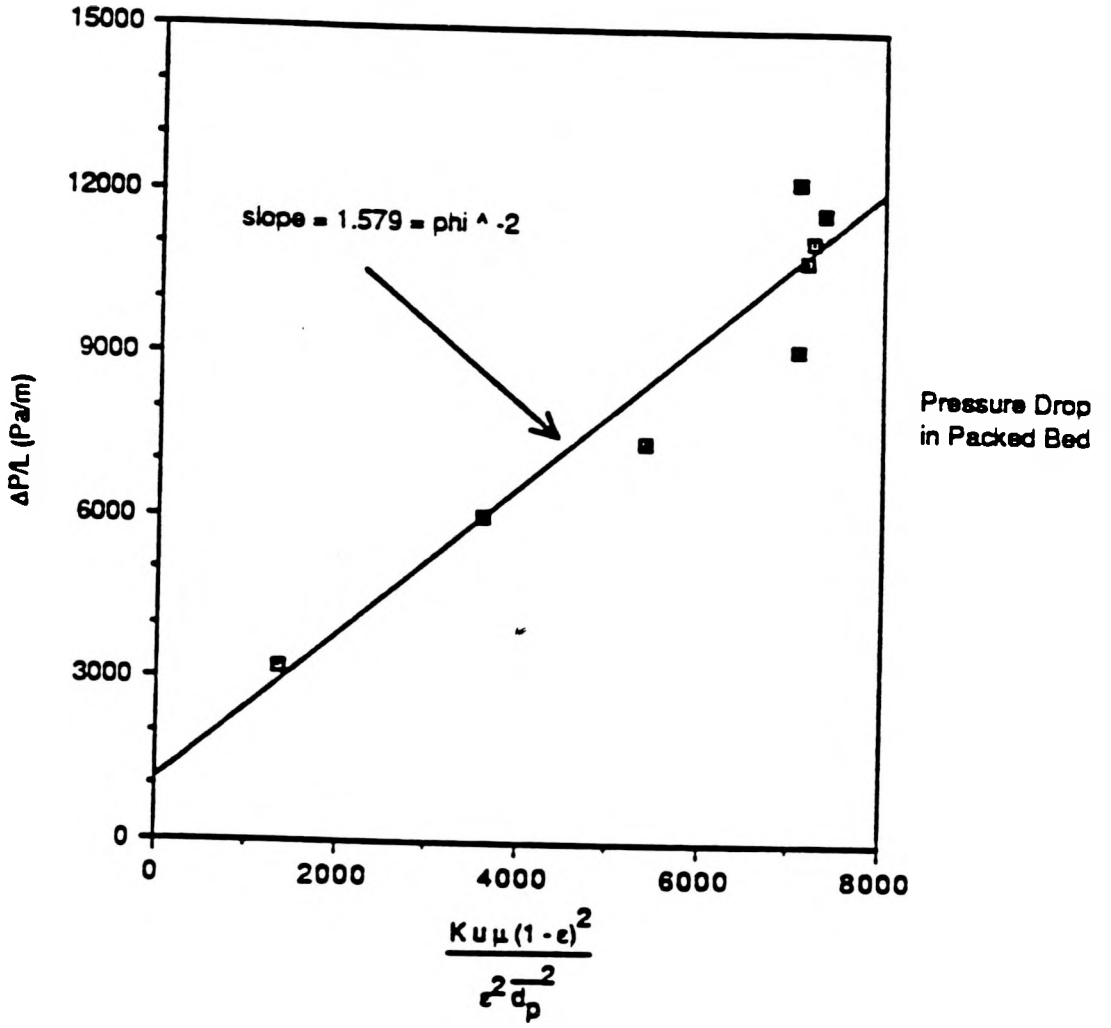

Figure 55. Determination of Shape Factor

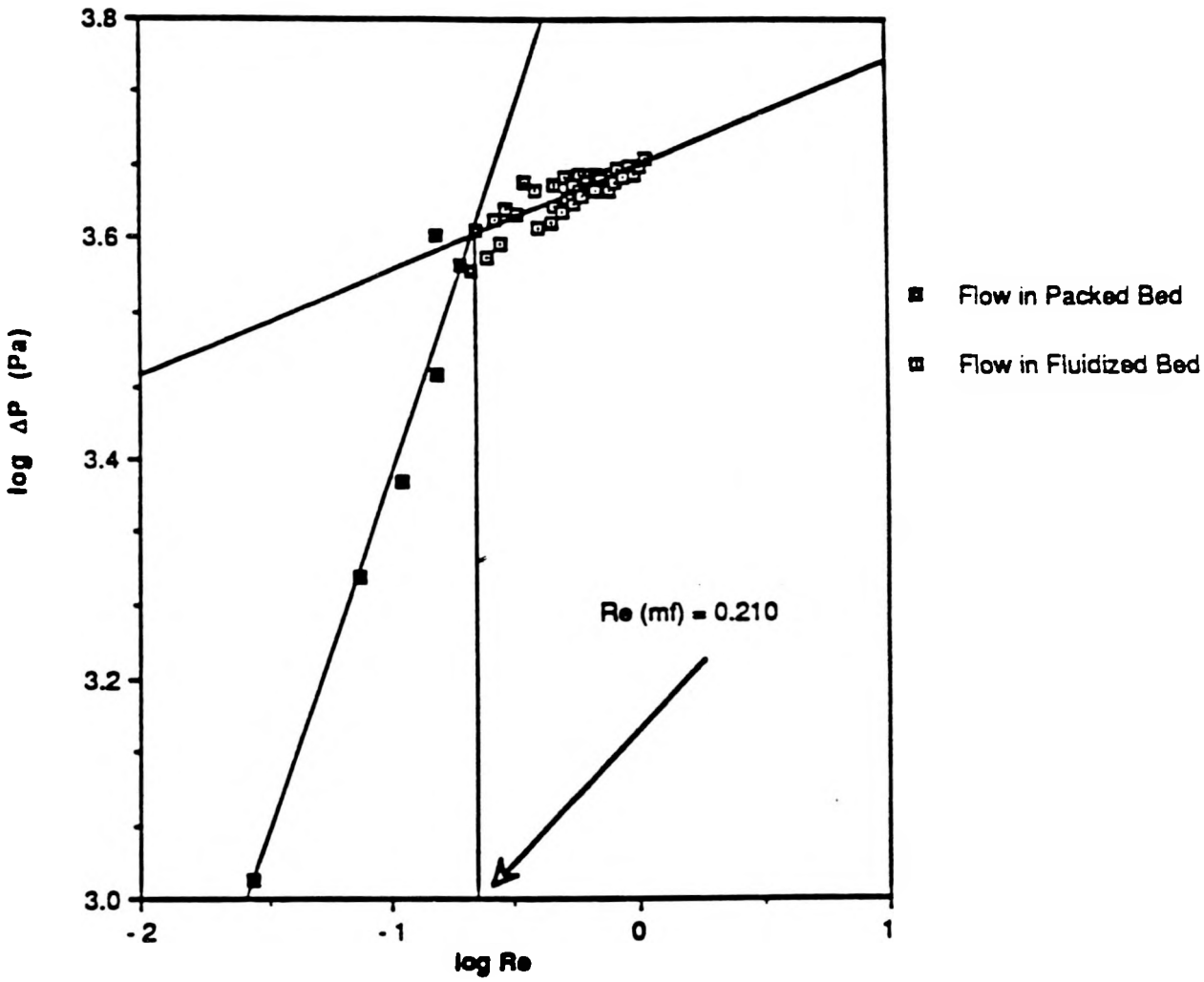

Figure 56. Determination of Minimum Fluidization Velocity

$$\frac{L}{L_{mf}} = 1 + \frac{u - u_{mf}}{0.711\sqrt{g\,d_b}} \qquad (25)$$

The void fraction can then be found from:

$$\varepsilon = 1 - \frac{V_s}{A_B L} \qquad (26)$$

The height of the bed, L, is plotted along with equation 25 in Figure 57. The agreement between experiment and theory is remarkably good. The value used for d_b is that predicted by equation 15 at the top of the bed.

The pressure drop across the bed at minimum fluidization, ΔP_{mf}, was determined to be 4051 Pa from Figure 56. Ideally, ΔP_{mf} can be found by dividing the weight (force) of sand in the bed by the cross-sectional area of the bed. This gives ΔP_{mf} (calc) = 4829 Pa, 19% higher than the measured value.

A cursory investigation of bubble size resulted in confirmation of the bubble growth model of Darton et al.[144] for freely bubbling beds (i.e., beds with no internals which are not slugging). The surface of the bed was photographed and the "eruption diameter" was measured upon playback of the tape. Fryer and Potter[169] claim that the equivalent bubble diameter, d_b, is equal to 0.78 times the measured "eruption diameter" in a freely bubbling bed. Despite the inexact method of measurement, the data are correlated surprisingly well by equation 15, as seen in Figure 58.

Some useful qualitative observations were made during the operation of the fluidized bed. Geldart[100] predicts that beds of sand will bubble immediately upon fluidization. This fact was visually confirmed. When the flow barely exceeded that required for minimum fluidization, small bubbles were observed, as indicated graphically in Figure 58.

The effect of the inserted vertical rods was rather difficult to identify experimentally. The surface of the bubbling bed was photographed both with and without the inserts. At flow velocities slightly above minimum fluidization, the bubbles are apparently slightly larger when pipes are present, as shown in Figure 58. This is surprising in light of the previous conclusion that the effect of internal vertical baffling tubes will be to limit the bubble size. Perhaps the effect of the pipes is to cause the bubbles to achieve a maximum size at relatively low flow rates, and to remain at a constant size with increasing fluid flow. Or, perhaps, there are other unknown phenomena at work in such a small (four-inch diameter) column.

Slugging was observed in the column with and without the inserts. It has been proposed by Harrison and Grace[122] and Volk et al.[125] that the presence of vertical tubes should prevent slugging, at least to some extent. However, wall effects may be significant in the column in which the experiments were done because the column diameter is only four inches,

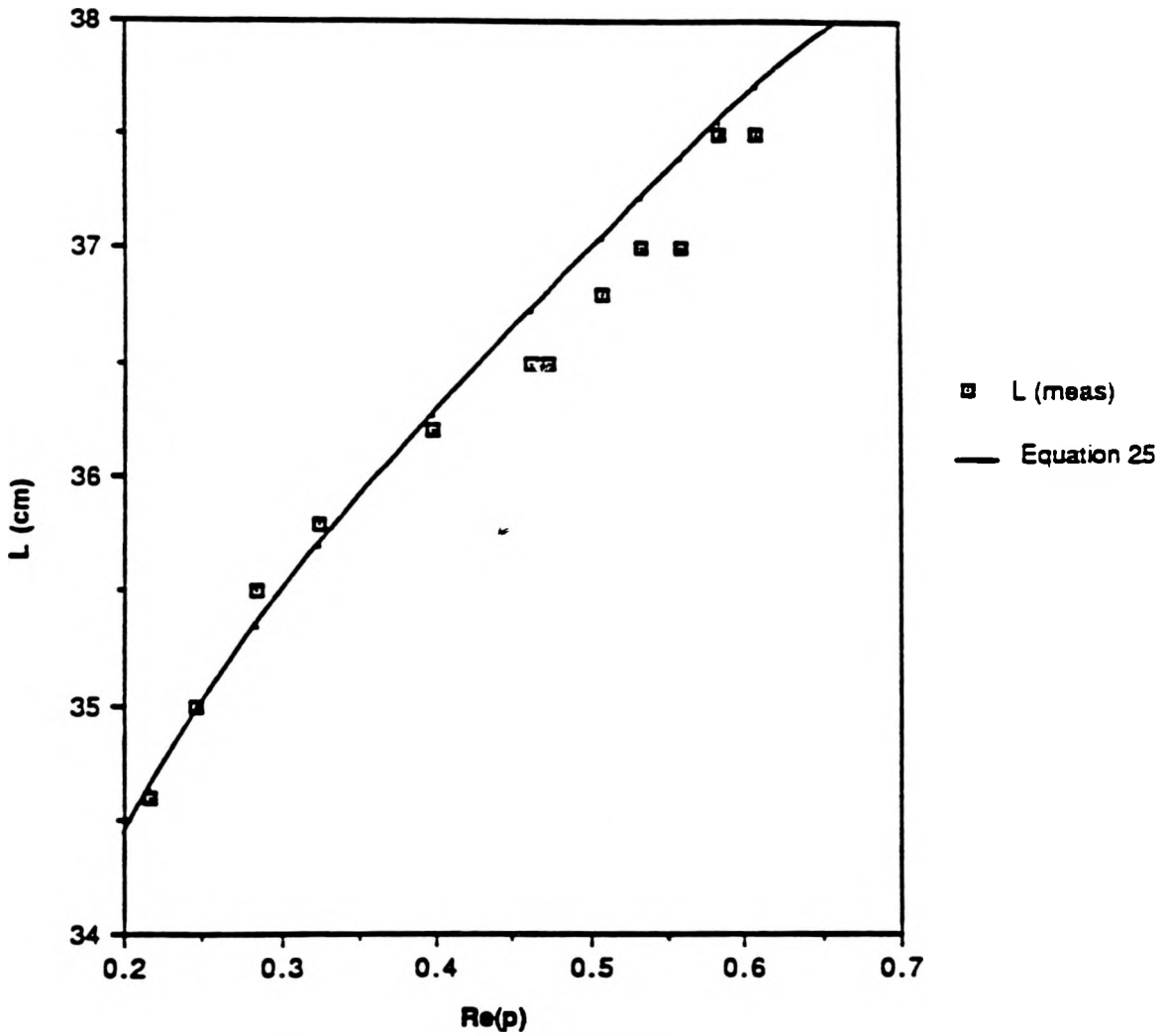

Figure 57. Effect of Reynolds Number on Bed Expansion

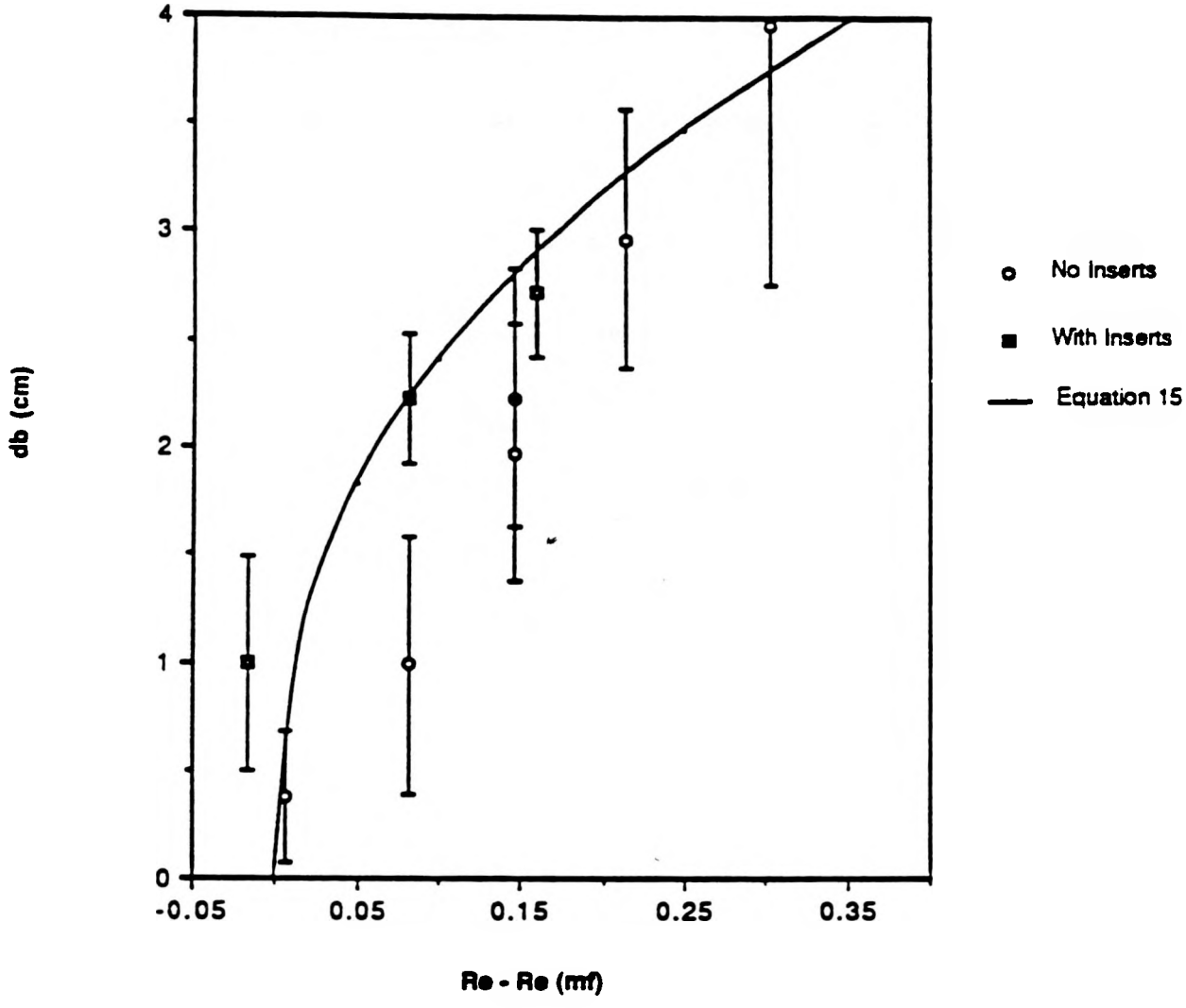

Figure 58. Effect of Reynolds Number on Bubble Size

and there were only three tubes present. Therefore, conclusions regarding slugging in such a small column will not be applied to a reactor of industrial scale.

Model

The equations which will be used to model the lower combustion bed have been derived according to the procedure outlined by Grace.[139] The primary features of this model are as follows:

1. The fluidized bed is said to have two phases: a bubble phase with low solids concentration, and a dense phase.

2. The void fraction in the dense phase stays constant at ε_{mf} at all fluidization conditions.

3. Essentially all of the gas flow passes through the bed in bubbles (i.e., there is no net flow of gas in the dense phase).

4. Gas is exchanged continuously between the two phases throughout the bed.

5. The solids are perfectly mixed throughout the bed.

6. The bubbles pass through in plug flow while exchanging mass with the dense phase.

7. The bed operates isothermally.

With the assumptions detailed above, a mass balance for component i in the bubble phase gives the following:

$$-u \frac{d C_{i,b}}{d z} + k_q a_b \varepsilon_b (C_{i,d} - C_{i,b}) + n_i^e \varepsilon_b + n_i^o \varepsilon_b = 0 \qquad (27)$$

and in the dense phase

$$k_q a_b \varepsilon_b (C_{i,b} - C_{i,d}) + n_i^e (1 - \varepsilon_b) + n_i^o (1 - \varepsilon_b) = 0 \qquad (28)$$

where i can be CO or O_2, superscript e indicates a heterogeneous reaction, and superscript o indicates a homogeneous reaction. In equation 27, the first term represents convection, the second term represents mass transfer between phases, and the last two terms are due to reaction. Equation 28 can be solved explicitly for the dense phase concentrations $C_{i,d}$, which can then be substituted into equation 27 for integration.

The energy balance around the combustion bed is somewhat more complex:

$$\Delta H_{sand} + \Delta H_C + \Delta H_{awO_2} + Q = 0 \tag{29}$$

where

$$\Delta H_{sand} = M_{CB}/A_B \; (1 - f_{cc}) \; C_{sand} \; (T_{pyr} - T_{CB}) \tag{30}$$

$$H_{awO_2} = N_T|O/A_B \; (1 - y_{O_2,0}) \int_{T_{CB}}^{T_{ent}} C_{p,awO_2} \, dT \tag{31}$$

$$Q = (T_T - T_{CB}) \; a_T \int_0^L h_T \; (z) \, dz \tag{32}$$

$$-\Delta H_C = \frac{M_{CB}}{A_B} \; f_{CC} \int_{T_{pyr}}^{T_{CB}} C_{coke} dT + u|_0 \; CO_2|0 \int_{T_{ent}}^{T} CB \; C_{p,O_2} \, dT + m\Delta H_1^{298} \tag{33}$$

$$+ \; n\Delta H_2^{298} + \int_{298}^{T_{CB}} \left\{ m \; C_{p,CO} + n \; C_{p,CO_2} - \left(\frac{M_{CB}}{A_B} \right) f_{CC} \overset{=}{x} \; C_{coke} + (u \; CO_2) \Big|_O^L \; C_{p,O_2} \right\} dT$$

$$m = \frac{2}{M_C} \left(\frac{M_{CB}}{A_B} \right) f_{CC} \overset{=}{x} + 2 \; (u \; CO_2) \Big|_0^L \tag{34}$$

$$n = \frac{-1}{M_C} \left(\frac{M_{CB}}{A_B} \right) f_{CC} \overset{=}{x} - 2 \; (u \; CO_2) \Big|_0^L \tag{35}$$

ΔH_1^{298} and ΔH_2^{298} are standard heats of reaction of the reactions in equations 17 and 16, respectively. These equations can be used to determine the combustion bed operating temperature, T_{CB}, in the case that it is unspecified.

The subroutine LSODA of ODEPACK has been selected to integrate the six variables necessary for the steady state temperature-specified case. This routine has the ability to determine the stiffness of a problem, and then to solve it appropriately. The ability of LSODA to numerically

approximate the Jacobian of the system makes it particularly desirable for this application.

The six variables which are integrated through the length of the bed are:

1. $u \cdot C_{CO,b}$;
2. $u \cdot C_{O_2,b}$;
3. ε;
4. dp/dz;
5. ε_b; and
6. $(r_{C,b} + r_{C,d})$.

The variables ε and ε_b are integrated so that an average of each throughout the bed can be computed.

During the integration, LSODA calls Subroutine DERIV with the current 3values of each of the six integrated variables given above. In order to determine the local rates of each reaction, the dense-phase concentration of CO and of O_2 must be known. These are found by applying a two-dimensional Newton-Ralphson algorithm to the dense phase mass balance equation above (equation 28) for integration over the height of the bed.

The bed height, L, is given by:

$$L = \frac{L_{mf}}{1 - \overline{\varepsilon_b}} \tag{36}$$

where $\overline{\varepsilon_b}$ is the average bubble phase volume fraction of the bed. However, to find $\overline{\varepsilon_b}$, we must integrate up to z = L, and hence an iterative procedure for finding L is indicated. We can make an initial guess for L based on an assumed $\overline{\varepsilon_b}$ by equation 36. Then the integration is carried out, and hence $\overline{\varepsilon_b}$ may be computed. L is recalculated and compared with the previous value. This procedure is repeated until satisfactory convergence is attained. The bounded Wegstein method is used to accelerate the convergence of L and $\overline{\varepsilon_b}$.

It is relatively simple to show that the above successive-substitution method will converge to the correct solution. Let the function defined above for determining L be $\phi(L)$, i.e., L_{n+1} $\phi(L_n)$. If $|\phi'(L)|<1$ near the solution, then ϕ is a contraction mapping of L and convergence is guaranteed for a suitable initial guess. Let $F = \int \varepsilon_b \, dz$. Then $\varepsilon_b =$ [F(L)] F(0)]/L, and we may rewrite equation 36:

$$\phi\ (L) = L + L_{mf} + F(L) - F(0) \tag{37}$$

so

$$\phi'(L) = F'(L) = \varepsilon_b(L) << 1 \tag{38}$$

Therefore, speedy convergence is guaranteed.

We assume that each particle leaving the upper pyrolysis bed is coated with a layer of coke of uniform thickness δ. Therefore, the volumetric flow rate of coke into the lower combustion bed is

$$\frac{f_{CC}M_{CB}}{\rho_C} = \sum_I \ (\textit{volume of coke in each particle size cut } i)$$

$$= \sum_I \frac{2\ M_{CB}(1 - f_{CC})\ w_i}{\rho_s} \left\{3\ (\frac{\delta}{d_i}) + 6\ (\frac{\delta}{d_i})^2 + 4\ (\frac{\delta}{d_i})^3\right\} \tag{39}$$

We can find δ easily by solving equation 39 with any nonlinear equation solver such as the secant method.

It may be assumed[113] that the particles in the fluidized bed are subject to an exit age distribution function similar to that of a CSTR:

$$E\ (t) = \frac{1}{\bar{t}} \exp\ (\frac{-t}{\bar{t}}) \tag{40}$$

where $\bar{t}$, the mean solid residence time in the bed, is uniform for all particles if we assume all elutriated particles are returned via a cyclone. If $\tau(d_{p,i})$ is the time required for complete combustion of the coke on a particle of size $d_{p,i}$, then any particles in the bed for a time greater than $\tau(d_{p,i})$ are not reacting. The fraction of particles of size $d_{p,i}$, which are in the bed for a time greater than $\tau(d_{p,i})$ is $1 - \int_0^{\tau(d_p)} E(t)\,dt$.

The rate of coke combustion throughout the bed is found by LSODA, and is designated I. Then the rate of combustion on a single particle can be found by assuming that this rate is uniformly distributed on all particles which are still reacting, i.e., this rate is $I\ A_p/A_c^T$ where $A_{p,i} = \pi d_{p,i}^2 \phi_s^2$ and A_C^T is the total surface area of all particles which have been in the bed for a time less than $\tau(d_p)$.

$$\frac{A_C^T}{A_B} = \frac{6\ L_{mf}(1-\varepsilon_{mf})}{\Phi_s} \sum_I \left[1-\exp\left(\frac{-\tau(d_I)}{\bar{t}}\right)\right] \frac{w_I}{d_i} \qquad (41)$$

Thus, we can compute the $\tau(d_i)$, and from that, the coke conversion on a particle as a function of time, x(t). To find the overall coke conversion, $\bar{\bar{x}}$, a procedure outlined by Kunii and Levenspiel[113] is followed.

$$1 - \bar{x}_I = \int_0^{\tau(d_I)} [1-x_I(t)]\, E(t)\, dt \qquad (42)$$

$$1-\bar{\bar{x}} = \frac{2(1-f_{CC})\,\rho_C}{f_{CC}\rho_s} \sum_I (1-\bar{x}_I)\, w_I \left\{3\left(\frac{\delta}{d_i}\right) + 6\left(\frac{\delta}{d_i}\right)^2 + 4\left(\frac{\delta}{d_i}\right)^3\right\} \qquad (43)$$

RESULTS

The reaction rates, gas concentrations, and bed void fraction have been determined for a typical Tar Sand Triangle case, with T_{CB} = 575 °C. The oxygen conversion profiles are presented in Figure 59. Equation 39 was solved by the secant method to find δ = 1.3 μm. A plot of $\tau(d_i)$ versus d_i is presented in Figure 60 for this same case. It may be surprising to note that $\tau(d_i)$ is inversely proportional to d_i. However, recall that the combustion reaction is treated as a surface reaction. Despite the fact that the smaller particles enter the bed with a smaller amount of coke, the smaller surface area causes a slower reaction.

FUTURE WORK

The model of the lower combustion bed is almost complete. However, it still remains to treat the operating temperature T_{CB} as an unknown, and to subsequently model the upper pyrolysis bed.

NOMENCLATURE

A	Constant in equation 10
a_b	Specific area of bubbles (m^2/m^3)
A_b	Cross-sectional area of bed (m^2)
A_C^T	Total surface area of particles in bed with unburned coke
A_p	Surface area of particle

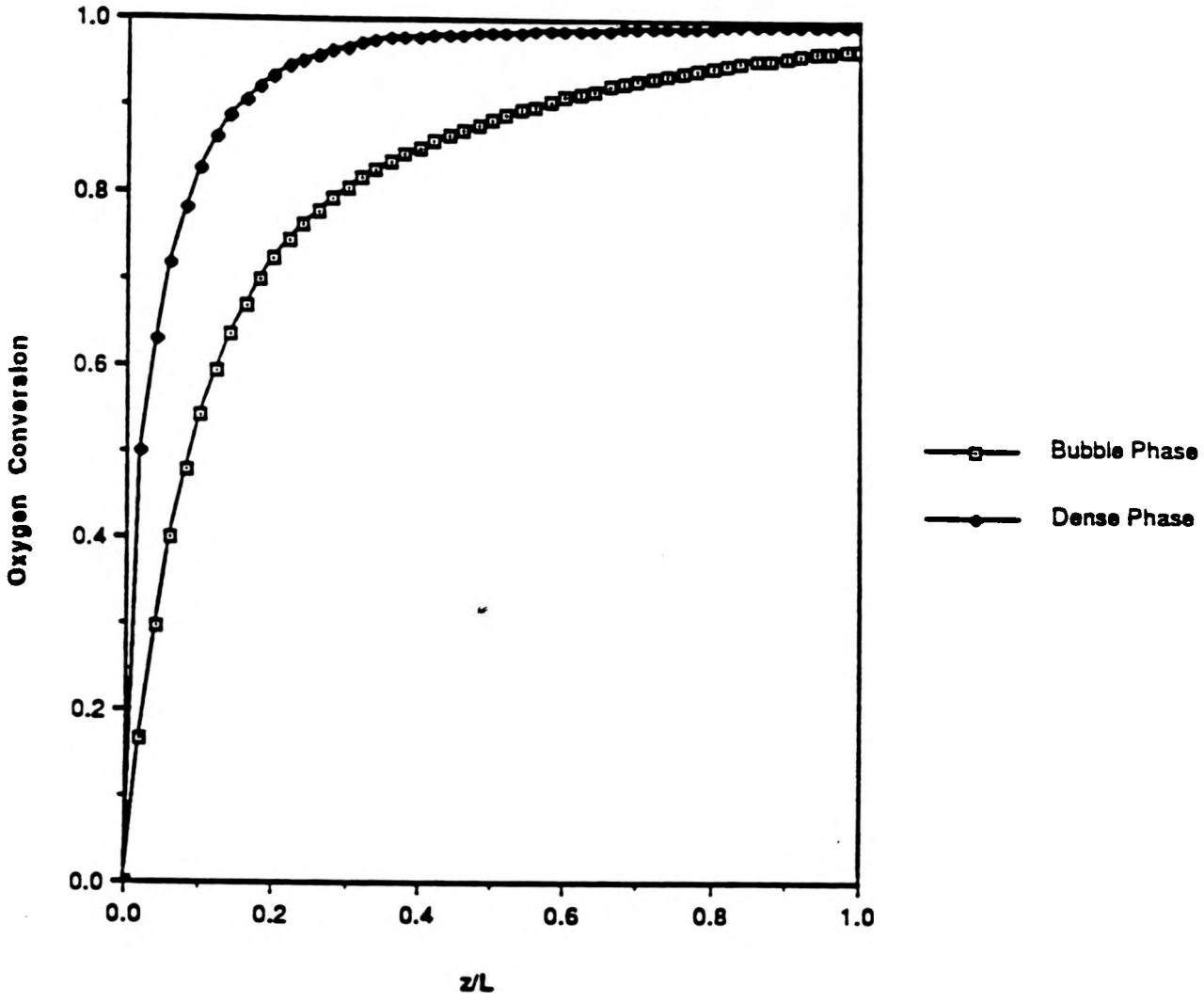

Figure 59. Oxygen Conversion Profiles

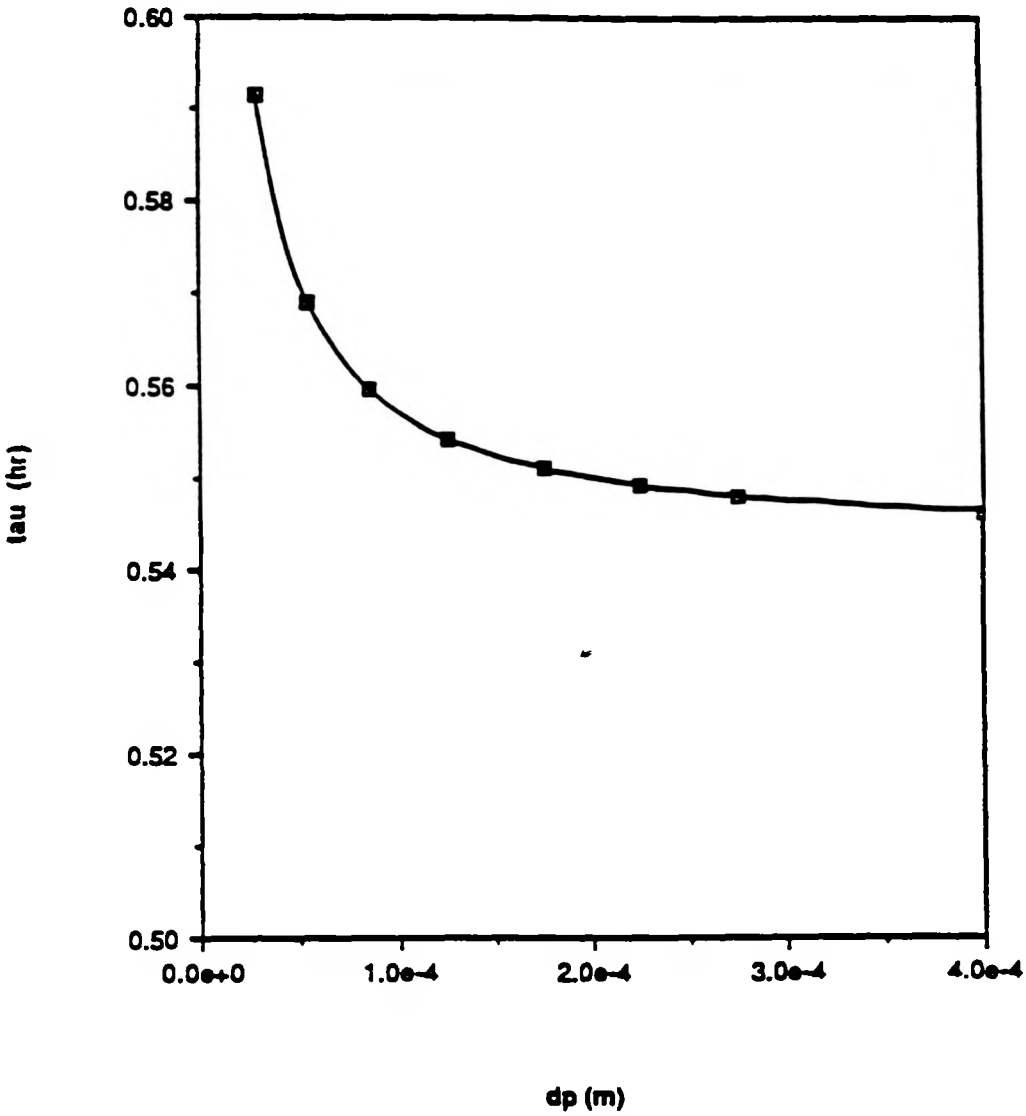

Figure 60. Time Required for Complete Combustion

A_r	Archimedes number defined in equation 11
A_0	Catchment area of distributor
B	Constant in equation 10
C_i	Heat capacity
C_g	Heat capacity of gas
C_s	Heat capacity of particles
d_b	Effective bubble diameter
d_p, $\overline{d_p}$	Average particle size
$d_{p,i}$	Arithmetic average of two screen width sizes for one sized cut--one above and one below
d_t	Vertical heat transfer tube diameter
E	Activation energy of combustion reaction
E(t)	Exit age distribution of particles leaving bed
F	$\int \varepsilon_b \, dz$, a function of z
f_{CC}	Mass fraction of entering solids which is coke
g	Acceleration of gravity
h_t	Heat transfer coefficient between fluidized bed and tube
I	Total rate of coke combustion in bed per area of bed
k_g	Thermal conductivity of gas
k_p	Surface reaction rate constant
k_q	Mass transfer coefficient (m/s)
k_o	Preexponential coefficient of k_p
K_1, K_2	Constants in equation 12
L	Total height of fluidized bed
m	Molar rate of heterogeneous CO production

M_{CB}	Mass flux of coked sand entering combustion bed
m_f	Mass fraction of fines; $d_p < 45$ μm
n	Molar rate of heterogeneous CO_2 production
$n_{i,p}$	Molar production rate of component i
$N_{T\|o}$	Total molar flow rate of inlet combustion gas (kg mol/s)
Nu_{max}	Maximum Nusselt number at some fluidizing velocity
Nu_p	Particle Nusselt number = $h_t\ d_p/k_g$
P	Pressure in bed
p_{O_2}	Partial pressure of oxygen
Q	Total heat transfer to heat pipes
r	Reaction rate
R	Gas law constant
Re, Re_p	Particle Reynolds number = $d_p u\ \rho_g/\mu_g$
Re_{mf}	Particle Reynolds number at minimum fluidization
s_H	Horizontal spacing of heat pipes
t	Time
$\bar{t}$	Average particle residence time in bed
T	Bed temperature
T_{CB}	Combustion bed temperature
T_{ent}	Entering combustion gas temperature
T_p	Particle temperature
T_T	Heat pipe temperature
u, u_o	Superficial velocity of gas through bed
u_k	Minimum gas velocity for the turbulent regime
u_{mb}	Minimum superficial velocity for bubbling

u_{mf}	Superficial velocity of gas through bed at minimum fluidization
u_{ms}	Minimum superficial velocity for slugging
V_s	Total volume of solids only in bed
w_i	Weight fraction of a size cut of particles
$x_i(t)$	Conversion of coke on particle size $d_{p,i}$ in bed
$\bar{x}$	Mean of coke on particles of size $d_{p,i}$ leaving bed
$\bar{\bar{x}}$	Mean exit conversion of coke
y_i	Mole fraction (in gas) of component i
z	Vertical ordinate through the bed

Greek

α, β	Temperature dependence characteristics of A given by Hartman and Svoboda
ΔH_C	Enthalpy change due to combustion in bed, per area of bed
ΔP	Bed pressure drop
δ	Thickness of residual coke on sand particles entering combustion bed
ε	Bed void fraction
ε_b	Volume fraction of bed occupied by bubbles
ε_{mf}	Bed void fraction at minimum fluidization
$\phi(L)$	Iteration scheme which converges to L
ϕ_s	Particle shape factor
π	3.14159...
τ	Time required for complete combustion of coke on a particle
μ_g	Viscosity of gas phase
ρ_c	Density of coke

ρ_g	Density of gas phase
ρ_s	Density of solid particles

Subscripts

awO_2	All entering combustion gas excluding oxygen
b	Bubble phase
d	Dense phase
i	Component
mf	Minimum fluidization condition
n	Iteration counter
p	Phase
0	Initial (entering) condition

Superscripts

e	Heterogeneous reaction
o	Homogeneous reaction
-	Mean

APPENDIX A

LISTING OF NON-LINEAR NUMERICAL INTEGRATION PROGRAM

```
      PROGRAM TEST
C
C        Main program for execute SIMPLEX under general conditions
C
      IMPLICIT REAL*8 (A-H, O-Z)
      CHARACTER #1 CC, CC1, CC2, CC3, CNAME*11
      DIMENSION X(6), XX(7,6), FX(7), C(6), Y(6), Z(6), V(6)
      EXTERNAL F
      WRITE(6,200)
200   FORMAT(//2X, 'the output file name: ', $)
      READ (5,210) CNAME
210   FORMAT (A11)
      OPEN (1, FILE=CNAME, STATUS='NEW')
      WRITE(6,150)
150   FORMAT(//2X, 'the dimension of parameter: ', $)
      READ(5,*) N
      WRITE(6,170)
      READ(5,*) ITMAX
      WRITE(6,190)
      READ(5,*) EPS
5     CONTINUE
      WRITE(6,230)
230   FORMAT(//2X, 'display the intermediate results on screen?(Y/N) ',
     1       $)
      READ(5,140) CC3
      IF (CC3 .EQ. 'Y' .OR. CC3 .EQ. 'y') THEN
         IP=1
       ELSE
         IP1=0
      ENDIF
      WRITE(1,220) N, ITMAX, EPS
220   FORMAT('1', 1X, 'Dimension of parameter:    ', I9,
     *       /2X, 'Maximum iteration time:     ', I9,
     *       /2X, 'Convergence criterion:     ', E9.2)
      WRITE(6,100)
100   FORMAT(//2X, 'input the initial value:',/)
      DO 10 I=1,N
      WRITE(6,110) I
110   FORMAT(5X, 'X(', I2, '0=? ', $)
      READ(5,*) X(I)
10    CONTINUE
      L=N/7+1
      WRITE(6,120) (X(I), I=1,N)
      WRITE(1,120) (X(I), I=1,N)
120   FORMAT (//2X, 'The initial value:',/<L>(4X, 7D18.10, :, /))
      CALL SIMPLEX(N, ITMAX, EPS, X, XX, FX, C, Y, Z, V, FY, 0, IP1, F)
      CALL STTEST(N, X, IP1)
      WRITE(6,130)
130   FORMAT (/2X, 'Going on with another initial value? (Y/N) ', $)
      READ(5,140) CC
140   FORMAT(A1)
      IF (CC .EQ. 'Y' .OR. CC .EQ. 'y') THEN
         WRITE(6,160)
160      FORMAT(//2X,
     1       'to change the max. number of iterations? (Y/N) ', $)
      READ(5,140) CC1
      IF (CC1 .EQ. 'Y' .OR. CC1 .EQ. 'y') THEN
```

```
            WRITE(6,170)
170         FORMAT(//2X, 'input the max. number of iterations: ', $)
            READ (5,*) ITMAX
         ENDIF
         WRITE(6,180)
180      FORMAT(//2X, 'to change the convergence criterion? (Y/N) ', $)
         READ(5,140) CC2
            IF (CC2 .EQ. 'Y' .OR. CC2 .EQ. 'y') THEN
               WRITE(6,190)
190            FORMAT(//2X, 'the convergence criterion: ', $)
               READ (5,*) EPS
            ENDIF
            GOTO 5
         ENDIF
         CLOSE (1)
         STOP
         END
C
C
         SUBROUTINE SIMPLEX(N, ITMAX, EPS, X, XX, FX, C, Y, Z, V, FY,
        2                   IP, IP1, F)
C
C           Simplex method for nonlinear program
C
C
C           Dummy arguments:
C
C              Name        Type          I/O                    Description
C              ----        ----          ---                    -----------
C              N            I             I          dimension of parameters
C              ITMAX        I             I          the max iteration times
C              EPS          R             I          the convergence criteria
C              X          array           I/O        input: initial values of parameters
C                                                     output: the result
C              XX         array           -          internal working unit,
C                                                        one row is the coordinate of a vertex
C              FX         array           -          internal working unit, storing the
C                                                        corresponding function values
C              C          array           -          internal working unit, the centroid
C                                                        coordinate
C              Y          array           -          internal working unit
C              Z          array           -          internal working unit
C              V          array           -          internal working unit
C              FY           R             O          the functional value at the opt. point
C              IP           I             I        a flag for printing intermediate results,
C                                                     1, the action taken, the coordinate and
C                                                        function value at the min. point,
C                                                        and the coordinate and function
C                                                        value at every vertex, and the
C                                                        coordinate of centroid
C                                                     else, the action taken, the coordinate and
C                                                        function value at the min. point
C              IP1          I             I        a flag for the location to write the
C                                                   intermediate result,
C                                                     1, on screen and in a file
C                                                     else, only in a file
C              F         function         -          the objective function
C
C
C        IMPLICIT REAL *8 (A-H, O-Z)
         CHARACTER ACTION*12, FLIP*5, ACTP*17
         DIMENSION X(N), XX(N+1,N), FX(N+1), C(N), Y(N), Z(N), V(N)
         EXTERNAL F
         DATA R, T, S/1.0D0, 2.0D0, 0.5D0/
         DATA FLIP/'Flip'/
C
C           Initialization
C
         ITER=0
```

```
            LINE=0
            IFLIP=0
            ACTION='
            ACTP = '
            L=N/7+1
C
C                 to calculate the coordinate of other N vertexes
C
            SQ1=SQRT(FLOAT(N+1))-1
            SQ=N*SQRT(2.0D0)
            P=(SQ1+N)/SQ
            Q=SQ1/SQ
            DO 200 I=1,N
            XX(1,I)=X(I)
200         CONTINUE
            DO 210 I=2,N+1
            I1=I-1
            DO 210 J=1,N
            IF (I1 .EQ. J) THEN
                XX(I,J)=X(J)+P
               ELSE
                XX(I,J)=X(J)+Q
            ENDIF
210         CONTINUE
5           CONTINUE
C
C               to calculate the function values at every vertex
C
            DO 10 I=1,N+1
            DO 8 J=1,N
            X(J)=XX(I,J)
8           CONTINUE
            CALL F(X,N,FX(I))
10          CONTINUE
C
C               search for the max. and the min. points
C
15          CONTINUE
            FMAX=-1.0D38
            FMIN=1.0D38
            DO 17 I=1,N+1
            IF (FX(I) .GT. FMAX) THEN
               FMAX=FX(I)
               IMAX=I
            ENDIF
            IF (FX(I) .LT. FMIN) THEN
               FMIN=FX(I)
               IMIN=I
            ENDIF
17          CONTINUE
C
C               print the title of intermediate results
C
            IF (MOD(LINE,53) .EQ. 0) THEN
               WRITE(1,1000)
               IF (IP1 .EQ. 1) WRITE(6,1000)
1000           FORMAT('1', 'No of IT', 2X, 'Action', 16X, 'F(min)',
     *              11X, 'X(min)',
     *                   /1X, '========', 2X, '======', 16X, '======',
     *              11X, '======',/)
            ENDIF
C
C               check to see if the action is combined with flip
C
            IF (IFLIP .EQ. 1) THEN
               ACTP=FLIP//ACTION
               IFLIP=0
            ELSE
               ACTP=ACTION
```

```
            ENDIF
C
C              print the intermediate results: iteration time, action taken,
C                 coordinate and function value at the min. point
C
            WRITE(1,1010) ITER, ACTP, FX(MIN), (XX(IMIN,J),J=1,N)
            IF (IP1 .EQ. 1)
           *    WRITE(6,1010) ITER, ACTP, FX(IMIN), (XX(IMIN,J),J=1,N)
1010        FORMAT(2X, I4, 5X, A17, D15.6, 2X, <N>D11.3)
            ACTP='                '
            LINE=LINE+1
C
C              check to see if the criterion is satisfied, if so, return
C
            SS=0.0D0
            DO 170 I=1,N+1
            SS=SS+(FX(I)-FX(IMIN))**2
170         CONTINUE
            SS=SQRT(SS/N)
            IF (SS .LT. EPS) THEN
               FY=FX(IMIN)
               DO 175 I=1,N
               X(I)=XX(IMIN,I)
175         CONTINUE
            WRITE(6,1020) ITER, FY, (X(I),I=1,N)
            WRITE(1,1020) ITER, FY, (X(I),I=1,N)
1020        FORMAT(/5X, 'No. of iterations:', I10,
           *       /5X, 'Function value(min):', D20.10/
           *        5X, 'The coordinate:', /<L>(4X, 7D18.10, :, /))
            RETURN
           ENDIF
C
C              check to see if the max. iteration times have been reached, if
C                 so, print a message and return
C
           IF (ITER .GT. ITMAX) THEN
            DO 180 I=1, N
            X(I)=XX(IMIN,I)
180         CONTINUE
            FY=FX(IMIN)
            WRITE(1,1030) ITMAX, ITER, FY, (X(I),I=1,N)
            WRITE(6,1030) ITMAX, ITER, FY, (X(I),I=1,N)
1030        FORMAT(//2X,' ** The max. iteration time,', I5, ' has been ',
           *            'reached, but the convergence is not satisfied.',
           *            /5X, 'No. of iterations:', I10,
           *            /5X, 'Function value(min):', D20.10,
           *            /5X, 'The coordinate:',/<L>(4X, 7D18.10, :, /))
            RETURN
           ENDIF
C
C              search the second max. point
C
            SS=-1.0D38
            DO 18 I=1,N+1
            IF (I .NE. IMAX) THEN
               IF (FX(I) .GT. SS) THEN
                  SS=FX(I)
                  IMAXS=I
               ENDIF
            ENDIF
18          CONTINUE
C
C              calculate the coordinate of the centroid
C
            DO 20 I=1,N
            C(I)=0.0D0
20          CONTINUE
            DO 22 I=1,N
            DO 22 J=1,N+1
```

```
            IF (J .NE. IMAX) C(I)=C(I)+XX(J,I)
22          CONTINUE
            DO 25 I=1,N
            C(I)=C(I)/N
25          CONTINUE
C
C              print the coordinate and function values at every vertex,
C                 and the coordinate of centroid if IP=1
C
            IF (IP .EQ. 1) THEN
               WRITE(2,1040) ITER, (C(I),I=1,N)
1040           FORMAT(/2X,'ITERATION TIME:', I10, 5X,'CC:',<N>F10.3)
               DO 270 I=1,N+1
               JJ=0
               DO 265 J=1,N
               IF (ABS (FX(J)) .LT. 1E-3) THEN
                  JJ=1
                  GOTO 267
                  ENDIF
265            CONTINUE
267            CONTINUE
               IF (JJ .EQ. 0) THEN
                  WRITE(2,1060) I, FX(I), (XX(I,J),J=1,N)
               ELSE
                  WRITE(2,1050) I, FX(I), (XX(I,J),J=1,N)
               ENDIF
1050           FORMAT(2X, 'FX(', I1, '):', E10.3, 5X, 'XX:', <N>F10.3)
1060           FORMAT(2X, 'FX(', I1, '):', F10.3, 5X, 'XX:', <N>F10.3)
270            CONTINUE
            ENDIF
            ITER=ITER+1
C
C              reflection
C
            DO 30 I=1,N
            Y(I)=C(I)+R*(C(I)-XX(IMAX,I))
30          CONTINUE
C
C              the function value at the new point
C
            CALL F(Y,N,FY)
               IF (FY .LT. FX(IMIN)) THEN
C
C                 expansion
C
                  DO 40 I=1,N
                  Z(I)=C(I)+T*(C(I)-XX(IMAX,I))
40                CONTINUE
                  CALL F(Z,N,FZ)
                  IF (FZ .LT. FY) THEN
C
C                    the expansion has succeeded
C
                     DO 45 I=1, N
                     XX(IMAX,I)=Z(I)
45                   CONTINUE
                     FX(IMAX)=FZ
                     ACTION='Expansion   '
                     GOTO 15
                  ELSE
                     DO 50 I=1,N
                     XX(IMAX,I)=Y(I)
50                   CONTINUE
                     FX(IMAX)=FY
                     ACTION='Reflection  '
                     GOTO 15
                  ENDIF
               ELSEIF (FY .LT. FX(IMAXS)) THEN
C
```

```
C                  exchange
C
                   DO 60 I=1,N
                   XX(IMAX,I)=Y(I)
60                 CONTINUE
                   FX(IMAX)=FY
                   ACTION='Exchange    '
                   GOTO 15
                ELSE
                   IF (FY .LT. FX(IMAX)) THEN
C
C                     flip
C
                      DO 70 I=1,N
                      XX(IMAX,I)=Y(I)
70                    CONTINUE
                      FX(IMAX)=FY
                      IFLIP=1
                   ENDIF
C
C                     contraction
C
                   DO 80 I=1,N
                   V(I)=C(I)+S*(XX(IMAX,I)-C(I))
80                 CONTINUE
                   CALL F(V,N,FV)
                   IF (FV .LT. FX(IMAX)) THEN
                      DO 90 I=1,N
                      XX(IMAX,I)=V(I)
90                    CONTINUE
                      FX(IMAX)=FV
                      ACTION='Contraction '
                      GOTO 15
                   ELSE
C
C                        shrink
C
                      DO 100 I=1,N+1
                      DO 100 J=1,N
                      XX(I,J)=0.5D0*(XX(I,J)+XX(IMIN,J))
100                   CONTINUE
                      ACTION='Shrink      '
                      GOTO 5
                   ENDIF
                ENDIF
                RETURN
                END
C
C
                SUBROUTINE F(X, N, FX)
C
C                  The objective function for SIMPLEX
C
C                  Dummy arguments:
C
C                     Name          Type          I/O              Description
C                     ----          ----          ---              -----------
C                     X             array         I              the parameters
C                     N               I           I              dimension of parameters
C                     FX              R           O              the function value
C
                IMPLICIT REAL *8 (A-H, O-Z)
                DIMENSION X(N), CONST(2)
                INCLUDE 'EXPT.DAT'
                DO 5 I=1,N
                XX(I)=X(I)
                IF (XX(I) .LT. 0.0D0) THEN
                   FX=1.0D10
                   GOTO 20
```

```
            ENDIF
5           CONTINUE
            FX=0.0D0
            DO 20 JCOL=1,NT
            TK=TEMP(JCOL)
            Y(1)=Y10
            Y(2)=Y20
            Y(3)=Y30
            Y(4)=Y40
            Y(5)=Y50
            CALL DIFFUN(NN,Y,DY)
            JEXP=1
            TIME1=TIME(JEXP,JCOL)
            DO 10 I=1,MAXS
            CALL RK2(NN, H, Y, DY, YC, Y1)
            IF (ABS(Y(1)-TIME1) .LE. 1.0D-8) THEN
               DIFA=A(JEXP,JCOL)-Y(2)
               DIFB=B(JEXP,JCOL)-Y(3)
               DIFC=C(JEXP,JCOL)-Y(4)
               DIFD=D(JEXP,JCOL)-Y(5)
               DIFA=SIGN( MIN( ABS( DIFA), 1.0D15), DIFA)
               DIFB=SIGN( MIN( ABS( DIFB), 1.0D15), DIFB)
               DIFC=SIGN( MIN( ABS( DIFC), 1.0D15), DIFC)
               DIFD=SIGN( MIN( ABS( DIFD), 1.0D15), DIFD)
               DIFA=DIFA/A(JEXP,JCOL)
               DIFB=DIFB/B(JEXP,JCOL)
               DIFC=DIFC/C(JEXP,JCOL)
               DIFD=DIFD/D(JEXP,JCOL)
               FX=FX + DIFA*DIFA + DIFB*DIFB + DIFC*DIFC + DIFD*DIFD
               JEXP=JEXP+1
               TIME1=TIME(JEXP,JCOL)
               IF (JEXP .GT. NUMBER(JCOL)) GOTO 20
            ENDIF
10          CONTINUE
20          CONTINUE
            RETURN
            END
C
C
            SUBROUTINE RK2 (N, H, Y, DY, YC, Y1)
C
C              Fixed step size Runge-Kutta method for the solution of the initial
C                 value problem of first order ordinary differential equations
C
C              Dummy arguments:
C
C                 Name          Type          I/O                Description
C                 ----          ----          ---                -----------
C                 N               I           I                   no. of equations
C                 H               R           I                   step size
C                 Y             array         I/O          dimension = N
C                                                          input: initial values for the first calling
C                                                          output: integration results
C                 DY            array         O            dimension = N
C                                                              the values of right function
C                 YC            array         -            dimension = N
C                                                              working unit
C                 Y1            array         -            dimension = N
C                                                              working unit
C
            IMPLICIT REAL *8 (A-H, O-Z)
            DIMENSION Y(N), DY(N), YC(N), Y1(N), A(4)
            A(1)=0.5D0*H
            A(2)=A(1)
            A(3)=H
            DO 1 I=1,N
            Y1(I)=Y(I)
1           CONTINUE
            DO 3 K=1,3
```

```
      DO 2 I=1,N
      YC(I)=Y1(I)+A(K)*DY(I)
      Y(I)=Y(I)+A(K+1)*DY(I)/3.0D0
2     CONTINUE
      CALL DIFFUN(N, YC, DY)
3     CONTINUE
      DO 4 I=1,N
      Y(I)=Y(I)+A(1)*DY(I)/3.0D0
4     CONTINUE
      CALL DIFFUN(N, Y, DY)
      RETURN
END
C
C
      SUBROUTINE DIFFUN(N,Y,DY)
C
C        The rate equations
C
C
C        Dummy arguments:
C
C           Name          Type          I/O              Description
C           ----          ----          ---              -----------
C           N               I           I                no. of equations
C           Y             array         I              dimension = N
C                                                      input: the previous integration results
C           DY            array         O              dimension = N
C                                                        the values of right function
C
      IMPLICIT REAL*8 (A-H,O-Z)
      DIMENSION Y(N),DY(N)
      COMMON /DIFFUN/TEMP, X(10)
      DO 10 I=2,N
      IF (Y(I) .LT. 0.0D0) Y(I)=0.0D0
      IF (Y(I) .GT. 1.0D0) Y(I)=1.0D0
10    CONTINUE
      DY(1)=1.0D0
      Y2=Y(2)
      Y3=Y(3)
      DY(2)=-X(1)*Y2
      DY(3)= X(1)*Y2-Y3(X(2)+X(3))
      DY(4)=X(2)*Y3-X(4)*Y(4)
      DY(5)=X(3)*Y3+X(4)*Y(4)
      RETURN
      END
C
C
      SUBROUTINE STTEST(N, X, IP1)
C
C        statistical test for the model parameters
C
C        Dummy arguments:
C
C           Name          Type          I/O              Description
C           ----          ----          ---              -----------
C           X             array         I              the parameters
C           N               I           I              dimension of parameters
C
      IMPLICIT REAL *8 (A-H, O-Z)
      DIMENSION X(N)
      INCLUDE 'EXPT.DAT'
      DIMENSION DIFFA(NP), DIFFB(NP), DIFFC(NP), DIFFD(NP), DIFFE(NP),
     1          YAA(NP), YBB(NP), YCC(NP), YDD(NP), YEE(NP),
     2          PERCTA(NP), PERCTB(NP), PERCTC(NP), PERCTD(NP),
     3          PERCTE(NP)
      DIMENSION DIFA(NT*NP),DIFB(NT*NP),DIFC(NT*NP),DIFD(NT*NP),
     1          DIFE(NT*NP)
      DO 5 I=1,N
      XX(I)=X(I)
```

```
5           CONTINUE
            ICOUNT=0
            AADA=0.0D0
            AADB=0.0D0
            AADC=0.0D0
            AADD=0.0D0
            DO 200 JCOL=1,NT
            TK=TEMP(JCOL)
            Y(1)=Y10
            Y(2)=Y20
            Y(3)=Y30
            Y(4)=Y40
            Y(5)=Y50
            NUM=NUMBER(JCOL)
            JEXP=1
            TIME1=TIME(JEXP,JCOL)
            CALL DIFFUN(NN,Y,DY)
            DO 10 I=1,MAXS
            CALL RK2(NN, H, Y, DY, YC, Y1)
            IF (ABS(Y(1)-TIME1) .LE. 1.0D-8) THEN
               DIFFA(JEXP) = A(JEXP,JCOL)-Y(2)
               DIFFB(JEXP) = B(JEXP,JCOL)-Y(3)
               DIFFC(JEXP) = C(JEXP,JCOL)-Y(4)
               DIFFD(JEXP) = D(JEXP,JCOL)-Y(5)
               ICOUNT=ICOUNT+1
               DIFA(ICOUNT)=DIFFA(JEXP)
               DIFB(ICOUNT)=DIFFB(JEXP)
               DIFC(ICOUNT)=DIFFC(JEXP)
               DIFD(ICOUNT)=DIFFD(JEXP)
               YAA(JEXP) = Y(2)
               YBB(JEXP) = Y(3)
               YCC(JEXP) = Y(4)
               YDD(JEXP) = Y(5)
               PERCTA(JEXP) = DIFFA(JEXP)/A(JEXP,JCOL)*100.0D0
               PERCTB(JEXP) = DIFFB(JEXP)/B(JEXP,JCOL)*100.0D0
               PERCTC(JEXP) = DIFFC(JEXP)/C(JEXP,JCOL)*100.0D0
               PERCTD(JEXP) = DIFFD(JEXP)/D(JEXP,JCOL)*100.0D0
               AADA = AADA + ABS(PERCTA(JEXP))
               AADB = AADB + ABS(PERCTB(JEXP))
               AADC = AADC + ABS(PERCTC(JEXP))
               AADD = AADD + ABS(PERCTD(JEXP))
               JEXP=JEXP+1
               TIME1=TIME(JEXP,JCOL)
               IF (JEXP .GT. NUM) GOTO 20
            ENDIF
10          CONTINUE
20          CONTINUE
            IF (IP1 .EQ. 1) WRITE(6,100) TK
            WRITE(1,100) TK
100         FORMAT(/5X, 'Temperature=', F7.2, ' K',
           1        /5X, 'Component A:')
            IF (IP1 .EQ. 1) WRITE (6,110)
            WRITE(1,110)
110         FORMAT(7X, 'Time', 4X, 'Observed', 12X, 'Predicted', 8X,
           1         'Difference', 5X, 'Percentage'/
           2        7X, '---', 4x, '--------', 12X, '----------', 8X
           3        '----------', 5X, '----------')
            DO 30 I=1,NUM
            IF (IP1 .EQ. 1)
           1 WRITE(6,120) TIME(I,JCOL), A(I,JCOL), YAA(I), DIFFA(I), PERCTA(I)
            WRITE(1,120) TIME(I,JCOL), A(I,JCOL), YAA(I), DIFFA(I), PERCTA(I)
30          CONTINUE
120         FORMAT(3X, F8.1, 2X, G13.5, G22.7, G18.7, G13.5)
            IF (IP1 .EQ. 1) WRITE(6,130)
            WRITE(1,130)
130         FORMAT(/5X, 'Component B:')
            IF (IP1 .EQ. 1) WRITE(6,110)
            WRITE(1,110)
            DO 40 I=1, NUM
```

```
      IF (IP1 .EQ. 1)
     1 WRITE(6,120) TIME(I,JCOL), B(I,JCOL), YBB(I), DIFFB(I), PERCTB(I)
      WRITE(1,120) TIME(I,JCOL), B(I,JCOL), YBB(I), DIFFB(I), PERCTB(I)
40    CONTINUE
      IF (IP1 .EQ. 1) WRITE(6,140)
      WRITE(1,140)
140   FORMAT(/5X, 'Component C:')
      IF (IP1 .EQ. 1) WRITE(6,110)
      WRITE(1,110)
      DO 50 I=1,NUM
      IF (IP1 .EQ. 1)
     1 WRITE(6,120) TIME(I,JCOL), C(I,JCOL), YCC(I), DIFFC(I), PERCTC(I)
      WRITE(1,120) TIME(I,JCOL), C(I,JCOL), YCC(I), DIFFC(I), PERCTC(I)
50    CONTINUE
      IF (IP1 .EQ. 1) WRITE(6,150)
      WRITE(1,150)
150   FORMAT(/5X, 'Component D:')
      IF (IP1 .EQ. 1) WRITE(6,110)
      WRITE(1,110)
      DO 60 I=1,NUM
      IF (IP1 .EQ. 1)
     1 WRITE(6,120) TIME(I,JCOL), D(I,JCOL), YDD(I), DIFFD(I), PERCTD(I)
      WRITE(1,120) TIME(I,JCOL), D(I,JCOL), YDD(I), DIFFD(I), PERCTD(I)
60    CONTINUE
200   CONTINUE
C
C        the square of the correlation coefficient
C
      S1=0.0D0
      DO 70 J=1,NT
      NUM=NUMBER(J)
      DO 70 I=1,NUM
      S1=S1+A(I,J)
      S1=S1+B(I,J)
      S1=S1+C(I,J)
      S1=S1+D(I,J)
70    CONTINUE
      S1=0.25D0*S1/ICOUNT
      RGS=0.0D0
      DO 80 J=1,NT
      NUM=NUMBER(J)
      DO 80 I=1,NUM
      RGS=RGS+(A(I,J)-S1)**2
      RGS=RGS+(B(I,J)-S1)**2
      RGS=RGS+(C(I,J)-S1)**2
      RGS=RGS+(D(I,J)-S1)**2
80    CONTINUE
      RSDA=0.0D0
      RSDB=0.0D0
      RSDC=0.0D0
      RSDD=0.0D0
      DO 90 I=1,ICOUNT
      RSDA=RSDA+DIFA(I)*DIFA(I)
      RSDB=RSDB+DIFB(I)*DIFB(I)
      RSDC=RSDC+DIFC(I)*DIFC(I)
      RSDD=RSDD+DIFD(I)*DIFD(I)
90    CONTINUE
      RSD=RSDA+RSDB+RSDC+RSDD
      R2=1.0D0-RDS/RGS
      AADA=AADA/ICOUNT
      AADB=AADB/ICOUNT
      AADC=AADC/ICOUNT
      AADD=AADD/ICOUNT
      WRITE(1,170) RSDA, AADA, RSDB, AADB, RSDC, AADC, RSDD, AADD
      IF (IP1 .EQ. 1) WRITE(6,170) RSDA, AADA, RSDB, AADB, RSDC, AADC,
     1                             RSDD, AADD
170   FORMAT(/5X, '  Comp.', 8X, 'SSE', 12X, 'AAD',
     1       /5X, '  -----', 8X, '---', 12X, '---',
     2        /8X, 'A', 3X, 2G16.5, /8X, 'B', 3X, 2G16.5,
```

```
     3        /8X, 'C', 3X, 2G16.5, /8X, 'D', 3X, 2G16.5)
       RETURN
       END
C
C
C          PROGRAM: EXPT.DAT
C
C          NN No. of equations
C          H  Step size
C          NT No. of temperature level
C          NP Max. no. of expt. points in every temp. level
C          TR Max. residence time
C
       PARAMETER NN=5, H=0.2D0,NT=1, NP=4, TR=40, MAXS=TR/H+1
       DIMENSION Y(NN), YC(NN), Y1(NN), DY(NN), TIME(NP,NT), A(NP,NT),
     1           B(NP,NT), C(NP,NT), D(NP,NT), E(NP,NT), TEMP(NT),
     2           NUMBER(NT), XX(10)
       COMMON /DIFFUN/TK, XX
C485
C      DATA NUMBER/3/
C      DATA TEMP/758.15D0/
C      DATA TIME/20.0D0, 30.0D0, 40.0D0, 0.0D0/
      DATA NUMBER/4/
      DATA TIME/12.0D0, 20.0D0, 30.0D0, 40.0D0/
      DATA TEMP/783.15D0/
C      DATA TEMP/808.15D0/
C      DATA TEMP/833.15D0/
C
C      DATA NUMBER/3,4,4,4/
C      DATA TIME/20.0D0, 30.0D0, 40.0D0, 0.0D0, 12.0D0, 20.0D0, 30.0D0,
C     1          40.0D0, 12.0D0, 20.0D0, 30.0D0, 40.0D0, 12.0D0, 20.0D0,
C     2           30.0D0, 40.0D0/
C
C          the unit of temperature is in K
C
C      DATA TEMP/758.15D0, 783.15D0, 808.15D0, 833.15D0/
C
C          Data for 4 lumps, weight fraction, RESIDUAL is included
C             with a set of different initial values
C
       DATA Y10, Y20, Y30, Y40, Y50/
     1      0.0D0, 0.65900D+00, 0.26600D+00, 0.07500D+00, 0.00000D+00
       DATA A/
C      1          0.40205D+00,     0.37744D+00,     0.35433D+00,     0.00000D+00/
       2          0.32844D+00,     0.31226D+00,     0.29314D+00,     0.27520D+00/
C      3          0.24893D+00,     0.23666D+00,     0.22218D+00,     0.20857D+00/
C      4          0.18142D+00,     0.17248D+00,     0.16192D+00,     0.15200D+00/
       DATA B/
C      1          0.19887D+00,     0.17121D+00,     0.20086D+00,     0.00000D+00/
       2          0.15682D+00,     0.13467D+00,     0.14197D+00,     0.13564D+00/
C      3          0.14171D+00,     0.10345D+00,     0.90710D-01,     0.80203D-01/
C      4          0.59053D-01,     0.49891D-01,     0.52439D-01,     0.44783D-01/
       DATA C/
C      1          0.39125D+00,     0.43809D+00,     0.41717D+00,     0.00000D+00/
       2          0.47078D+00,     0.50059D+00,     0.50333D+00,     0.51647D+00/
C      3          0.52674D+00,     0.55973D+00,     0.57627D+00,     0.58816D+00/
C      4          0.51428D+00,     0.52358D+00,     0.51754D+00,     0.52939D+00/
       DATA D/
C      1          0.78330D-02,     0.13261D-01,     0.27635D-01,     0.00000D+00/
       2          0.43853D-01,     0.52475D-01,     0.61567D-01,     0.72689D-01/
C      3          0.82617D-01,     0.10015D+00,     0.11084D+00,     0.12307D+00/
C      4          0.24525D+00,     0.25405D+00,     0.26810D+00,     0.27382D+00/
```

APPENDIX B

LISTINGS OF PROGRAM FILE AND RUN-TIME COMMAND FILE FOR SIMUSOLV

```
        PREPARE TIME, R, T, M, G

        PROC DATA1
          SET TSTOP=40.0
          DATA
             TIME          R              T              M              G
              0.00       0.6590         0.2660         0.0750         0.0000
             20.00       0.4021         0.1989         0.3912         0.0078
             30.00       0.3774         0.1712         0.4381         0.0133
             40.00       0.3543         0.2009         0.4172         0.0276
  END
END

PROC DATA2
  SET TSTOP=40.0
  DATA
        TIME              R              T              M              G
         0.00          0.6590         0.2660         0.0750         0.0000
        12.00          0.3284         0.1569         0.4708         0.0439
        20.00          0.3123         0.1347         0.5006         0.0525
        30.00          0.2931         0.1420         0.5033         0.0616
        40.00          0.2752         0.1356         0.5165         0.0727
  END
END

PROC DATA3
  SET TSTOP=40.0
  DATA
        TIME              R              T              M              G
         0.00          0.6590         0.2660         0.0750         0.0000
        12.00          0.2489         0.1417         0.5267         0.0826
        20.00          0.2367         0.1035         0.5597         0.1002
        30.00          0.2222         0.0907         0.5763         0.1108
        40.00          0.2086         0.0802         0.5882         0.1231
  END
END


PROC DATA4
  SET TSTOP=40.0
  DATA
        TIME              R              T              M              G
         0.00          0.6590         0.2660         0.0750         0.0000
        12.00          0.1814         0.0591         0.5143         0.2452
        20.00          0.1725         0.0499         0.5236         0.2541
        30.00          0.1619         0.0524         0.5175         0.2681
        40.00          0.1520         0.0448         0.5294         0.2738
  END
END

PROC P1
  PLOT R,T,M,G, 'OVER'
END

PROC D1
  DISPLAY K1,K2,K3,K4
  DISPLAY FUNOPT
END
```

```
PROC S1
  SET K1=0.01,K2=0.01,K3=0.01,K4=0.01
END

PROC S2
  SET K1=0.1,K2=0.1,K3=0.1,K4=0.1
END
PROGRAM

  INITIAL
        VARIABLE TIME=0.0
        CONSTANT R0=.659, T0=.266, M0=.075, G0=0.0,...
                 K1=0.05, K2=0.05, K3=0.02, K4=0.02, TSTOP=40.0

        CINT = TSTOP/120
  END

  DYNAMIC
        DERIVATIVE
             DRDT = -K1*R
             DTDT =  K1*R - K2*T - K3*T
             DMDT =  K2*T - K4*M
             G    =  R0 + T0 + M0 + G0 - R - T - M

             R    =  INTEG(DRDT, R0)
             T    =  INTEG(DTDT, T0)
             M    =  INTEG(DMDT, M0)
        END

        TERMT (TIME .GE. TSTOP)

        CONVR = 100.0*(R0-R)/R0
        CONVT = 100.0*(T0-T)/T0
        CONVM = 100.0*(M0-M)/M0
  END

  TERMINAL
        TOTAL = R+M+T+G

        PCR   = 100.0*R/TOTAL
        PCT   = 100.0*T/TOTAL
        PCM   = 100.0*M/TOTAL
        PCG   = 100.0*G/TOTAL
  END
END
```

APPENDIX C

UNIVERSITY OF UTAH TAR SANDS BIBLIOGRAPHY

Theses and Dissertations

Sepulveda, J.E. *Hot water separation of bitumen from Utah tar sands.* M.S. thesis, Univ. Utah, Salt Lake City, Utah, 1977.

Weeks, J.K. Jr. *Fluidized-bed processing of Utah tar sands.* M.S. thesis, Univ. Utah, Salt Lake City, Utah, 1977.

Bunger, J.W. *Processing Utah tar sand bitumen.* Ph.D. dissertation, Univ. Utah, Salt Lake City, Utah, 1979.

Jayakar, K.M. *The thermal recovery of oil from tar sand.* Ph.D. dissertation, Univ. Utah, Salt Lake City, Utah, 1979.

Venkatesan, V.N. *Fluidized-bed thermal recovery of synthetic crude from bituminous sands of Utah.* Ph.D. dissertation, Univ. Utah, Salt Lake City, Utah, 1979.

Hanks, K.C. *Chemistry of oil production from tar sand.* M.S. thesis, Univ. Utah, Salt Lake City, Utah, 1979.

Smith, R. *Asphalt Ridge tar sands--flotation behavior and process design.* M.S. thesis, Univ. Utah, Salt Lake City, Utah, 1981.

Aguilar, R. *Physical separation of bitumen from Utah tar sands.* M.S. thesis, Univ. Utah, Salt Lake City, Utah, 1981.

Brechtel, C.E. *Hydrotreating Utah tar sand products.* M.S. thesis, Univ. Utah, Salt Lake City, Utah, 1981.

Umoh, R.A. *Steam cracking of Utah tar sand bitumen in a Kellogg millisecond furnace.* M.S. thesis, Univ. Utah, Salt Lake City, Utah, 1981.

Bezama, R.J. *An energy efficient method for thermal processing of Utah tar sands.* Ph.D. dissertation, Univ. Utah, Salt Lake City, Utah, 1983.

Wang, J. *The production of hydrocarbon liquids from a bitumen-impregnated sandstone in a fluidized bed pyrolysis reactor.* M.S. thesis, Univ. Utah, Salt Lake City, Utah, 1983.

Wang, C.J. *The solubility of carbon dioxide in tar sand bitumens.* M.S. thesis, Univ. Utah, Salt Lake City, Utah, 1984.

Smart, L.M. *Thermal processing of tar sands.* M.S. thesis, Univ. Utah, Salt Lake City, Utah, 1984.

Dorius, J.C. *The pyrolysis of bitumen impregnated sandstone from the P.R. Spring (Utah) deposit in a fluidized bed.* Ph.D. dissertation, Univ. Utah, Salt Lake City, Utah, 1985.

Tsai, C.H. *Reaction kinetics and mechanisms of hydropyrolysis processing of tar sand bitumen and related materials.* M.S. thesis, Univ. Utah, Salt Lake City, Utah, 1987.

Lin, L.C. *The kinetics of the pyrolysis of tar sands and of the combustion of coked sands.* Ph.D. dissertation, Univ. Utah, Salt Lake City, Utah, 1988.

Sung, SH. *The fluidized bed pyrolysis of bitumen-impregnated sandstone in a large diameter reactor.* M.S. thesis, Univ. Utah, Salt Lake City, Utah, 1988.

Final Reports

Oblad, A.G.; Bunger, J.W.; Miller, J.D.; Seader, J.D. 1977. Recovery of oil from Utah's tar sands. *Final Report.* Grant ASR74-21867, Natl. Sci. Found. RANN Program.

Oblad, A.G.; Bunger, J.W.; Hanson, F.V.; Miller, J.D.; Seader, J.D. 1979. Recovery of oil from Utah's tar sands. *Final Report, 1977-79.* U.S. Dept. Energy (DOE) Contract # ET77-S-03-1762. 140 pp.

Bunger, J.W.; Wells, H.M. 1980. Economic evaluation of tar sand resources located in the state of Utah. Phase I. *Final Report.* Utah Eng. Exp. Stn., 211 pp.

Wells, H.M.; Bunger, J.W.; Jensen, G.F. 1984. Economic evaluation of oil shale and tar sands located in the state of Utah. *Final Report.* Utah Eng. Exp. Stn. 5 volumes.

Oblad, A.G.; Bunger, J.W.; Hanson, F.V.; Miller, J.D.; Seader, J.D. 1984. Recovery of oil from Utah's tar sands. *Final Report.* DOE Contract #DE-AS20-80LC10332.

Oblad, A.G.; Bunger, J.W.; Hanson, F.V.; Miller, J.D.; Seader, J.D. 1984. Recovery and hydropyrolysis of oil from Utah's tar sands. *Final Report.* DOE Contract #DE-AS20-82LC10942.

Oblad, A.G.; Bunger, J.W.; Hanson, F.V.; Miller, J.D.; Seader, J.D. 1985. Recovery and upgrading of oil from Utah tar sands. *First Annual Report.* DOE Contract #DE-FG20-84LC11057.

Oblad, A.G.; Bunger, J.W.; Hanson, F.V.; Miller, J.D.; Seader, J.D. 1986. Recovery and upgrading of oil from Utah tar sands. *Second Annual Report.* DOE Contract #DE-FG20-84LC11057.

Oblad, A.G.; Bunger, J.W.; Hanson, F.V.; Miller, J.D.; Seader, J.D. 1987. Recovery and upgrading of oil from Utah tar sands. *Final Report*. DOE Contract #DE-FG20-84LC11057.

Oblad, A.G.; Hanson, F.V. Production of bitumen-derived hydrocarbon liquids from Utah's tar sands. *Final Technical Report*. DOE Contract # DE-FG21-87MC11090.

Patents

Miller, J.D.; Sepulveda, J.E. Oct. 17, 1978. Separation of bitumen from dry tar sands. *U.S. Patent 4,120,776*.

Seader, J.D.; Jayakar, K.M. July 10, 1979. Process and apparatus to produce synthetic crude oil from tar sands. *U.S. Patent 4,160,720*.

Oblad, A.G.; Shabtai, J.S. Nov. 3, 1981. Hydropyrolysis of tar sand bitumens and heavy petroleum oils. *U.S. Patent 4,298,487*.

Hanson, F.V.; Miller, J.D.; Oblad, A.G. June 29, 1982. Process for obtaining products from tar sands. *U.S. Patent 4,337,143*.

Hanson, F.V.; Miller, J.D.; Oblad, A.G. Oct. 11, 1983. Process for recovering products from tar sand. *U.S. Patent 4,409,090*.

Miller, J.D.; Hupka, J. Sept. 11, 1984. Bitumen recovery from tar sands. *U.S. Patent 4,470,899*.

Miller, J.D.; Misra, M. Dec. 4, 1984. Process for separating high viscosity bitumen from tar sands. *U.S. Patent 4,486,294*.

Publications

1976

Bunger, J.W.; Mori, S; Oblad, A.G. 1976. Processing of tar sand bitumens. Part I. Thermal cracking of Utah and Athabasca tar sand bitumens. *Preprints, Div. Fuel Chem.*, ACS, 21(6):147.

Oblad, A.G.; Seader, J.D.; Miller, J.D.; Bunger, J.W. 1976. Recovery of bitumen from oil-impregnated sandstone deposits of Utah. *Oil Shale and Tar Sands. AIChE Symp. Ser. 72*, No. 155, p. 69.

Sepulveda, J.E.; Miller, J.D.; Oblad, A.G. 1976. Hot water extraction of bitumen from Utah tar sands. I. *Symp. on Oil Shale, Tar Sands and Related Materials--Production and Utilization of Synfuels, Preprints, Div. Fuel Chem.*, ACS 21(6):110.

1977

Bunger, J.W. 1977. Development of Utah tar sands--A status report, *Mines and Mineral Rep.* No. 5, 1-10, October.

Bunger, J.W. 1977. Techniques of analysis of tar sand bitumens. *Preprints, Div. Pet. Chem.*, ACS 22(2):716-26.

Bunger, J.W.; Cogswell, D.E.; Oblad, A.G. 1977. Thermal processing of a Utah tar sand bitumen. *Proc. Canada-Venezuela Oil Sand Symp.-77.* Edmonton, Alberta, Canada; The oil sands of Canada-Venezuela-1977, ed. D.A. Redford, A.G. Winestock. 1978. *CIM Special* 17:178-82.

1978

Sepulveda, J.E.; Miller, J.D. 1978. Separation of bitumen from Utah tar sands by a hot water digestion-flotation technique. *Mining Eng.* 30(9):1311 (also published in *Trans SME/AIME*, Sept. 1978).

Sepulveda, J.E.; Miller, J.D.; Oblad, A.G. 1978. Hot water extraction of bitumen from Utah tar sands. III. *Mining Eng.* 30:1311.

Bunger, J.W.; Cogswell, D.E.; Oblad, A.G. 1978. Influence of chemical factors on primary processing of Utah tar sand bitumen. *Preprints, Div. Fuel Chem.*, ACS 23(4):98-109.

1979

Bunger, J.W.; Cogswell, D.E.; Oblad, A.G. 1979. Catalytic cracking of Asphalt Ridge bitumen. *Refining of Synthetic Crude Oils*, ACS Adv. Chem., Ser. 179, 67.

Venkatesan, V.N.; Hanson, F.V.; Oblad, A.G. 1979. The thermal recovery of synthetic crude from the bituminous sands of the Sunnyside (Utah) deposit. *Proc. First Int. Conf. on the Future of Heavy Crude and Tar Sands.* Edmonton, Alberta, Canada, June 4-12.

1980

Hanson, F.V.; Miller, J.D.; Oblad, A.G. 1980. A combined hot water-thermal pyrolysis strategy for the production of bitumen-derived liquids. *15th Intersoc. Energy Conversion Conf.* Seattle, WA, August.

1981

Bunger, J.W.; Cogswell, D.E. 1981. Characteristics of tar sand bitumen asphaltenes as studied by conversion of bitumen by hydropyrolysis. *Chemistry of Asphaltenes*, ACS Adv. Chem. Ser., ed. J.W. Bunger, N.C. Li. No. 195, pp. 219-36. ACS, Washington, D.C.

Miller, J.D.; Misra, M. 1981. Hot water process development for Utah tar sands. Presented at the *90th Natl. AIChE Meet.* Houston, TX, Apr. 5-8.

Smith, R.J.; Miller, J.D. 1981. Flotation behavior digested Asphalt Ridge tar sands, *Mining Eng.* 33(12):1724.

Misra, M.; Miller, J.D. 1981. Surface chemistry features in the hot water processing of Utah tar sands. Presented at the *Symp. on Separation Sci. and Technol.*, Gatlinburg, TN, May 5-8; *Separation Sci. Technol.* 16(10):1523-44.

Bunger, J.W.; Cogswell, D.E.; Oblad, A.G. 1981. Hydropyrolysis--potential for primary upgrading. *Oil Shale, Tar Sands and Related Material*, ed. H. Stauffer. ACS Symp. Ser., No. 163: pp. 369-80.

1982

Venkatesan, V.N.; Hanson, F.V.; Oblad, A.G. 1982. A fluidized bed-thermal process for the recovery of a bitumen-derived liquid from the bitumen-impregnated sandstone deposits of Utah. *AIChE, Symp. Ser. 216*, 78:42-55.

Hupka, J.; Miller, J.D.; Aguilar, R.; Cortes, A. 1982. Modified hot water processing of domestic tar sands. *AIME Ann. Meet.*, Dallas, TX, Feb. 14-18, 1982. *Preprint No. 82-85.*

Miller, J.D.; Misra, M. 1982. Hot water process development for Utah tar sands. *Fuel Proc. Tech.* 6:27-59.

Miller, J.D.; Misra, M. 1982. Concentration of Utah tar sands by an ambient flotation process, *Int. J. Miner. Proc.* 9:269-87.

1983

Wang, J.; Hanson, F.V.; Oblad, A.G. 1983. The fluidized bed pyrolysis of the bitumen-impregnated sandstone from the Whiterocks (Utah) deposit, *Preprint AIChE Symp. Adv. Tar Sand Technol.* Denver, CO, August.

Hupka, J.; Miller, J.D.; Oblad, A.G. 1983. Hot water processing of U.S. tar sands--hot water recycle and tailing disposal, *4th Int. Conf. for Protection of the Environment.* Toulouse, France, Sept. 20-23.

Hupka, J.; Miller, J.D.; Cortes, A. 1983. The importance of bitumen viscosity in the hot water processing of domestic tar sands. *SME/AIME, Mining Eng.* 35(12):1635-41, December.

1984

Hatfield, K.E.; Oblad, A.G. 1984. Pilot plant program for upgrading of heavy oils by hydropyrolysis. *Proc. of the Second Int. Conf. Heavy Crude and Tar Sand.* Caracas, Venezuela, Feb. 7-17, UNITAR 1175-79.

Bunger, J.W. 1984. Upgrading Utah tar sand bitumen to syncrude. *Proc. WRI-DOE Tar Sand Symp.* Vail, CO, June 26-29.

Dorius, J.C.; Hanson, F.V.; Oblad, A.G. 1984. The pyrolysis of the bitumen-impregnated sandstone from the P.R. Spring (Utah) deposit in a fluidized-bed. *Proc. WRI-DOE Tar Sand Symp.* Vail, CO, June 26-29.

Smart, L.; Seader, J.D. 1984. Thermal recovery of bitumen. *Proc. WRI-DOE Tar Sand Symp.* Vail, CO, June 26-29.

1985

Bunger, J.W.; Oblad, A.G. 1985. Upgrading of bitumen by hydropyrolysis--a process for low coke and high syncrude yields. *Proc. Third Int. Conf. on Heavy Crude and Tar Sands*, UNITAR/UNDP Inf. Ctr. New York City, NY/Los Angeles, CA, pp. 1717-26, July 22-31.

Bunger, J.W. 1985. Reactions of hydrogen during hydropyrolysis processing of heavy crudes. *Preprints, Div. Pet. Chem.*, Am. Chem. Soc. 30(4):658-63.

Bunger, J.W. 1985. Inhibition of coke formation in hydropyrolysis of residual oils. *Preprints, Div. Pet. Chem.*, Am. Chem. Soc. 30(3):549-54.

1986

Bunger, J.W.; Tsai, C.H.; Russell, C.P. 1986. Competing reactions during hydropyrolysis upgrading of tar sand bitumen and residual materials. *Proc. WRI/DOE Tar Sand Symp.*, ed. J.D. Westhoff, L.C. Marchant. Jackson, WY, July 7-10.

Seader, J.D.; Bezama, R.J.; Charavarty, T. 1986. Design and economic evaluation of an energy-integrated thermal process for recovery of oil from tar sands. *Proc. WRI/DOE Tar Sand Symp.*, ed. J.D. Westhoff, L.C. Marchant. Jackson, WY, July 7-10.

Lin, L.C.; Hanson, F.V.; Oblad, A.G. 1986. A preliminary mathematical model of the pyrolysis of bitumen-impregnated sandstone in a fluidized bed. *Proc. WRI/DOE Tar Sand Symp.*, ed. J.D. Westhoff, L.C. Marchant. Jackson, WY, July 7-10.

1987

Hupka, J.; Miller, J.D.; Oblad, A.G. 1987. Diluent-assisted hot water processing of tar sands, *AOSTRA J. Res.*

Lin, L.C.; Hanson, F.V.; Oblad, A.G.; Westhoff, J.D. 1987. The pyrolysis of bitumen-impregnated sandstone in short-contact time reactors. I. Cyclone Reactor. *Fuel Proc. Tech. 16*, 173-190.

Oblad, A.G.; Bunger, J.W.; Hanson, F.V.; Miller, J.D.; Ritzma, H.R.; Seader, J.D. 1987. Tar sand research and development at the University of Utah. *Ann. Rev. Energy.* *12*:283-356.

1988

Hanson, F.V.; Oblad, A.G. 1988. The fluidized bed pyrolysis of bitumen-impregnated sandstone from the tar sand deposits of Utah. *Proceedings UNITAR/UNDP International Conference on Heavy Crude and Tar Sands*, Paper No. 155. Edmonton, Alberta, Canada.

1989

Lin, L.C.; Hanson, F.V.; Oblad, A.G. 1989. Mathematical model of the pyrolysis of bitumen-impregnated sandstone particles. I. Diffusion dominant transport regime. *Fuel Proc. Tech.*

1990

Deo, M.D.; Wang, C.J.; Hanson, F.V. I&EC Research, in press.

Lin, L.C.; Deo, M.D.; Hanson,F.V.; Oblad, A.G. AIChE J, in press.

Lin, L.C.; Deo, M.D.; Hanson, F.V., submitted for publication in AIChE J.

Lin, L.C.; Deo, M.D.; Hanson, F.V., submitted for publication in I&EC Research.

REFERENCES

1. Aris, R., and Gavalas, G.R., "On the Theory of Reactions in Continuous Mixtures," *Phil. Trans. Roy. Soc. London*, A260, 1966, p. 351-393.

2. Aris, R., "Prolegomena to the Rational Analysis of Systems of Chemical Reactions," *Arch. Rational Mach. Anal., 19*, 1965, p. 81-99.

3. Aris, R., "Prolegomena to the Rational Analysis of Systems of Chemical Reactions. II. Some Addenda," *Arch. Rational Mech. Anal., 27*, 1968, p. 356-364.

4. Wei, J., and Kuo, J.C.W., "A Lumping Analysis in Monomolecular Reaction Systems. Analysis of the Exactly Lumpable System," *Ind. Eng. Chem. Fundam., 8*, No. 1, 1969, p. 114-123.

5. Kuo, J.C.W., and Wei, J., "A Lumping Analysis in Monomolecular Reaction Systems. Analysis of Approximately Lumpable System," *Ind. Eng. Chem. Fundam., 8*, No. 1, 1969, p. 124-133.

6. Hutchinson, P., and Luss, D., "Lumping of Mixtures with Many Parallel First Order Reactions," *Chem. Eng. J., 1*, 1970, p. 129-136.

7. Luss, D., and Hutchinson, P., "Lumping of Mixtures with Many Parallel N-th Order Reactions," *Chem. Eng. Sci., 26*, 1971, p. 172-178.

8. Luss, D., "Uniqueness Criteria for Lumped and Distributed Parameter Chemically Reacting systems," *Chem. Eng. Sci., 26*, 1971, p. 1713-1721.

9. Bailey, J.E., "Lumping Analysis of Reactions in Continuous Mixtures," *Chem. Eng. J., 3*, 1972, p. 52-61.

10. Golikeri, S.V., and Luss, D., "Analysis of Activation Energy of Grouped Parallel Reactions," *AIChE J., 18*, 1972, p. 277-282.

11. Ozawa, Y., "The Structure of a Lumpable Monomolecular System for Reversible Chemical Relations," *Ind. Eng. Chem. Fundam., 12*, No. 2, 1973, p. 191-196.

12. Liu, Y.A., and Lapidus, L., "Observer Theory for Lumping Analysis of Monomolecular Reaction Systems," *AIChE J., 19*, 1973, p. 467-473.

13. Golikeri, S.V., and Luss, D., "Aggregation of Many Coupled Consecutive First Order Reactions," *Chem. Eng. Sci., 29*, 1974, p. 845-855.

14. Luss, D., and Golikeri, S.V., "Grouping of Many Species Each Consumed by Two Parallel First-Order Reactions," *AIChE J., 21*, 1975, p. 865-872.

15. Lee, H.H., "Kinetic Behavior of Mixtures with Many First-Order Reactions," *AIChE J., 23*, 1977, p. 116-117.

16. Lee, H.H., "Synthesis of Kinetic Structure of Reaction Mixtures of Irreversible First-Order Reaction," *AIChE J.*, *24*, **1978**, p. 116-123.

17. Li, G., "A Lumping Analysis in Mono- or/and Bimolecular Reaction Systems," *Chem. Eng. Sci.*, *39*, **1984**, p. 1261-1270.

18. Ho, T.C., and Aris, R., "On Apparent Second-Order Kinetics," *AIChE J.*, *33*, **1987**, p. 1050-1051.

19. Coxson, P.G., and Bischoff, K.B., "Lumping Strategy. 1. Introductory Techniques and Applications of Cluster Analysis," *Ind. Eng. Chem. Res.*, *26*, **1987a**, p. 1239-1248.

20. Coxson, P.G., and Bischoff, K.B., "Lumping Strategy. 2. A System Theoretic Approach," *Ind. Eng. Chem. Res.*, *26*, **1987b**, p. 2151-2157.

21. Astarita, G., "Lumping Nonlinear Kinetics," *AIChE J.*, *35*, **1988**, p. 1299-1309.

22. Astarita, G., "Lumping Nonlinear Kinetics: Apparent Overall Order of Reaction," *AIChE J.*, *35*, **1989**, p. 529-532.

23. Chou, M.Y., and Ho, T.C., "Continuum Theory for Lumping Nonlinear Reactions," *AIChE J.*, *34*, **1988**, p. 1519-1527.

24. Chou, M.Y., and Ho, T.C., "Lumping Coupled Nonlinear Reactions in Continuous Mixtures," *AIChE J.*, *35*, **1989**, p. 533-538.

25. Aris, R., "Reactions in Continuous Mixtures," *AIChE J.*, *35*, **1989**, p. 539-548.

26. Weekman, V.W., Jr., "A Model of Catalytic Cracking Conversion in Fixed, Moving, and Fluid-Bed Reactors," *Ind. Eng. Chem. Process Des. Dev.*, *7*, **1978**, p. 90-95.

27. Weekman, V.W., Jr., and Nace, D.M., "Kinetics of Catalytic Cracking Selectivity in Fixed, Moving, and Fluid Bed Reactors," *AIChE J.*, *16*, **1970**, p. 397-404.

28. Nace, D.M., Voltz, S.E., and Weekman, V.W., Jr., "Application of a Kinetic Model for Catalytic Cracking--Effects of Charge Stocks," *Ind. Eng. Chem. Process Des. Dev.*, *10*, **1971**, p. 530-537.

29. Voltz, S.E., Nace, D.M., and Weekman, V.W., Jr., "Application of a Kinetic Model for Catalytic Cracking--Some Correlations of Rate Constants," *Ind. Eng. Chem. Process Des. Dev.*, *10*, **1971**, p. 538-541.

30. Voltz, S.E., Nace, D.M., and Weekman, V.W., Jr., "Application of a Kinetic Model for Catalytic Cracking. III. Some Effects of Nitrogen Poisoning and Recycle," *Ind. Eng. Chem. Process Des. Dev.*, *11*, **1972**, p. 261-265.

31. Paraskos, J.A., Shah, Y.T., McKinney, J.D., and Carr, N.L., "A Kinematic Model for Catalytic Cracking in a Transfer Line Reactor," *Ind. Eng. Chem. Process Des. Dev.*, *15*, **1976**, p. 165-169.

32. Jacob, S.M., Gross, B., Voltz, S.E., and Weekman, V.W., Jr., "A Lumping and Reaction Scheme for Catalytic Cracking," *AIChE J., 22*, **1976**, p. 701-713.

33. Weekman, V.W., Jr., "Lumps, Models, and Kinetics in Practice," AICHE Monograph Series, 75(11), 1979, p. 3-29.

34. Wen, L.C., Wrench, R.E., and Ong, A.S., "Reaction Kinetic Correlation Equation Predicts Fluid Catalytic Cracking Coke Yields," *Oil & Gas J.*, Jan 11, **1988**, p. 67-70.

35. Zhorov, Y.M., Panchenkov, G.M., Tatarintseva, G.M., Kuz'min, S.T., and Zen'kovskii, S.M., "Chemical Scheme and Structure of Mathematical Description of Hydrocracking," *Int. Chem. Eng., 11*, **1971**, p. 256-258.

36. Stangeland, B.E., and Kittrell, J.R., "Jet Fuel Selectivity in Hydrocracking," *Ind. Eng. Chem. Process Des. Dev., 11*, **1972**, p. 15-20.

37. Stangeland, B.E., "A Kinetic Model for the Prediction of Hydrocracker Yields," *Ind. Eng. Chem. Process Des. Dev., 13*, **1974**, p. 71-76.

38. Cronauer, D.C., Shah, Y.T., and Ruberto, R.G., "Kinetics of Thermal Liquefaction of Belle Ayr Subbituminous Coal," *Ind. Eng. Chem. Process Des. Dev., 17*, **1978**, p. 281-288.

39. Shalabi, M.A., Baldwin, R.M., Bain, R.L., Gary, J.H., and Golden, J.O., "Noncatalytic Coal Liquefaction in a Donor Solvent. Rate of Formation of Oil, Asphaltenes, and Preasphaltenes," *Ind. Eng. Chem. Process Des. Dev., 18*, **1979**, p. 474-479.

40. Hatate, Y., Louh, C.J., and Wen, C.Y., "A Mathematical Model for Coal Liquefaction in the Solvent Refined Coal Process," AIChE Symp. Ser., No. 202, 77, 1981, p. 11-22.

41. Ghosh, A.K., Prasad, G.N., Agnew, J.B., and Sridhar, T., "Generalized Kinetic Model for the Uncatalyzed Hydroliquefaction of Coal," *Ind. Eng. Chem. Process Des. Dev., 25*, **1986**, p. 464-471.

42. Prasad, G.N., Wittman, C.V., Agnew, J.B., and Sridhar, T., "Modeling of Coal Liquefaction Kinetics Based on Reactions in Continuous Mixtures. Part 1: Theory," *AIChE J., 32*, **1986**, 1277-1287.

43. Prasad, G.N., Agnew, J.B., and Sridhar, T., "Modeling of Coal Liquefaction Kinetics Based on Reactions in Continuous Mixtures. Part II: Comparison with Experiments on Catalyzed and Uncatalyzed Liquefaction of Coals of Different Ranks," *AIChE J., 32*, **1986**, p. 1288-1300.

44. Gertenbach, D.D., Baldwin, R.M., and Bain, R.L., "Modelling of Bench-Scale Coal Liquefaction Systems," *Ind. Eng. Chem. Process Des. Dev., 21*, **1982**, p. 490-500.

45. Shabtai, J.S., Ramakrishnan, R., and Oblad, A.G., "Hydropyrolysis of Model Compounds," in *Thermal Hydrocarbon Chemistry*; Oblad et al., Ed.; *Adv. in Chem. Ser. 183*, Am. Chem. Soc., Washington D.C., 1979, 297-329.

46. Bunger, J.W.. "Processing Utah Tar Sand Bitumen," Ph.D. Dissertation, University of Utah, Salt Lake City, Utah, 1979.

47. Wen, Y.H., "Hydropyrolysis of Partially Hydrogenated Synfuels and Related Naphthenoaromatic Compounds," Ph.D. Dissertation, University of Utah, Salt Lake City, Utah, 1986.

48. Tsai, C.H., "Reaction Kinetics and Mechanisms of Hydropyrolysis Processing of Tar Sand Bitumen and Related Materials," M.S. Thesis, University of Utah, Salt Lake City, Utah, 1987.

49. Bunger, J.W., Cogswell, D.E., Wood, R.E., and Oblad, A.G., "Hydropyrolysis: The Potential for Primary Upgrading of Tar Sand Bitumen," in *Oil Shale, Tar Sands and Related Materials*; Stauffer, H.C., Ed.; ACS Symp. Ser.:163, 1981, p. 369-380.

50. Bunger, J.W., and Cogswell, D.E., "Characteristics of Tar Sand Bitumen Asphaltenes as Studied by Conversion of Bitumen by Hydropyrolysis," in *Chemistry of Asphaltenes*; Bunger, J.W., and Li, N.C., Eds.; Adv. in Chem. Series: 195, 1981, p. 219-236.

51. Oblad, A.G., Bunger, J.W., Hanson, F.V., Miller, J.D., and Seader, J.D., "Recovery and Hydropyrolysis of Oil from Utah's Tar Sands," 1982-1984 Final Report, U.S. Department of Energy, Contract # DE-AS-20-82LC10942.

52. McColgan, E.C., and Parsons, B.I., "The Hydrocracking of Residual Oils and Tars, Part 2: The Catalytic Hydrocracking of Athabasca Bitumen," Mines Branch Report R-253, Department of Energy, Mines and Resources, Ottawa, Canada, 1972.

53. Qader, S.A., and Hill, G.R., "Rate Data of Tar Hydrocracking," *Fuel, 51*, 1972, p. 54-56.

54. Qader, S.A., and Hill, G.R., "Hydrocracking of Gas Oil," *Ind. Eng. Chem. Process Des. Dev., 8*, 1969, p. 98-105.

55. Qader, S.A., and Hill, G.R., "Catalytic Hydrocracking. Hydrocracking of a Low-Temperature Coal Tar," *Ind. Eng. Chem. Process Des. Dev., 8*, 1969, p. 450-455.

56. Qader, S.A., and Hill, G.R., "Catalytic Hydrocracking. Mechanism of Hydrocracking of Low Temperature Coal Tar," *Ind. Eng. Chem. Process Des. Dev., 8*, 1969, p. 456-461.

57. Qader, S.A., and Hill, G.R., "Hydrocracking of Petroleum and Coal Oils," *Ind. Eng. Chem. Process Des. Dev., 8*, 1969, p. 462-469.

58. Banerjee, D.K., Laidler, K.J., Nandi, B.N., and Patmore, D.J., "Kinetic Studies of Coke Formation in Hydrocarbon Fractions of Heavy Crudes," *Fuel, 65*, 1986, p. 480-484.

59. Köseoglu, R.Ö., and Phillips, C.R., "Kinetic Models for the Non-Catalytic Hydrocracking of Athabasca Bitumen," *Fuel, 67*, 1988, p. 906-915.

60. Guin, J.A., Tarrer, A.R., Pitts, W.S., and Prather, J.W., "Kinetics and Solubility of Hydrogen in Coal Liquefaction Reactions," in *Liquid Fuels from Coal*; Ellington, R.T., Ed.; Academic Press, New York, 1979, p. 133-151.

61. Bunger, J.W., "Inhibition of Coke Formation in Hydropyrolysis of Residual Oils," Preprints, Div. Pet. Chem., Am. Chem. Soc., *30*(3), 1985, p. 549-554.

62. Bunger, J.W., "Reactions of Hydrogen During Hydropyrolysis Processing of Heavy Crudes," Preprints, Div. Pet. Chem., Am. Chem. Soc., *30*(4), 1985, p. 658-663.

63. Lewis, I.C., "Chemistry of Carbonization," *Carbon, 20*(6), 1982, p. 519-529.

64. Rebick, C., "Pyrolysis of Heavy Hydrocarbons," in *Pyrolysis - Theory and Industrial Practice*; Albright, L.F., Crynes, B.L., and Corcoran, W.H., Eds.; Academic Press, New York, 1983, p. 69-87.

65. Green, L.E., Schmauch, L.J., and Worman, J.C., "Simulated Distillation by Gas Chromatography," *Anal. Chem., 36*, 1964, p. 1512-1516.

66. Bunger, J.W., "Characterization of a Utah Tar Sand Bitumen," in *Shale Oil, Tar Sands, and Related Fuel Sources*; Yen, T.F., Ed.; Adv. in Chem. Series: 151, 1976, p. 121-136.

67. Worman, J.C., and Green, L.E., "Simulated Distillation of High Boiling Petroleum Fractions," *Anal. Chem., 37*, 1965, p. 1620-1621.

68. Bunger, J.W., Thomas, K.P., and Dorrence, S.M., "Compound Types and Properties of Utah and Athabasca Tar Sand Bitumens," *Fuel, 58*, 1979, p. 183-195.

69. Ryu, H., and Bunger, J.W., University of Utah, unpublished results.

70. Steinder, E.C., Blau, G.E., and Agin, G.L., "Introductory Guide - Simusolv;" Mitchell and Gauthier Associates: 1987.

71. Steinder, E.C., Blau, G.E., and Agin, G.L., "Reference Guide - Simusolv;" Mitchell and Gauthier Associates: 1987.

72. Hangos, K.M., and Toth, J., "Maximum Likelihood Estimation of Reaction Rate Constants," *Computers and Chemical Engineerings, 12*, 1988, p. 135-139.

73. Miale, J.N., Chen, N.Y., "Catalysis by Aluminosilicates," *J. Catal., 6*, 287-287 (1966).

74. Oblad, A.G., Milken, T.H., and Mills, G.A., "Chemical Characteristics and Structure of Cracking Catalyst," Advances in Catalysis, 3, 199 (1949).

75. Bunger, J.W., Thomas, J.P., and Dorrence, S.M., *Fuel, 58*, 183-195 (1979).

76. Miller, J.D., and Misra, M., *International Journal of Mineral Processing, 9*, 269-287 (1982).

77. Sepulveda, J.E., and Miller, J.D., *Mining Engineering, 30* (9) 1311-1320 (1978).

78. Hupka, J., Miller, J.D., and Cortez, A., *Mining Engineering, 35*, 1635-1641 (1983).

79. Takamura, K., *AOSTRA Journal of Research, 2* (1), 1-10 (1985).

80. Smith, R.J., and Miller, J.D., *Mining Engineering, 33*, (12) 1719-1724 (1980).

81. Hupka, J., Oblad, A.G., and Miller, J.D., *AOSTRA Journal of Research, 3*, 95-102 (1987).

82. Fu, B.C.H., and Phillips, C.R., *Fuel, 58*, 554-556 (1979).

83. Marvillet, J., Proceedings of the Association of Asphalt Technologists, 44, 416-443 (1975).

84. Brule, B., Ramond, G., and Such, C., *Transportation Research Record, 1096*, 22-34 (1986).

85. Cormack, D.E., Kenchington, J.M., Phillips, C.R., and Leblanc, P.J., *Canadian Journal of Chemical Engineering, 55*, 572-580 (1977).

86. Funk, E.W., *Canadian Journal of Chemical Engineering, 57*, 333-341 (1979).

87. Misra, M., and Miller, J.D., *Mining Engineering, 32*, 302-311 (1980).

88. Menon, V.B., and Wasan, D.T., *Colloids and Surfaces, 19*, 89-105 (1986).

89. Menon, V.B., and Wasan, D.T., *Colloids and Surfaces, 19*, 107-122 (1986).

90. Menon, V.B., and Wasan, D.T., *Colloids and Surfaces, 25*, 387-396 (1987).

91. Gonzalez, G., and Middea, A., *Journal of Dispersion Science and Technology, 8*, (5,6) 525-548 (1987).

92. Kotlyar, L.S., Ripmeester, J.A., Sparks, B.D., and Woods, J., *Fuel, 67*, p. 1529-1535 (1988).

93. Long, R.B., "Chemistry of Asphaltenes," Advances in Chemistry Series-1985; Bunger, J.W., and Li, N.C., Eds.: American Chemical Society, Washington, p. 17-27 (1981).

94. Axelson, D.E., *Fuel Processing Technology, 16*, 257-278 (1987).

95. Thiel, J., and Grey, M., *AOSTRA J. Research*, Vol. 4, pp. 63-73 (1988).

96. Thiel, J., and Wachowska, H., *Fuel*, Vol. 68, pp. 758-762 (1989).

97. Rhoads, C.A., Painter, P.C., and Given, P.H., *Int. J. Coal Geol., 8*, 69-83 (1987).

98. Geldart, D., and Abrahamsen, A.R., "The Effect of Fines on the Behavior of Gas Fluidised Beds of Small Particles," in *Fluidization*; Grade, J.R., and Matsen, J.M., Eds.: Plenum Press, New York (1980) 453.

99. Jayakar, K.M., "The Thermal Recovery of Oil from tar Sands," Ph.D. Dissertation, Univ. of Utah (1979).

100. Geldart, D., "Types of Gas Fluidization," *Powder Technol., 7* (1973) 285.

101. Grace, J.R., "Modelling and Simulation of Two Phase Fluidized Bed Reactors," *Chemical Reactor Design and Technology*, H. de Lasa, ed., Martinus Nijhof Pub., den Haag, Netherlands (1986a).

102. Kunii, D., and Levenspiel, O., "Bubbling Bed Model," *Ind. Eng. Chem. Fund., 7* (1968) 446.

103. Yerushalmi, J., and N.T. Cankurt, "Further Studies of the Regimes of Fluidization," *Powder Technol., 24* (1979) 187.

104. Di, Guo, and Seader, J.D., "Development of a Correlation for Minimum Fluidization Velocity for Sand at Elevated Temperatures," unpublished paper, 1988.

105. Mathur, A., Saxena, S.C., and Zhang, Z.F., "Hydrodynamic Characteristics of Gas-Fluidized Beds Over a Broad Temperature Range," *Powder Technol., 47* (1986) 247.

106. Saxena, S.C., and Mathur, A., "Comments on Recent Publications on 'Minimum Fluidization Velocity at High Temperatures'," *Ind. Eng. Chem. Res., 26* (1987) 859.

107. Yang, W.-C., Chitester, D.C., Kornosky, R.M., and Keairns, D.L., "A Generalized Methodology for Estimating Minimum Fluidization Velocity at Elevated Pressure and Temperature," *AIChE J., 31* (7) (1985) 1086.

108. Shrivastava, S., Mathur, A., and Saxena, S.C., "On the Determination of Minimum Fluidization Velocity by the Method of Yang et al." *AIChE J., 32* (7) (1986) 1227.

109. Ergun, S., "Flow Through Packed Columns," *Chem. Eng. Progr., 48* (2) (1952) 89.

110. Bin, A.K., "Minimum Fluidization Velocity at Elevated Temperatures and Pressures," *Can. J. Chem. Eng., 64* (1986) 854.

111. Wen, C.Y., and Yu, Y.H., "A Generalized Method for Predicting the Minimum Fluidization Velocity," *AIChE J., 12* (3) (1966) 610.

112. Bourgeois, P., and Grenier, P., *Can. J. Chem. Eng., 46* (1968) 325.

113. Kunii, D., and Levenspiel, O., *Fluidization Engineering*, Wiley & Sons, New York (1969).

114. Saxena, S.C., and Vogel, G.J., "The Measurement of Incipient Fluidisation Velocities in a Bed of Coarse Dolomite at Temperature and Pressure," *Trans. Inst. Chem. Eng., 55* (1977) 184.

115. Babu, S.P., Shah, B., and Talwalker, A., "Fluidization Correlations for Coal Gasification Materials - Minimum Fluidization Velocity and Fluidized Bed Expansion Ratio," *AIChE Symp. Ser. 176, 174* (1978) 176.

116. Vaid, R.P., and Gupta, P.S., "Minimum Fluidization Velocity in Beds of Mixed Solids," *Can. J. Chem. Eng., 56* (1978) 292.

117. Richardson, J.F., and Jeronimo, M.A. da S., "Velocity-Voidage Relations for Sedimentation and Fluidisation," *Chem. Eng. Sci., 34* (1979) 1419.

118. Nakamura, M., Hamada, Y., Toyama, S., Fouda, A.E., and Capes, C.E., "An Experimental Investigation of Minimum Fluidization Velocity at Elevated Temperatures and Pressures," *Can. J. Chem. Eng., 63* (1985) 8.

119. Hartman, M., and Svoboda, K., "Predicting the Effect of Operating Temperature on the Minimum Fluidizing Velocity, *Ind. Eng. Chem. Process Des. Dev., 25* (1986) 649.

120. Lucas, A., Arnaldos, J., Casal, J., and Puigjaner, L., "Improved Equation for the Calculation of Minimum Fluidization Velocity," *Ind. Eng. Chem. Process Des. Dev., 25* (1986) 426.

121. Chen, J.C., and J.G. Withers, "An Experimental Study of Heat Transfer from Plain and Finned Tubes in Fluidized Beds," *AIChE symp. Ser.* No. 174, Vol. 74 (1978) 327.

122. Harrison, D., and Grace, J.R., "Fluidized Beds with Internal Baffles," Ch. 13 in *Fluidization*; Davidson, J.F., and Harrison, D., Eds.; Academic Press, New York (1971).

123. Yates, J.G., Cheesman, D.J., Mashingaidze, T.A., Howe, C., and Jefferis, G., "The Effect of Vertical Rods on Bubbles in Gas Fluidized Beds," *Fluidization*; Kunii, D., and Toei, R., Eds.; Engineering Foundation, New York (1983) 103.

124. Sitnai, O., and Whitehead, A.B., "Immersed Tubes and Other Internals," Ch. 14 in *Fluidization* (2nd edition); Davidson, J.F., Clift, R., and Harrison, D., Eds.; Academic Press, London (1985).

125. Volk, W., Johnson, C.A., and Stotler, H.H., "Effect of Reactor Internals on Quality of Reactor Fluidization," *Chem. Eng. Prog., 58* (3) (1962) 44.

126. Rowe, P.N., and Nienow, A.W., "Particle Mixing and Segregation in Gas Fluidised Beds. A Review," *Powder Technol., 15* (1975) 141.

127. Rowe, P.N., and Partridge, B.A., *Trans. Inst. Chem. Engrs., 43* (1965) T157.

128. Davidson, J.F., Harrison, D., *Fluidised Particles*, Cambridge University: London (1963).

129. Nienow, A.W., and Cheesman, D.J., "The Effect of Shape on the Mixing and Segregation of Large Particles in a Gas-Fluidised Bed of Small Ones," in *Fluidization*; Grace, J.R., and Matsen, J.M., Eds.; Plenum Press, New York (1980) 373.

130. Chen, J.L.-P., and Keairns, D.L., "Particle Segregation in a Fluidized Bed," *Can. J. Chem. Eng., 53* (1975) 395.

131. Yoshida, K., Kameyama, H., and Shimizu, F., "Mechanism of Particle Mixing and Segregation in Gas Fluidized Beds," in *Fluidization*; Grace, J.R., and Matsen, J.M., Eds.; Plenum Press, New York (1980) 389.

132. Urabe, S., Hiraki, I., Yoshida, K., and Kunii, D., "Behavior of Particles in Fluidized Beds," *Kagaku Kogaku* (abridged edition) 4 (1) (1966) 151.

133. Thomas, W.J., Grey, P.J., and Watkins, S.B., *Brit. Chem. Eng., 80* (1961) 176.

134. Grace, J.R., Chapter 11, *Gas Fluidization Technology*; Geldart, D., Ed.; John Wiley & Sons Pub., Great Britain (1986b).

135. Orcutt, J.C., J.F. Davidson, and R.C. Pigford, "Reaction Time Distributions in Fluidized Catalytic Reactors," *AIChE Symp. Ser. 58, 38* (1962) 1.

136. Kato, K., and Wen, C.Y., "Bubble Assemblage Model for Fluidized Bed Catalytic Reactors," *Chem. Eng. Sci., 24* (1969) 1351.

137. Darton, R.C., "A Bubble Growth Theory of Fluidised Bed Reactors," *Trans. I. Chem. E., 57* (1979) 134.

138. Darton, R.C., LaNauze, R.D., Davidson, J.F., and Harrison, D., "Bubble Growth Due to Coalescence in Fluidized Beds," *Trans. I. Chem. E., 55*, (1977) 274.

139. Grace, J.R., "Generalized Models for Isothermal Fluidized-Bed Reactors," *Recent Advances in Engineering Analysis of Chemically Reacting Systems*; Doraiswami, L.K., Ed.; Wiley Eastern, New Delhi (1984), ch. 13.

140. Johnsson, J.E., Grace, J.R., and Graham, J.J., "Fluidized-Bed Model Verification on a Reactor of Industrial Scale," *AIChE J.* (1987) 619.

141. Skinner, F.D., and Smoot, L.D., "The Heterogeneous Reactions of Char and Carbon," Chap. 9 in *Pulverised-Coal Combustion and Gasification*; Smoot, L.D., and Pratt, P.T., Eds.; Plenum: New York (1979).

142. Field, M.A., Gill, D.W., Morgan, B.B., Hawksley, P.G.W., *Combustion of Pulverised Coal*; Cheney and Sons: Banbury, England (1967).

143. Arthur, J.A., "Reactions Between Carbon and Oxygen," *Trans. Faraday Soc., 47* (1951) 164.

144. Smoot, L.D., and Smith, P.J., *Coal Combustion and Gasification*; Plenum: New York (1985).

145. Mulcahy, M.F.R., and Smith, I.W., "Kinetics of Combustion of Pulverized Fuel: A Review of Theory and Experiment," *Rev. Pure and Appl. Chem., 19* (1969) 81.

146. Walsh, D.E., and Green, G.J., "A Laboratory Study of Petroleum Coke Combustion: Kinetics and Catalytic Effects," *Ind. Eng. Chem. Res., 27* (1988) 1115.

147. Lewis, B., and von Elbe, G., *Combustion, Flames, and Explosions of Gases*; Academic, New York (1951).

148. Minkoff, G.J., and Tipper, C.F.H., *Chemistry of Combustion Reactions*; Butterworths: London (1962).

149. Hottel, H.C., Williams, G.C., Nerheim, N.M., and Schneider, G.R., "Kinetic Studies in Stirred Reactors: Combustion of Carbon Monoxide and Propane," *Tenth Symp. (International) on Combustion*; Combustion Institute (1965) 111.

150. Tang, S.K., and Churchill, S.W., "A Theoretical Model for Combustion Reactions Inside a Refractory Tube," *Chem. Eng. Commun., 9* (1981) 137.

151. Cherian, M.A., Rhodes, P., Simpson, R.J., and Dixon-Lewis, G., "Kinetic Modelling of the Oxidation of Carbon Monoxide in Flames," *Eighteenth Symp. (International) on Combustion*; Combustion Institute (1981) p. 385.

152. Rajan, R.R., and Wen, C.Y., "A Comprehensive Model for Fluidized Bed Coal Combustors," *AIChE J., 26* (4) (1980) 642.

153. Verma, R.S., and Saxena, S.C., "Heat Transfer from an Immersed Vertical Tube to a Gas Fluidized Bed," *Energy, 8* (12) (1983) 909.

154. Gelperin, N.I., and Einstein, V.G., "Heat Transfer in a Fluidized Bed," Chapter 10 in *Fluidization*; Davidson, J.F., and Harrison, D., Eds.; Academic Press, New York (1971).

155. Zabrodsky, S.S., *Hydrodynamics and Heat Transfer in Fluidized Beds*, M.I.T. Press, Cambridge, Mass. (1966) 289.

156. White, T.R., Mathur, A., and Saxena, S.C., "Effect of Vertical Tube Diameter on Heat Transfer Coefficients in a Gas Fluidized Bed," *Chem. Eng. J., 32* (1986) 1.

157. Noe, A.R., and Knudsen, J.G., "Local and Average Heat Transfer Coefficients in a Fluidized Bed Heat Exchanger," *AIChE Symp. Ser., 64* (82) (1968) 202.

158. Saxena, S.C., Grewal, N.S., Gabor, J.D., Zabrodsky, S.S., and Galershtein, D.M., "Heat Transfer Between a Gas Fluidized Bed and Immersed Tubes," *Adv. in Heat Trans., 14* (1978) 149.

159. Baskakov, A.P., "Radiative Heat Transfer in Fluidized Bed" in *Fluidization* (2nd edition); Davison, J.F., Clift, R., and Harrison, D., Eds.; Academic: London (1985), Chapter 13b.

160. Martin, H., "The Effect of Pressure and Temperature on Heat Transfer to Gas-Fluidized Beds of Solid Particles," in *Heat and Mass Transfer in Fixed and Fluidized Beds*; van Swaaij, W.P.M., and Afghan, N.H., Eds.; Hemisphere: New York (1986) 143.

161. Wender, L., and Cooper, G.T., "Heat Transfer Between Fluidized-Solids Beds and Boundary Surfaces - Correlation of Data," *AIChE J., 4* (1) (1958) 15.

162. Xavier, A.M., and Davidson, J.F., "Convective Heat Transfer in Fluidized Beds," in *Fluidization* (2nd edition); Davidson, J.F., Clift, R., and Harrison, D., Eds.; Academic: New York (1985) Chapter 13a.

163. Bezama, R.J., "Energy-Efficient Thermal Processing of Utah Tar Sands," Ph.D. Dissertation, Univ. of Utah (1983).

164. Zabrodsky, S.S., Antonishin, N.V., and Parmas, A.L., "On Fluidized Bed-to-Surface Heat Transfer," *Can. J. Chem. Engr., 54* (1976) 52.

165. Smith, G.D., "Fluidization Experiment," B.S. Thesis, Univ. of Utah (1986).

166. Casal, J., Lucas, A., and Arnaldos, J., "A New Method for Determination of Shape Factor and Particle Density," *Chem. Eng. J., 30* (1985) 155.

167. Leva, M., *Fluidization*; McGraw-Hill: New York (1959).

168. Yates, J.G., *Fundamentals of Fluidized-Bed Chemical Processes*; Butterworths: Boston (1983).

169. Fryer, C., and Potter, O.E., "Experimental Investigation of Models for Fluidized Bed Catalytic Reactors," *AIChE J., 22* (1) (1976) 38.